THE WELDING INSTITUTE

5547/19/87
October 1987

FATIGUE PERFORMANCE OF REPAIRED TUBULAR JOINTS

For: A group of sponsors

By: P.J. Tubby

REPORT

-03143/

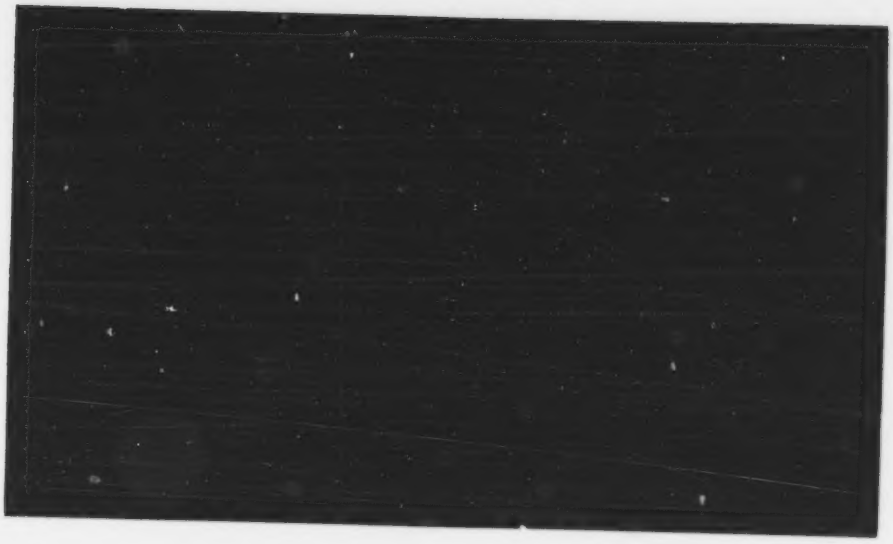

REQ. NO 4-9304

CONTRACT REPORT NO. UKL84-1059-01

5547/19/87
October 1987

FATIGUE PERFORMANCE OF REPAIRED TUBULAR JOINTS

For: A group of sponsors

By: P.J. Tubby

THE WELDING INSTITUTE
Abington Hall, Abington, Cambridge. CB1 6AL

Telephone 0223 891162 Telex 81183

158pp

MICROMEDIA

CONTENTS

		Page no.
	NOMENCLATURE	
	SUMMARY	1
1.	INTRODUCTION	2
2.	EXPERIMENTAL DETAILS	3
	2.1. Tubular joint tests	3
	2.1.1. Specimen design	3
	2.1.2. Materials	3
	2.1.3. Specimen manufacture	3
	2.1.4. Strain gauge instrumentation	3
	2.1.5. Fatigue testing details	3
	2.1.6. Repair methods	4
	2.1.7. Strain measurements on repaired specimens	5
	2.2. Fatigue crack growth tests on hyperbaric weld metal	5
	2.2.1. Specimen manufacture	5
	2.2.2. Testing details	5
3.	TEST CONDITIONS AND RESULTS	6
	3.1. Tubular joint tests	6
	3.1.1. Strain distribution in unrepaired joints	6
	3.1.2. Results of fatigue precracking	6
	3.1.3. Repair welded specimens	7
	3.1.4. Results for specimens repaired by hole drilling and cold expansion	7
	3.1.5. Results for specimens repaired by grinding alone	8
	3.2. Results of crack growth measurements in hyperbaric weld metal	9
4.	DISCUSSION	9
	4.1. Data obtained from fatigue precracking tubular joints	9
	4.2. Stress concentrations in repair welded joints	10
	4.3. Efficacy of the repair methods	10
	4.3.1. Repair welded specimens	10
	4.3.2. Hole drilling and cold expansion	12
	4.3.3. Specimens repaired by grinding alone	12
	4.4. Comparison of repair methods	14
	4.5. Crack growth in hyperbaric weld metal	14
5.	CONCLUSIONS	14
6.	ACKNOWLEDGEMENTS	15
	REFERENCES	15
	TABLES	
	FIGURES	
	APPENDICES	

NOMENCLATURE

C	constant in S-N curve
K_e	stress concentration factor due to excavation
K_t	stress concentration factor due to tubular joint geometry
m	index in S-N curve
N	endurance
N_1	endurance for first detected cracking
N_2	endurance for through-thickness cracking
R	stress ratio (minimum stress/maximum stress)
S	stress range
σ_1, σ_2	principal stresses
σ_{max}	maximum value of σ_1 determined in excavation
σ_{nom}	nominal stress in brace.

5547/19/87
October 1987

FATIGUE PERFORMANCE OF REPAIRED TUBULAR JOINTS

By: P.J. Tubby

SUMMARY

This report describes a series of fatigue tests on welded tubular T joints in steel in which fatigue cracks were repaired by a number of alternative methods. The principal objectives were to establish a ranking for the repair methods in terms of residual fatigue performance and to establish whether it is necessary to repair the entire joint, or only the cracked region. The joints were tested in out-of-plane bending.

The repair methods investigated were as follows:

1. Repair welding. Cracks were removed by grinding, and the resulting excavation filled by manual metal arc welding.
2. Repair welding and burr grinding. Repair welds made as described above were fully burr ground to remove the repair weld toe and to achieve a smooth finish on the repair weld face.
3. Hole drilling and cold expansion. The fatigue crack tips were removed by drilling through-thickness holes, which were then cold expanded to induce compressive residual stresses in the hole circumference.
4. Grinding alone. Part wall cracks were removed by burr grinding and the resulting excavations left unrepaired.

Repair welding was carried out in air at atmospheric pressure under shop conditions, rather than trying to reproduce conditions likely to be met in repairing an offshore structure. In a subsidiary investigation, fatigue crack growth rates were measured in weld metal deposited under hyperbaric conditions to establish whether hyperbaric repair welds would give results similar to those for one-atmosphere repairs.

The principal findings are summarised below:

1. Expressed in terms of the hot spot stress range, the fatigue strength of as-welded repair welds is marginally lower than that of unrepaired joints. However, this is compensated by the fact that in making the repair, the overall weld leg length is increased, which leads to a reduction in the stress range at the repair weld toe. As a result, if the applied loading is of the same magnitude after repair as before, the fatigue endurance for through-thickness cracking after repair is on average similar to, or marginally greater than, that before repair.
2. Burr grinding the repair weld may considerably improve the fatigue strength, although a smooth surface finish must be achieved to avoid premature crack initiation on the weld face. Where the applied loading continues unchanged after repair, the fatigue life for through-thickness cracking may be in excess of five times that before repair.
3. Through-thickness and part-wall weld repairs behave similarly. Under the mode of loading investigated, relatively large lack of penetration defects can be tolerated at the root in through-thickness repairs.
4. Cold expanded holes at the crack tips were not effective as a means of delaying crack propagation.
5. Removal of part-wall flaws by grinding is an effective repair method giving endurances after repair equal to or up to four times greater than the mean for unrepaired joints. Data are presented which allow the likely residual life to be estimated for a given excavation depth.

6. It is necessary to burr grind the unrepaired weld toes on both the chord and the brace to avo premature failure.

7. The crack growth rates in hyperbaric repair welds would be expected to be similar to those the one-atmosphere repairs studied here.

1. INTRODUCTION

The vast majority of fixed and mobile offshore structures are fabricated from tubular steel members These are ideally suited for offshore structural applications since they possess a high strength t weight ratio and provide a minimum restriction to the flow of water around the member, thu minimising environmental loads. However, high stress concentrations exist at joints betwee tubular members due to the localised displacements which occur as loads are transmitted throug the joint. Thus, it is at these joints that fatigue cracking is most likely to occur under the arduou conditions which can exist offshore, particularly in the North Sea.

Although every effort is made at the design stage to avoid the occurrence of fatigue cracks during the service life of an offshore structure, this may not always be achieved. An increasing number of instances of fatigue cracking in fixed offshore structures has been reported.[1,2,3] In view of the confidentiality that many oil companies apply to instances of fatigue cracking in their installations, the problem may in fact be more extensive than the reports suggest. Furthermore, as many structures move into the middle years of their design lifetime it is likely that instances of cracking will become more prevalent. It is also known through confidential work carried out at The Welding Institute that examples of fatigue cracking in mobile offshore structures are equally common.

Although it may be feasible for structures to exist with fatigue cracks for a period of time without their performance or safety being impaired, if any significant extension in the life of the structure is to be obtained, cracked joints must eventually be repaired. Although repair may be difficult and expensive and may result in significant downtime and consequential loss, this cost will be considerably lower than the cost of replacing the structure.

In addition to repairs to fatigue cracks, repairs are also carried out in situations where surface discontinuities are detected during inspection. The origin of these discontinuities is often uncertain; they may be defects which have extended during service, or manufacturing defects which were not detected during fabrication. Repairs may also be necessary following mechanical damage such as that occurring as the result of ship impact.

A number of different types of repair can be carried out. These range from a basic weld repair to the use of mechanical fixings or grouted connections. When evaluating which repair technique is the most suitable in any particular situation, a large number of factors must be taken into consideration. However, relatively little is known about the likely fatigue performance of cracked tubular joints which have been repaired. Repair welds on an offshore structure will of necessity be made under adverse conditions. Normally they will be made from one side only, possibly with poor weld preparation and no stress relief. In these circumstances the quality of the repair weld produced is likely to be lower than that of the original weld. Limited information available on the fatigue performance of repaired joints in flat plates[4] suggests that their fatigue lives can be lower than those of the original joint, even when the repairs have been made under ideal laboratory conditions.

The object of the present investigation was to obtain fatigue data for tubular T-connections tested in out-of-plane bending which had been repaired after fatigue precracking. A number of alternative repair methods were investigated including repair welding (at atmospheric pressure), crack retardation by hole drilling and cold expansion and removal of part-wall cracks by grinding without subsequent rewelding. Tests on welded joints in flat plates[5,6] have shown that the last two methods can be effective in prolonging the fatigue life. Furthermore, they are particularly attractive since they avoid the expense and difficulty of making a weld repair. In addition, fatigue crack growth rates were measured in weld metal deposited under hyperbaric conditions to establish whether hyperbaric repair welds would be expected to give similar fatigue strengths to repairs made at atmospheric pressure.

2. EXPERIMENTAL DETAILS

2.1. Tubular joint tests

2.1.1. Specimen design

The tubular joint specimens were T joints with chord dimensions of 457mm outer diameter and 16mm wall thickness and brace dimensions of 229 × 12mm wall thickness. The design is shown in Fig.1.

2.1.2. Materials

The chord material was node quality BS 4360 Grade 50E (modified) while the brace tube was API 5LX X52N steel. The chemical compositions and tensile properties are given in Tables 1 and 2 respectively.

2.1.3. Specimen manufacture

The brace tubes were hand-profiled to match the contour of the chord and chamfered to give a weld preparation angle of 50-55°. A root gap of 2-3mm was adopted to ensure full penetration. The welds were made by manual metal arc welding in the HV position using electrodes conforming to BS 639 E51 33B (AWS E7018). No preheat was required. Further details of the welding procedure are given in Table 3. All the joints were made by a single welder in order to minimise differences arising from welding technique. A balanced welding sequence in which welding was confined to one quadrant at a time was adopted to ensure that the brace was set-on normal to the chord.

2.1.4. Strain gauge instrumentation

Each specimen was instrumented with electrical resistance strain gauges. The basic gauge plan is shown in Fig.2. Strip gauges, comprising five elements of 1mm gauge length at 2mm spacing, were attached on the brace and chord in the region of expected stress hot spots on the brace centreline. The gauge positions were selected to cover the region in which strains are conventionally assumed to vary linearly with distance according to the guidance of Ref. 7 and 8. For the specimen geometry adopted here these regions (expressed in terms of the distance from the weld toe) were as follows:

Chord: 7.4-20mm
Brace: 7.4-24mm

Six strain measurement positions were included in the designated region on the chord and two on the brace. After the strain distribution in a number of specimens had been established in detail, the gauge plan was reduced in later tests to that shown in Fig.3. Gauges were incorporated on both sides of the joint since at this stage the stress ratio was changed from R = 0 to R = −1 as indicated in Section 2.1.5 below. The gauge plan of Fig.3 was also adopted for repair welded specimens. As described in Section 2.1.7 below, an alternative gauge plan was adopted for specimens with cracks removed by grinding alone.

The gauge readings were measured and recorded using a computerised data logging system supplied by Intercole Systems.

2.1.5. Fatigue testing details

All specimens were fatigue tested under constant amplitude sinusoidal loading in the same testing machine which was a purpose-built load frame with a hydraulic actuator of 70kN capacity which applied out-of-plane bending to the end of the brace via a spherical bearing. Figure 4 shows a specimen set up in the load frame ready for testing. The chord was clamped into the load frame at each end to prevent rotation. The tests were conducted under load control using a load cell interposed between the actuator and the brace.

Prior to fatigue testing, each specimen was subjected to a programme of incremental static loads to stabilise the gauges and to establish the strain distribution in the hot spot positions. Hot spot strains were determined in accordance with Ref.7 by extrapolating strains perpendicular to the toe (see Appendix B). The hot spot stress was then estimated from the extrapolated strain value together with the strain measured parallel to the toe by a single gauge as shown in Fig.2 and 3. (Young's modulus was taken as 207×10^3 N/mm^2 and Poisson's ratio as 0.3.) The fatigue load range was then

selected to achieve the desired hot spot stress range, and the test commenced. The tests covered hot spot stress ranges from 140 to 420 N/mm^2 approximately. Details of the test conditions for each specimen are given in Section 3.1 below.

A number of preliminary tests were conducted with an applied stress ratio, R (minimum stress divided by maximum stress), of zero, the remainder with R = −1. The tests were all performed in laboratory air at room temperature. The testing frequency was within the range 0.5-5Hz.

Surface crack growth was monitored by visual inspection with the aid of soap solution and coloured inks to highlight the crack mouth. The chord member was pressurised with air at low pressure for detection of through-thickness cracking. A pressure switch was used to interrupt the fatigue loading when internal pressure was lost. A number of specimens were precracked to a required crack depth (nominally 25 or 50% of the chord wall thickness) as indicated by alternating current potential drop (ACPD) measurements with a Unit Inspection Crack Microgauge.

Fatigue loading was continued until the desired extent of fatigue cracking was obtained. The test was then suspended whilst the specimen was repaired, after which the loading was continued at the same applied load range, although in a number of instances, as described below, a higher load range was adopted. Tests on repaired specimens were terminated when through-thickness cracking had developed in the chord.

2.1.6. **Repair methods**

2.1.6.1. Repair welding

A combination of disc and burr grinding was employed to remove the crack and provide a suitable preparation for repair welding. Dye penetrant was used to ensure that the crack was followed and completely removed. A final check was made by magnetic particle inspection prior to rewelding. For through-thickness repairs the intention was to leave a ligament of approximately 1-2mm thickness at the root to provide a suitable root face to be fused by the repair weld. This was in preference to removing the fatigue crack completely leaving a comparatively wide root gap to be bridged. As discussed later in the report, the technique adopted was not always entirely successful in fusing the root.

The repair welds were made by manual metal arc welding in the flat position without preheat. Typical welding conditions for a through-thickness and a part-wall crack are given in Table 4.

A further complication encountered in making some of the repairs was that the fatigue cracking was not confined to the weld toe but had branched into the chord. In such instances the branch cracks were excavated and repaired first, followed by excavation and repair of the main toe crack.

Figure 5 shows a typical specimen after repair welding.

2.1.6.2. Repair welding followed by burr grinding

A number of specimens were burr ground after repair welding. A 10mm diameter single helix burr was used in an air pistol operating at 37000rpm. The toe and the full face of the repair welds were treated. First, the repair weld toe was ground to achieve a depth of penetration of approximately 0.5mm below any undercut present. The repair weld face was then treated until a smooth surface was achieved with all traces of the interrun toes removed. No attempt was made to modify the profile of the repair weld by grinding. The original (unrepaired) weld toes were initially left untreated, but where cracks developed in these locations during the retest they were removed immediately by further burr grinding. Figure 6 shows a specimen after repair welding and burr grinding.

2.1.6.3. Hole drilling and cold expansion

This technique was attempted on two tubular joint specimens in this investigation. The method used was the Boeing split sleeve cold expansion process which is illustrated in Fig.7. The crack tips were located by magnetic particle inspection and holes centred on the crack tip or slightly ahead of it were accurately drilled to 13.41mm diameter in each location. The holes were then treated by the Boeing process which consists of drawing a mandrel through the hole using a dry lubricated split sleeve liner which prevents damage to the edge of the hole. The liner is removed after the expansion process is complete. The hole is plastically deformed giving an increase in diameter of approximately 6%. Since

the surrounding material remains elastic, compressive residual stresses are produced in the hole circumference. The equipment is designed for use on a flat surface rather than at a weld toe and it was found necessary to manufacture spacer pieces from soft aluminium to allow the puller nosecap to be seated adequately against the weld face. The holes were left open after treatment, although in practice they would need to be sealed in non-flooded submerged members.

2.1.6.4. Crack removal by grinding alone

The burr grinding conditions given in Section 2.1.6.2 were used to excavate the cracks. Dye penetrant checks ensured that the crack path was closely followed and that all cracking had been removed. The excavations were extended by a further 1-2mm in depth and approximately 25mm in surface length after the last crack indication. A final check was carried out by magnetic particle inspection. The uncracked areas of the joint were left untreated. Figure 8 shows a specimen on completion of crack excavation.

2.1.7. Strain measurements on repaired specimens

With the exception of the specimens repaired by hole drilling, all the repaired specimens were regauged after repair. For repair welded specimens the strain gauge plan was the same as that used during fatigue precracking (shown in Fig.3), except that the gauges were positioned relative to the new weld toe which was slightly further from the joint intersection as a result of the increased leg length of the weld.

The basic gauge plan adopted for specimens with ground excavations is shown in Fig.9. Small single element gauges (1mm gauge length) were attached in the bottom of the excavation at right angles to the excavation (*i.e.* in the radial direction with respect to the brace). Figure 10 shows a gauged specimen prior to retesting. It was necessary to clean up the surface of the excavation locally using fine emery paper to provide a suitable surface preparation. The gauges were left in position during the fatigue test.

In selected specimens with ground excavations the stress distribution in the excavation was investigated using a SPATE system (stress pattern analysis by thermal emission). This is a non-contacting instrument which detects infra-red emissions from a cyclically stressed surface. By scanning the surface, a full field image of the stress pattern is built up. The instrument can resolve detail down to 0.5mm, with a sensitivity in steel of approximately 1 N/mm^2. The parameter measured is the sum of the principal stresses. The experimental method employed was to scan the excavation, whilst the specimen was cycled at a reduced load range, typically 10% of full load, to establish the position of maximum stress. A load frequency in excess of 2Hz was required to achieve satisfactory results. A strain gauge rosette of 1mm gauge length was then attached at this position and strains monitored under incremental static loads up to the full test load. Prior to continuing the fatigue loading, the strain gauges were removed and the excavation lightly burr ground to remove the effect of surface preparation at the strain gauge locations.

2.2. Fatigue crack growth tests on hyperbaric weld metal

2.2.1. Specimen manufacture

Two test butt welds were made in 10mm thick steel plate BS 4360 Grade 50E in a hyperbaric chamber under conditions equivalent to a water depth of 30m in a helium 2% oxygen environment. The welding consumable was the same as that used in manufacturing the tubular joint specimens (BS 639 E51 33B). The welds were deposited automatically. Details of the welding parameters and the run sequence are shown in Table 5. Chemical analyses of the parent plate and the weld metal, and mechanical properties of the parent plate are given in Table 6.

The butt welded panels were stress-relieved at 600°C for one hour prior to cold sawing to form blanks for the crack growth specimens which were machined to the form shown in Fig.11.

2.2.2. Testing details

Specimens were loaded in three-point bending in a servohydraulic testing machine of 50kN capacity. Two specimens were tested in air at room temperature at frequencies in the range 1-6Hz and three tests were conducted in synthetic sea water at 5°C ($\pm$ 1°C) with a loading frequency of

0.16Hz. The synthetic seawater complied with the requirements of ASTM D1141 (without the addition of stock solution 3 containing the heavy metal ions). The volume of the seawater cell was approximately 25 litres and the flow rate of the order of 2 l/min. The tests were performed under freely corroding conditions.

Crack length measurement was by the direct current potential drop method using a continuous current of 20A. Further details of the measurement method and calibration are given in Ref.9. All specimens were precracked at high frequency in air at the loads to be used in the fatigue tests. The tests were conducted using a span to width ratio of 8:1 and a stress ratio R = 0.01. Load ranges were selected to cover a reasonable range of stress intensities. The results were reduced to derive the stress intensity factor range using a standard K-calibration.[9] The crack growth rates were estimated by the seven point incremental polynomial method recommended in ASTM E647.

3. TEST CONDITIONS AND RESULTS

3.1. Tubular joint tests

Twenty-five tubular joints were fatigue tested, of which twenty-four were repaired and retested. For the remaining specimen, the loading was continued without repair to examine the crack development after through-thickness cracking. The repair methods, fatigue stresses and endurances are given in Table 7 for both the preliminary testing, that is the fatigue precracking, and the continuation of each test after repair. The lives quoted after repair exclude the cycles applied during precracking.

The majority of specimens failed in the chord at the hot spot positions on both sides of the joint which were designated A and B, side A being the front of the specimen as positioned in the test frame (see Fig.4). The endurances recorded were the number of cycles at which cracking was first detected visually, N_1, and the number of cycles for the development of cracking through the chord wall, N_2. (Note: the N_2 results for fatigue precracking in Table 7 are the number of cycles to achieve the target precrack depth indicated.)

Figures showing the extent of the cracks in each specimen at N_1 and N_2 are given in Appendix A. Strain distributions measured in each specimen before and after repair are given in Appendix B, and macrosections of typical repaired joints are given in Appendix C. The results are presented in detail in the following sections.

3.1.1. Strain distribution in unrepaired joints

The results from specimens instrumented with the full strain gauge plan of Fig.2 were used to examine the stress distribution in the joint area. Figure 12 shows a typical strain distribution in the vicinity of the hot spot in specimen No.2 (side A). As would be expected for the out-of-plane loading mode, the maximum hot spot strain in the chord occurs in the saddle area on the centreline of the brace. Stress concentration factors, K_t, for the chord and brace obtained from the strain measurements on specimen No.2 are compared with those predicted using the parametric formulae derived by various researchers (see Ref.8) in the Table below.

	K_t	
Source	Chord	Brace
Measured values (specimen No.2)	7.78	3.63
Kuang	6.78	7.19
Gibstein	8.41	6.21
Wordsworth and Smedley	8.38	6.28

As indicated by these values, hot spot strains in the brace were consistently lower than expected and in later tests they were not measured in detail.

3.1.2. Results of fatigue precracking

In all specimens, cracks developed at the weld toe in the chord and propagated in the through-thickness direction in the chord wall. In a few specimens, cracks also developed at the toe

between the first and second weld runs in the weld cap adjacent to the chord. No cracks were observed at the weld toe in the brace. As indicated in Table 7, cracks were grown to different target depths, namely 25, 50 and 100% of the chord wall thickness. In specimens which cracked on both sides, the loading was stopped when the deeper of the two cracks indicated the target depth. Whilst it was not possible to measure the actual crack depths achieved, the depth of grinding required to remove part-wall cracks in specimens repaired by welding or by grinding alone indicated that the target depths were achieved generally to within ±1mm.

Figure 13 shows the extent of cracking in specimen No.3 revealed by magnetic particle inspection after the crack had propagated through the chord wall thickness. Several branch cracks have developed from irregularities in the weld toe and propagated roughly parallel to the axis of the chord. As will be seen in the Figures in Appendix A, this behaviour was observed in many of the specimens precracked to the full thickness of the chord, with branch cracks up to 50mm long in some instances.

The precracking results are plotted in terms of the hot spot stress range versus endurance on logarithmic axes in Fig.14. Since, in most specimens, cracks developed on both sides of the joint, two values of N_1 (the endurance for first detected cracking) are plotted for each test. It is felt that both these values are valid since the strain distribution on the uncracked side was little affected by cracking on the other side of the joint. Different symbols are used in Fig.14 to indicate the crack depth at which each test was terminated. S-N curves from Ref.8 are plotted in Fig.14 for comparison with the test results. These are the mean and mean minus two standard deviations curves for through-thickness cracking in joints of 16mm chord wall thickness, and the T design curve for thickness up to 32mm.

3.1.3. Repair welded specimens

Thirteen specimens were repaired by welding, of which eight were retested in the as-welded condition and five were burr ground as described in Section 2.1.6.2. All specimens were retested at the same load range with the exception of numbers 1 and 23 where higher hot spot stresses after repair, as indicated in Table 7, were achieved by increasing the load range.

In the as-repaired specimens, failure occurred in the chord at the repair weld toe, although in several specimens cracks also grew at the toes between the first and second capping passes in the repair, as indicated in Appendix A. Of the five specimens retested with burr ground repair welds, two failed by fatigue cracking which initiated on the ground repair weld face close to the chord toe, and the others were unfailed after either two million or five million cycles, as indicated in Table 7. In several of these tests cracks developed at the untreated toe in the brace and were removed by burr grinding to allow the test to continue. Details are given in Table A1 of Appendix A.

The majority of specimens with through-thickness repairs contained defects at the repair weld root where the original fatigue crack was not completely fused, as described in Section 2.1.6.1. As will be seen in the macrosections in Appendix C, some of the defects extended slightly by fatigue during the retest, but they do not seem to have contributed significantly to failure since in every case, cracks initiated at the outside surface of the joint and propagated inwards through the chord wall.

Figure 15 shows specimen No.3 (as-welded through-thickness repair) after retesting. Figure 16 shows the fracture surfaces in specimen No.20 (as-welded part-wall repair). The fracture surface markings (caused by the soap solution used during inspection) show the crack development.

The fatigue test results for all repair welded specimens are plotted in terms of the hot spot stress range measured after repair, in Fig.17. For comparison with the other repair methods, the results are also plotted in terms of the precracking hot spot stress range, in Fig.18.

3.1.4. Results for specimens repaired by hole drilling and cold expansion

As indicated in Table 7 two specimens were investigated, one precracked to nominally 50% of the chord wall (specimen No.8) and one with through-thickness cracks (specimen No.7). Figures 19 and 20 show the positions of the holes and the extent of cracking after the retest. Further detail is shown in the relevant diagrams in Appendix A. In specimen No.7 a large proportion of the joint circumference was cracked at the weld toe and, in addition, five branch cracks had grown away from the toe into the chord. It was therefore necessary to treat a total of nine crack tips. At one crack

tip the hole was incorrectly positioned, so a second was drilled as shown in Fig.19b. In specimen No.8, cracking was less extensive and only four holes were necessary. (Note: The three separate toe cracks on side B of specimen 8 (see Appendix A) were treated as a single crack, *i.e.* only the two extreme crack tips were treated.)

The progress of cracking after loading recommenced is shown in the figures in Appendix A. The first new cracking to develop in specimen No.7 was a branch from an irregularity in the original toe crack on side B. It is possible that this branch could have been present at the time the holes were drilled but was too small to be noticed by magnetic particle inspection. This was rapidly followed by crack initiation at the edges of the holes opposite the initial cracking. Since the specimen was precracked through the chord wall, a true N_2 value could not be obtained in this test. Cycling was continued until substantial new cracking had developed from all the holes, at which stage the weld toe was cracked around the full circumference. In specimen No.8, a crack approximately 10mm long was found at the weld toe away from the treated area within 700 cycles of commencing the retest. Since it was uncertain whether this was a new crack, or one missed during previous inspection, it was removed by burr grinding before continuing the test. Subsequently, cracking initiated from the holes as in specimen No.7. There was also a tendency for cracks to initiate at the chord toe ahead of those spreading from the holes. The fatigue fracture surfaces are shown in Fig.21. The test was terminated when the original crack between the holes on side A had propagated through the thickness, as indicated by ACPD measurement.

The test results are plotted in terms of the hot spot stress range measured during precracking versus endurance, in Fig.22. Figure 23 shows the crack development expressed in terms of the surface crack length versus cycles after repair. The results for specimen No.2, which was tested to final failure without repair at a similar hot spot stress range, are plotted for comparison. The treated specimens show a step increase in surface length where the holes were introduced, since each crack tip effectively advances by a proportion of the hole diameter. It should be noted that the apparently large step increase in crack length for specimen 8B is a result of considering the three separate toe cracks as one after hole drilling; the crack length plotted before this is the sum of the three lengths. In addition, in order to simplify the plots, only the main cracking at the toes is represented and the branch cracks have not been included.

3.1.5. Results for specimens repaired by grinding alone

Nine specimens were tested as indicated in Table 7. Failure was by multiple crack initiation within the ground excavations followed by coalescence and growth along the excavation and the untreated weld toe in the chord. Branch cracks developed into the chord before through-thickness cracking, as observed with the other repair methods. Figure 24 shows a typical specimen after retesting, and Fig.25 shows the fracture surfaces for this specimen (No.11). Cracking also initiated on the inside surface of the chord wall beneath the excavation and propagated outwards to meet that growing in from the bottom of the excavation. In two specimens cracks also appeared at the untreated weld toes in the chord adjacent to the ends of the excavation, and were removed by burr grinding (see Table A1 in Appendix A).

Details of the strain distributions and excavation profiles are given in Appendix D. In addition, the macrosections given in Appendix C show the excavation shapes on the brace centreline in each joint. Maximum depths for each excavation are given in Table 8 together with principal stresses in the excavations estimated as described further below. The test results are plotted in terms of the hot spot stress measured during precracking versus endurance in Fig.26.

In two specimens (22 and 25) N_1 results were obtained for a range of excavation depths by grinding out cracks each time they were detected in the excavation. The results are given in Table 9. At each depth the stress distribution within the excavation was examined using the SPATE technique and strain gauge rosettes, as described in Section 2.1.7 above.

The test on specimen No.22 was only partially successful since the load range used during SPATE measurements was accidentally set too high and was not maintained constant throughout, with the result that several cracks developed in the excavation before the stress measurements were completed. At this stage, since the applied loads, and hence the extent of fatigue damage accumulated in the excavation were not accurately known, it was decided to grind both excavations to approximately 50% of the chord wall thickness before continuing. In the event, the excavation on

side B had to be taken slightly deeper to remove surface blemishes, assumed to be imperfections in the plate, which appeared in the bottom of the groove. Finally, stress measurements were made on the second excavation using the SPATE system with the test load reduced to 10% of the full range, and rosette gauges subsequently attached at the hot spots to measure the principal strains at full load. The test was then continued until through-thickness cracking. The results given in Table 9 relate to the second excavation depth only.

N_1 results were successfully obtained for three excavation depths in specimen No.25 as indicated in Table 9. Each time cracking was detected both excavations were immediately ground out to the next required depth. Finally, at a depth of 6mm, cracking was allowed to progress until both excavations were cracked, and subsequently to through-thickness cracking on side B.

The remaining seven specimens were tested with a single excavation depth rather than attempting to obtain results for a range of depths. In three of these (10, 14 and 17) the stress distribution was examined using the SPATE system and strains measured at the hot spot positions by rosette gauges. Strains in the other four specimens were measured with single element gauges in the excavation (Fig.9).

Assuming elastic conditions, strains measured by the rosette gauges were converted to principal stress ranges which are given in Table 8. In all cases the maximum principal stress direction was close to the radial direction with respect to the brace (*i.e.* transverse to the excavation). The extent of biaxiality (σ_2/σ_1) varied little from one specimen to another within the range 0.27-0.34, with an average value of 0.3.

Assuming that the extent of biaxiality and the principal stress direction were similar in all specimens, the strain ranges obtained from the single element gauges have also been used to estimate principal stresses. The maximum value for each excavation is given in Table 8.

The data in Table 8 have been used to estimate stress concentration factors, K_e, for each excavation as follows:

$$K_e = \frac{\text{maximum principal stress range in excavation}}{\text{hot spot stress range during precracking}}$$

The results are plotted against excavation depth in Fig.27 and the test endurances, N_1 and N_2, are plotted against the maximum principal stress range in the excavation in Fig.28.

3.2. Results of crack growth measurements in hyperbaric weld metal

The results of the crack growth tests performed in air and synthetic seawater are presented together in Fig.29 as a logarithmic graph of crack propagation rate versus stress intensity factor range. Two scatterbands based on published data are plotted for comparison. These are:

i. Crack growth rates measured in air at room temperature for a range of structural steels including weld metal, heat affected zones and parent materials.[10]

ii. Data for parent steel to BS 4360 Grade 50D freely corroding in seawater at temperatures in the range 5-20°C and with loading frequencies between 0.1 and 1.0Hz.[11]

4. DISCUSSION

4.1. Data obtained from fatigue precracking tubular joints

The test results for first detected cracking, N_1, are rather widely scattered as seen in Fig.14. This is to be expected as a result of local variations in weld toe geometry, and has been observed in other investigations.[8] In addition, the early detection of cracks is a function of both experimental technique and inspection frequency. Whilst it is possible to detect surface cracks of the order of 1-2mm length with the visual inspection technique employed in this study, cracking had in many cases progressed to greater than 10mm before detection, as can be seen in the figures in Appendix A. Generally inspections were carried out at a minimum frequency of once every 12 hours, and the loading rate was kept at 0.5-1Hz until crack initiation, so that the minimum inspection frequency was once in 2-4 $\times 10^4$ cycles. In addition, more frequent checks were made during the first few hours of running, up

to approximately 10^4 cycles. It is therefore unlikely that more frequent inspections would have reduced the scatter significantly.

The results for N_2 in Fig.14 generally fall on or slightly above the mean N_2 line for joints of 16mm wall thickness obtained in a survey of available data.[8] All the data are well above both the mean minus two standard deviations line and the T design curve. It is therefore concluded that the fatigue characteristics of the joint geometry investigated in this study are consistent with the established database. The results for joints precracked to 25 or 50% of the chord wall thickness lie in a fairly narrow scatterband between the N_1 and N_2 points.

Linear regression analysis of the ten N_2 data points in Fig.14 yields a mean S-N curve as follows:

$m = 2.92$ and $C = 7.32 \times 10^{12}$
(for a curve of the form $S^mN = C$).

This curve is not shown in Fig.14 for clarity but lies above the 16mm mean line by a factor of roughly 1.4 on endurance within the stresses covered by the data. In view of the few data points considered, and the fact that they are not evenly spread over the range of stresses of interest, it is more appropriate to use the 16mm mean line as a basis for comparison with the other test results as described below since it is based on a much larger data population.

4.2. Stress concentrations in repair welded joints

As indicated earlier, the hot spot stress ranges measured after repair welding were generally lower than those during precracking as a result of the increased leg length and more favourable profile of the repair welds. In Table 10 the hot spot stress range after repair is expressed as a proportion of the precracking hot spot stress range for the repair welded specimens. Average values are 0.80 for as-welded repairs and 0.74 for burr ground repairs, indicating that there is a slight additional benefit in terms of stress reduction to be gained by grinding. However, the lowest value of 0.58 was obtained with an as-welded repair (5B). Examination of the macrosection in Appendix C indicates that the repair weld leg length was particularly large since the welder had deposited a number of extra weld passes after excavating and repairing the main fatigue crack. As indicated in Table 7, this repair did not fail on retesting which suggests that the reduction in hot spot stress was beneficial. Figure 30 illustrates the relationship between hot spot stress and repair weld leg length.

The results in Table 10 also indicate that one joint, No.13, gave higher hot spot stress values after repair. This specimen was in fact repaired twice because a larger than usual number of branch cracks had developed during precracking, and one or two on each side of the joint were missed during repair. In carrying out a second repair, the first repair weld cap was ground flush with the chord, as can be seen in the macrosections in Appendix C. As a result the final repair was much narrower than that in most other repair specimens and, hence gave higher hot spot stresses on retesting. Failure occurred at the weld toe of the second repair as seen in the macrosection.

These observations indicate that there is some benefit to be achieved in making a broad weld repair, even to the extent of applying additional capping passes, to move the weld toe further from the joint intersection. It is however likely that there is a limit to the advantage to be gained in this way since in a very broad, flat repair, the stress concentration at the interpass weld toes would be as high as, or higher than, that at the chord toe.

4.3. Efficacy of the repair methods

4.3.1. Repair welded specimens

Considering the as-welded repairs in Fig.17, there appears to be no consistent difference between the through-thickness repairs (1, 3, 4, 13 and 19) and part-wall repairs (5, 9 and 20). Although the results are few, both sets appear to follow a similar trend, and will be considered together in the following discussion. In view of the difficulties of achieving full penetration at the root in full thickness repairs, it was expected that at least those tested under alternating loading, which gives rise to partly tensile stresses on the inside surface of the chord, would give lower endurances than the part-wall repairs, since in previous work on simple plate specimens loaded in tension[4] an inferior fatigue performance had been obtained where the pre-existing fatigue crack was not fully removed during repair. The fact that the endurances of part-wall and through-thickness repairs were similar in

the present study, and the observation that defects at the root appear to have propagated little if at all, possibly indicates that the residual stress distribution is favourable, *i.e.* compressive, at the root of the repair.

The as-welded repairs taken together still form a relatively small sample (nine results in all) for the purposes of comparison with data for unrepaired joints in Fig.17. Nevertheless, the N_2 results tend to lie on or below the mean curve for 16mm thickness, whereas the precracking data tend to lie on or above the line as indicated earlier. Analysing the N_2 results for as-repaired joints by linear regression gave the following constants for the S-N curve (of the form $S^m N = C$):

$m = 3.64$
$C = 1.94 \times 10^{14}$

The line represented by the above expression cuts the 16mm mean line at a hot spot stress range of 145 N/mm^2 approximately, and at 300 N/mm^2 lies below the 16mm mean line by a factor of approximately 1.6 on endurance. It is therefore concluded that the fatigue strengths of the repair welds (expressed in terms of the measured hot spot stress range after repair) are marginally lower than those of the unrepaired joints. As indicated below, the marginal difference in fatigue strength is largely mitigated by the reduction in hot spot stress after repair.

Referring to the results for burr ground repair welds in Fig.17, it is clear that grinding markedly increases the fatigue strength in general, although a single poor result was obtained (specimen No.15). The fracture faces for specimen No.15 show that failure initiated from a small area of porosity in the repair weld which had been opened to the surface by grinding. As noted for the as-welded repairs, the small lack of root fusion in specimen No.15 (see Appendix C) did not play a significant part in the failure, although there was some slight crack growth into the root pass. Specimen No.16 also failed by cracking from the ground weld face, although the N_2 result was much better than that for specimen No.15. Compared with the mean curve for 16mm joints, the N_2 results for specimen No.16 represent an increase in fatigue strength by a factor of about two. These two results indicate the importance of achieving a good surface finish when grinding the weld face and of ensuring that subsurface defects are not revealed by grinding. It is likely that the use of an additional process such as polishing with emery bands to improve the surface finish would give a more consistent improvement in fatigue strength. In addition, the weld face should be thoroughly inspected by magnetic particle inspection and any surface blemishes removed by further grinding or polishing.

The above discussion has evaluated the repair welds in terms of their fatigue strengths. An alternative method is to compare the endurances before and after repair. Direct comparison in terms of N_2 is possible only for specimens precracked through the thickness, which are listed in the Table below.

Specimen number	Repair method*	Endurance ratio, $\left(\frac{N_2 \text{ after repair}}{N_2 \text{ before repair}}\right)$
3	R	1.11
13	R	0.42
19	R	1.00
4	R	0.55
6	RG	>6
15	RG	2.81

*R — repair welded
RG — repair welded and ground

On this basis the as-welded repairs appear rather unfavourable since the endurance after repair may be only about 40% of the original life. In view of the scatter in the data, a better appreciation is obtained from Fig.18 where the results for all repair welded joints are plotted in terms of the hot spot stress range during precracking. Taking the 16mm mean curve as the datum, the N_2 results for as-repaired joints in general lie on the line, with two results slightly below and two significantly above. The burr ground results are all well to the right of the datum, the lowest (No.15) being a factor of approximately five times on endurance above the mean. One may therefore conclude that, when

retested with the same load range, on average the fatigue endurance of as-welded repairs is equivalent to that of the original joint, whilst burr ground repairs gave endurances at least five times that of the original.

It must be emphasised that, as illustrated by the incidence of cracking in Table A1, these favourable results for burr ground repairs would not be achieved without grinding the unrepaired weld toe in the brace. Furthermore, since the results are strongly dependent on the surface finish on the repair weld face, it may be difficult in practice to achieve the fatigue performance obtained in this study, especially where the grinding is carried out in awkward circumstances such as under water. For submerged joints it is also important to ensure full corrosion protection at all times, since the occurrence of corrosion pitting on the ground surface would be detrimental.

4.3.2. Hole drilling and cold expansion

In Fig.22 the N_2 results for specimen No.8 (precracked to 50% of the chord wall) lie close to the mean curve for 16mm joints implying a favourable result. However, this is rather a false impression since the number of cycles required to precrack the specimen was also quite high in relation to the curve (1.66×10^5 cycles at 353 N/mm^2). When expressed in terms of the total endurance *i.e.* the sum of the cycles before and after hole drilling (3.37×10^5 cycles), the result is similar to those in Fig.14 at the same hot spot stress range, implying that the treatment has not significantly extended the life.

The plot of surface crack development in Fig.23 also indicates that the treatment did not significantly delay crack propagation in specimen No.8, although it was slightly more effective in specimen No.7, especially on side A. It should, however, be born in mind that only the main toe cracks are represented in the graph and that branch cracks were developing while the main toe crack in 7A was dormant (see Appendix A). Better results may have been achieved if the uncracked weld toe had been burr ground at the time the holes were drilled, thereby reducing the tendency for cracks to initiate away from the treated area. Light grinding would, in any case, normally be carried out as an aid to magnetic particle inspection. Clearly, this additional treatment would not have affected the holes away from the toe at the branch cracks and, as seen in Appendix A, cracking reinitiated rapidly at these points in specimen No.7.

Perhaps the most significant observation in relation to the hole drilling and cold expansion process is the fact that the first cracking to appear on retesting specimen No.7 was a branch from the main toe crack on side B. In practice it would be difficult to find and treat all such areas, and irrespective of the efficacy of the treatment at crack tips successfully located, a single untreated branch may be catastrophic. Burr grinding or possibly hammer peening the mouth of the main crack may reduce the risk of branching but is unlikely to eliminate the risk completely.

A final point to note with respect to Fig.22 is that although the results for specimen No.7 are shown as N_1 data, effectively they represent N_2 lives since at this stage a growing through-thickness crack was present, which then continued to propagate as shown in Fig.23.

The conclusion with respect to the hole drilling and cold expansion technique therefore must be that it was not effective in the two specimens investigated.

4.3.3. Specimens repaired by grinding alone

The results of Fig.26 indicate that this method of repair is successful even for joints with relatively deep excavations (*e.g.* specimens No.11, 17, 21 and 22 all had excavations greater than 60% of the chord wall thickness). All the N_2 data are above the datum S-N curve, with the best result (21B, excavation depth 63% of chord wall) lying above the curve by a factor of approximately 4 on endurance.

The fact that in some instances cracks initiated on the inside surface of the chord as well as in the bottom of the excavation indicates that no greater fatigue strength could have been achieved. If cracking in the excavation could have been prevented, failure may still have occurred from inside the chord. It is therefore unlikely that further treatment of the excavation, for example by polishing or hammer peening, would provide additional benefit. As indicated in Section 3.1.5 above and Table A1 of Appendix A, in two specimens, cracks developed at the untreated weld toe in the chord adjacent to the ends of the excavation prior to initiation in the excavation itself. These cracks were removed by burr grinding so that they would not affect the test results. In practice it is likely that these areas

would be lightly ground as an aid to magnetic particle inspection while removing the main crack, but in the light of the results it is essential that both weld toes are carefully treated to avoid premature failure outside the excavation.

The results in Fig.27 and 28, though rather scattered, provide a means of predicting the likely useful life remaining in joints repaired in this way. For a given depth of cracking, the maximum likely stress concentration in the resulting excavation may be estimated from the upper limit of the scatterband in Fig.27. The maximum pseudo-elastic principal stress in the excavation, σ_{max}, is then estimated as follows:

$$\sigma_{max} = K_e K_t \sigma_{nom}$$

where K_e is the stress concentration due to the excavation, K_t is the stress concentration due to the joint geometry (estimated by the published parametric formulae) and σ_{nom} is the nominal stress range in the brace. The likely residual life is then estimated from the mean or mean minus two standard deviations curves in Fig.28. Coefficients of the curves are given in Table 11.

In view of the few specimens investigated, Fig.28 must be interpreted with caution, but for the N_i results, data from two other sources[6,12] compare favourably with those obtained in the present study, as shown in Fig.31. Experimental details for these two studies were briefly as follows.

Reference 6 describes tests on fillet welded and cruciform joints in 12.5mm steel plate axially loaded. As in the present tests, fatigue cracks were allowed to propagate to target depths. They were then removed by machining with a milling cutter. Excavation depths in the range 20-50% were studied. Crack initiation was detected by visual inspection with the aid of soap solution, as in the present study. The results obtained in the work described in Ref.12 were for tubular T joints loaded in-plane, with chord dimensions of 900mm diameter × 25mm wall thickness and the brace of 460mm diameter × 12.7mm wall thickness. Crack initiation was detected by fluorescent magnetic particle inspection. The excavations, which were made by burr grinding, covered a range of depths from 10-50% of the brace wall thickness. For each joint studied, N_i data were obtained for a number of groove depths.

In both investigations strain measurements within the excavation were limited, so that the position of maximum stress could not have been determined as precisely as in the present study. Furthermore, single element gauges were used rather than rosettes, so that the maximum principal stresses were not determined. For comparison with the present study, the principal stresses have been estimated by assuming that the stress direction was transverse to the excavation, and that the ratio of the principal stresses was 0.17-0.21 for the plate specimens, as indicated by rosette gauges adjacent to the ends of the excavation, and 0.33 for the tubular specimens as reported in Ref.12.

As will be seen in Fig.31, the data from the three sources cover a very broad scatterband which is probably a reflection of the experimental differences outlined above. In general, excavations in the plate specimens gave longer initiation lives than those in the tubular joints, almost certainly as a result of the improved surface finish obtained by machining as opposed to burr grinding. There is also a tendency for the data of Ref.12 to lie below the rest, possibly as a result of the very sensitive inspection technique and high inspection frequency adopted. Nevertheless, the mean and lower bound curves for the whole data set shown in the Figure are very similar to those of Fig.28. Coefficients of the mean and lower bound curves of Fig.31 are given in Table 11.

The data obtained in the present study relate to a range of excavation depths and profiles as indicated in Appendix D. In general, the excavation shape was dictated by the profile of the precrack, and no attempt was made to optimise the shape once the last trace of cracking was removed. In practice it would be preferable to achieve a smoother excavation profile without abrupt variations in depth which may act as stress raisers. It is also recommended that the total excavation length is minimised since the maximum stress in the excavation will be governed by the extent to which loading can be redistributed to other parts of the joint circumference. Further work is required to establish an optimum excavation shape to minimise stress and hence provide the maximum residual life.

As mentioned above in connection with the burr ground repair welds, the surface finish in the excavation should be the best which can be achieved and, ideally, should not degrade during

subsequent service as a result of corrosion pitting. Full corrosion protection at all times is therefore essential.

(Note: when considering the application of remedial grinding in practice, it would be necessary also to assess the static strength of the joint, especially for long, deep excavations where a significant portion of the load bearing area is removed.)

4.4. Comparison of repair methods

Figure 32 shows all the N_1 and N_2 results for repaired joints plotted together in terms of the hot spot stress range measured during precracking. Whilst the graph is a little congested, it allows a general comparison of the methods investigated. In terms of the endurance achieved after repair, the burr ground repairs are undoubtedly the best followed by grinding alone, unground repair welds and hole drilling in that order.

Table 12 gives estimates of the relative costs of the repair methods in terms of man hours, and the cost of consumable items (electrodes, grinding burrs, penetrants, *etc*). The estimates are for the joint size investigated here, assuming that both sides of the joint are to be repaired. Clearly the methods not involving welding are far more economical. Furthermore, where a repair weld is required to be made under water in a hyperbaric chamber the costs would be much higher than those estimated here, whereas the hole drilling and grinding repairs could be carried out 'wet' by divers.

With respect to the hole drilling and cold expansion method, it may prove difficult to drill holes to the required tolerance under water, especially in areas of restricted access. There is also the risk that holes may be incorrectly positioned and miss the crack tip, as was found under the ideal laboratory conditions of this investigation. Both the hole drilling and grinding methods clearly rely heavily on the inspection technique employed, since any small areas of cracking left untreated would greatly reduce the residual life. Where repair welding is carried out, the small additional cost of burr grinding the repair provides a substantial benefit in terms of improved endurance.

A final observation which applies to all the repair methods considered is that, in view of the tendency for cracks to appear outside the treated area, it would be prudent to burr grind the weld toes on both members for the full joint circumference. The additional cost involved is trivial by comparison with that of the principal repair procedure.

4.5. Crack growth in hyperbaric weld metal

The crack growth rates measured in hyperbaric weld metal in air (Fig.29) lie within the scatterband obtained by Maddox[10] for structural steel weld metals, heat affected zones and parent plate. In seawater under free corrosion conditions, the growth rates measured were between 1.5 and 3 times faster than those in air, but were between the mean and the lower bound rates for BS 4360 Grade 50D steel quoted in the review by Booth.[11]

It is therefore concluded that the hyperbaric weld metal investigated has similar crack growth characteristics to weld metal deposited at one atmosphere, and to that of parent plate. Hence, in terms of crack propagation behaviour, hyperbaric repairs would be expected to behave in a similar manner to the one atmosphere repairs investigated here.

5. CONCLUSIONS

The present study has investigated the fatigue behaviour of tubular joints with fatigue cracks repaired by four alternative methods. In addition, fatigue crack growth rates in air and freely corroding in seawater have been measured in hyperbaric weld metal. The following conclusions may be drawn on the basis of the results obtained.

1. Before repair the fatigue strength of the joints investigated was marginally higher than the mean for joints of similar thickness based on published results.
2. Hot spot stresses measured in repair welded specimens were, on average, 20% lower than those in the original joints as a result of the increased leg length of the repair welds. Burr grinding the repair weld further reduced the hot spot stresses by a small margin.
3. The fatigue strength of as-welded repairs is marginally lower than the mean for unrepaired joints. However, the reduction in hot spot stress brought about by making the repair makes up

for the reduction in fatigue strength. As a result, when loading continues with the same range after repair, the endurance for through-thickness cracking in as-welded repairs is on average close to, or greater than, that before repair.

4. Burr grinding the repair weld (both the weld toe and the weld face) may considerably improve the fatigue strength, although a good surface finish must be achieved to avoid premature crack initiation on the repair weld face. In terms of the endurance for through-thickness cracking, of five ground repairs tested in the present study, the poorest result was five times better than the mean endurance for unrepaired joints.

5. In through-thickness repair welds, incomplete penetration defects at the weld root propagated only slightly during retesting and did not affect the primary failure which was from the repair weld toe in as-welded repairs, or from the repair weld face in burr ground repairs.

6. Cold expanded holes at the crack tips were ineffective as a means of delaying crack propagation.

7. Removal of part-wall flaws by burr grinding is an effective repair method. Nine specimens investigated, which included excavations of up to 60% of the chord wall in depth, gave endurances for through-thickness cracking up to four times greater than the mean for unrepaired joints.

8. Data derived here (Fig.27 and 28) allow the likely residual life to be estimated for a given excavation depth in joints of similar thickness.

9. It is necessary to burr grind the unrepaired weld toes in both the chord and the brace in order to achieve residual lives of the order indicated by the results presented here.

10. Fatigue crack growth rates for hyperbaric weld metal (deposited in a helium — 2% oxygen mixture at a water depth equivalent to 30m) in air and freely corroding in synthetic seawater are similar to those in parent plate or in welds made in air at ambient pressure. The crack propagation behaviour of hyperbaric repairs would therefore be expected to be similar to that of the one atmosphere repairs studied here.

6. ACKNOWLEDGEMENTS

The Sponsor Group who supported the project comprised the following organisations: Amoco, British Gas, BP, Britoil, Brown and Root, Chevron Corp., CAN/MET, Conoco, Department of Energy, Lloyd's Register of Shipping, Shell, and Union Oil of California. The author is grateful to these organisations and, in particular, to Mr Derek Hurden of Conoco who chaired the Sponsor Group meetings. He is also grateful to British Gas for the provision of additional data.

The author is also glad to acknowledge the assistance of many colleagues at The Welding Institute, especially the staff of Fatigue Laboratory II under the supervision of Roy Pettit and welding staff responsible to John Haugh.

REFERENCES

1 Dadson J: 'North Sea clamp down on oil rig crack-ups.' ***New Civil Engineer*** 17 July 1980.

2 Grubbs C E and Seth O W: 'Underwater wet welding with manual arc electrodes.' Intl Seminar on 'Underwater welding for offshore structures', The Welding Institute, London, 1976.

3 Fisher P J: 'Summary of current design and fatigue correlation.' Conf 'Fatigue in offshore structural steel.' Inst. of Civil Engineers, February 1981.

4 Wylde J G: 'The fatigue performance of fillet welded joints with weld repairs.' Welding Institute Members Report 215/83, May 1983.

5 Gurney T R and Nunn D E: 'Studies of the use of drilled holes to control fatigue cracks in welded structures.' Intl Conf 'Fatigue of welded constructions', The Welding Institute, Brighton, 1987.

6 Wylde J G and Haswell J: 'Fatigue of fillet welds with toe cracks removed by grinding.' Intl Conf 'Fatigue of welded constructions', The Welding Institute, Brighton, 1987.

7 Irvine N M: 'Review of stress analysis techniques used in UKOSRP.' Conf 'Fatigue in offshore structural steel', Inst. of Civil Engineers, February 1981.

8 'Background to new fatigue design guidance for steel welded joints in offshore structures.' Department of Energy, HMSO, London, 1984.

9 Booth G S and Iwasaki T: 'Corrosion fatigue crack propagation in structural steel.' Welding Institute Members Report 254/1984, November 1984.
10 Maddox S J: 'Fatigue propagation data obtained from parent plate weld metal and HAZ structural steel.' ***Welding Research Intl*** 1974 **4** (1).
11 Booth G S and Dobbs S J: 'Corrosion fatigue crack growth in BS 4360 Grade 50D steel — an analysis.' ***Welding Institute Research Bulletin*** 1986 **27** (9).
12 Haswell J. British Gas Engineering Research Station, Killingworth. Private communication.

Table 1 Chemical analysis of materials used in fabrication of the tubular joints

Tube	Specification	Cast number	Element, wt%										
			C	Si	Mn	P	S	Cr	Mo	Ni	Al	Cu	Nb
Chord	BS 4360 Grade 50E (modified)	C7048B	0.17	0.31	1.28	0.008	0.007	0.04	0.01	0.04	0.041	0.07	0.023
		4569	0.15	0.36	1.33	0.011	0.005	0.06	0.03	0.10	0.037	0.08	0.029
Brace	API 5LX X52N	C6539B	0.15	0.30	1.29	0.02	0.006	0.08	0.04	0.09	0.035	0.18	0.01

Table 2 Mechanical properties of tube materials

		Yield strength, N/mm^2	Tensile strength, N/mm^2	Elongation, %	Reduction of area, %
Chord	Cast no. C7048B	398	542	29	72
		367	534	28	75
	Average	383	538	29	74
	Cast no.4569	372	533	24	75
		378	543	27	72
		379	542	28	72
	Average	376	539	26	73
Brace		376	562	26	72
		389	562	26	74
		396	562	26	70
	Average	387	562	26	72

Table 3 Welding conditions for tubular joint fabrication

Welding process:	Manual metal arc
Electrode specification:	BS 639 E51 33B
Electrode drying:	450°C for 1hr
Electrode storage temperature:	150°C
Welding position:	HV
Interpass temperature:	150°C

Run number	1 (root)	2 – 19
Electrode diameter, mm	3.25	4
Current, A	120/125	150/160
AC, DC	DC–	DC+
Arc voltage, V	20/21	22/23
Energy input, kJ/mm	1.2	1.5

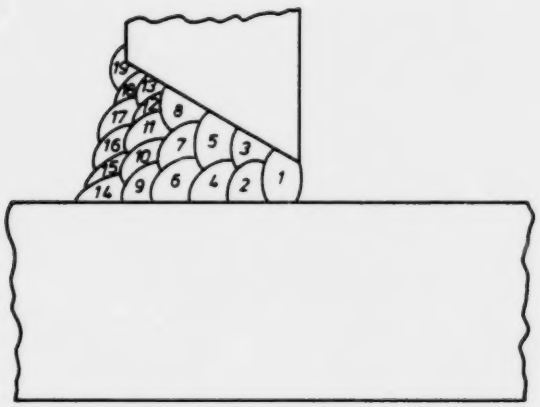

Table 4 Typical repair welding conditions for a through-crack and a part-wall crack

Welding process:	Manual metal arc
Electrode specification:	BS 639 E51 33B
Electrode drying:	450°C for 1hr
Electrode storage temperature:	150°C
Welding position:	1G
Interpass temperature:	100°C
Preheat:	None

	Through-crack repair		Part-wall repair
Run number	1	2-11	1-5
Electrode diameter, mm	3.25	4	4
Current, A	115	150	150
AC, DC	DC+	DC+	DC+
Arc voltage, V	21	23	23
Run out length	180	280	280

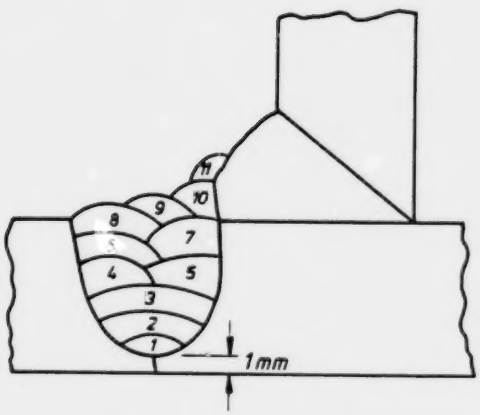

Through - crack

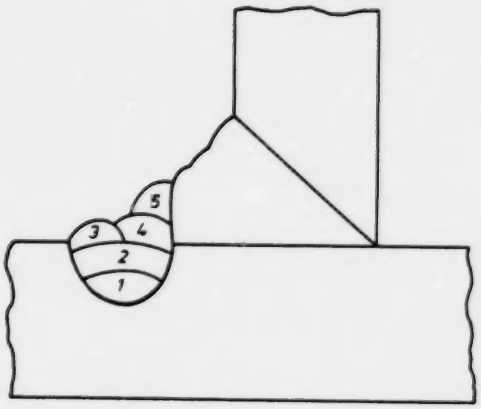

Part - wall crack

Table 5 Details of welding parameters for hyperbaric test welds

Plate size:	200 × 120 × 10mm
Consumables:	4mm diameter AWS E7018 Murex Fortrex
Polarity:	DC electrode negative
Welding current:	150A
Voltage (AVC):	20V
Welding speed:	300 mm/min
Run sequence:	Stringer beads — see below
Pressurising gas:	Helium — 2% oxygen
Pressure:	3 bar

Note: Root side. Ground back to sound metal and inspected using dye penetrant prior to deposition of run No.3.

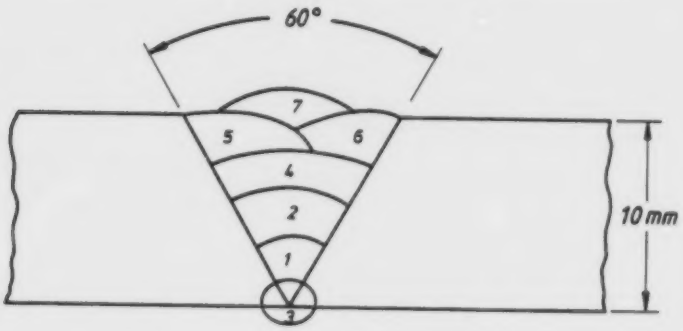

Table 6 Chemical analysis of the parent plate and weld metal of the hyperbaric test welds used for fatigue crack growth measurement

	Element, wt %															
	C	S	P	Si	Mn	Ni	Cr	Mo	V	Cu	Nb	Ti	Al	B	Sn	Co
Parent plate (BS 4360 Grade 50E)	0.13	0.005	0.010	0.35	1.34	0.14	0.07	0.03	<0.002	0.17	0.030	<0.002	0.047	<0.0003	<0.005	<0.005
Weld metal	0.13	0.013	0.012	0.31	0.69	0.06	0.04	0.01	0.01	0.17	0.005	0.005	0.003	<0.0003	<0.005	0.005

Mechanical properties of parent plate

	Yield strength, N/mm²	Tensile strength, N/mm²	Elongation, %	Reduction of area, %
	380	510	29	75
	381	510	28	74
	382	513	33	77
Average	381	511	30	75

Table 7 Fatigue testing conditions and results for tubular joints

Specimen number*	Repair method	Target precrack depth (% of chord wall)	Stress ratio	Precracking					After repair					Comments
				Radial strain range, με	Circumferential strain range, με	Hot spot stress range, N/mm²	Cycles		Radial strain range, με	Circumferential strain range, με	Hot spot stress range, N/mm²	Cycles		
							N_1**	N_2**				N_1*	N_2*	
2A	None		0	1500	167	352.6	21,110	247,044						
1A	R	100	0	1000	114	235.3	16,300	491,642	1210	153	285.7	20,490	196,779	Repaired side A only. (Retest load
1B									1520	208	360.0	38,235		increased 25%.)
3A	R	100	0	1150	94	268.0	47,985	366,050	1030	112	241.9	71,410	405,066	Repaired side A only
3B												8170	405,066	
13A	R	100	−1	700	82	164.8	173,970	4326,250	740	88	174.3	674,872	1793,500	
13B				590	73	139.2	371,600		640	117	153.6	498,500	1793,500	
19A	R	100	−1	1010	136	239.0	35,700	678,783	910	113	214.7	74,982	677,000	
19B				1000	130	236.3	49,600		850	103	200.4	491,690		
4A	R	100	−1	1430	147	335.3	21,475	413,590	1110	126	261.1	24,708	229,830	
4B				1660	147	387.6	259,270		11,090	132	257.0	64,635		
9A	R	50	−1	760	90	179.0	155,200	666,670	650	92	154.1			Failed side B only
9B				780	82	183.4	276,600		585	81	138.6	906,080	3700,819	
20A	R	50	−1	1010	134	238.9	62,240	248,500	900	111	212.3	152,700	491,339	
20B				1020	126	240.6	100,130		870	115	205.7	152,700		
5A	R	50	−1	1600	183	376.4	63,150		1200	170	284.6	73,402	413,306	
5B				1540	168	361.8	39,030	189,825	885	122	208.6			
6A	RG	100	−1	1430	149	335.5	10,780	309,840	920	137	218.6	$>2 \times 10^6$		Unfailed after repair
6B				1500	147	351.2	10,780		1130	139	266.5			
15A	RG	100	−1	1600	221	379.0	22,930	223,050	1180	179	280.6	532,000		Brace toe cracked — Table A1.
15B				1700	189	399.6	22,930	223,050	1000	202	241.3	384,000	626,282	
23A	RG	50	−1	1000	132	236.5	269,000		1350	157	317.8	$>5 \times 10^6$		Retested at increased load. Unfailed.
23B				1000	122	235.8	112,950	269,000	1060	157	251.8			Brace toe cracks — Table A1.
24A	RG	50	−1	1350	170	318.7	64,000		1210	141	284.9	$>5 \times 10^6$		Unfailed after repair. Brace
24B				1330	162	313.6	64,000	129,900	1110	164	263.7			toe cracks — Table A1.
16A	RG	50	−1	1590	199	375.3	43,435		1220	176	289.5			Extensive brace toe cracks
16B				1820	220	429.0	43,435	68,750	1200	200	286.6	1544,200	2929,405	— Table A1.
7A	HD	100	−1	1490	170	350.5	19,900	304,885				29,590	315,100	
7B				1465	183	338.9	101,600					9760	315,100	
8A	HD	50	−1	1500	183	353.7	66,500	166,300				13,000	190,300	N_2 detected by potential
8B				1310	178	310.1	103,225					6000	190,300	drop measurements

R Repair welded
RG Repair welded and burr ground
HD Hole drilling and cold expansion

* A and B refer to the two 'saddle' positions on each joint
** N_1 is number of cycles for first detected cracking
N_2 is number of cycles for through-thickness cracking (or 25% or 50% of wall thickness during precracking)

Table 7 contd

Specimen number*	Repair method	Target precrack depth (% of chord wall)	Stress ratio	Precracking					After repair					Comments
				Radial strain range, με	Circumferential strain range, με	Hot spot stress range, N/mm²	Cycles N_1**	Cycles N_2**	Radial strain range, με	Circumferential strain range, με	Hot spot stress range, N/mm²	Cycles N_1*	Cycles N_2*	
17A	G	50	−1	890	109	209 9	99,500	772,500				1634,600		
17B				860	82	201 2	99,500					9226	2105,600	
21A	G	50	−1	960	113	226 1	103,750					1111,650		Cracks outside excavation — Table A1.
21B				1060	118	249 2	64,000	310,100				860,500	1797,900	
11A	G	50	−1	1415	172	333 6	16,700	83,979				28,024	266,430	
11B				1535	185	361 8	16,700					28,024	266,430	
10A	G	25	−1	785	80	176 0	305,800	862,882						Failed side B only.
10B				750	84	184 3	323,900					63,800	3742,920	
18A	G	25	−1	1040	134	245 7	42,200	164,951				142,200	649,300	
18B				1030	132	243 3	42,200					206,285		
12A	G	25	−1	1540	189	363 2	36,800					118,700		
12B				1520	216	360 5	20,700	81,380				34,280	176,635	
14A	G	25	−1	1650	207	389 5	22,170	58,000				23,225	181,500	
14B				1600	205	378 0	22,170					23,225		
22A	G	25	−1	1750	258	415 7	11,000	50,010						N_1 determined for several excavation depths, Table 9
22B				1860	231	438 9	17,800							
25A	G	·	−1	1175	146	277 2	126,600							
25B				1260	121	294 9	126,600							

G Ground only
* A and B refer to the two 'saddle' positions on each joint
** N_1 is number of cycles for first detected cracking
N_2 is number of cycles for through-thickness cracking (or 25% or 50% of wall thickness during precracking)

Table 8 Excavation depths and measured stress levels in specimens repaired by grinding alone

Specimen number	Precracking hot spot stress range, N/mm²	Maximum excavation depth, % of chord wall	Maximum principal stress range in excavation	Stress concentration factor**, K_e
10A	176.0	22	451.8*	2.57
B	184.3	38	449.0*	2.44
14A	389.5	41	1004.3*	2.58
B	378.0	34	1028.7*	2.72
17A	209.9	44	570.3*	2.72
B	201.2	69	681.6*	3.39
22A	415.7	28	650.8*	1.57
B	438.9	13	767.1*	1.75
22A	415.7	59	1422.7*	3.42
B	438.9	66	728.8*	1.66
25A	277.2	13	497.8	1.8
B	294.9	13	518.2*	1.76
25A	277.2	25	693.3*	2.50
B	294.9	25	765.7*	2.60
25A	277.2	38	670.1*	2.42
B	294.9	38	797.8*	2.71
11A	333.6	63	980.8†	2.94
B	361.8	44	1003.8†	2.77
18A	245.7	25	480.0†	1.95
B	243.3	14	450.0†	1.85
12A	363.2	11	773.1†	3.13
B	360.0	39	1038.5†	2.88
21A	226.1	13	452.2†	1.90
B	249.2	63	474.1†	2.72

* Values determined from rosette gauges attached at the positions of maximum stress range indicated by SPATE analysis.

† Values estimated from single element gauges assuming $\sigma_2/\sigma_1 = 0.3$

** Defined as $K_e = \dfrac{\text{maximum principal stress range}}{\text{precracking hot spot stress range}}$

Table 9 Fatigue test results for specimens used to investigate crack initiation at different excavation depths

Specimen number	Maximum excavation depth, mm	N_1, cycles	N_2, cycles
22A	9.5	5 300	168 240
B	10.5	5 300	168 240
25A	2.0	197 101	—
B	2.0	—	—
25A	4.0	79 550	—
B	4.0	—	—
25A	6.0	121 925	—
B	6.0	235 500	720 200

Table 10 Comparison of hot spot stress ranges before and after repair for repair welded joints

Specimen number	Repair method †	Target precrack depth, %	Hot spot stress range ratio*	
3A	R	100	0.90	Range 0.58-1.1 Average 0.84 (Average without specimen No.13:0.80)
13A	R	100	1.06	
B			1.10	
19A	R	100	0.90	
B			0.85	
4A	R	100	0.78	
B			0.66	
9A	R	50	0.86	
B			0.75	
20A	R	50	0.89	
B			0.85	
5A	R	50	0.76	
B			0.58	
6A	RG	100	0.65	Range 0.60-0.89 Average 0.74
B			0.76	
15A	RG	100	0.74	
B			0.60	
24A	RG	50	0.89	
B			0.84	
16A	RG	50	0.77	
B			0.67	

† Repair methods
R — repair welded
RG — repair welded and burr ground

* Ratio = $\frac{\text{hot spot stress range after repair}}{\text{hot spot stress range before repair}}$

(Note: specimens Nos 1 and 23 omitted since the retest load range was increased.)

Table 11 Linear regression analysis of data for specimens repaired by grinding alone

	m*	C*
Present study (Fig.28)		
N_1 mean curve	3.262	1.480×10^{14}
N_1 mean − 2 standard deviations	3.262	1.269×10^{13}
N_2 mean curve	2.426	5.029×10^{12}
N_2 mean − 2 standard deviations	2.426	1.231×10^{12}
All data (Fig.31)		
N_1 mean curve	3.017	3.840×10^{13}
N_1 mean − 2 standard deviations	3.017	3.533×10^{12}

(*Coefficients of the S-N curves of the form $S^mN = C$)

Table 12 Cost of repair methods

Repair method	Man hours	Cost of consumables (at current prices) £
Through-thickness repair weld	35	50
Part-wall repair weld	21	25
Burr ground repair welds	As above plus 2	As above plus 10
Cracks removed by grinding alone	2	10
Hole drilling and cold expansion	1 per hole	Negligible

Note: The man hours quoted are for repairs carried out under favourable laboratory conditions. They take no account of the difficulties of access, environment, *etc* which contribute significantly to the costs of repairs carried out offshore.

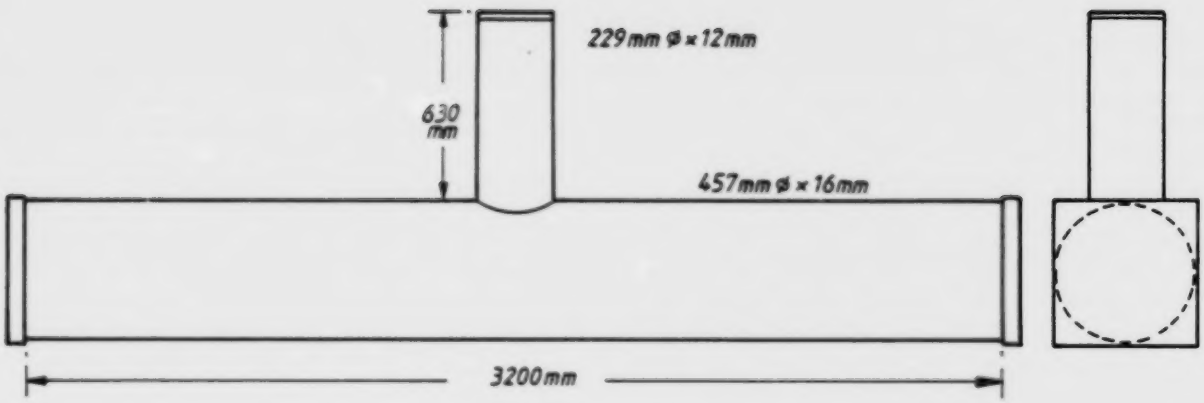

1 *Tubular joint specimen geometry.*

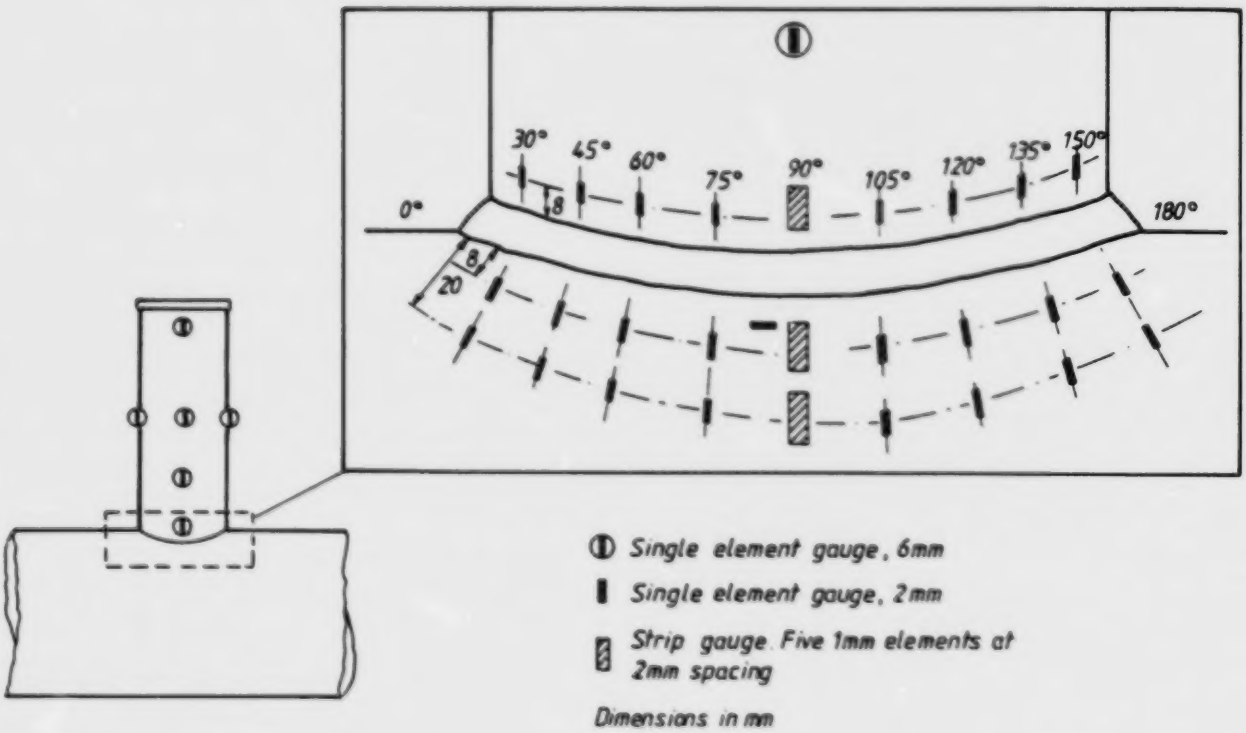

2 *Basic gauge plan for specimens tested under zero-tension loading.*

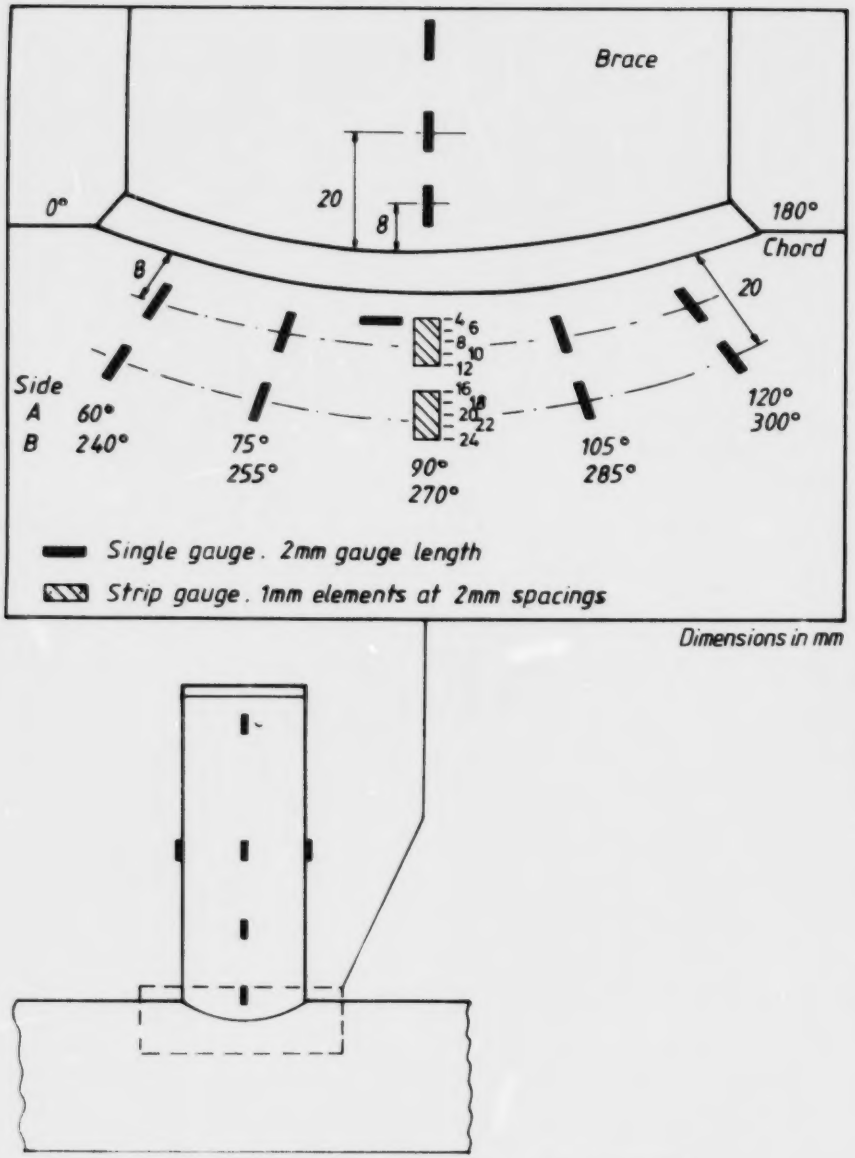

3 *Strain gauge plan adopted for specimens tested under alternating loading.*

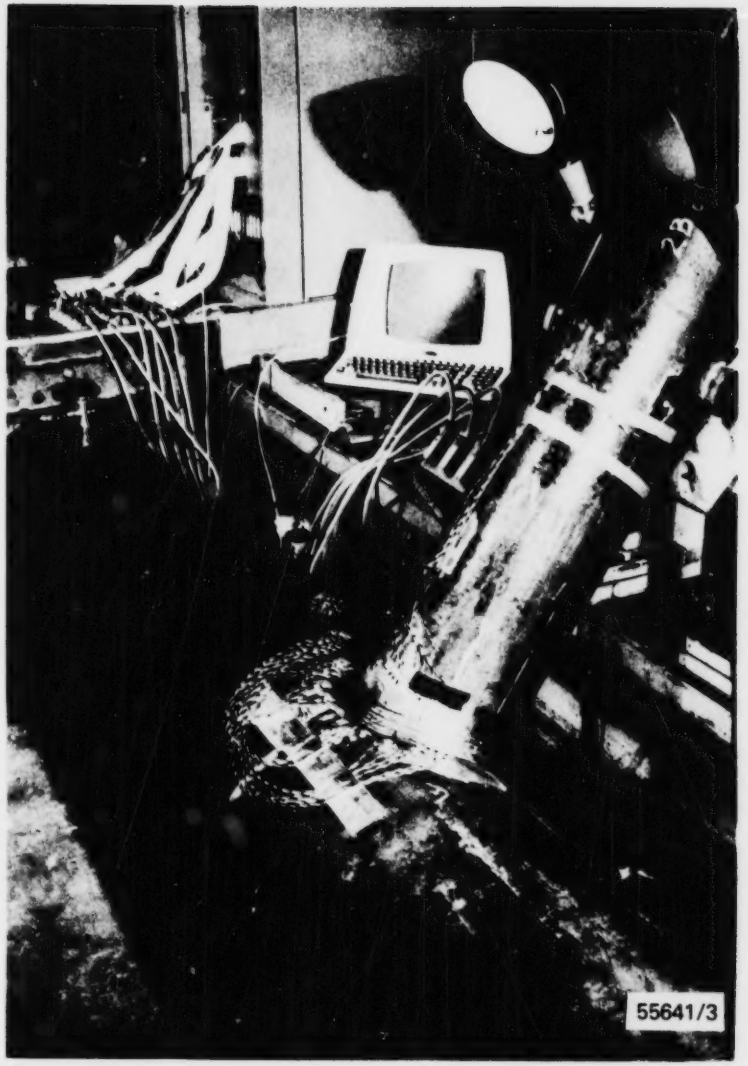

4 *Strain gauged specimen set up and ready for fatigue testing.*

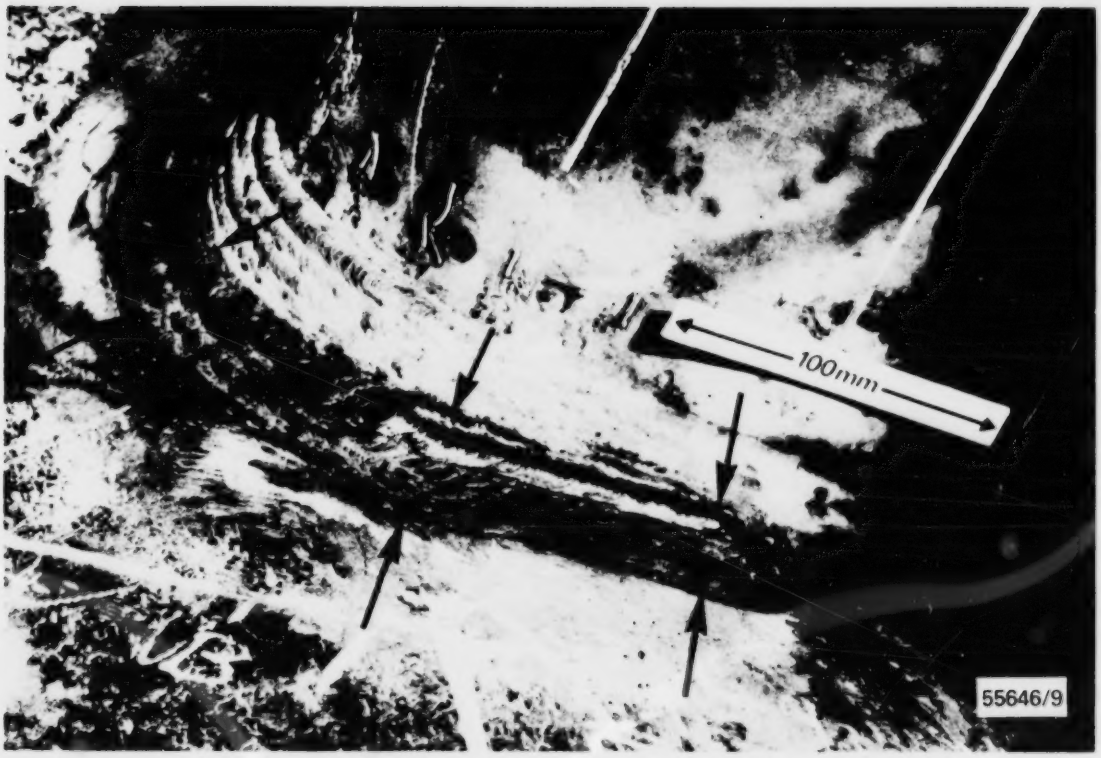

5 *Repair weld (arrowed) in specimen No.1.*

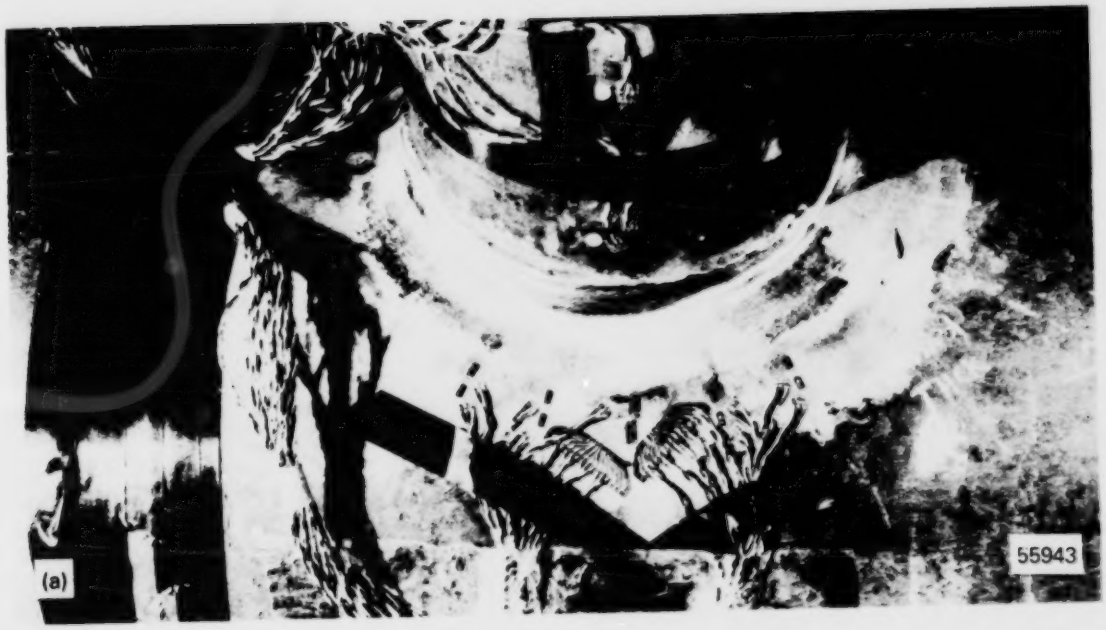

6 *Specimen No.6 prior to retesting showing burr ground repair weld.*

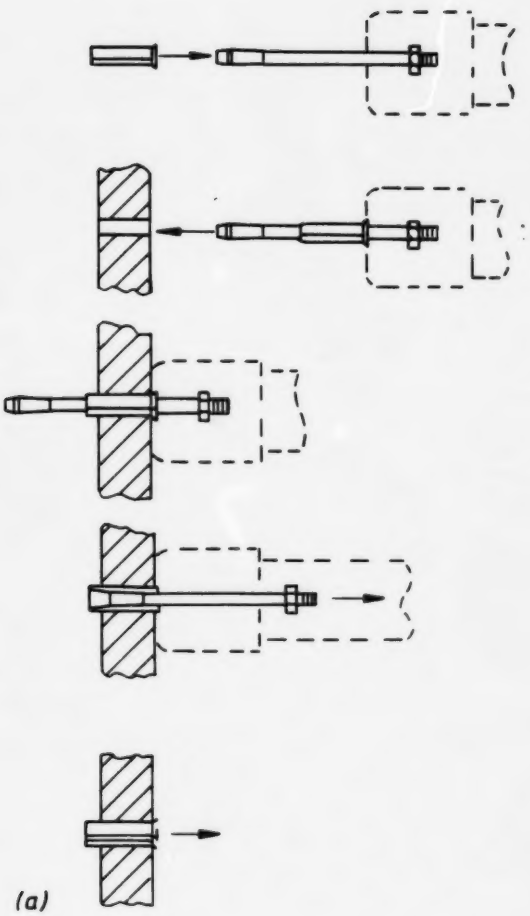

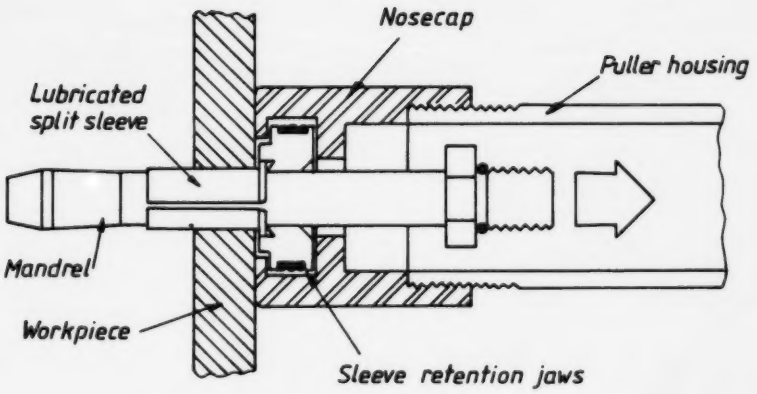

7 *Details of the cold expansion process:* a) *Sequence of operation;* b) *System components.*

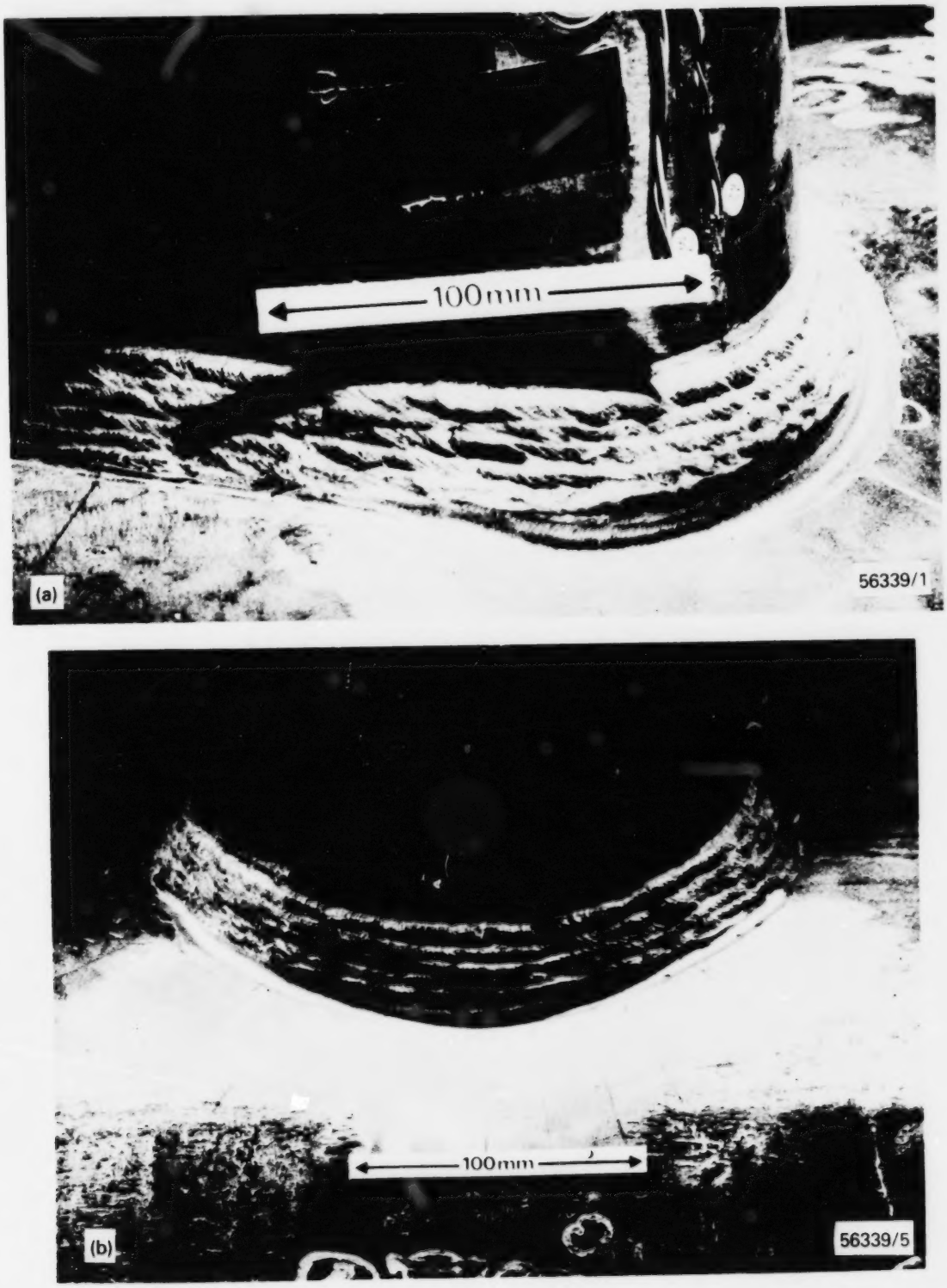

8 *Specimen No.11 showing ground excavation:* a) *Side A;* b) *Side B.*

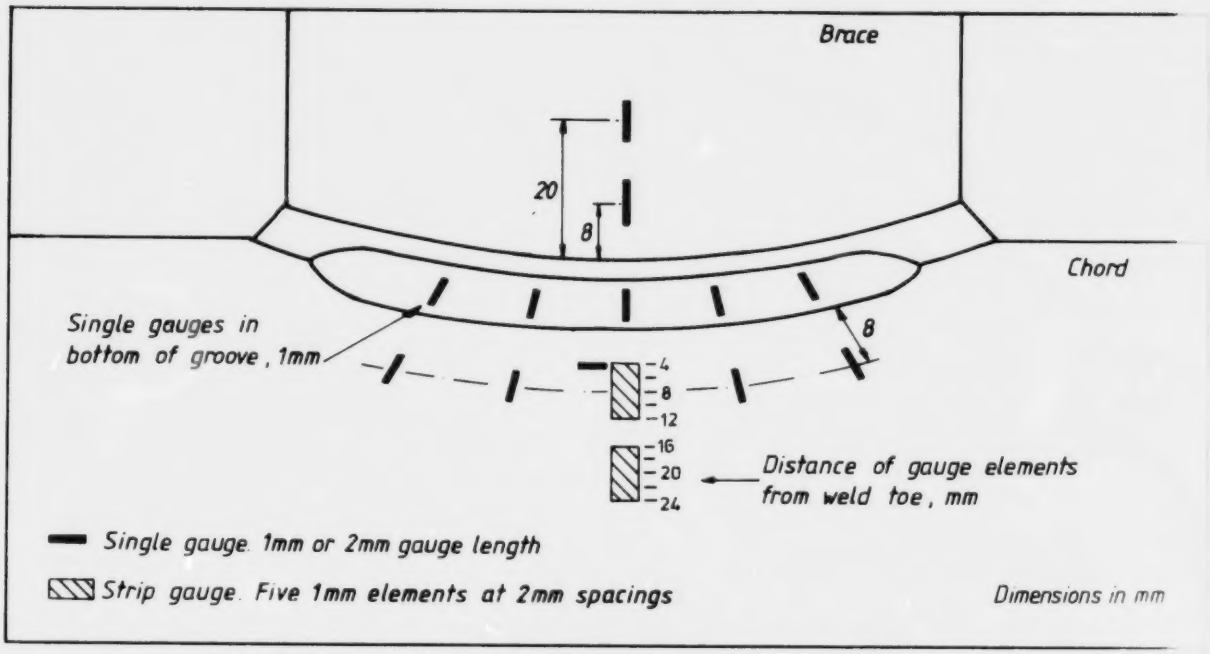

9 *Strain gauge plan for specimens with toe cracks excavated by burr grinding.*

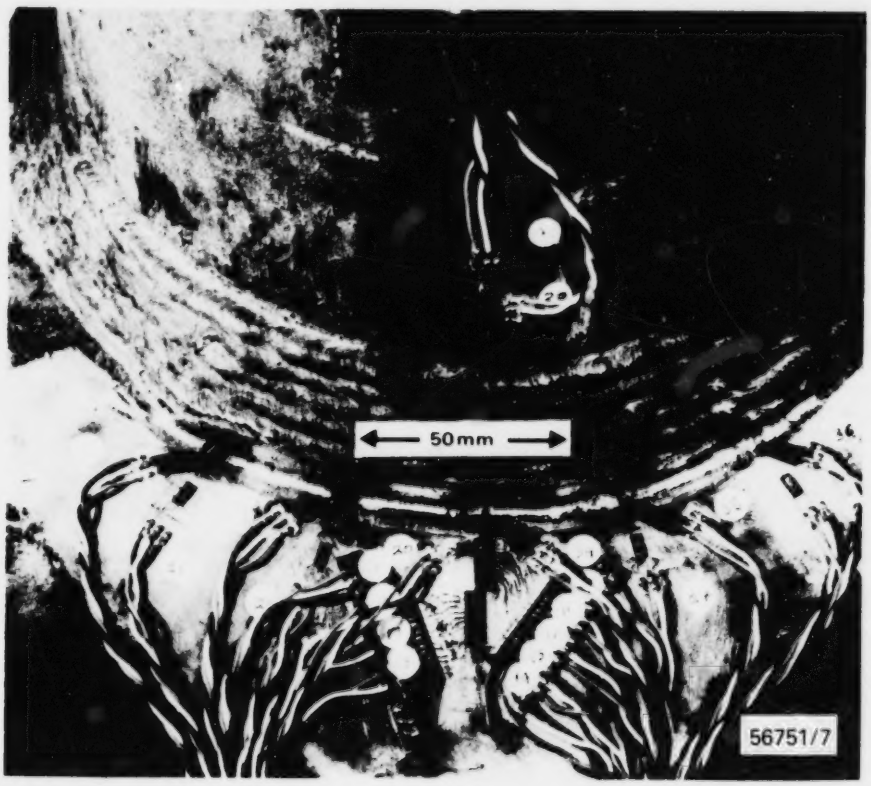

10 *Specimen No.21 showing the strain gauge pattern in the ground excavation.*

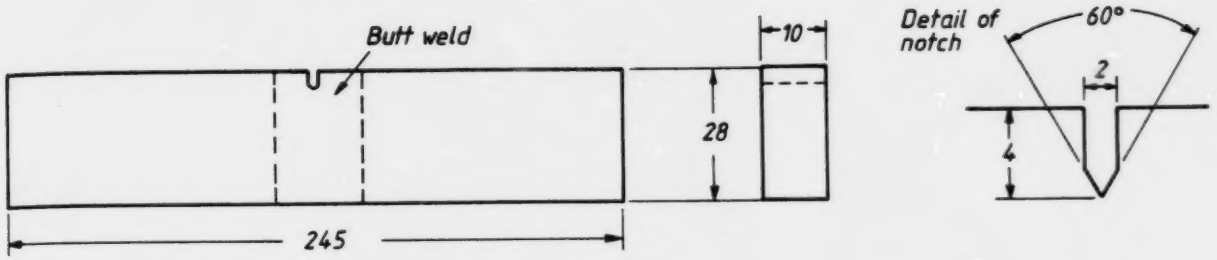

11 *Specimen geometry for fatigue crack growth study. (Dimensions in mm.)*

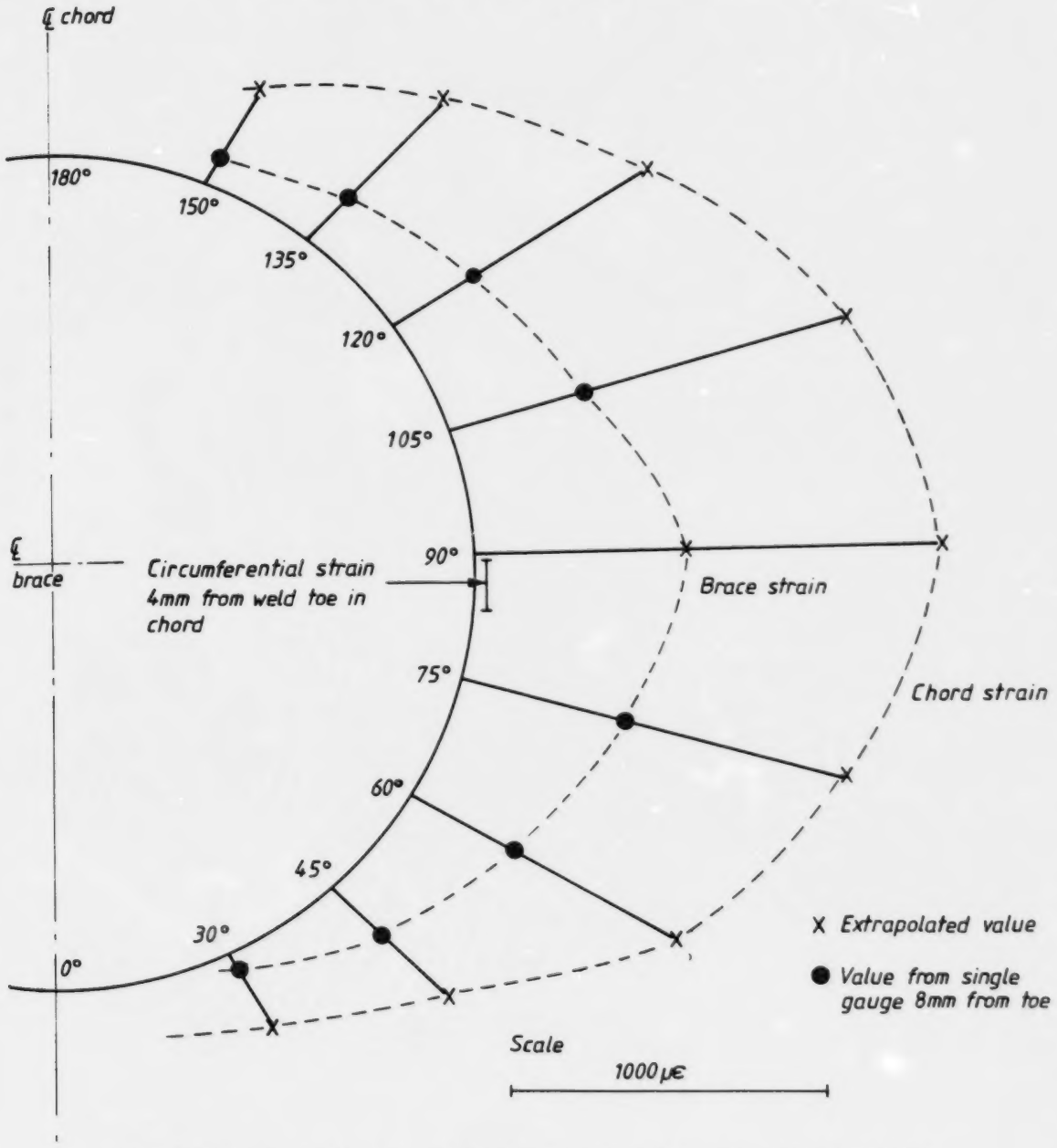

12 *Radial strain variation around the tubular joint circumference (specimen No.2, side A).*

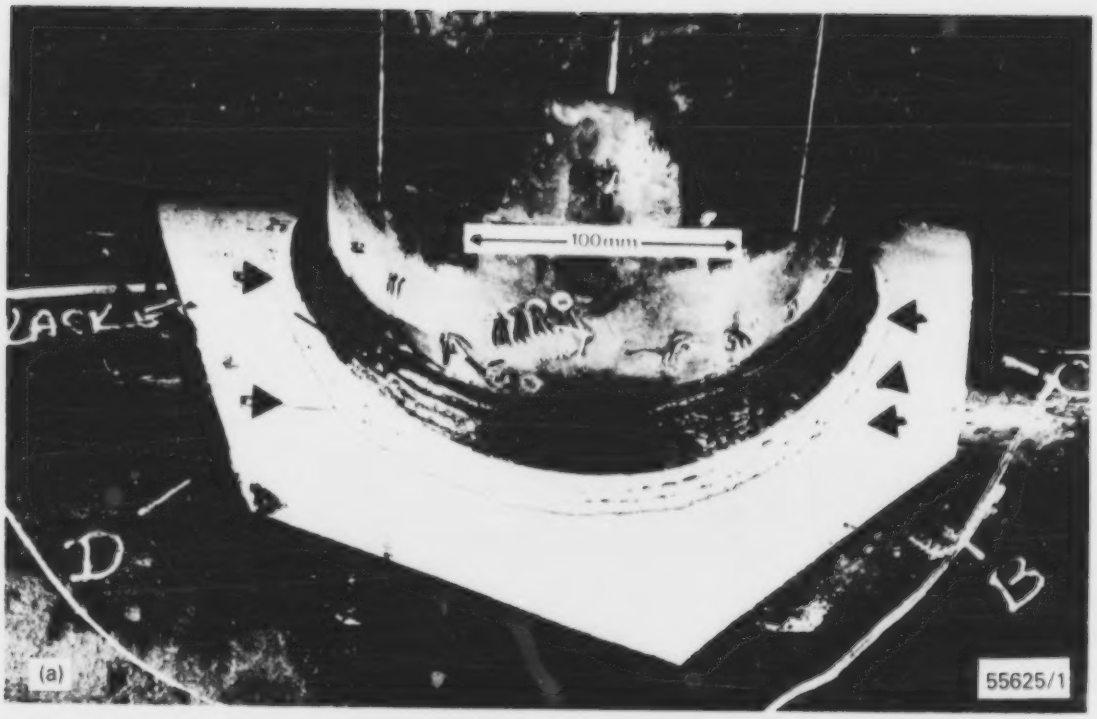

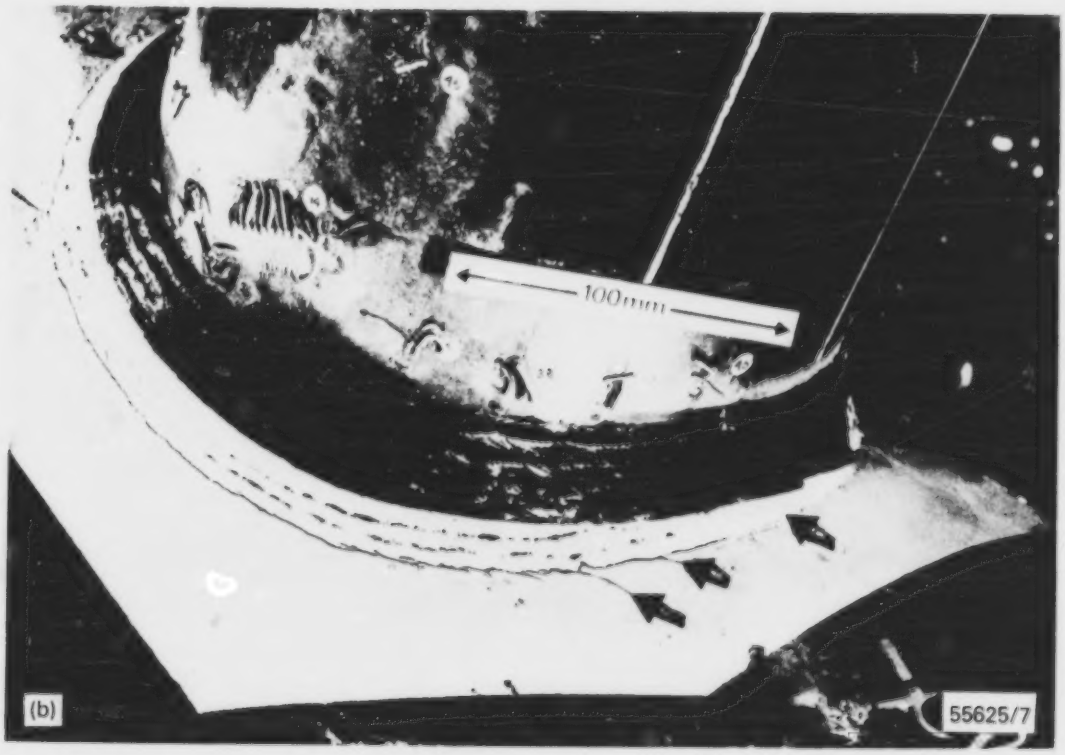

13 *Magnetic particle inspection of specimen No.3 after precracking through the chord wall thickness (the arrows indicate the crack tips).*

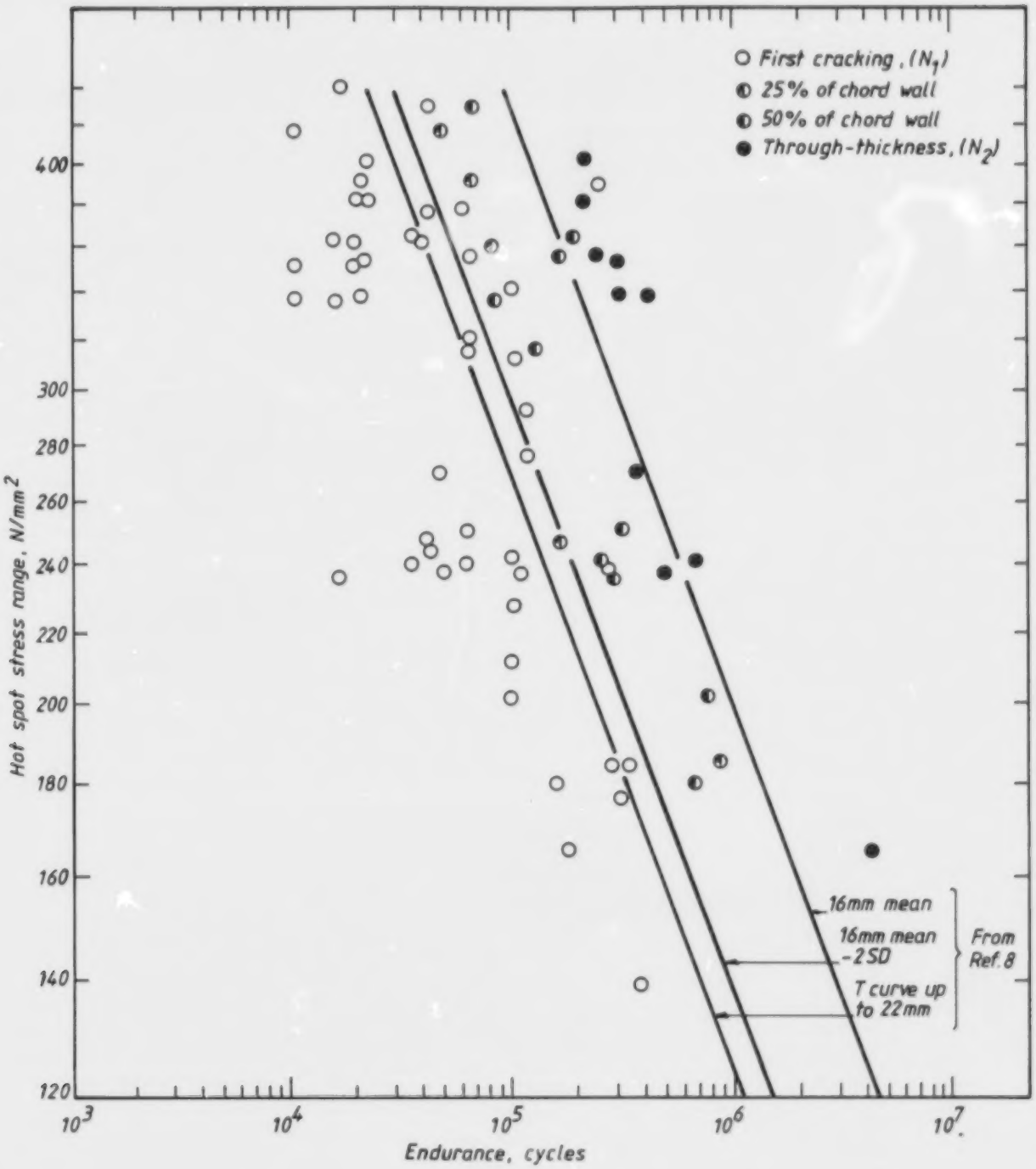

14 *Fatigue test results obtained during precracking tubular joint specimens.*

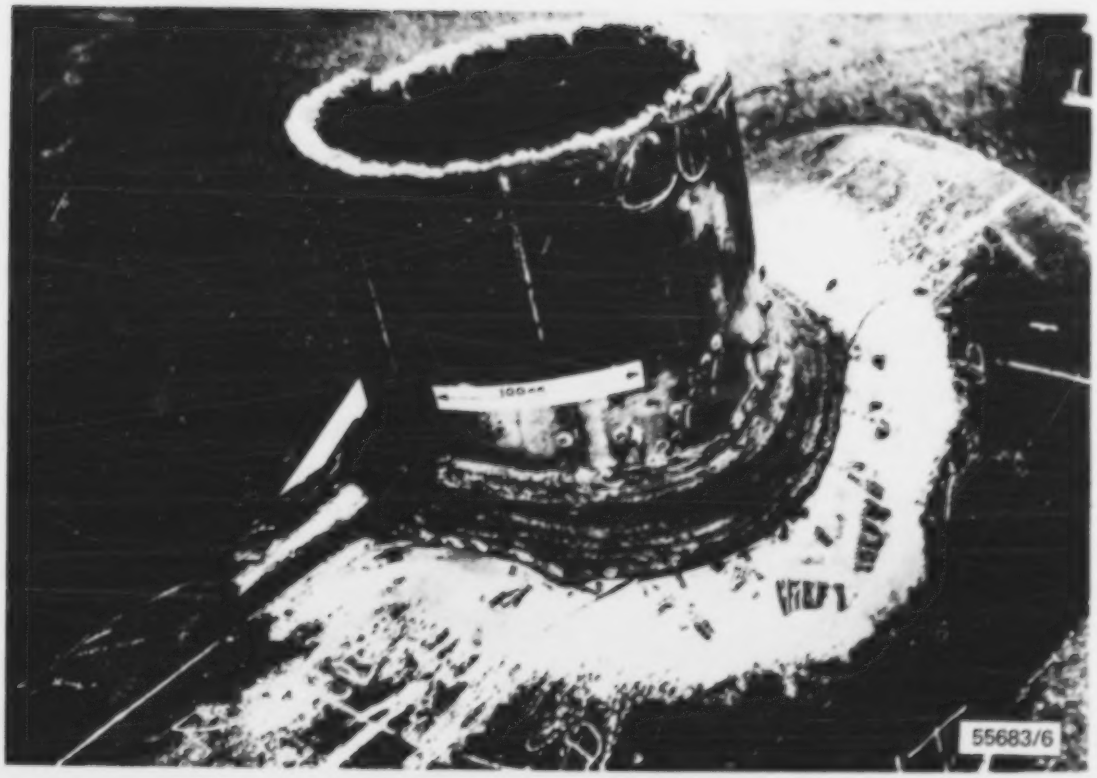

15 *Fatigue cracking in specimen No.3 (repair welded).*

16 a) *Fatigue fracture surfaces in repair welded specimen No.20, side A.*

16 b) *Fatigue fracture surfaces in repair welded specimen No.20, side B.*

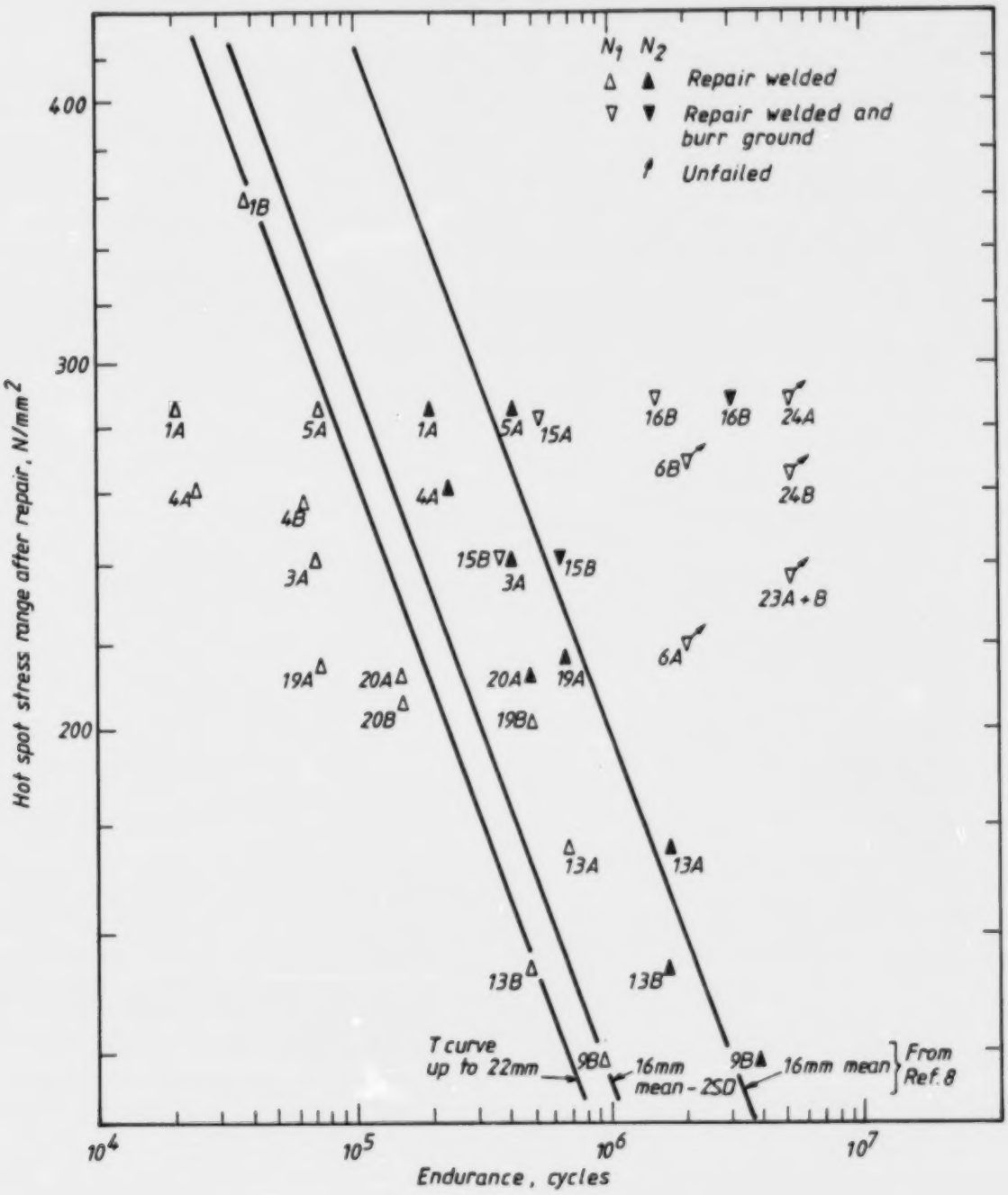

17 *Fatigue test results for repair welded tubular joints plotted in terms of the measured hot spot stress range after repair.*

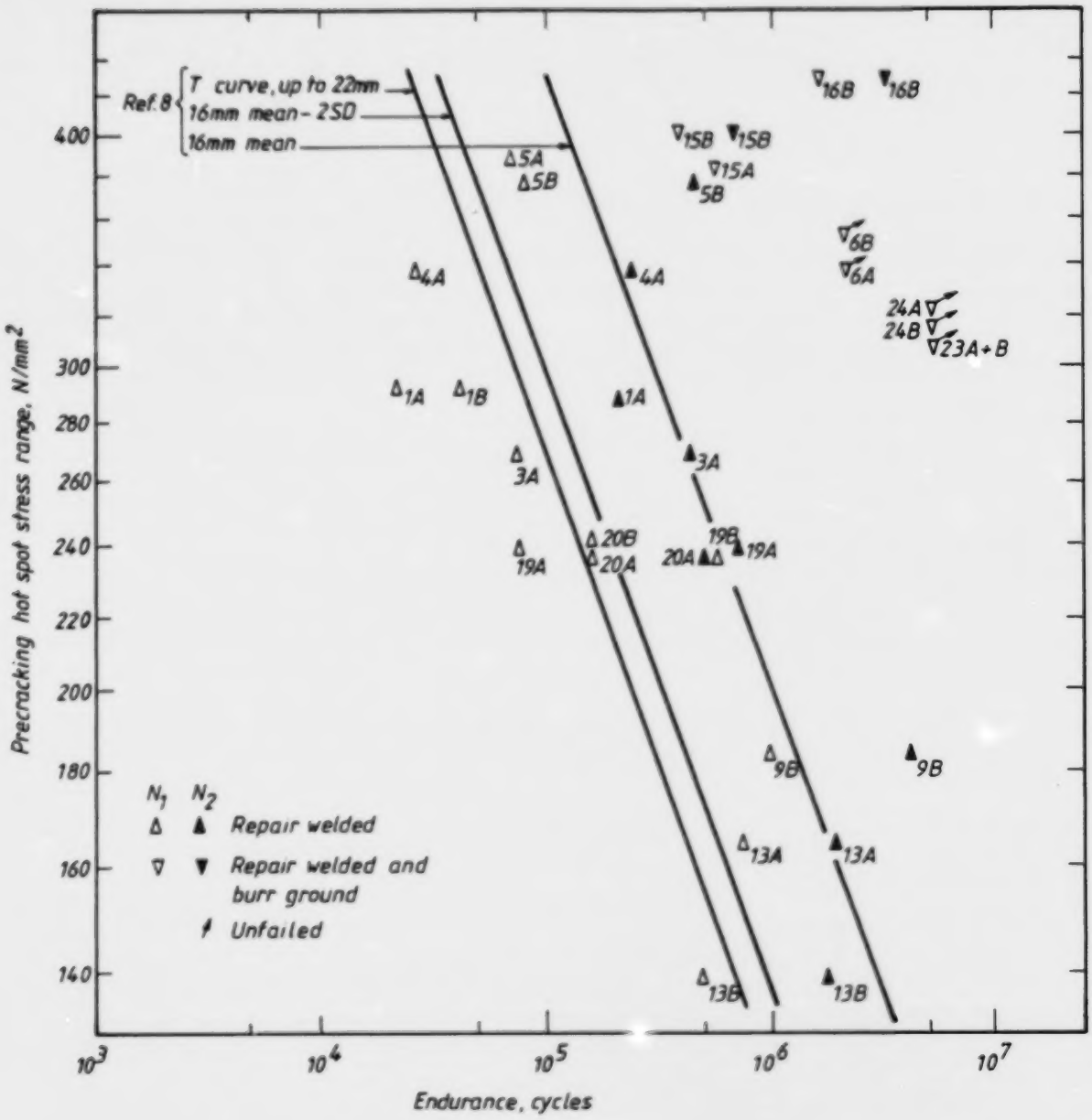

18 *Fatigue test results for repair welded tubular joints plotted in terms of the hot spot stress range during precracking.*

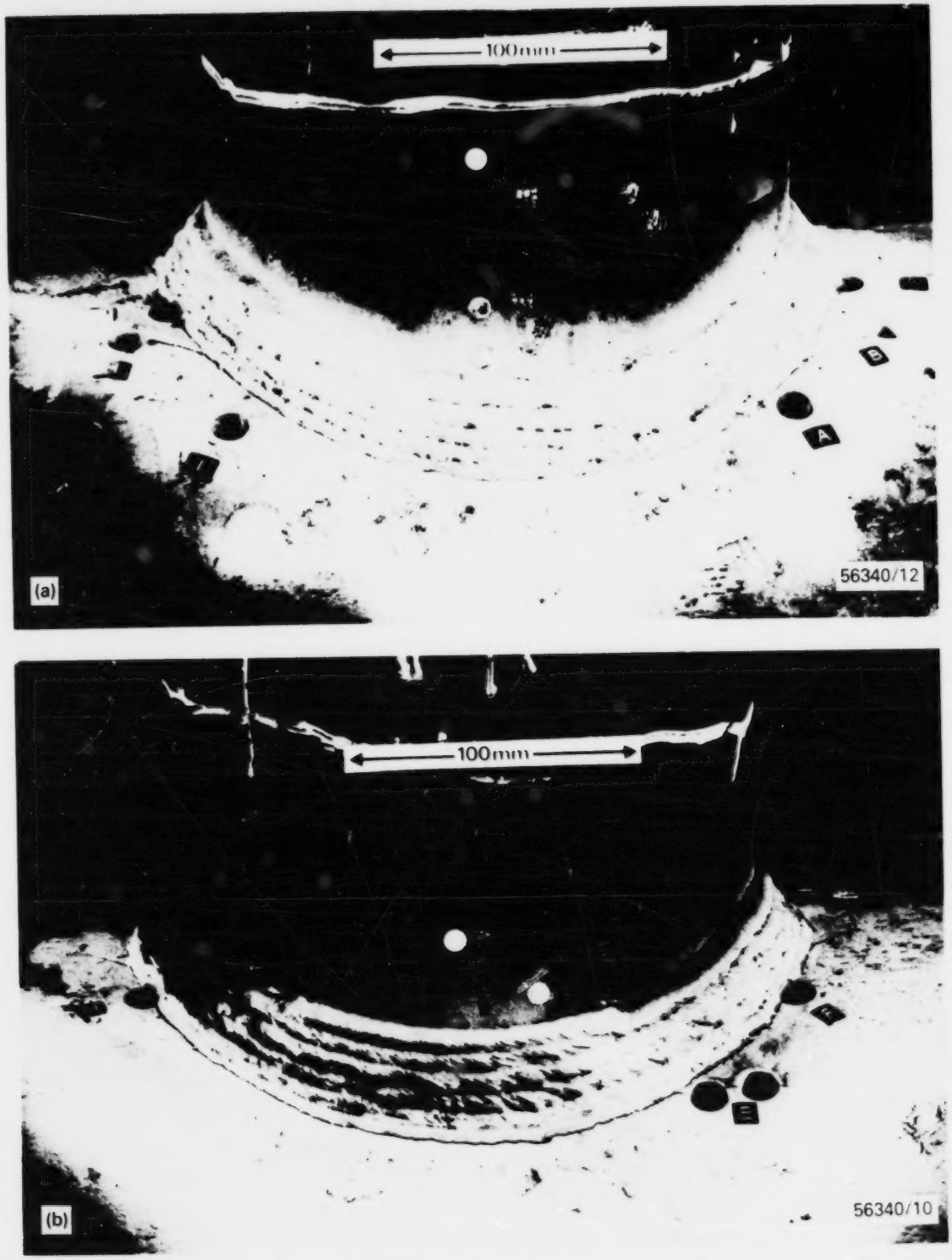

19 *Magnetic particle inspection of specimen No.7 after retesting:* a) *Side A;* b) *Side B.*

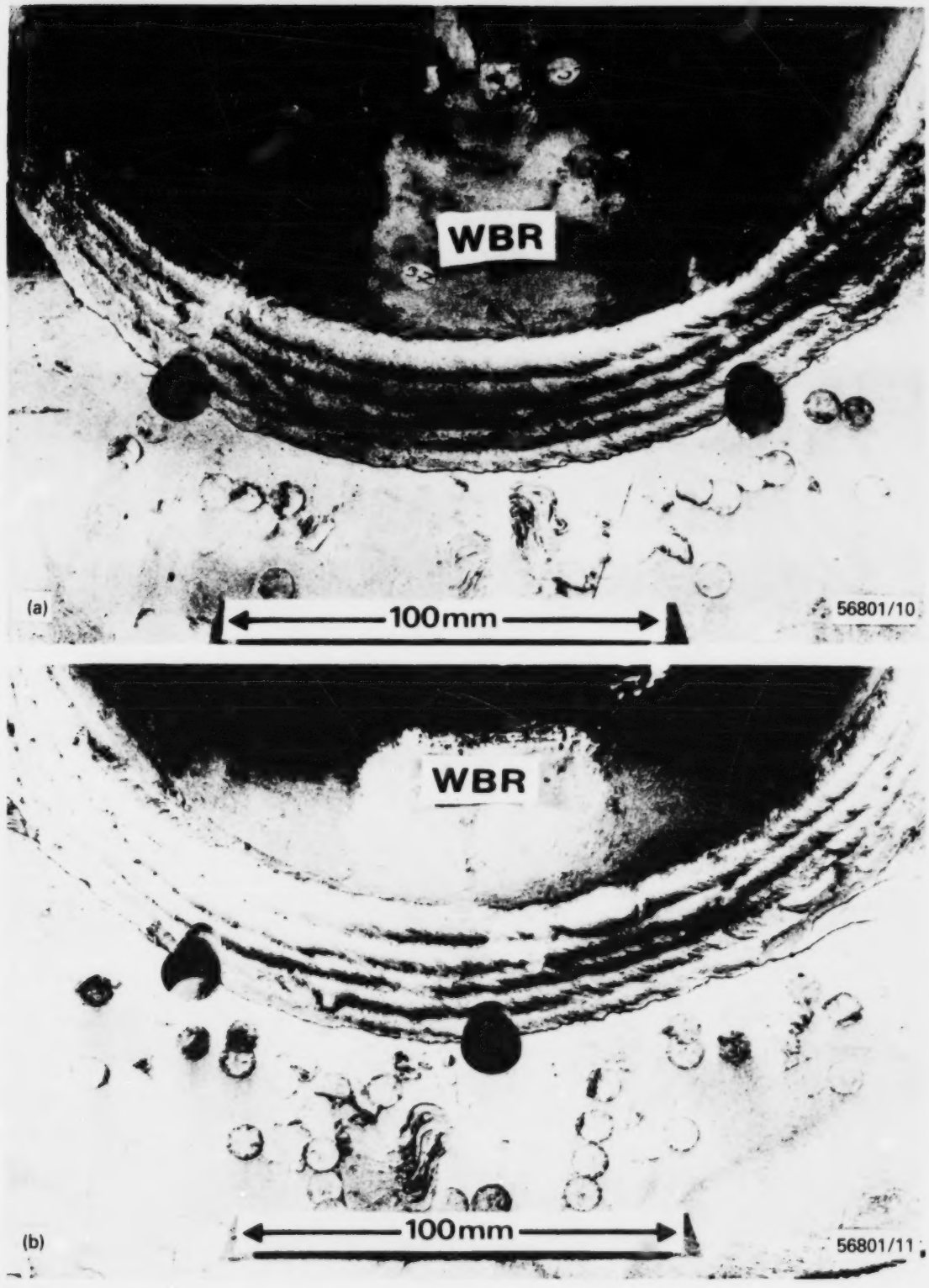

20 *Magnetic particle inspection of specimen No.8 after retesting:* a) *Side A;* b) *Side B.*

21 a) *Fatigue fracture surfaces in specimen repaired by hole drilling and cold expansion (specimen No.8, side A).*

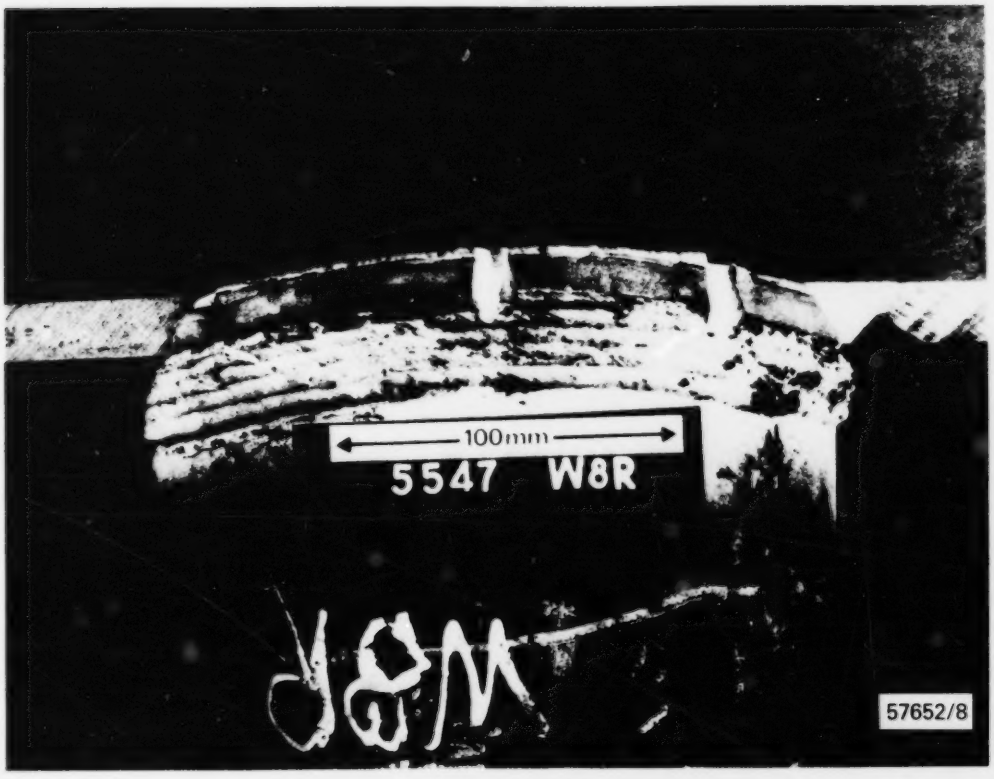

21 b) *Fatigue fracture surfaces in specimen repaired by hole drilling and cold expansion (specimen No.8, side B).*

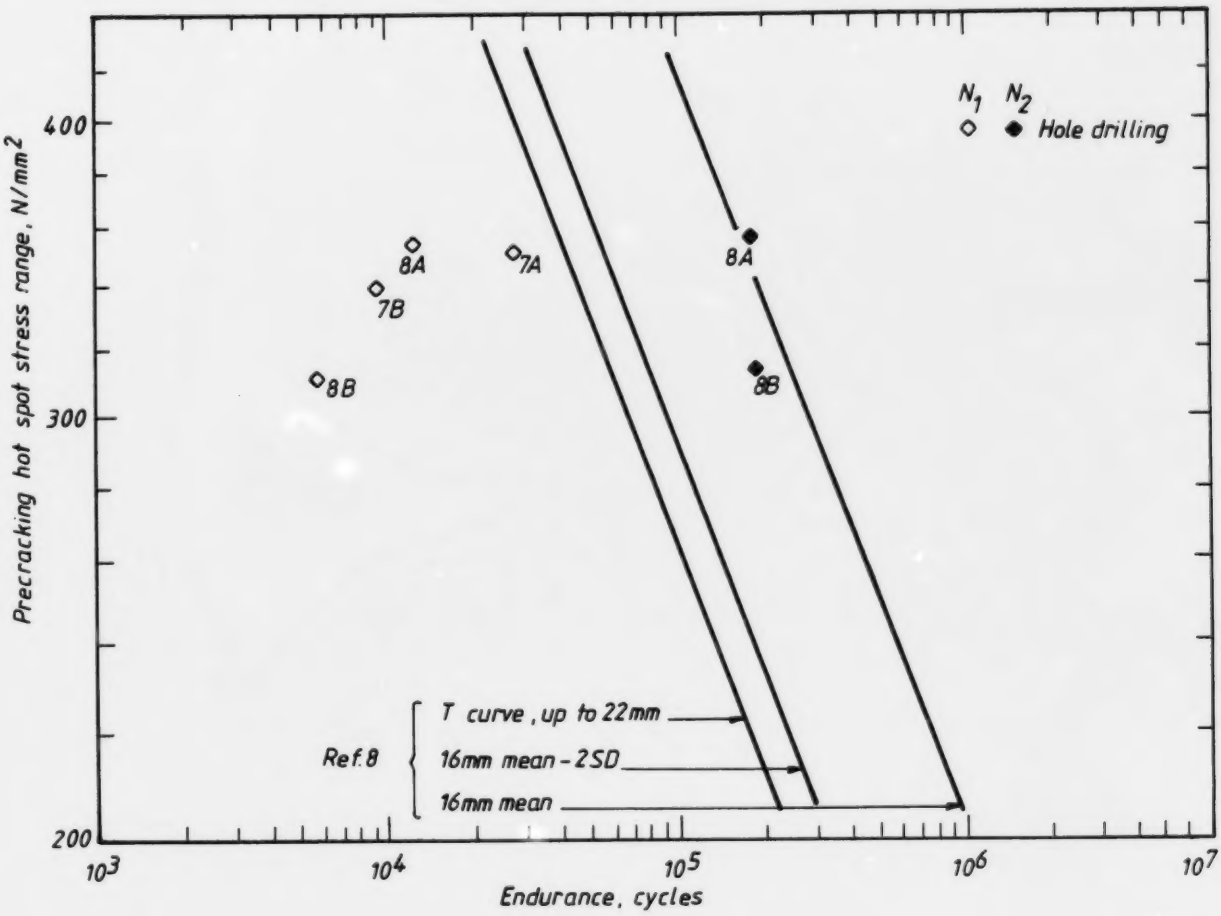

22 *Fatigue test results obtained for tubular joints repaired by hole drilling and cold expansion plotted in terms of the hot spot stress range during precracking.*

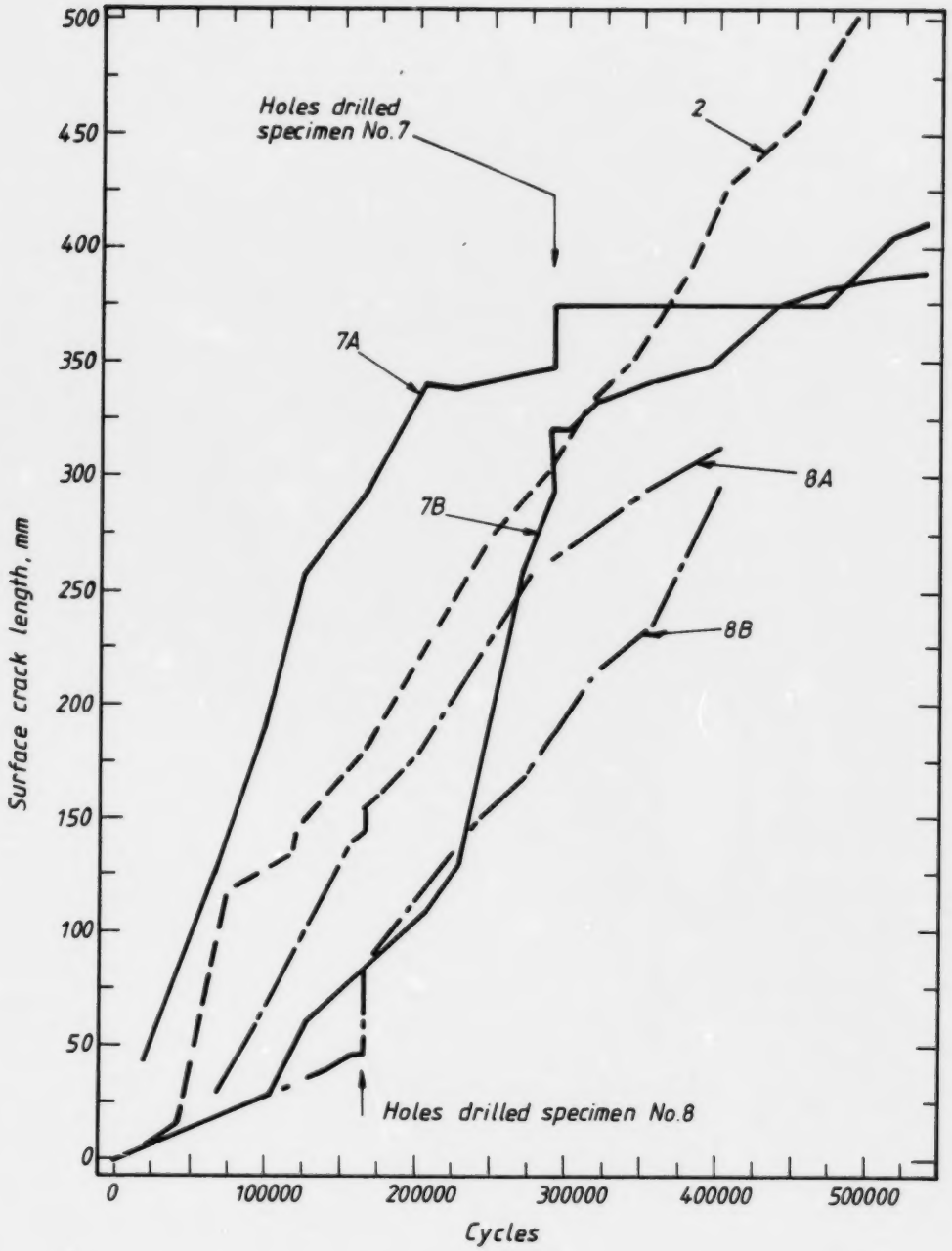

23 *Surface crack development in specimens repaired by hole drilling (No.7 and 8) compared with that in an unrepaired specimen (No.2).*

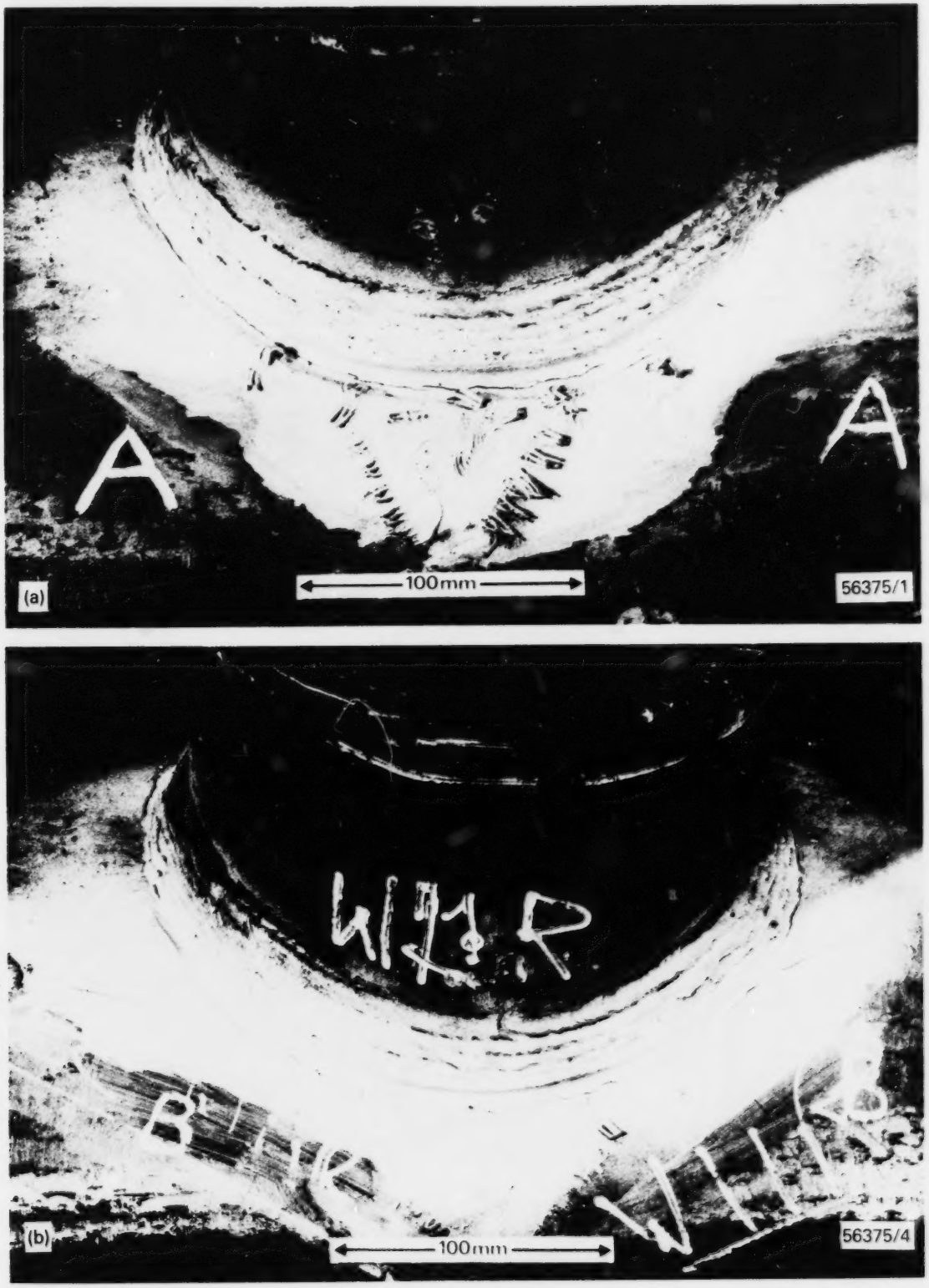

24 *Magnetic particle inspection of specimen (No.11) repaired by grinding alone:* a) *Side A;* b) *Side B.*

25 a) *Fatigue fracture surfaces in specimen with ground excavation (specimen No.11, side A).*

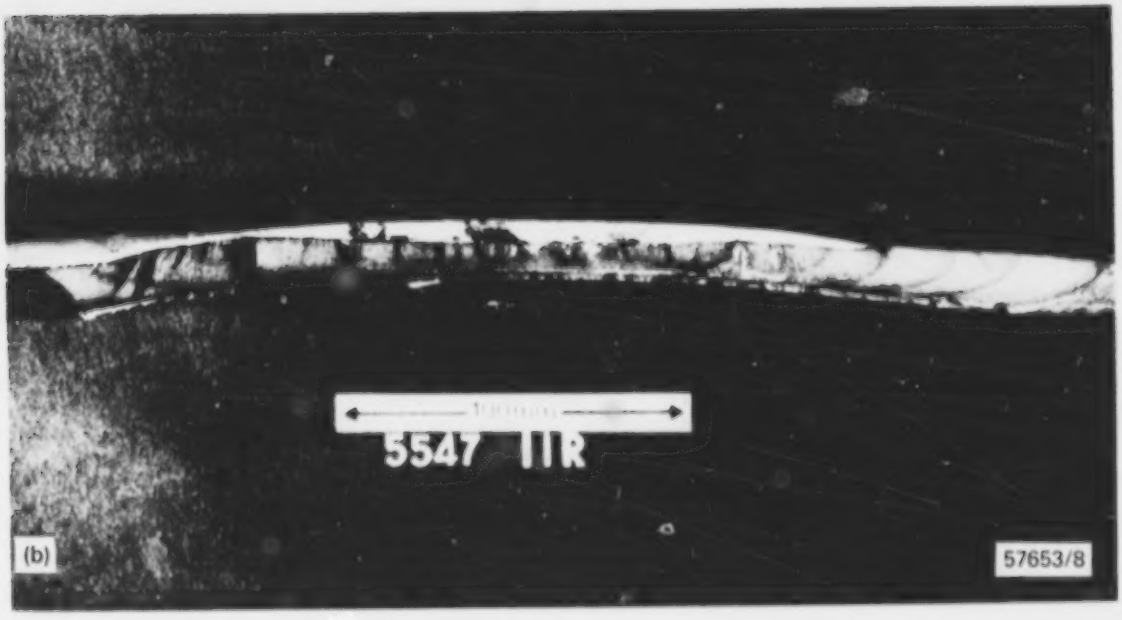

25 b) *Fatigue fracture surfaces in specimen with ground excavation (specimen No.11, side B).*

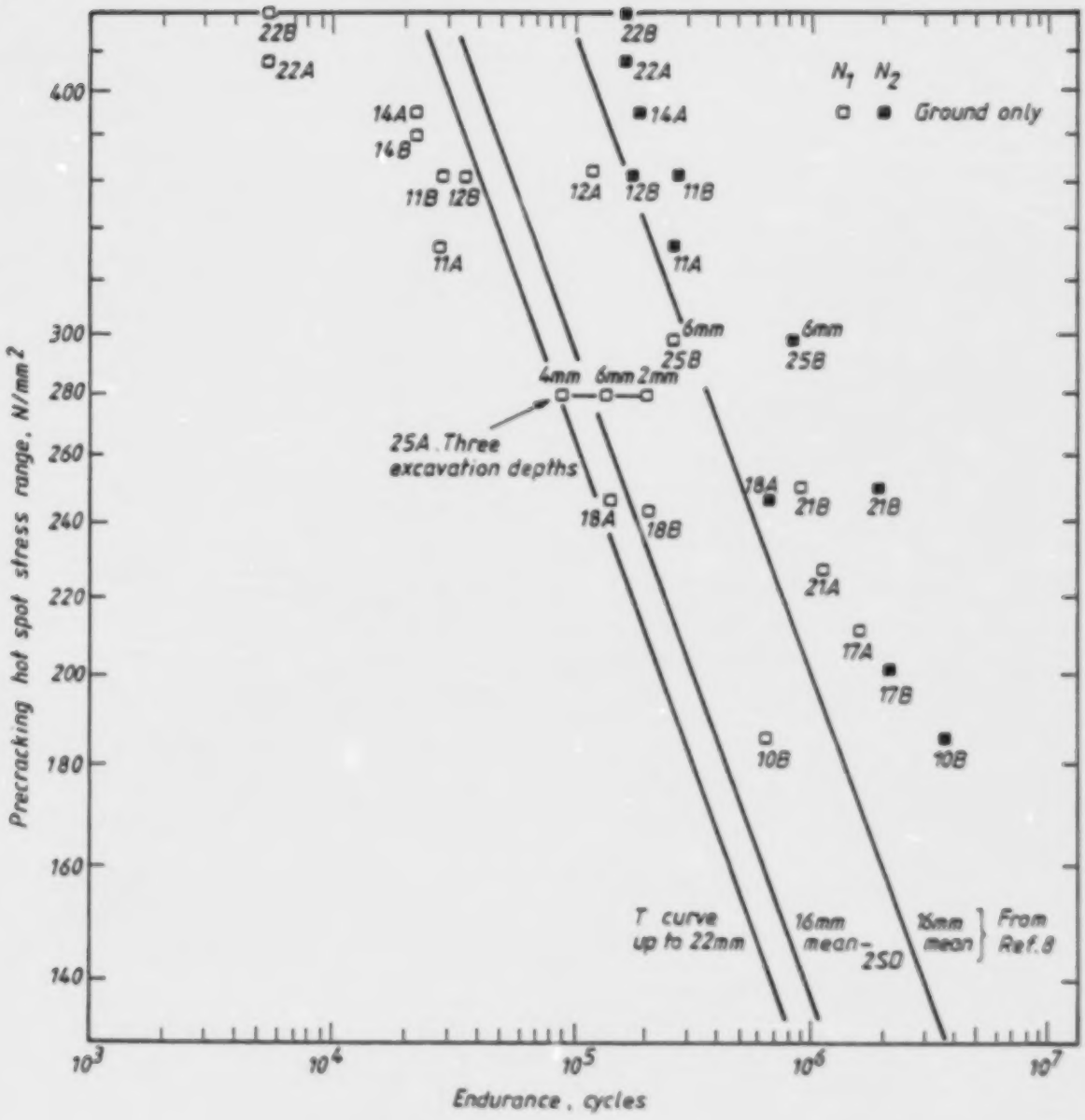

26 *Fatigue test results for tubular joints repaired by grinding alone plotted in terms of the hot spot stress range during precracking.*

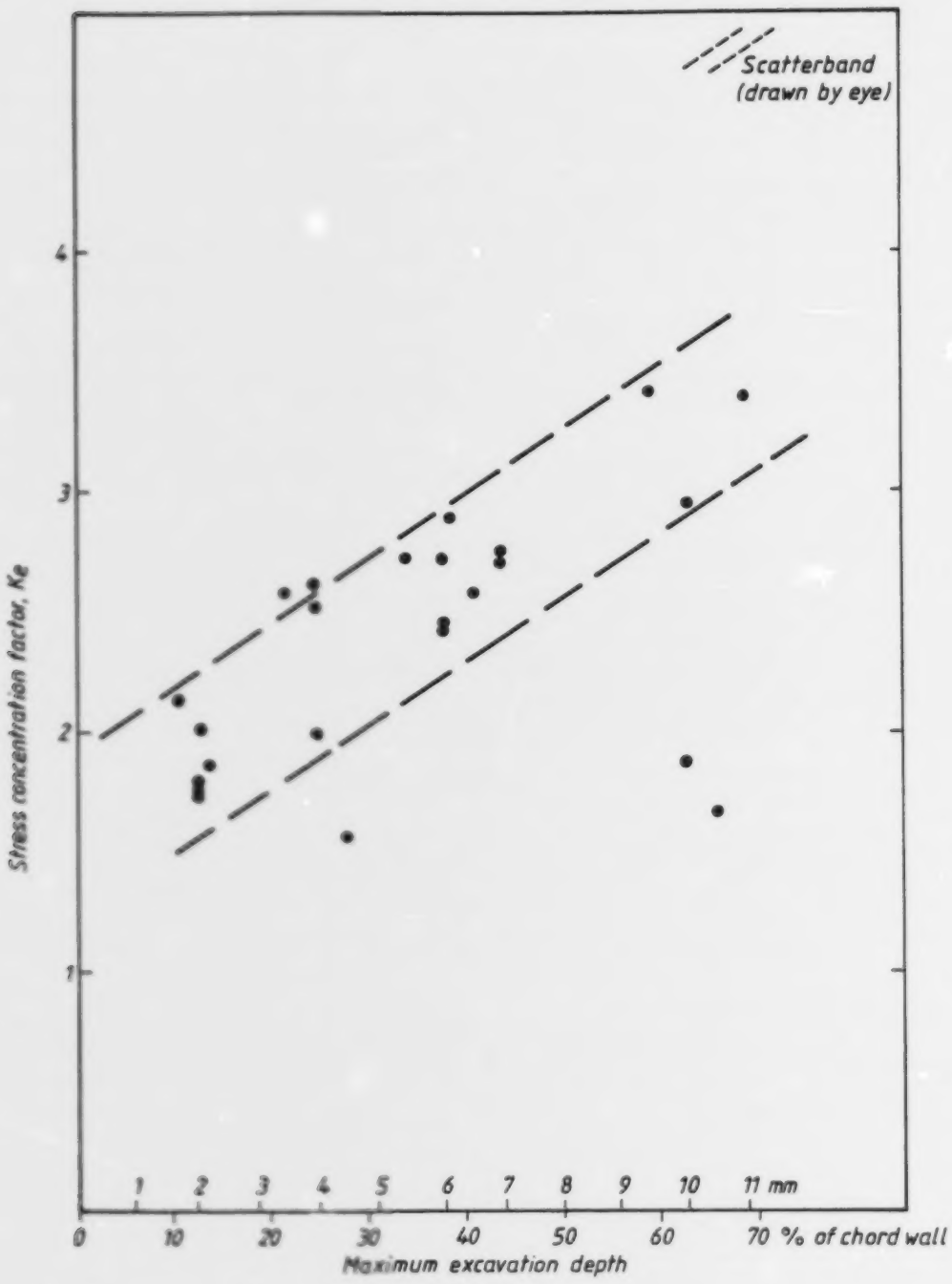

27 *Stress concentration factors for the ground excavations plotted against maximum excavation depth.*

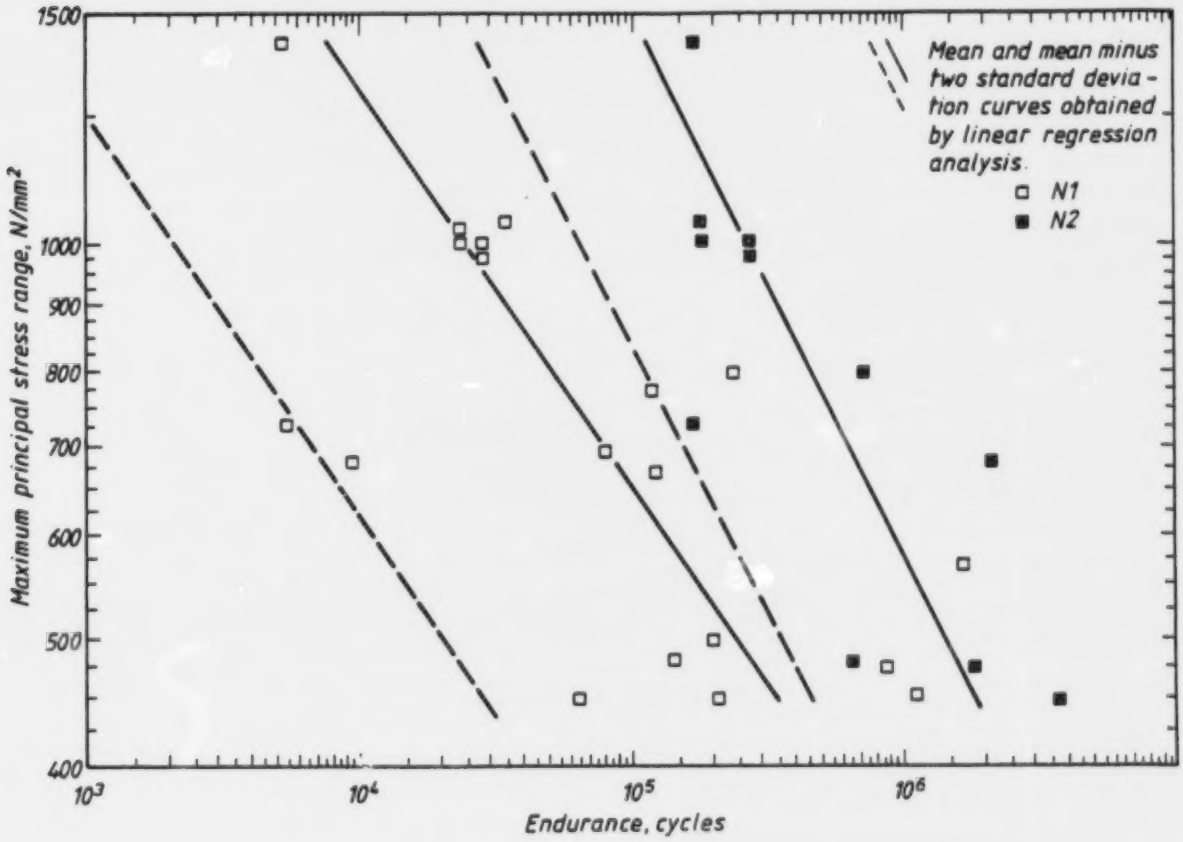

28 *Test lives for specimens repaired by grinding alone plotted in terms of the maximum pseudo-elastic principal stress range measured within the excavation.*

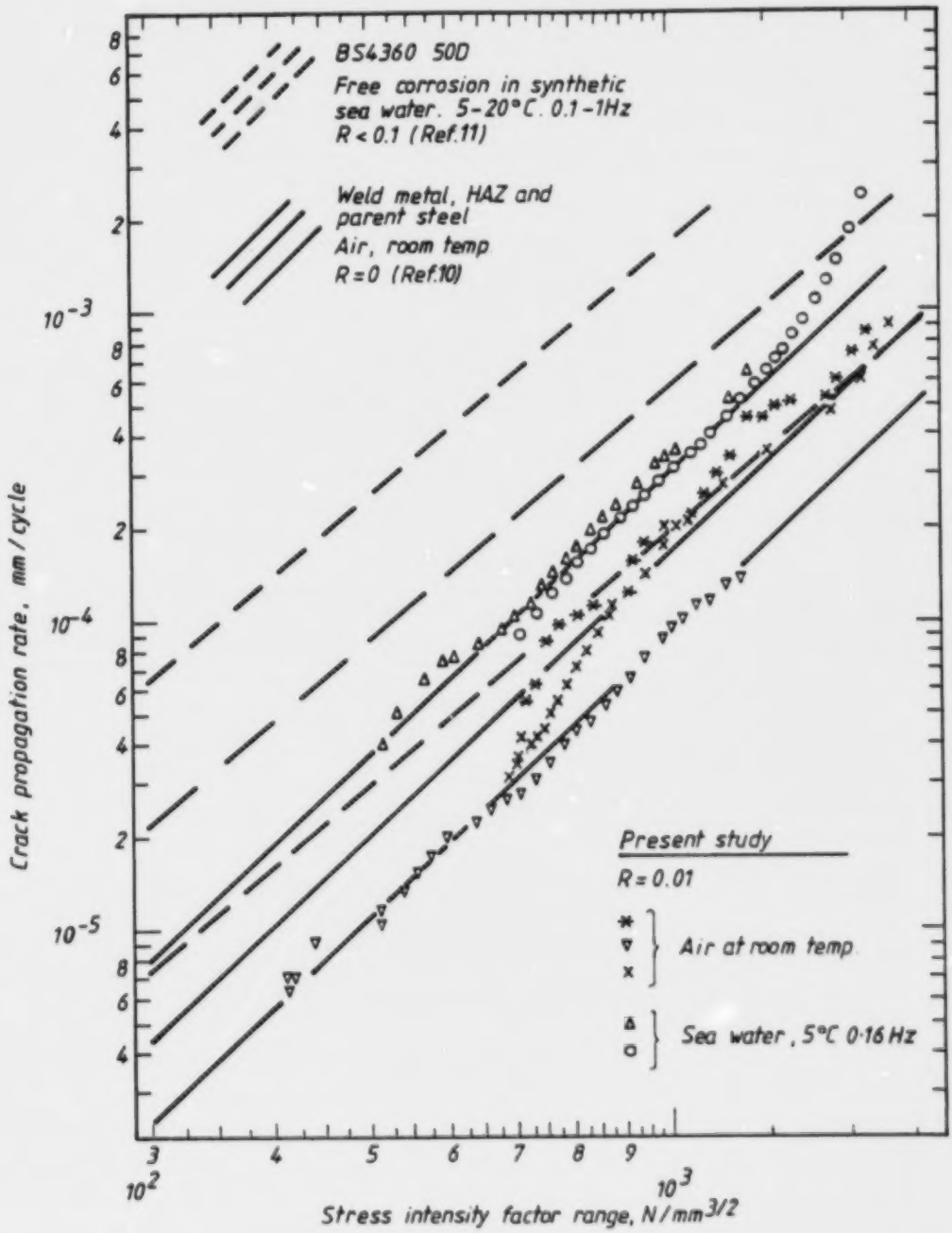
BS4360 50D
Free corrosion in synthetic sea water. 5-20°C. 0.1-1Hz
R < 0.1 (Ref.11)
Weld metal, HAZ and parent steel
Air, room temp.
R = 0 (Ref.10)
Present study
R = 0.01
Air at room temp.
Sea water, 5°C 0·16 Hz
Crack propagation rate, mm/cycle
Stress intensity factor range, N/mm^3/2

29 *Results of fatigue crack growth study on hyperbaric weld metal tested in air and freely corroding in synthetic sea water.*

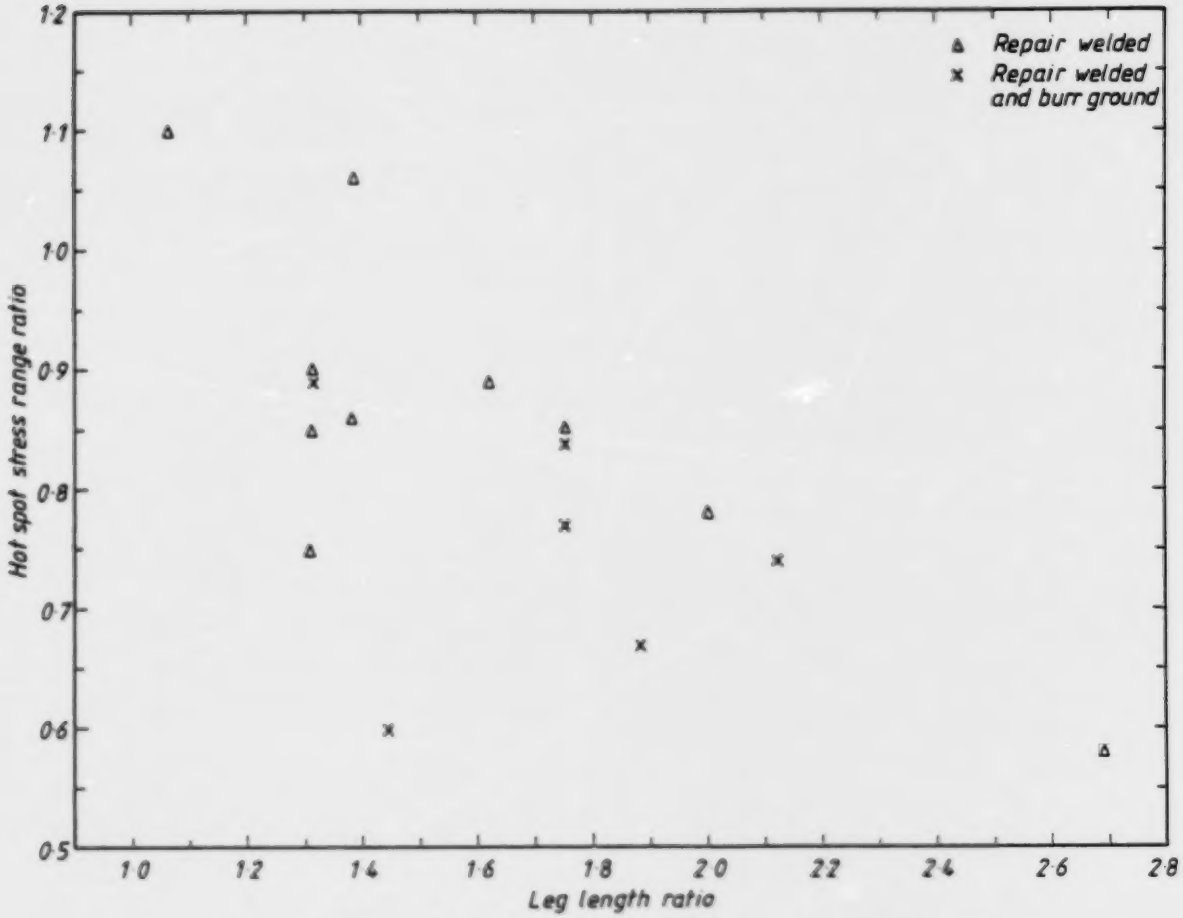

30 *Relationship between hot spot stress and weld leg length before and after repair.*

Note: Hot spot stress range ratio $= \dfrac{\text{hot spot stress range after repair}}{\text{hot spot stress range before repair}}$

$$\text{Leg length ratio} = \frac{\text{leg length after repair}}{\text{leg length before repair}}$$

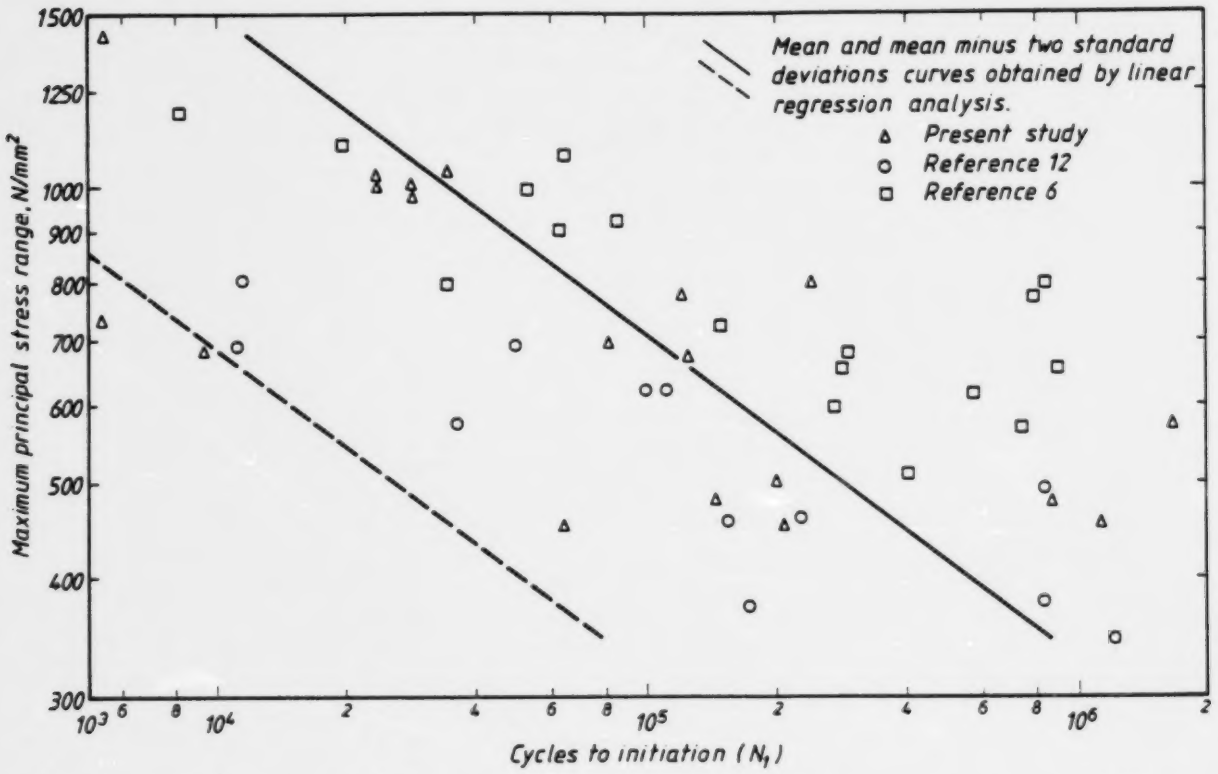

31 *Comparison of N_i data for specimens repaired by grinding alone from the present study with data from Ref. 6 and 12.*

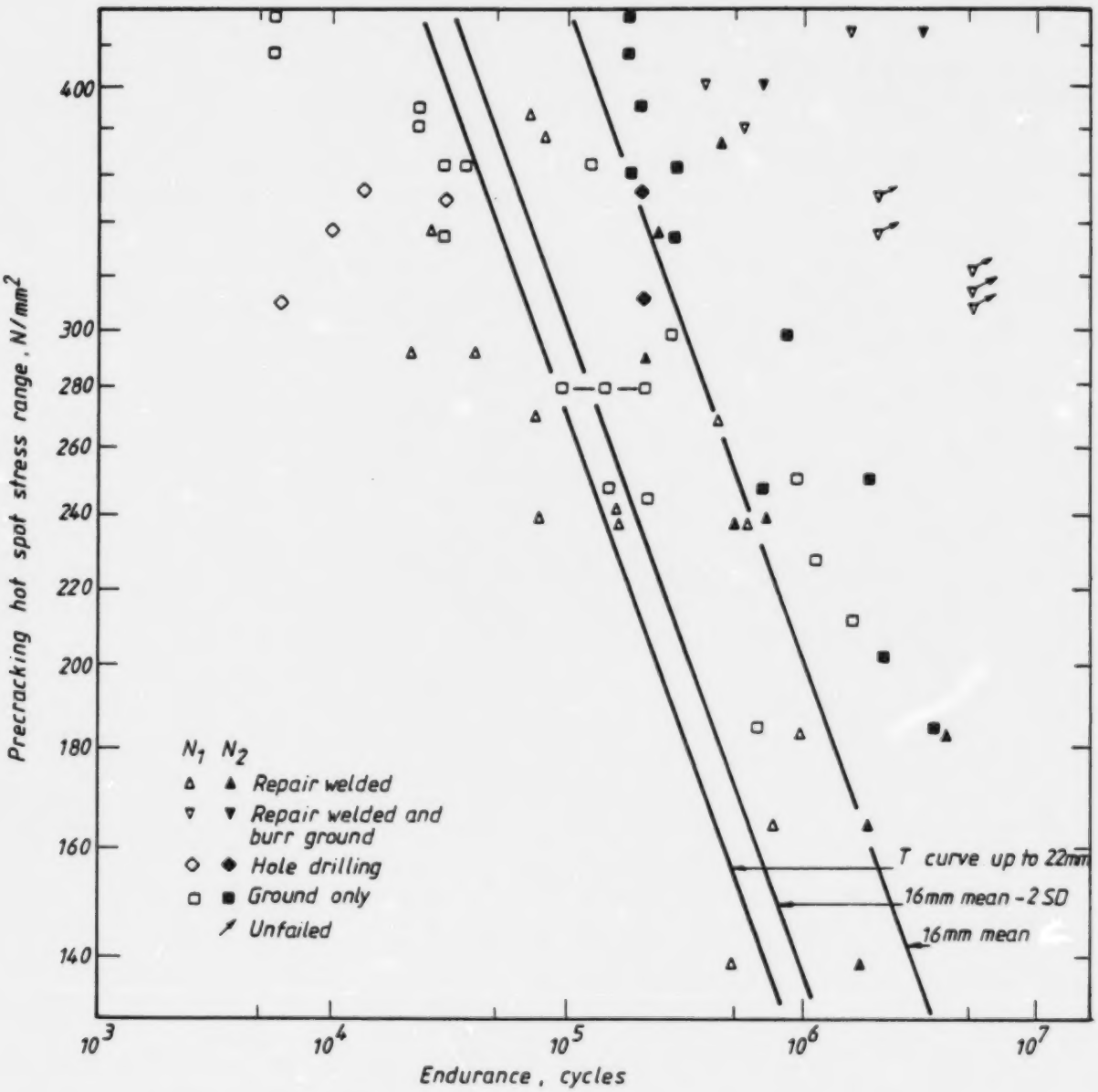

32 *Fatigue test results for all repaired tubular joints plotted in terms of the hot spot stress range during precracking.*

APPENDIX A — Extent of cracking in tubular joints

The following Figures illustrate the extent of surface cracking in each of the tubular joint specimens after precracking and after retesting. The crack lengths at first cracking are also shown. The plots represent a development of the chord, that is the outside surface of the chord is represented as though rolled flat. In this way the cracks can be plotted as true lengths. The plots also show the approximate outline shapes of the repair welds and ground excavations. For specimens No.7 and 8 (repaired by hole drilling and cold expansion) additional information is given to illustrate the progress of cracking with cycles after repair. The plots are grouped according to repair method and are shown in the order in which they appear in Table 7 of the main text.

In a number of specimens, cracks appeared outside the repaired area at the original weld toe in the chord or brace, and were removed by light burr grinding to allow the test to continue. For clarity this is not shown in the following cracking diagrams, but the incidence is listed in Table A1.

Table A1 Incidence of cracking at unrepaired weld toe in brace or chord

Specimen No.	Repair method*	Position** on joint circumference, °	Total surface crack length, mm	Endurance (on retest), cycles	Cracking position on brace (B) or chord (C)	
15A	RG	95	12	1.26×10^3	B	
15A	RG	85	9	3.84×10^3	B	
15B	RG	285	15	1.26×10^3	B	
16A	RG	95	16	1.54×10^5	B	
16A	RG	110	7	7.29×10^5	B	
16B	RG	260	9	1.54×10^5	B	
16B	RG	270	5	1.79×10^5	B	
16B	RG	280	5	4.82×10^5	B	
16B	RG	235	13	1.54×10^5	B	
23A	RG	100	4	2.86×10^4	B	
23A	RG	80	13	7.05×10^5	B	
23B	RG	255	47	5.28×10^5	B	
23B	RG	290	12	1.22×10^6	B	
24A	RG	90	50	3.42×10^5	B	
24A	RG	110	10	2.18×10^6	B	
21A	G	115	8	3.75×10^5	C	
21B	G	231	5	1.48×10^5	C	
21B	G	225	5	3.21×10^5	C	
21B	G	310	7	3.21×10^5		
25A	G	40	6	7.61×10^4	C	Note
A	G	132	4	7.61×10^4	C	excavation
25B	G	321	6	7.61×10^4	C	depth 6mm

* RG — repair welded and burr ground; G — ground only

**For reference the 'saddle' positions are: Side A: 90°, Side B: 270°

APPENDIX A: Extent of cracking in tubular joints

Specimen No. 2
Precracking

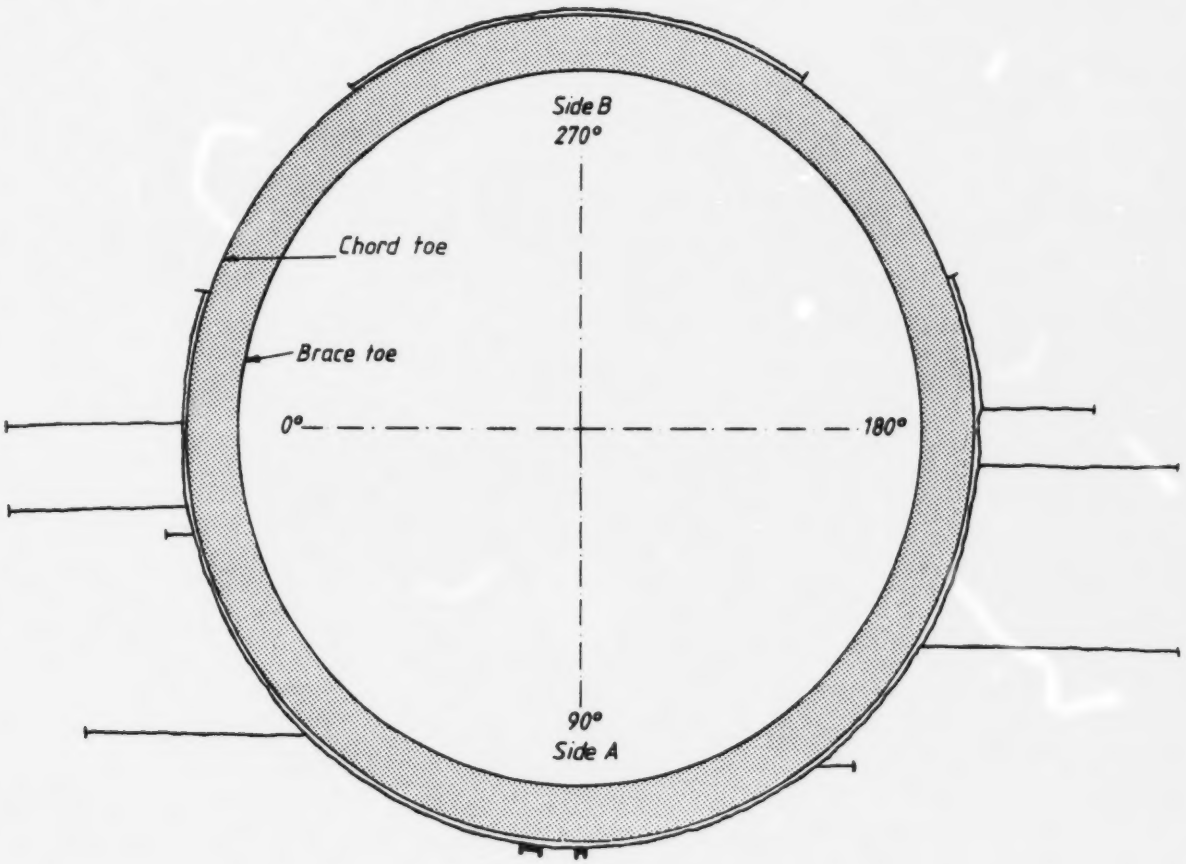

10mm

First detected cracking

Extent of final crack

APPENDIX A: Extent of cracking in tubular joints

Specimen No1
Precracking

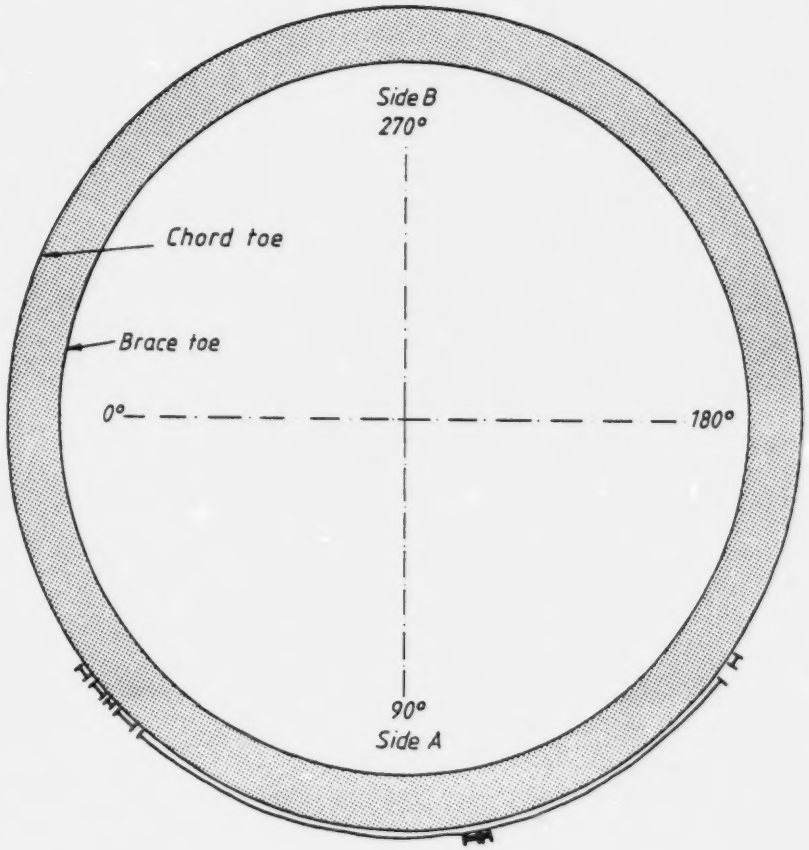

10mm

First detected cracking

Extent of final crack

APPENDIX A: Extent of cracking in tubular joints

Specimen No. 1
Repair welded

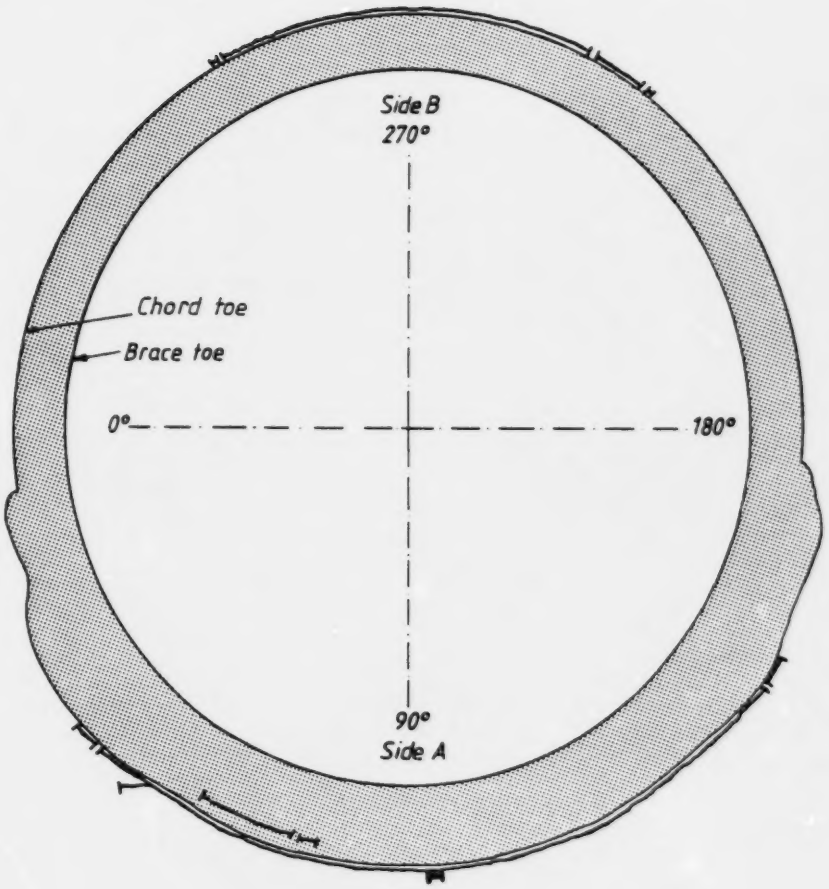

10mm

First detected cracking

Extent of final crack

APPENDIX A: Extent of cracking in tubular joints

Specimen No.3
Precracking

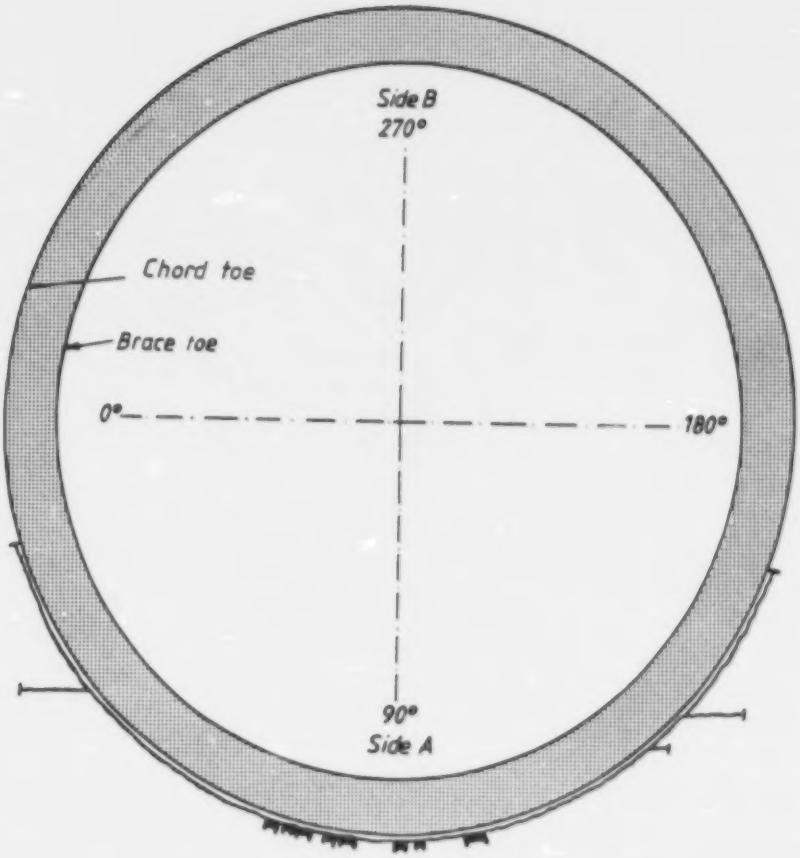

10mm

First detected cracking

Extent of final crack

APPENDIX A: Extent of cracking in tubular joints

Specimen No. 3
Repair welded

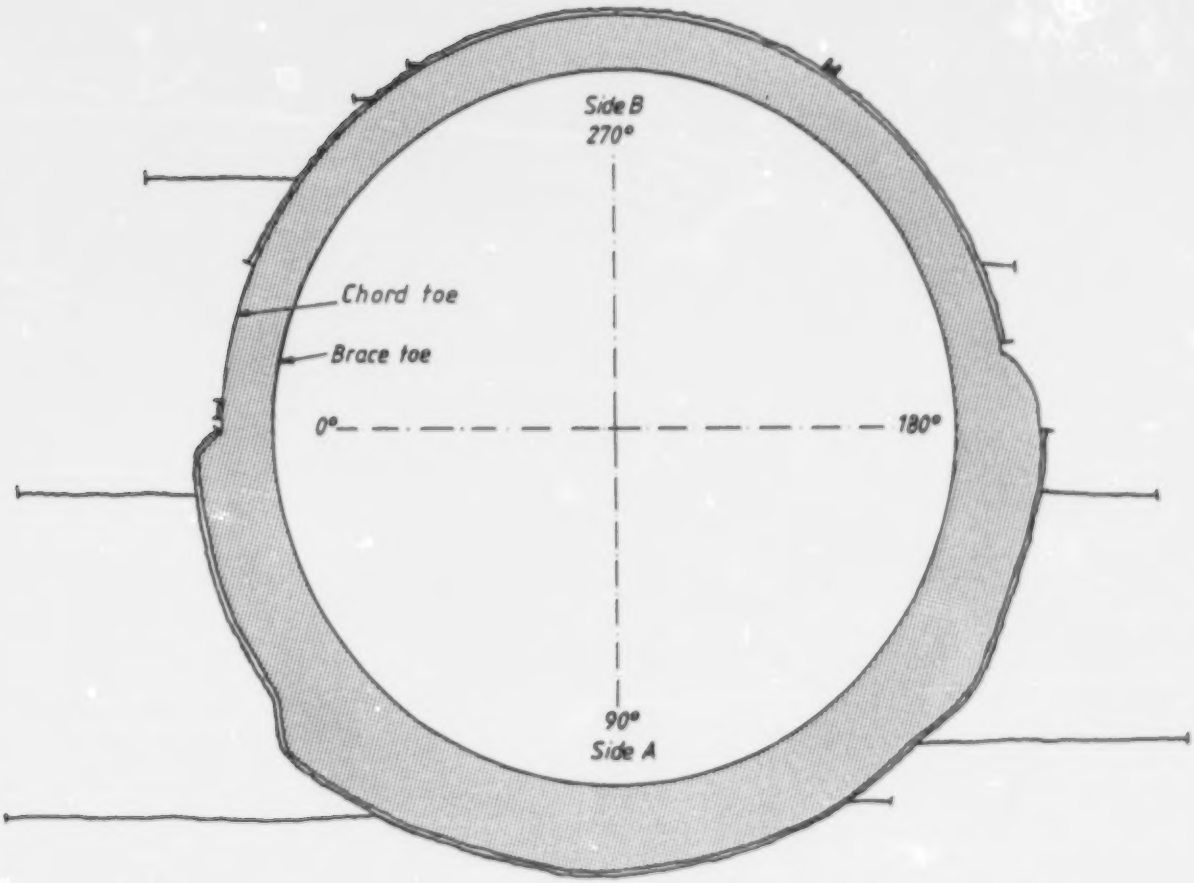

10mm

First detected cracking

Extent of final crack

APPENDIX A: Extent of cracking in tubular joints

Specimen No.13
Precracking

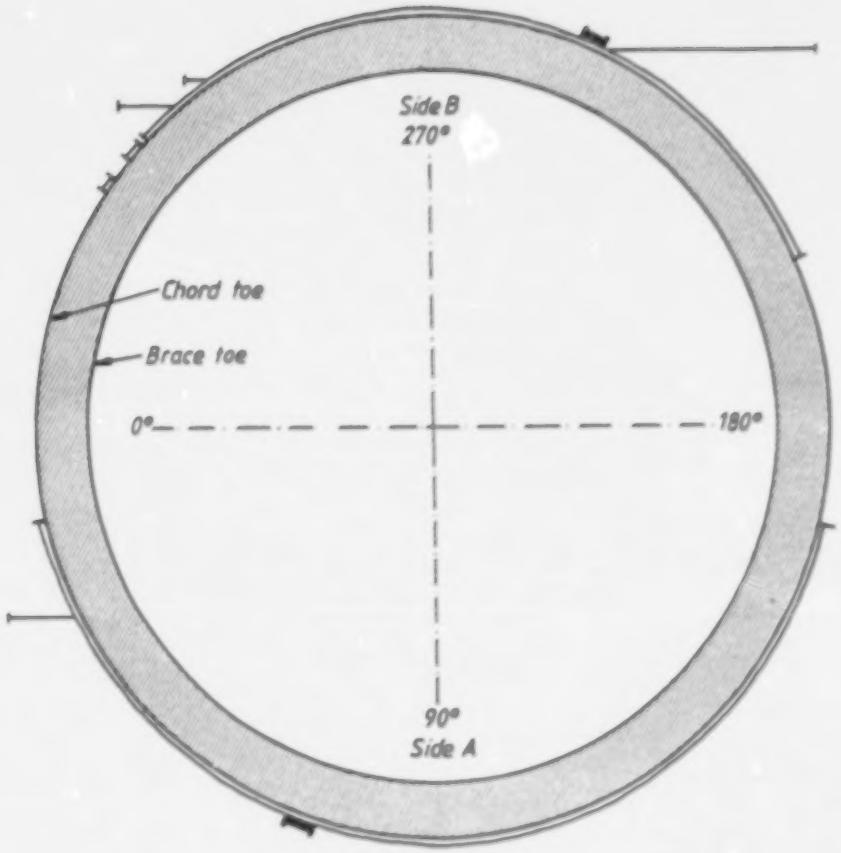

10mm

First detected cracking

Extent of final crack

APPENDIX A: Extent of cracking in tubular joints

Specimen No. 13
Repair welded

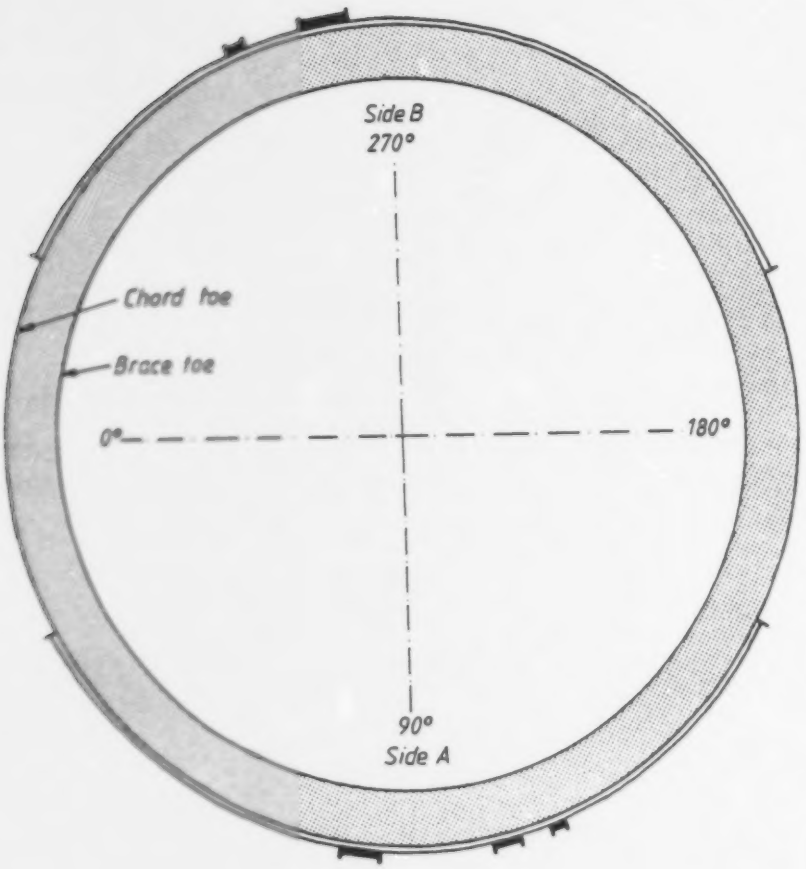

10mm

First detected cracking

Extent of final crack

APPENDIX A: Extent of cracking in tubular joints

Specimen No. 19
Precracking

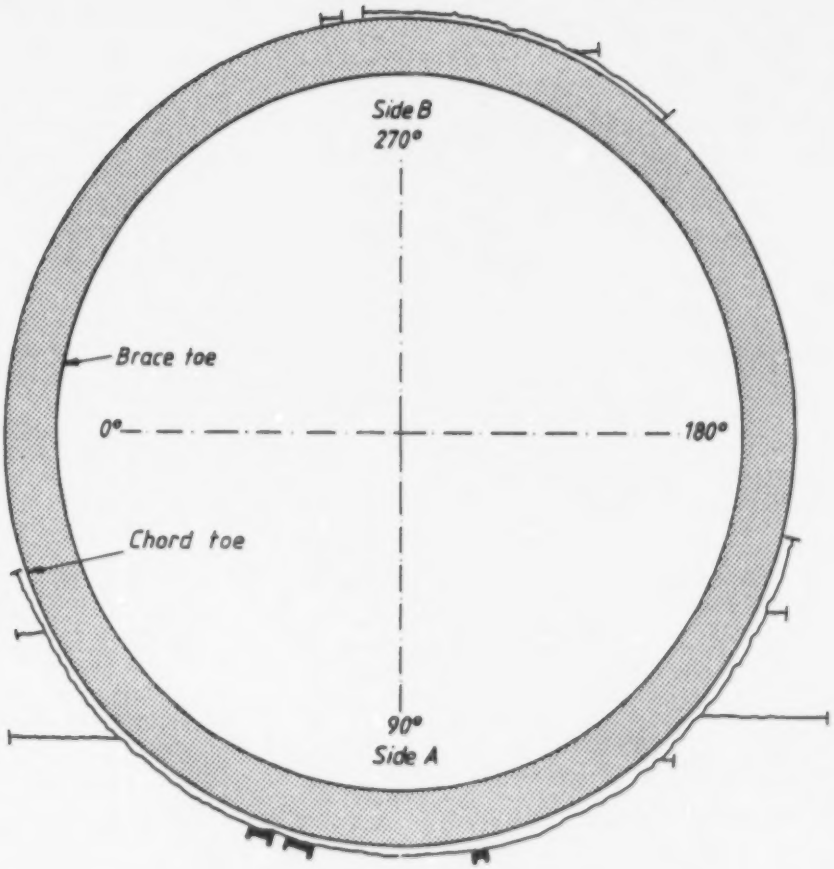

10mm

First detected cracking

Extent of final crack

APPENDIX A: Extent of cracking in tubular joints

Specimen No 19
Repair welded

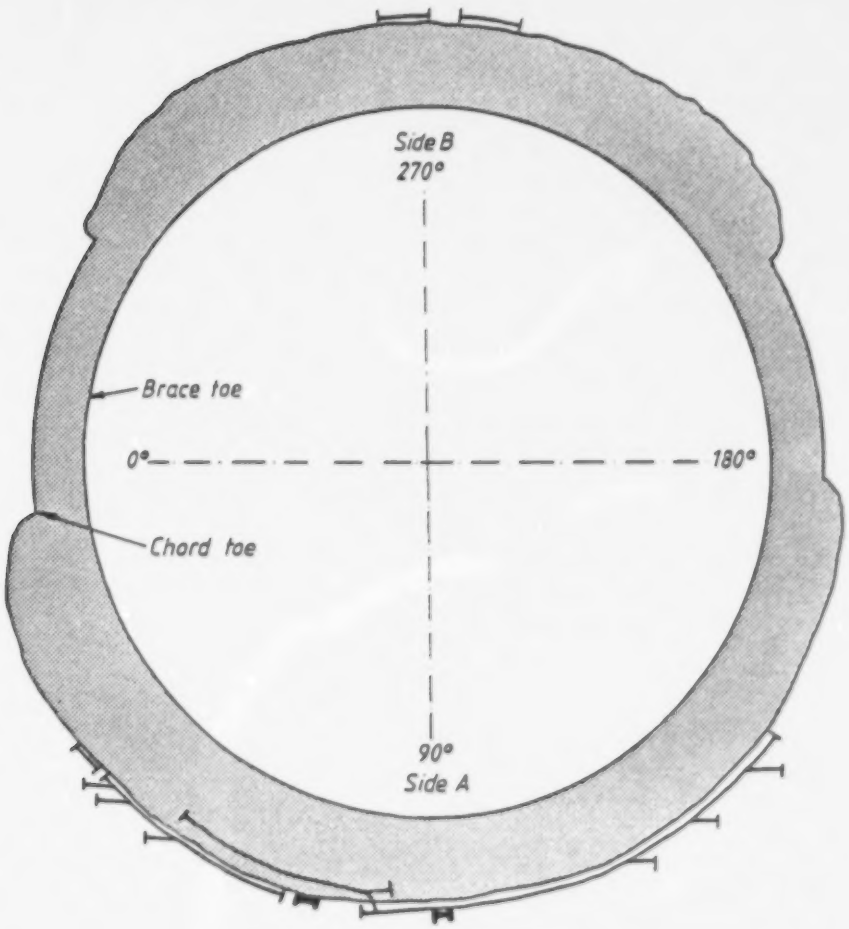

10mm

First detected cracking

Extent of final crack

APPENDIX A: Extent of cracking in tubular joints

Specimen No. 4
Precracking

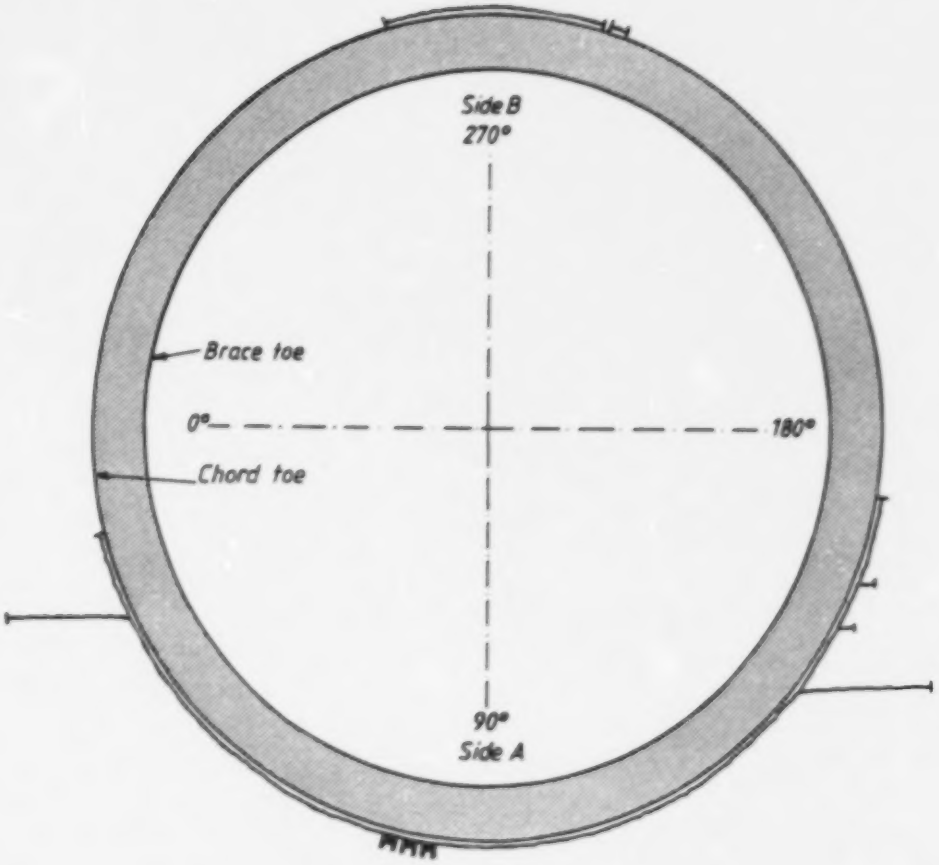

10mm

First detected cracking

Extent of final crack

APPENDIX A: Extent of cracking in tubular joints

Specimen No. 4
Repair welded

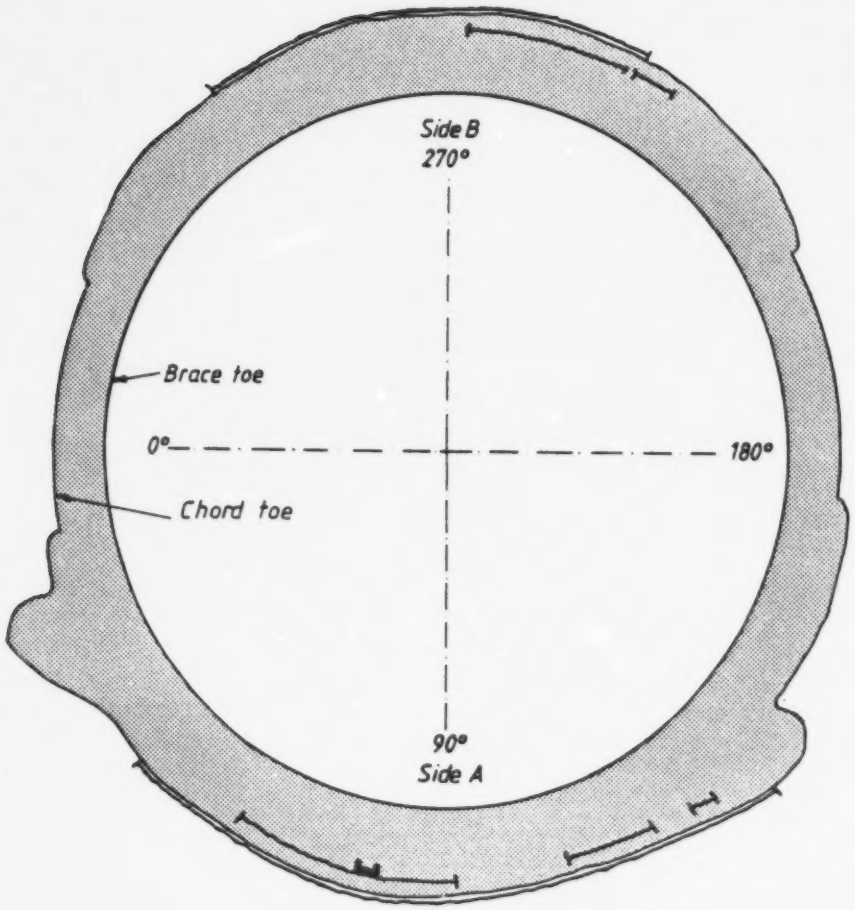

10mm

First detected cracking

Extent of final crack

APPENDIX A: Extent of cracking in tubular joints

Specimen No.9
Precracking

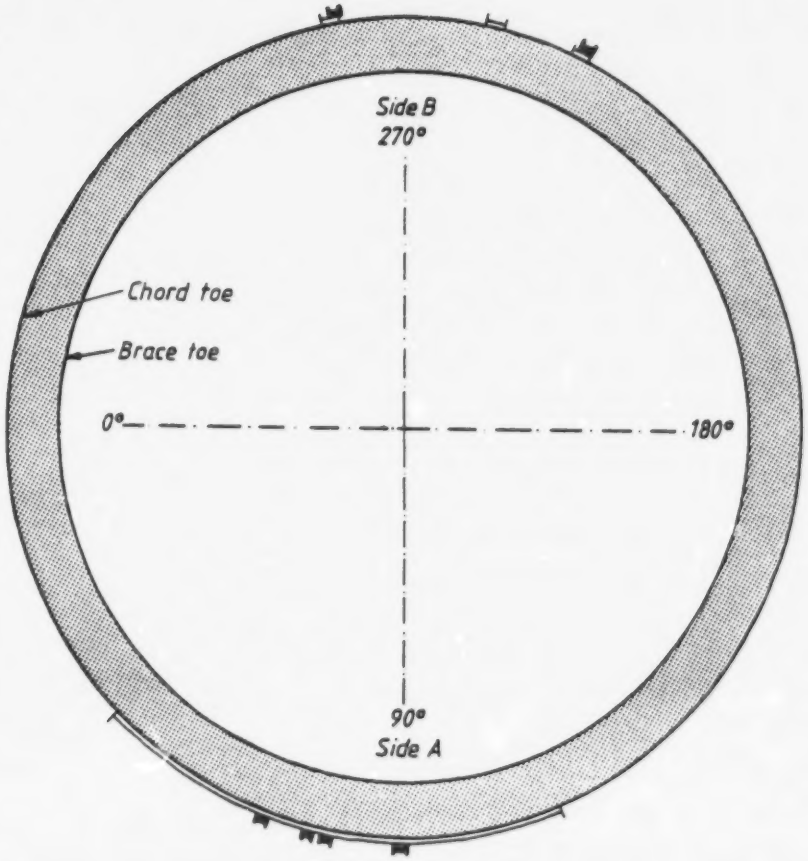

10mm

First detected cracking

Extent of final crack

APPENDIX A: Extent of cracking in tubular joints

Specimen No. 9
Repair welded

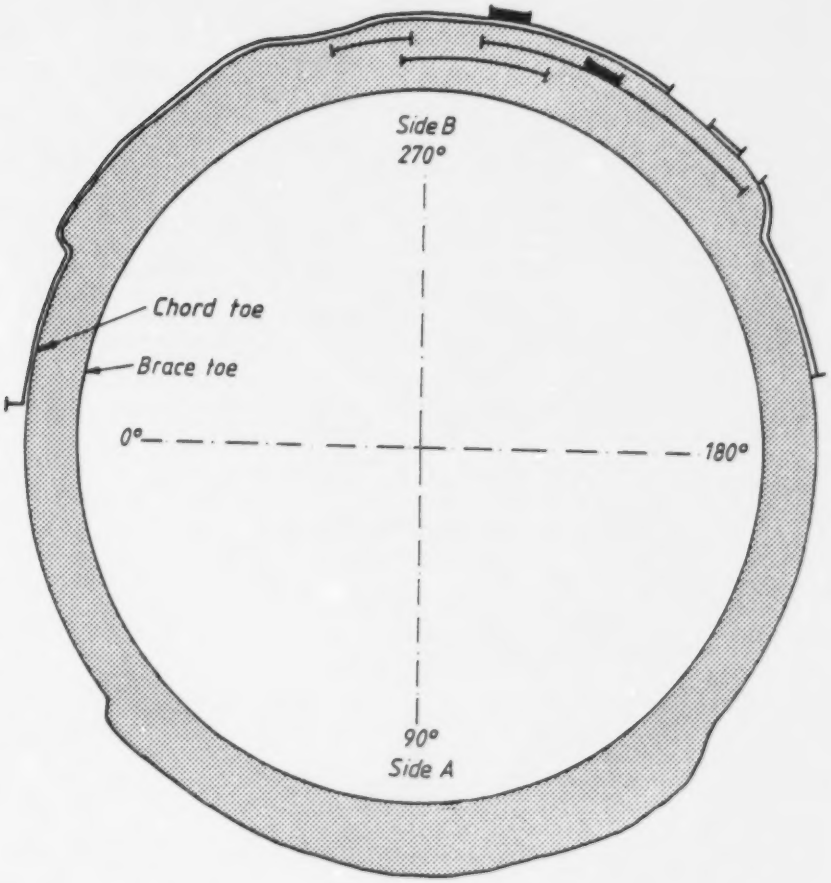

10mm

First detected cracking

Extent of final crack

APPENDIX A: Extent of cracking in tubular joints

Specimen No.20
Precracking

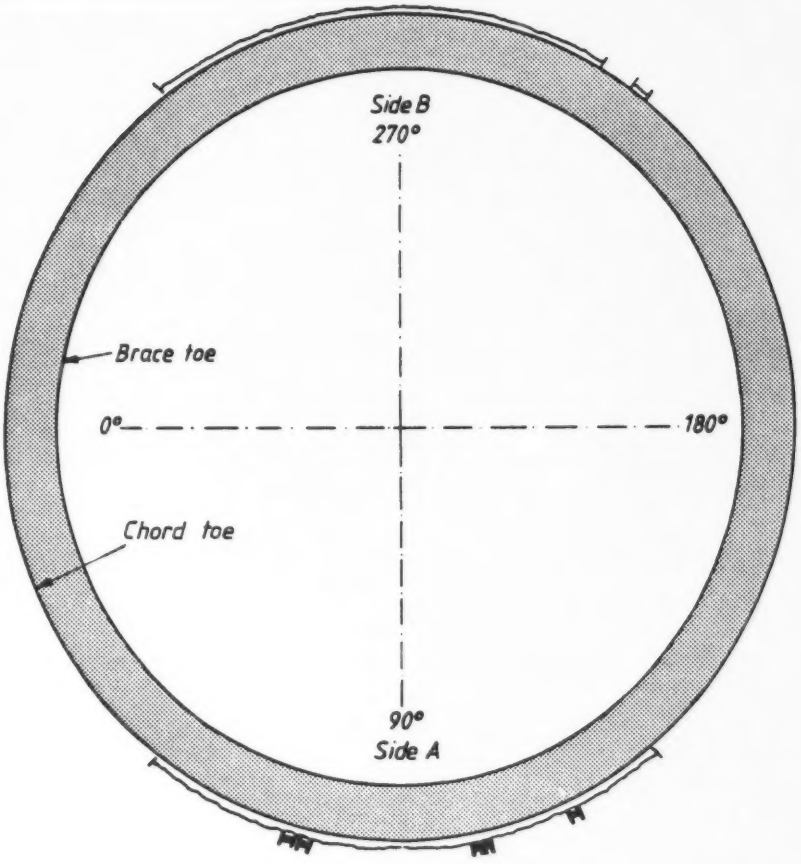

10mm

First detected cracking

Extent of final crack

APPENDIX A: Extent of cracking in tubular joints

Specimen No. 20

Repair welded

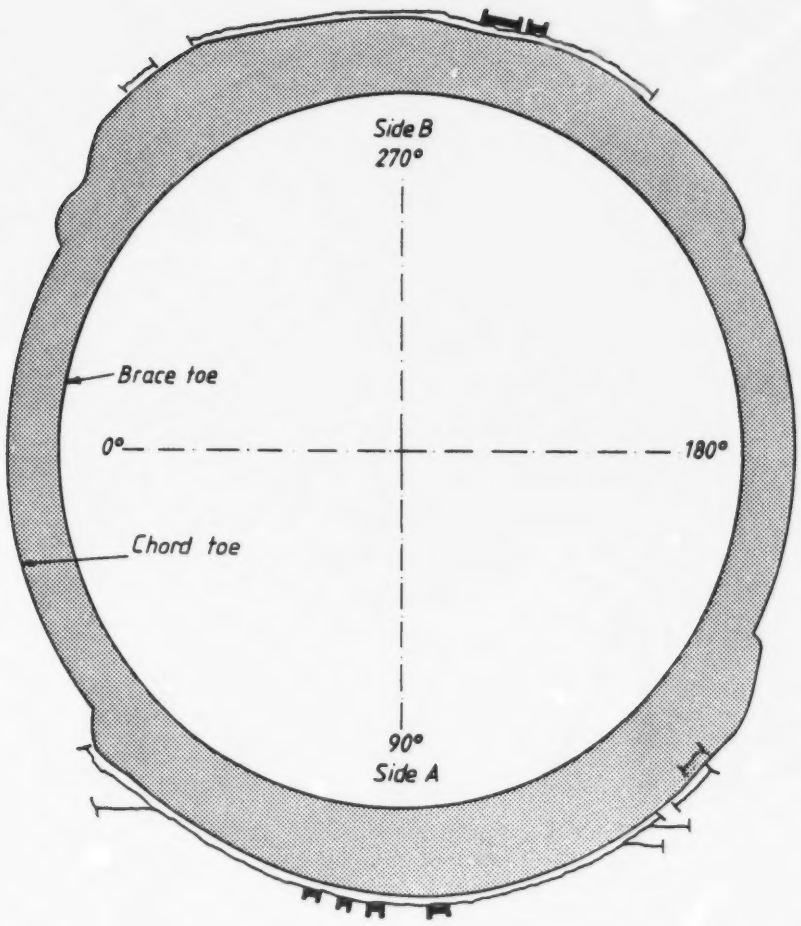

10mm

First detected cracking

Extent of final crack

APPENDIX A: Extent of cracking in tubular joints

Specimen No. 5
Precracking

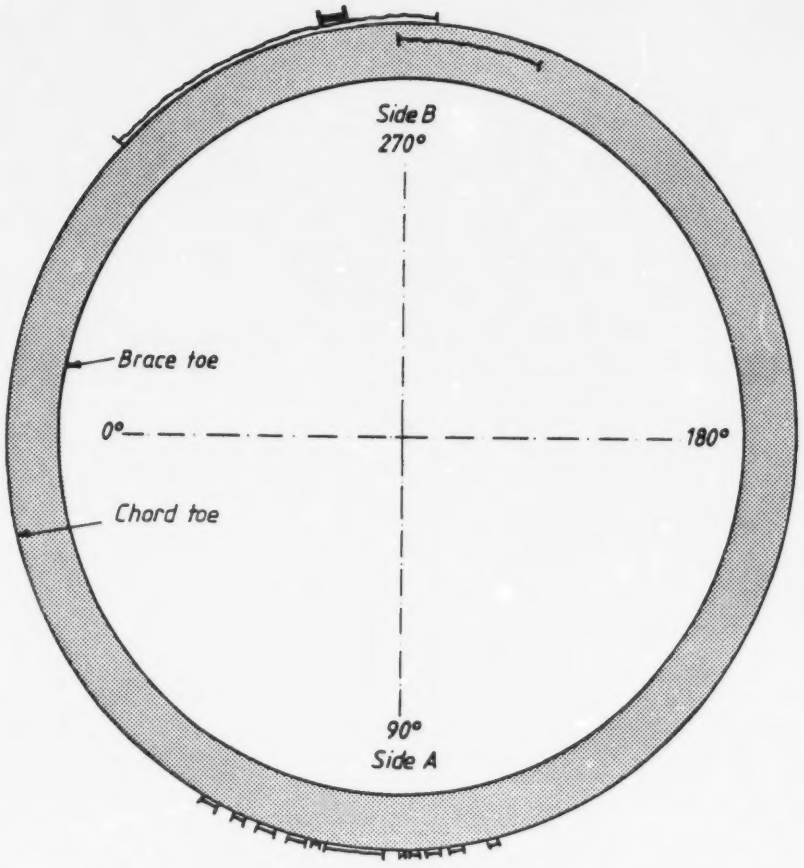

10mm

First detected cracking

Extent of final crack

APPENDIX A: Extent of cracking in tubular joints

Specimen No. 5
Repair welded

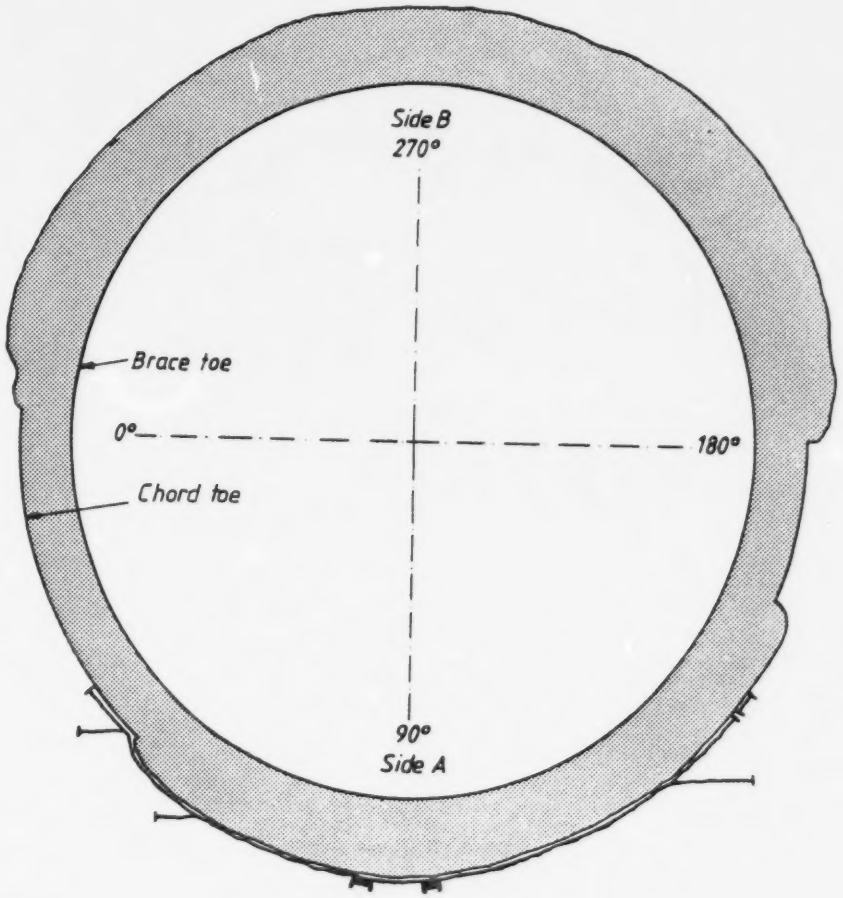

10mm

First detected cracking

Extent of final crack

APPENDIX A: Extent of cracking in tubular joints

Specimen No.6
Precracking

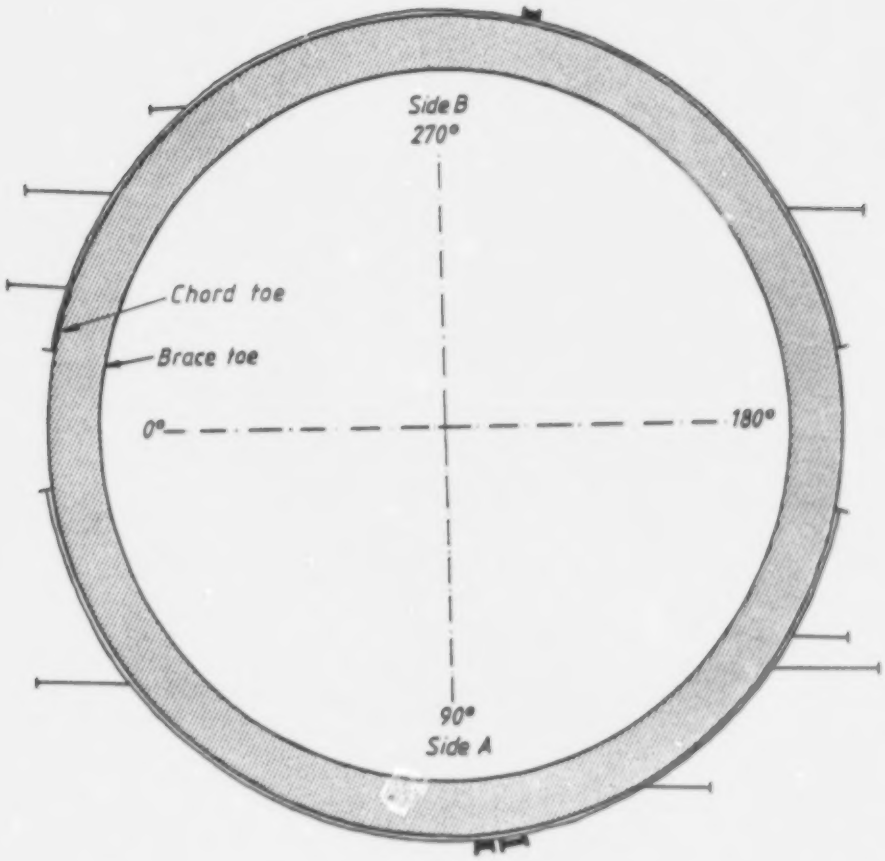

10mm

First detected cracking

Extent of final crack

APPENDIX A: Extent of cracking in tubular joints

Specimen No.15
Precracking

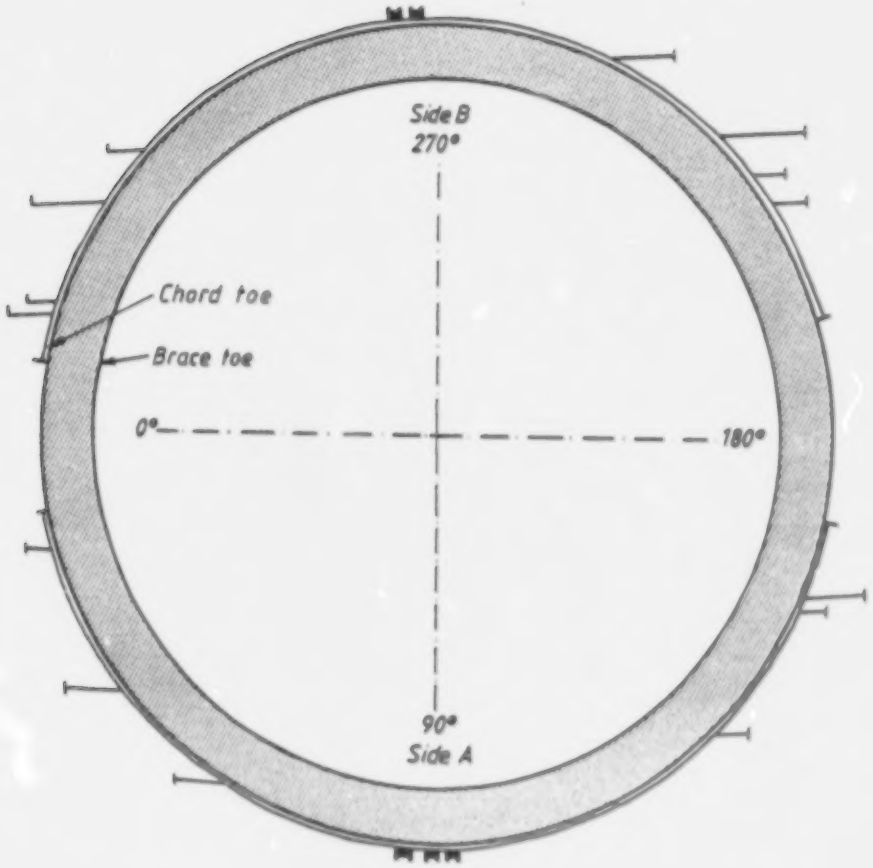

10mm

First detected cracking

Extent of final crack

APPENDIX A: Extent of cracking in tubular joints

Specimen No.15
Repair welded and burr ground

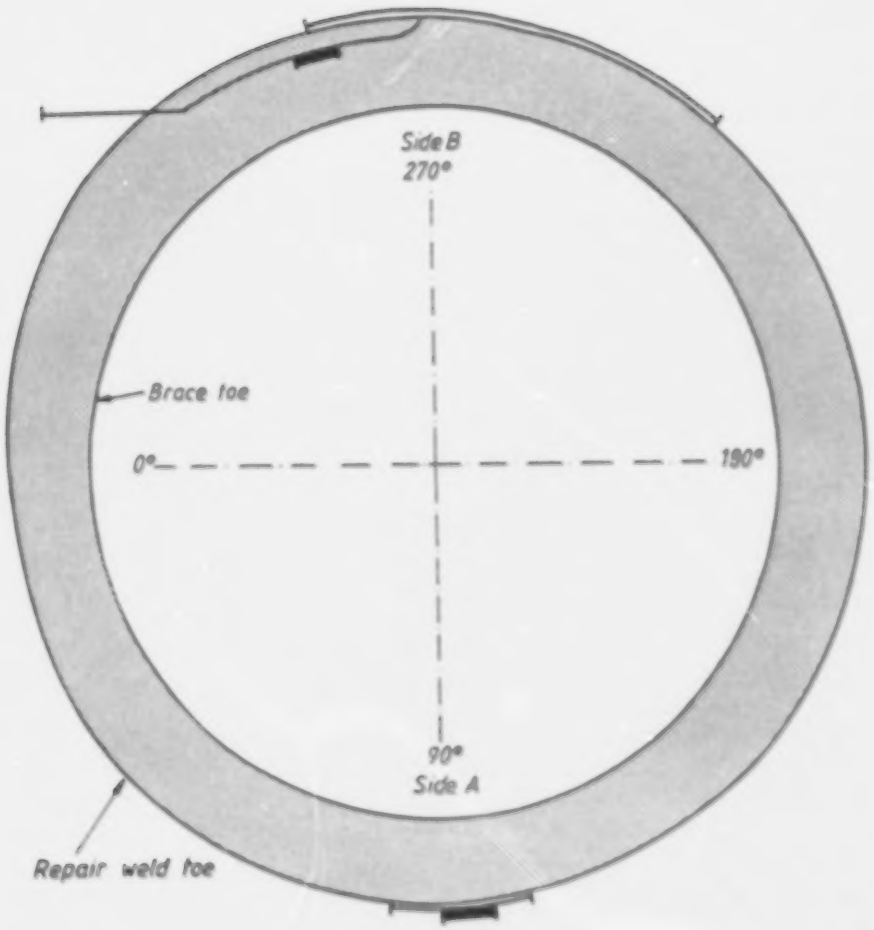

10mm

First detected cracking

Extent of final crack

APPENDIX A: Extent of cracking in tubular joints

Specimen No. 23
Precracking

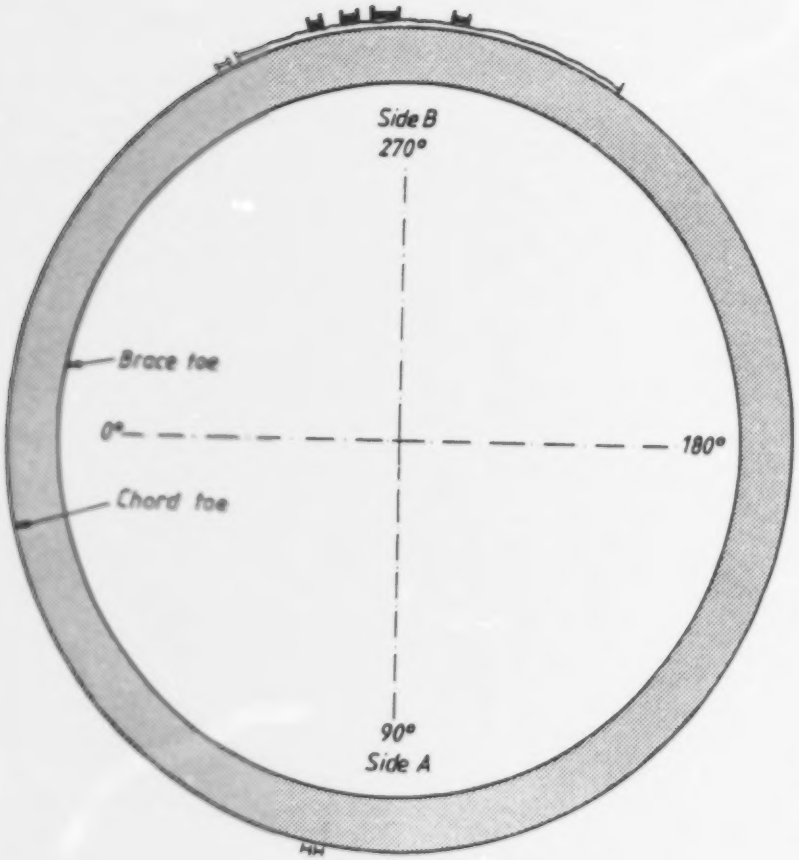

10mm

First detected cracking

Extent of final crack

APPENDIX A: Extent of cracking in tubular joints

Specimen No. 24
Precracking

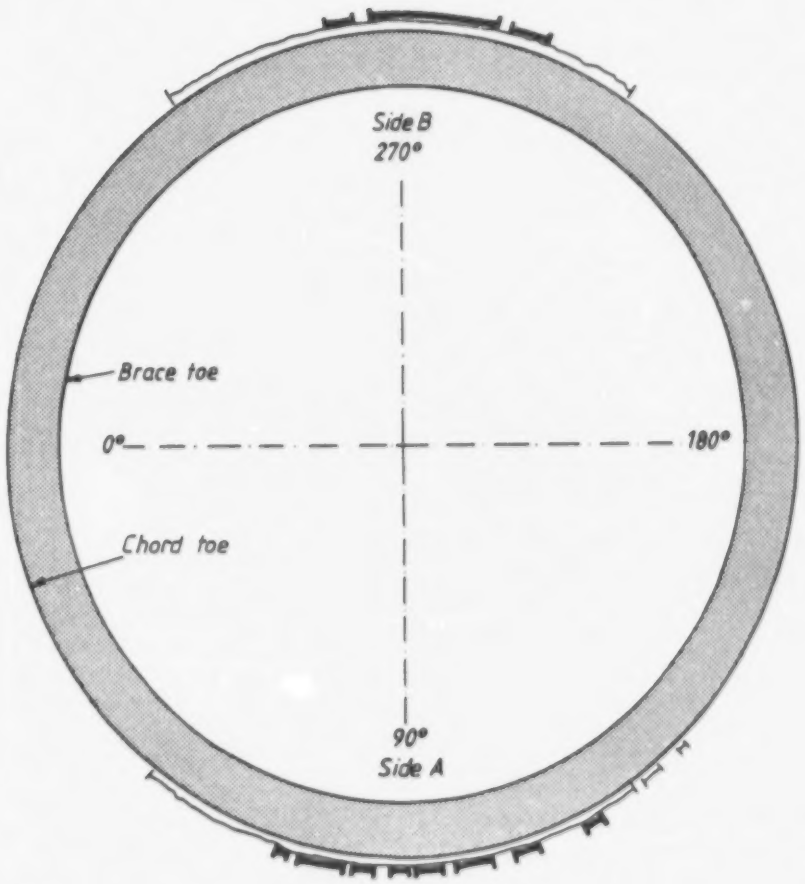

10mm

First detected cracking

Extent of final crack

APPENDIX A: Extent of cracking in tubular joints

Specimen No. 16
Precracking

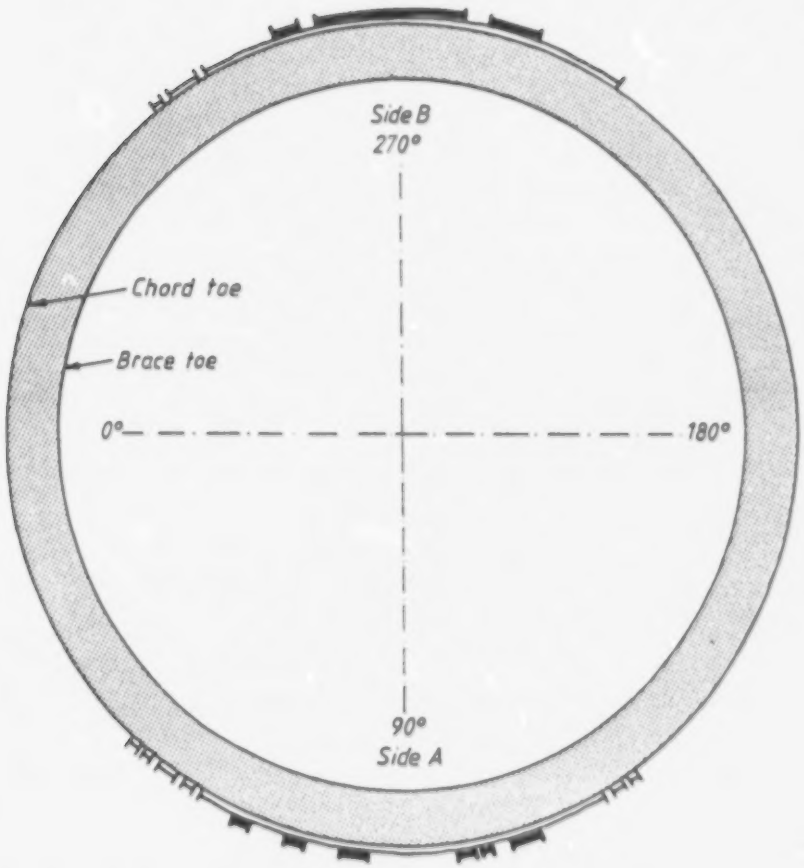

10mm

First detected cracking

Extent of final crack

APPENDIX A: Extent of cracking in tubular joints

Specimen No. 16
Repair welded and burr ground

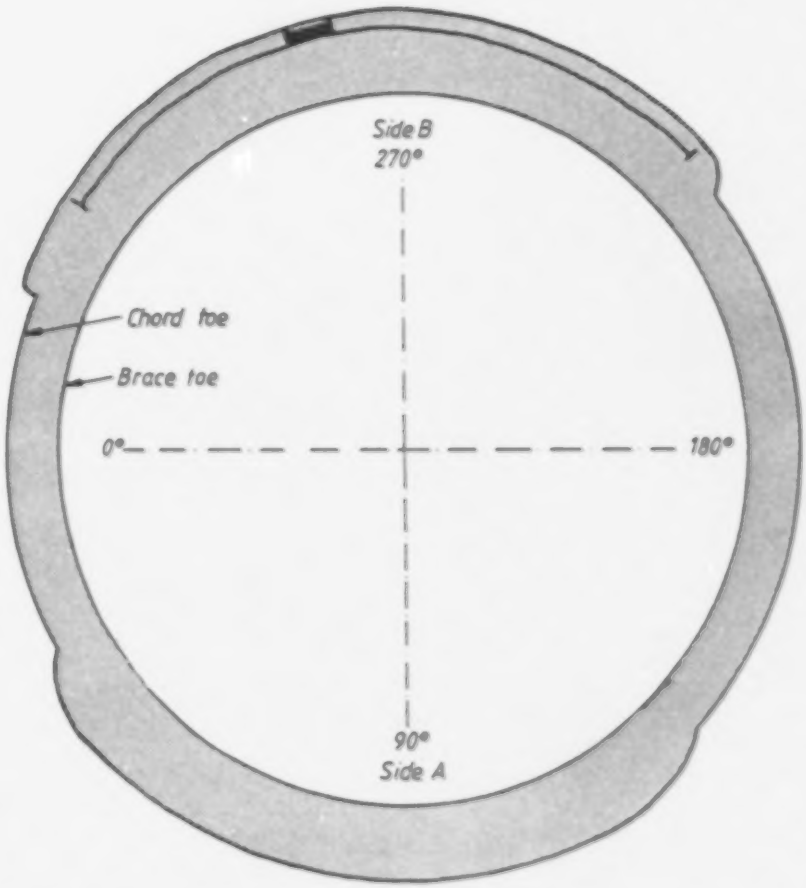

10mm

First detected cracking

Extent of final crack

APPENDIX A: Extent of cracking in tubular joints

Specimen No.7
Precracking

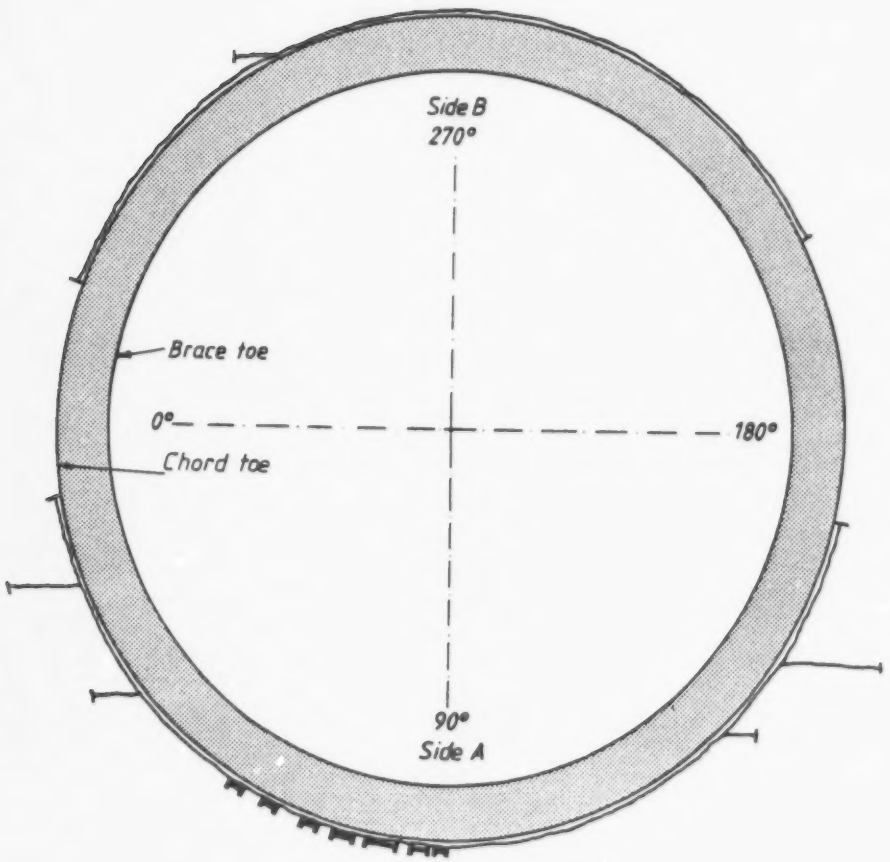

10mm

First detected cracking

Extent of final crack

APPENDIX A: Extent of cracking in tubular joints

Specimen No.7
Hole drilling

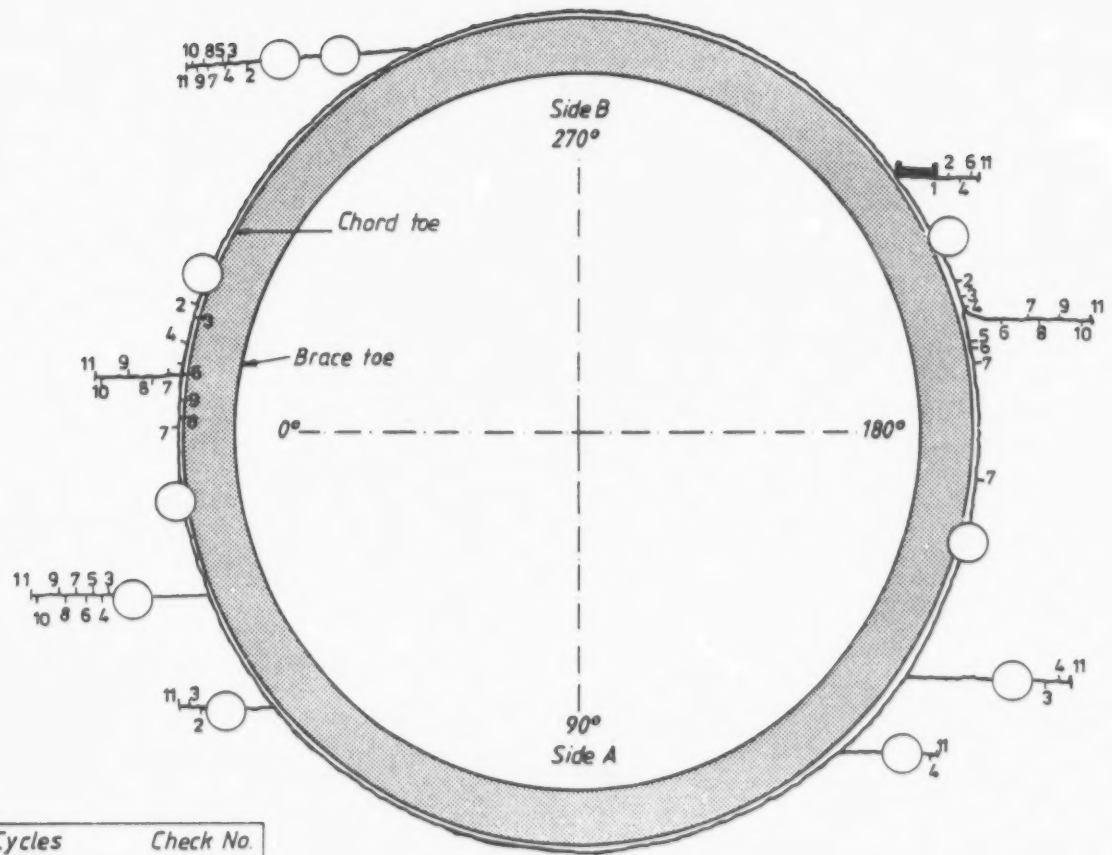

Cycles	*Check No.*
9760	*1*
29591	*2*
67060	*3*
104690	*4*
151306	*5*
179340	*6*
226580	*7*
247450	*8*
261980	*9*
304600	*10*
315100	*11*

10mm

First detected cracking

Extent of final crack

APPENDIX A: Extent of cracking in tubular joints

Specimen No. 8
Precracking

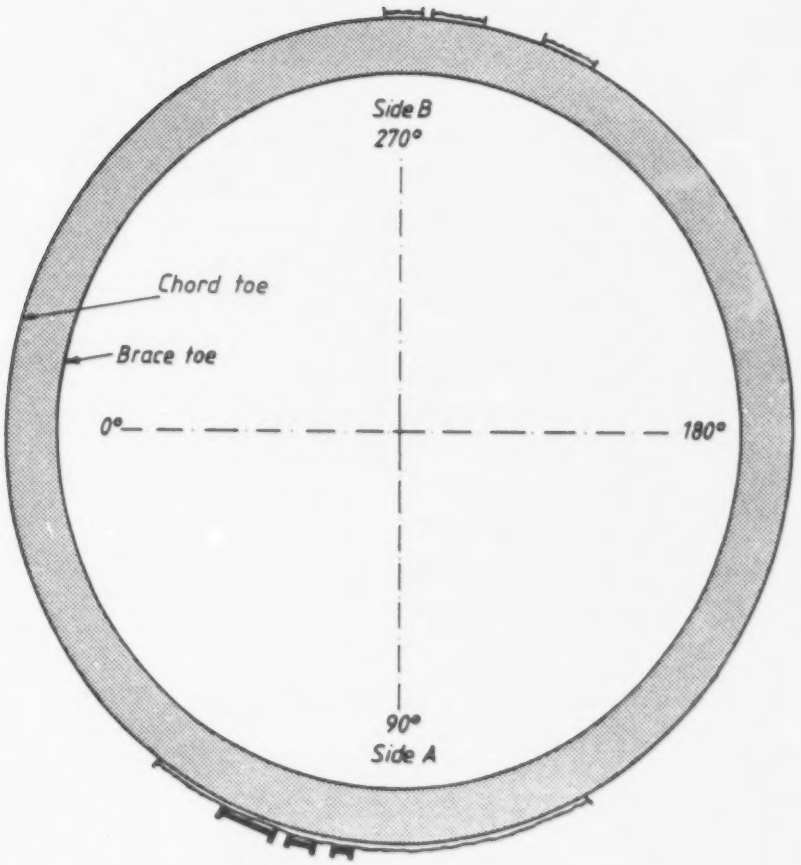

10mm

First detected cracking

Extent of final crack

APPENDIX A: Extent of cracking in tubular joints

Specimen No.8
Hole drilling

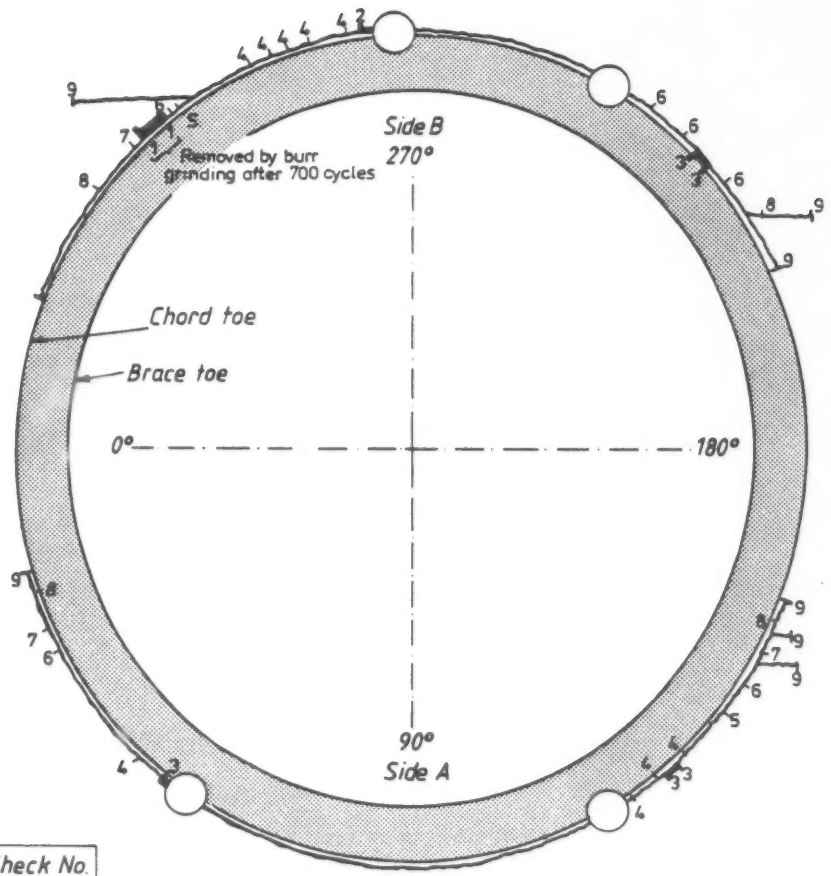

Cycles	Check No.
700	1
6000	2
13000	3
37200	4
75000	5
109400	6
150800	7
190300	8
235500	9

10mm

First detected cracking

Extent of final crack

APPENDIX A: Extent of cracking in tubular joints

Specimen No.17
Precracking

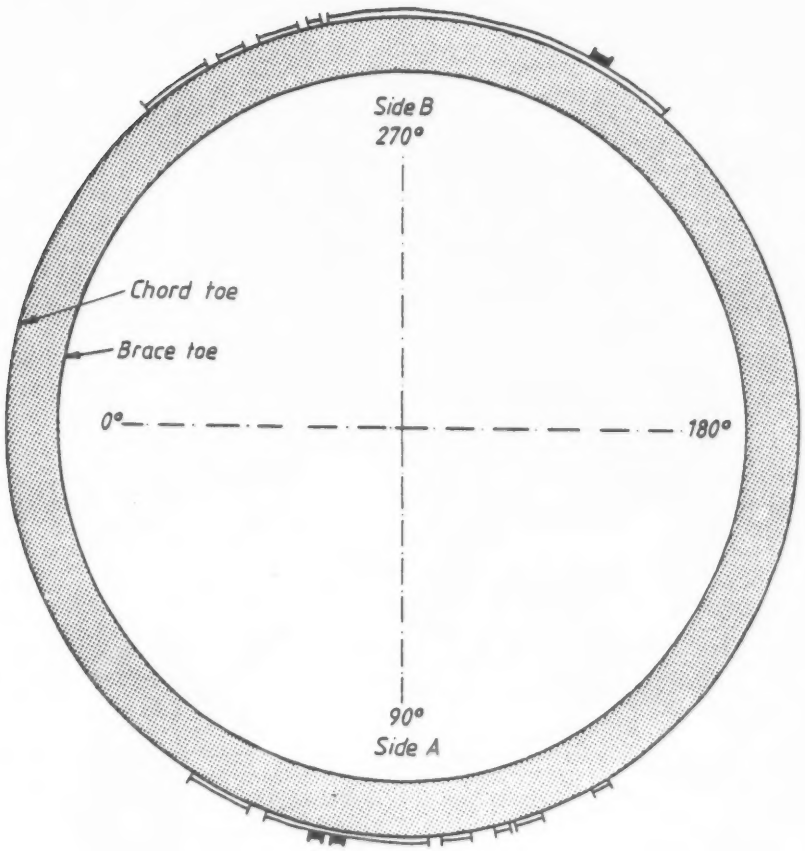

10mm

First detected cracking

Extent of final crack

APPENDIX A: Extent of cracking in tubular joints

Specimen No.17
Burr ground

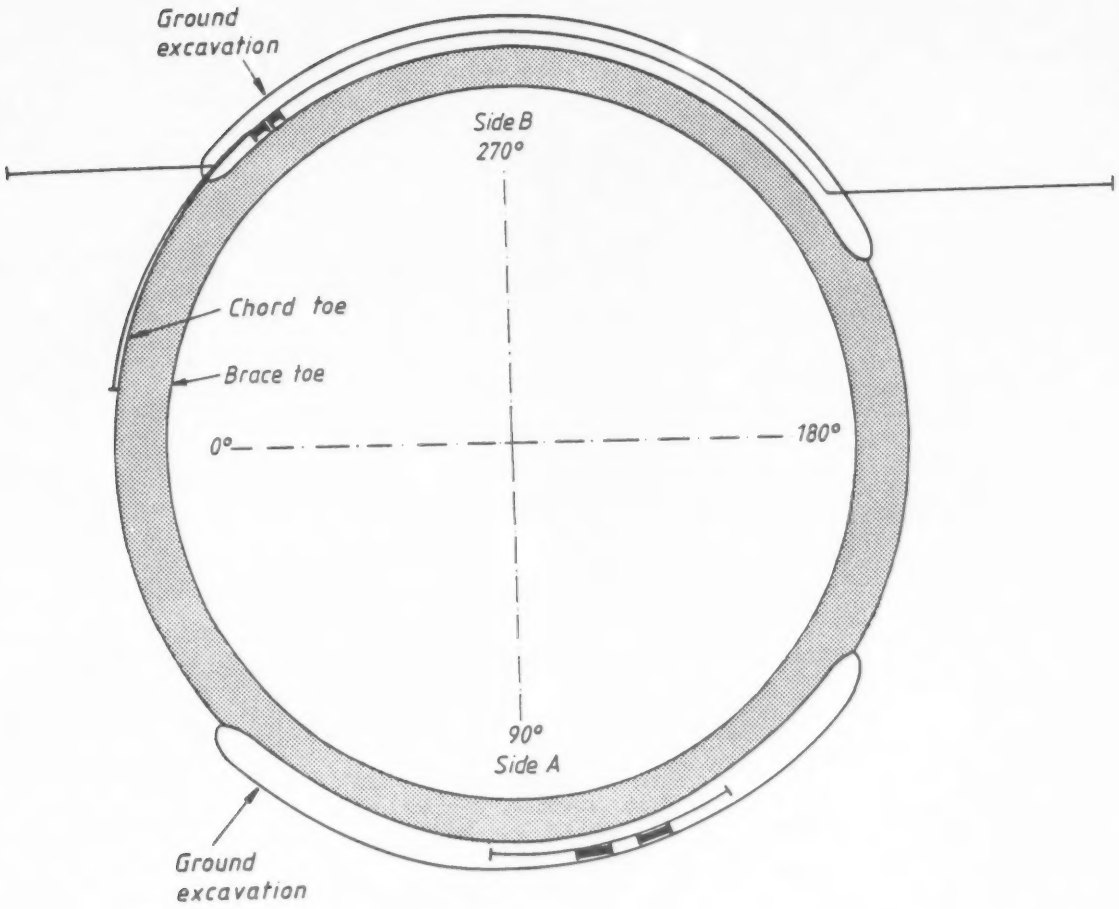

10mm

First detected cracking

Extent of final crack

APPENDIX A: Extent of cracking in tubular joints

Specimen No. 21
Precracking

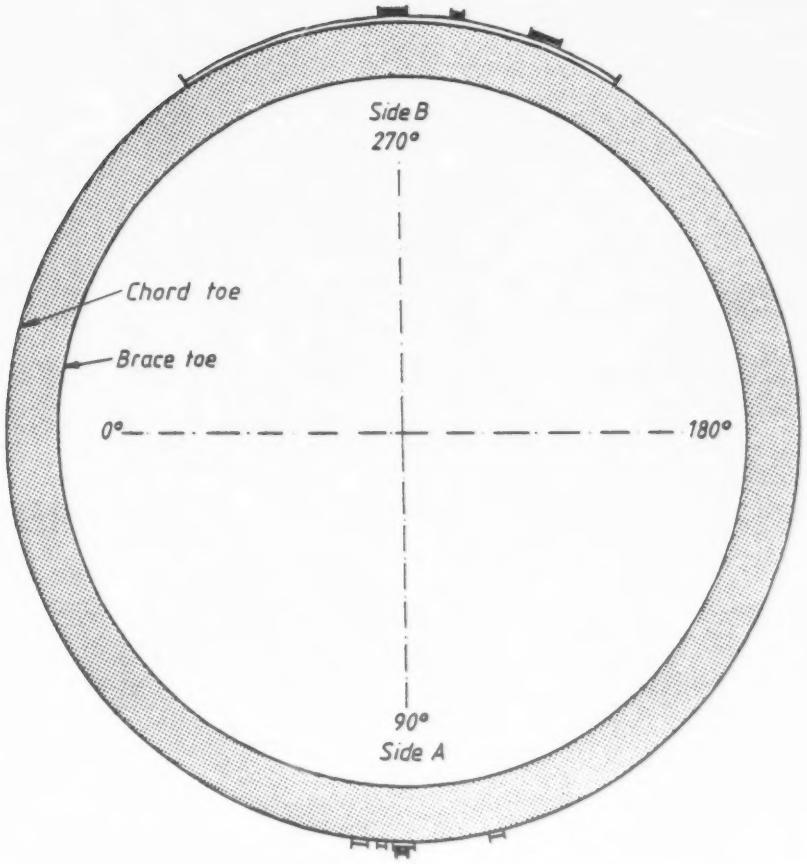

10mm

First detected cracking

Extent of final crack

APPENDIX A: Extent of cracking in tubular joints

Specimen No. 21
Burr ground

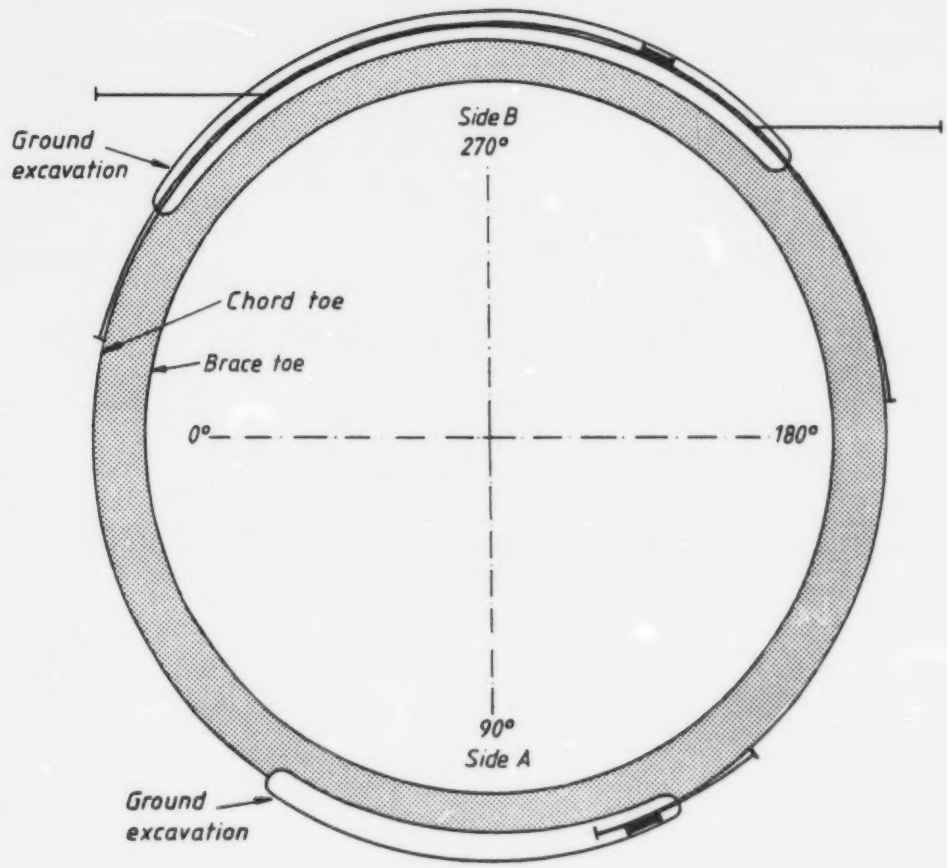

10mm

First detected cracking

Extent of final crack

APPENDIX A: Extent of cracking in tubular joints

Specimen No.11
Precracking

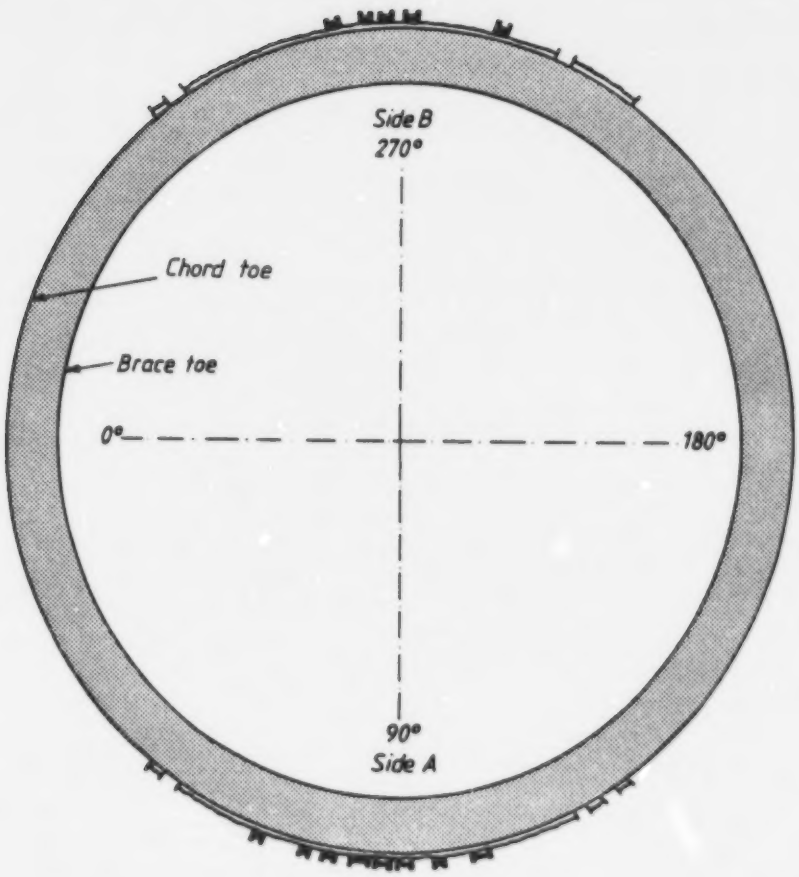

10mm

First detected cracking

Extent of final crack

APPENDIX A: Extent of cracking in tubular joints

Specimen No.11
Burr ground

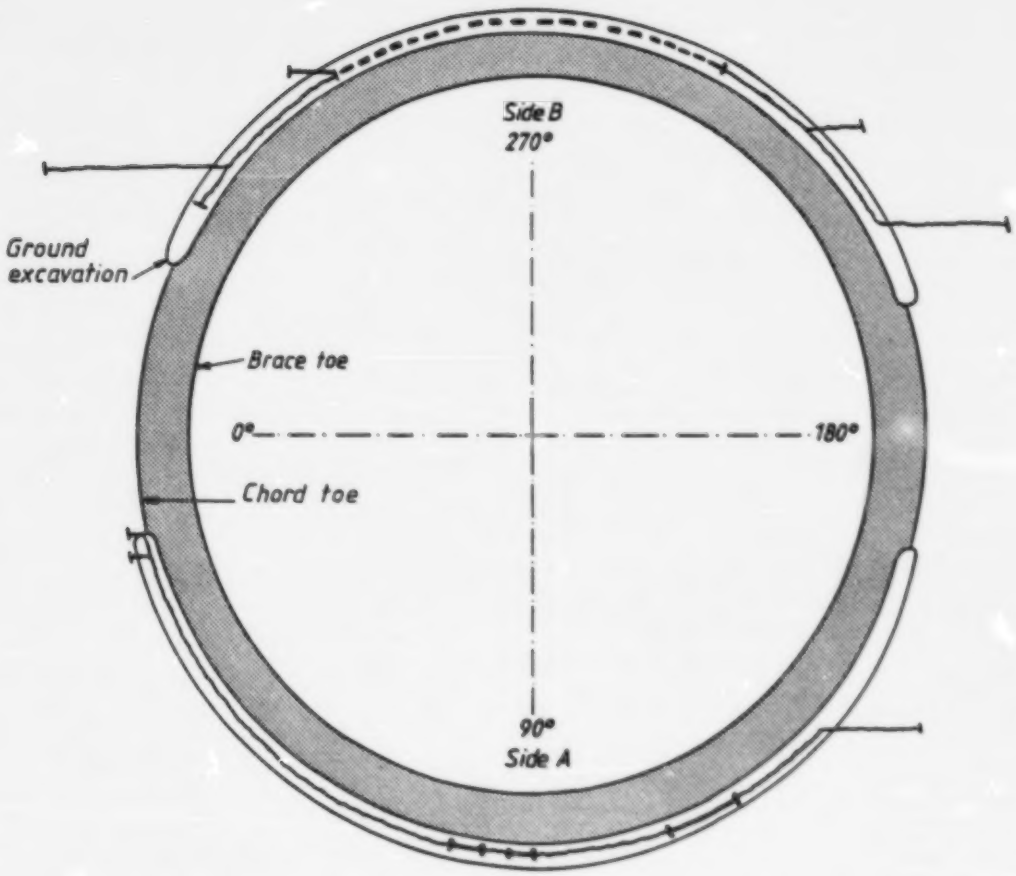

10mm

First detected cracking

Extent of final crack

APPENDIX A: Extent of cracking in tubular joints

Specimen No. 10
Precracking

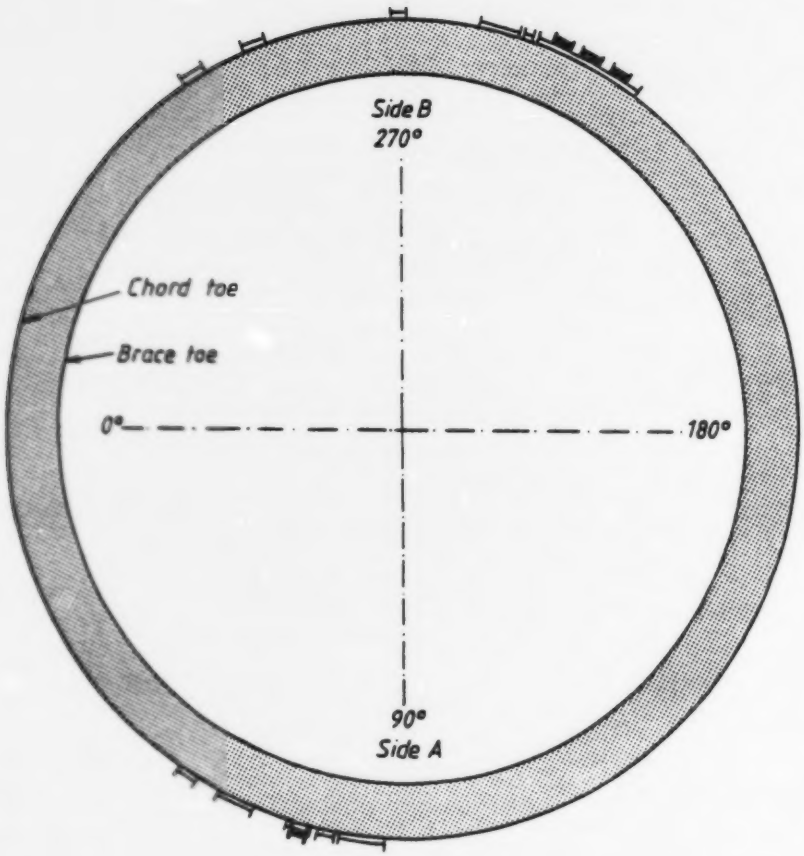

10mm

First detected cracking

Extent of final crack

APPENDIX A: Extent of cracking in tubular joints

Specimen No.10
Burr ground

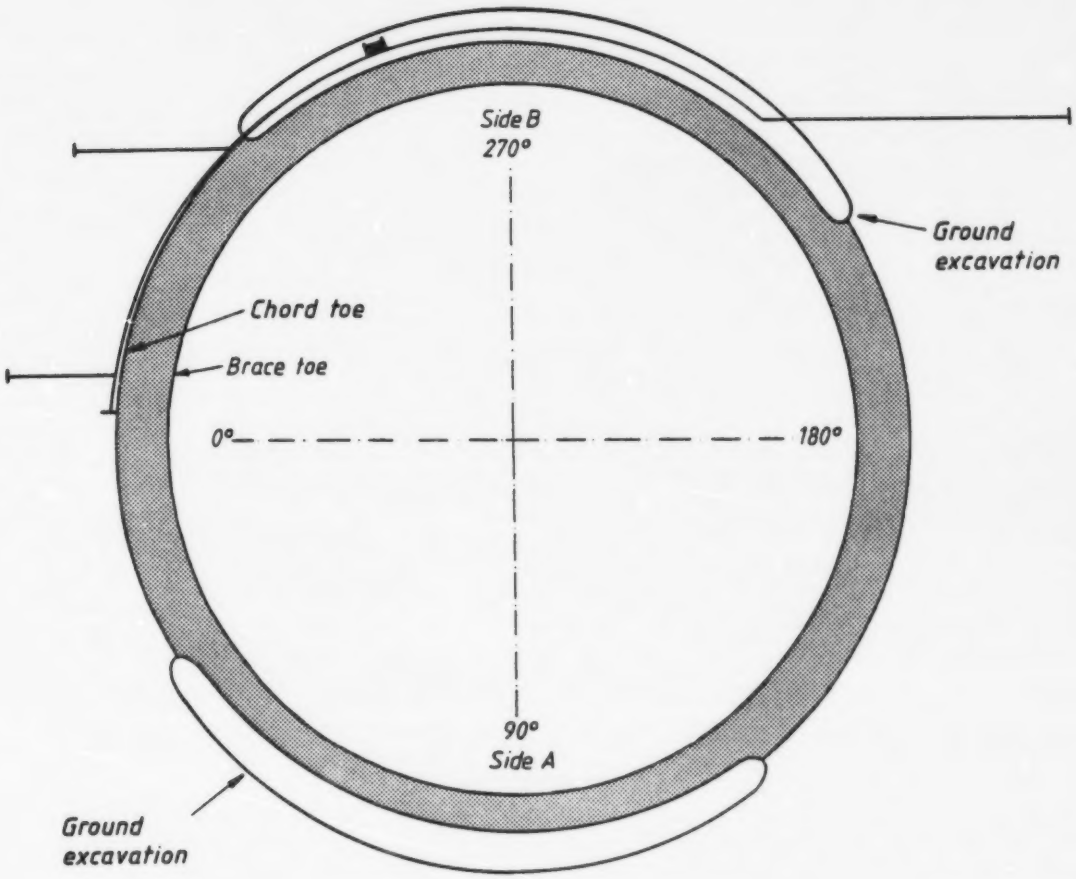

10mm

First detected cracking

Extent of final crack

APPENDIX A: Extent of cracking in tubular joints

Specimen No.18
Precracking

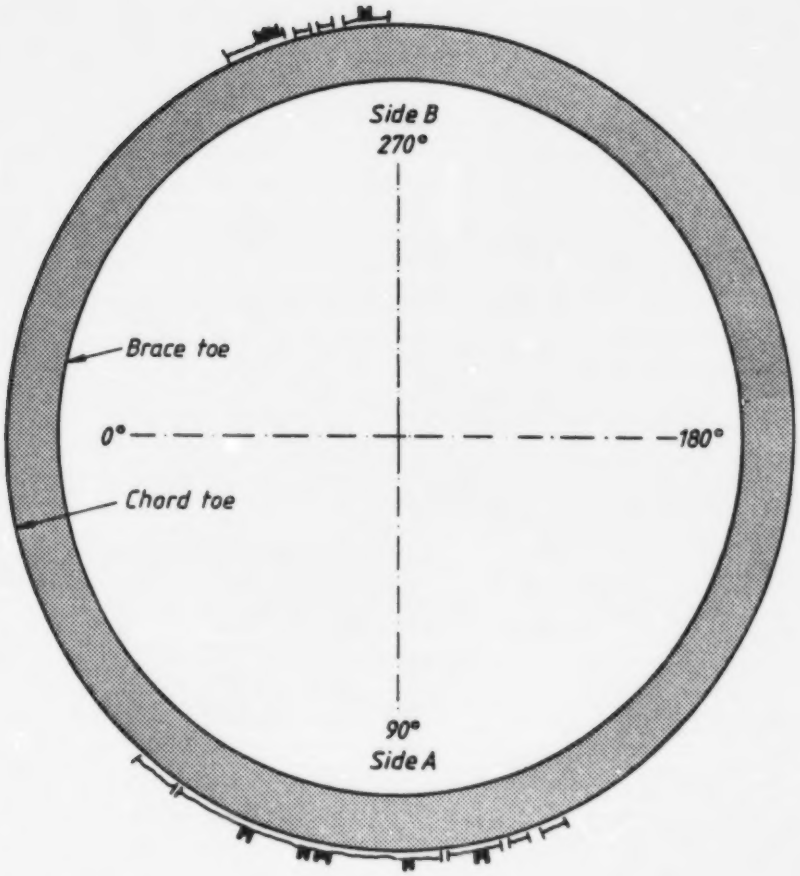

10mm

First detected cracking

Extent of final crack

APPENDIX A: Extent of cracking in tubular joints

Specimen No. 18
Burr ground

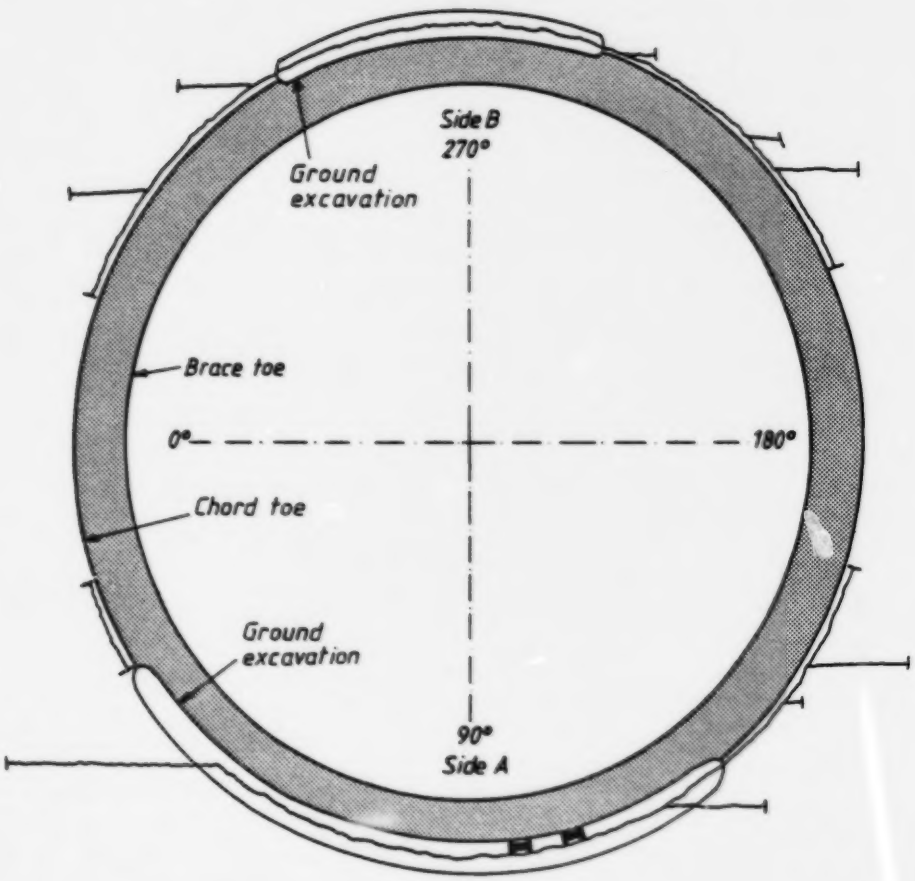

10mm

First detected cracking

Extent of final crack

APPENDIX A: Extent of cracking in tubular joints

Specimen No. 12
Precracking

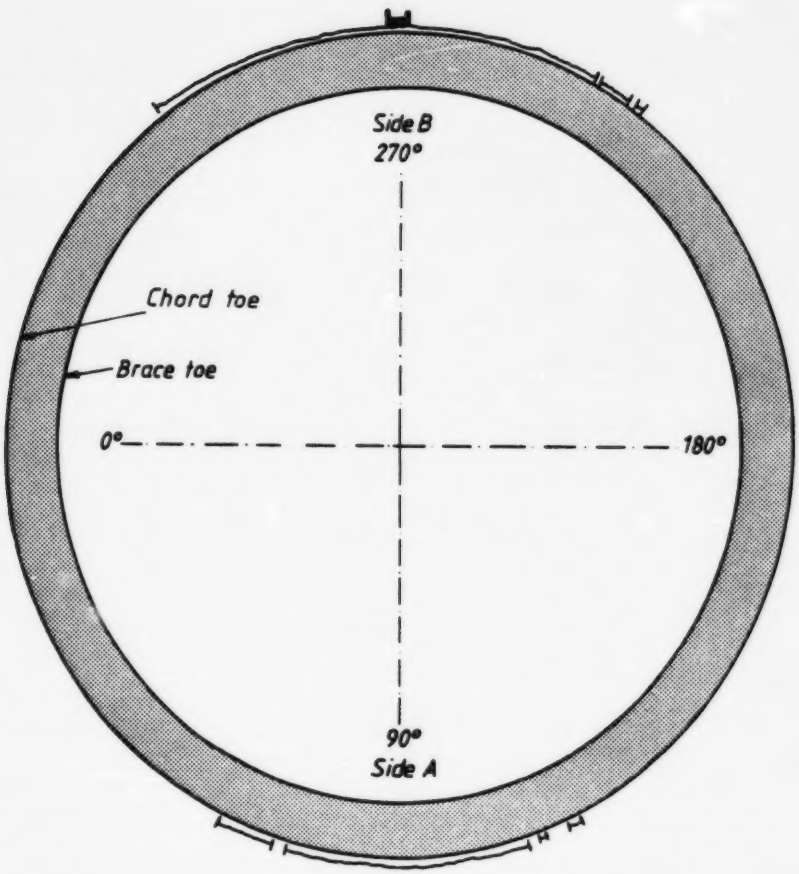

10mm

First detected cracking

Extent of final crack

APPENDIX A: Extent of cracking in tubular joints

Specimen No.12
Burr ground

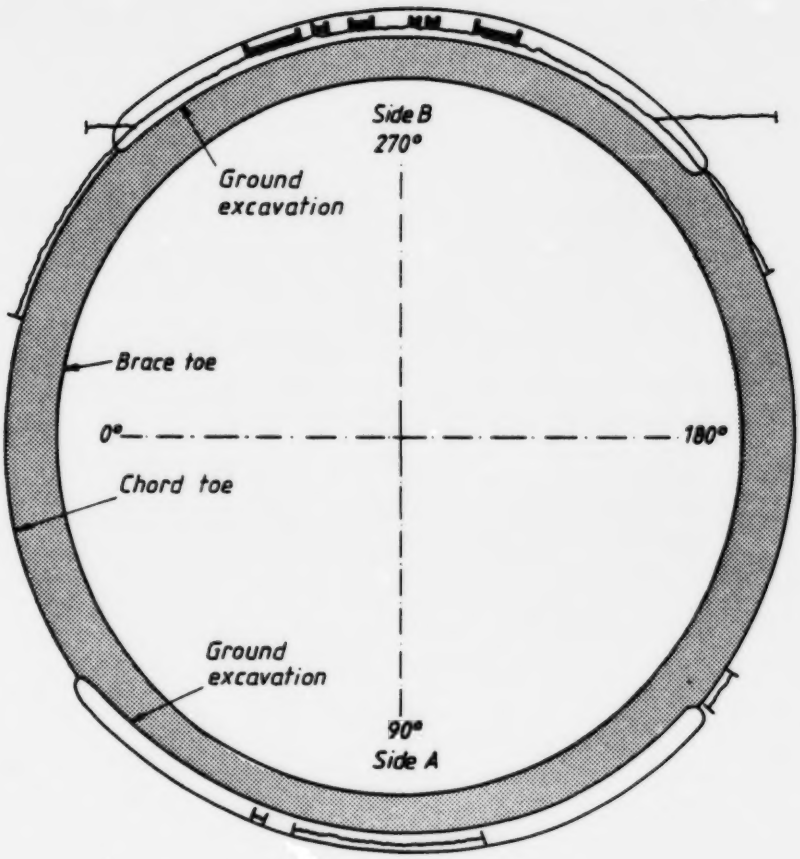

10mm

First detected cracking

Extent of final crack

APPENDIX A: Extent of cracking in tubular joints

Specimen No.14
Precracking

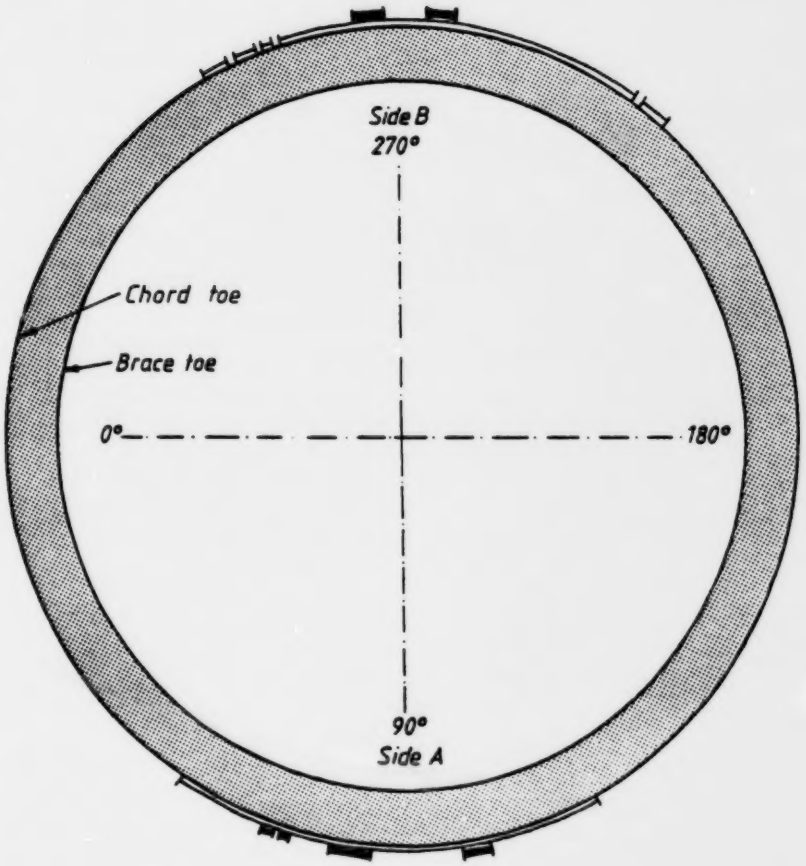

10mm

First detected cracking

Extent of final crack

APPENDIX A: Extent of cracking in tubular joints

Specimen No.14
Burr ground

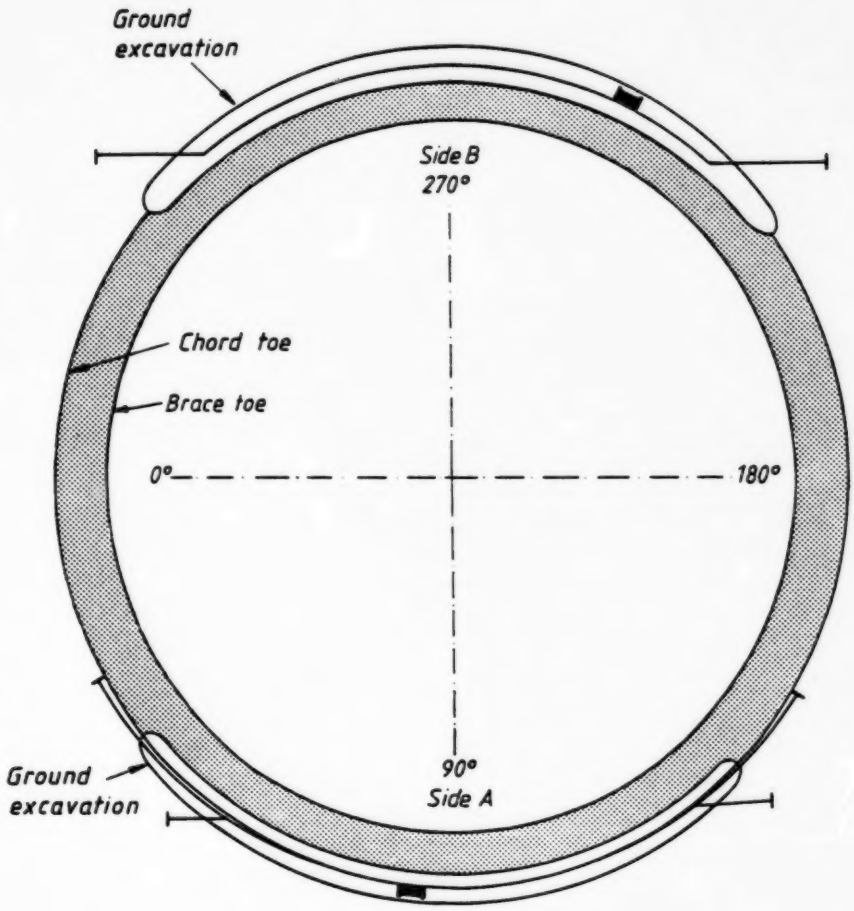

10mm

First detected crackin

Extent of final crack

APPENDIX A: Extent of cracking in tubular joints

Specimen No. 22
Precracking

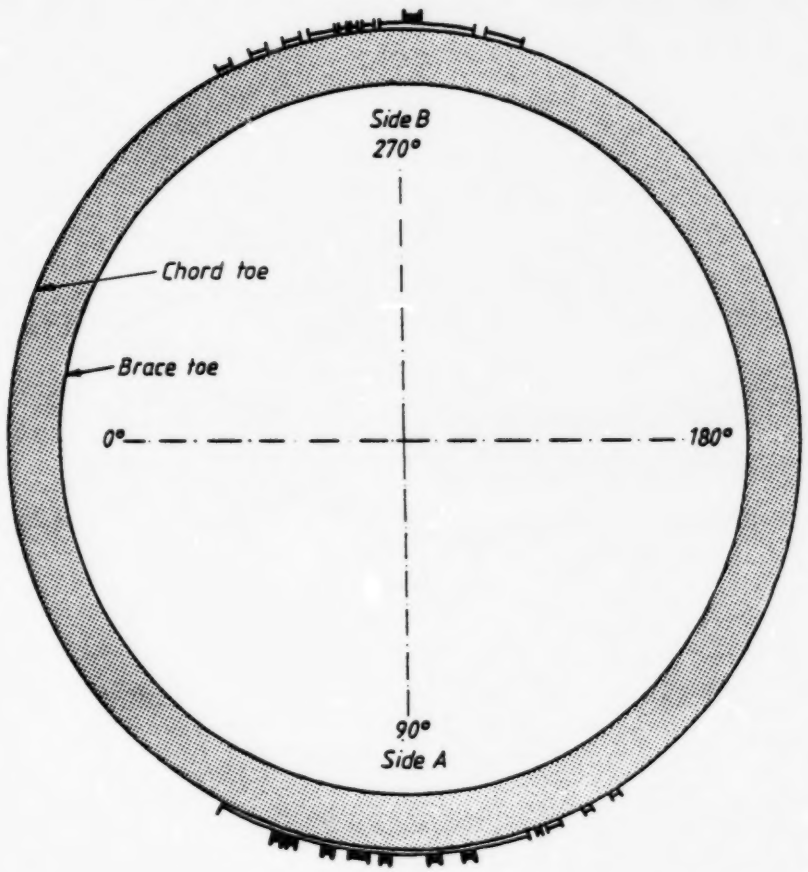

10mm

First detected cracking

Extent of final crack

APPENDIX A: Extent of cracking in tubular joints

Specimen No. 22
Burr ground

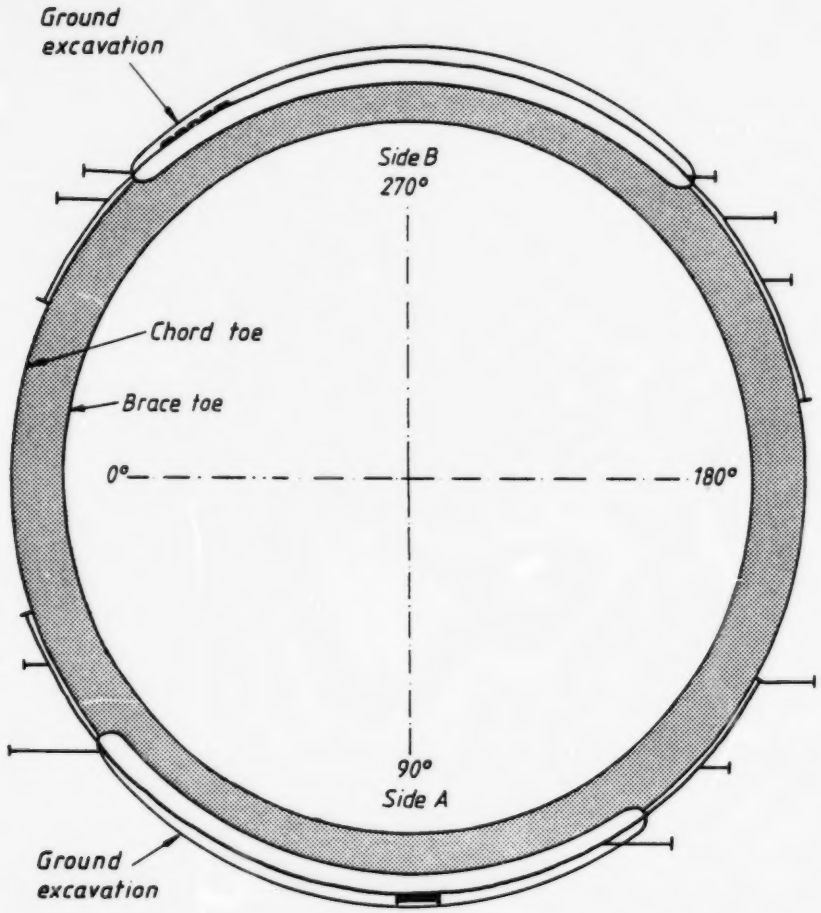

10mm

First detected cracking

Extent of final crack

APPENDIX A: Extent of cracking in tubular joints

Specimen No. 25
Precracking

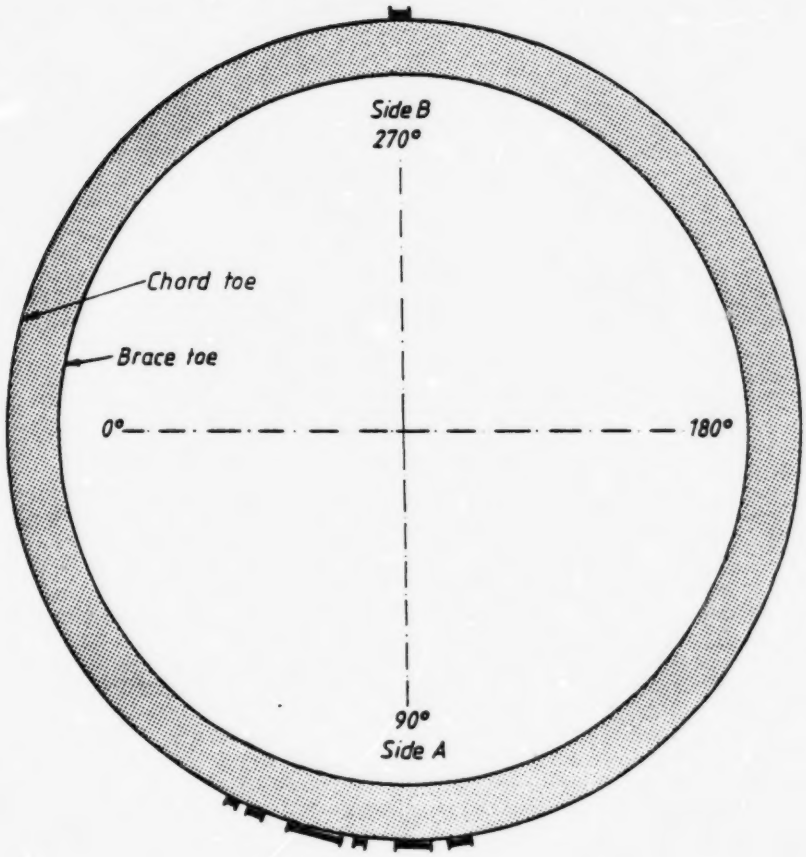

10mm

First detected cracking

Extent of final crack

APPENDIX A: Extent of cracking in tubular joints

Specimen No. 25
Burr ground
(2mm deep)

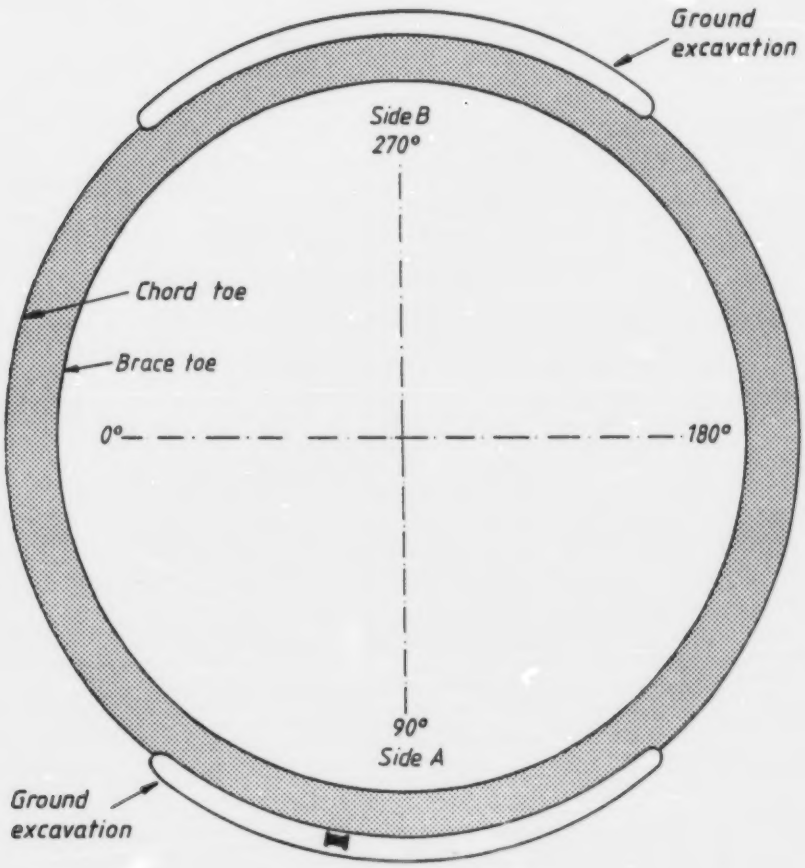

10mm

First detected cracking

Extent of final crack

APPENDIX A: Extent of cracking in tubular joints

Specimen No. 25
Burr ground
(4mm deep)

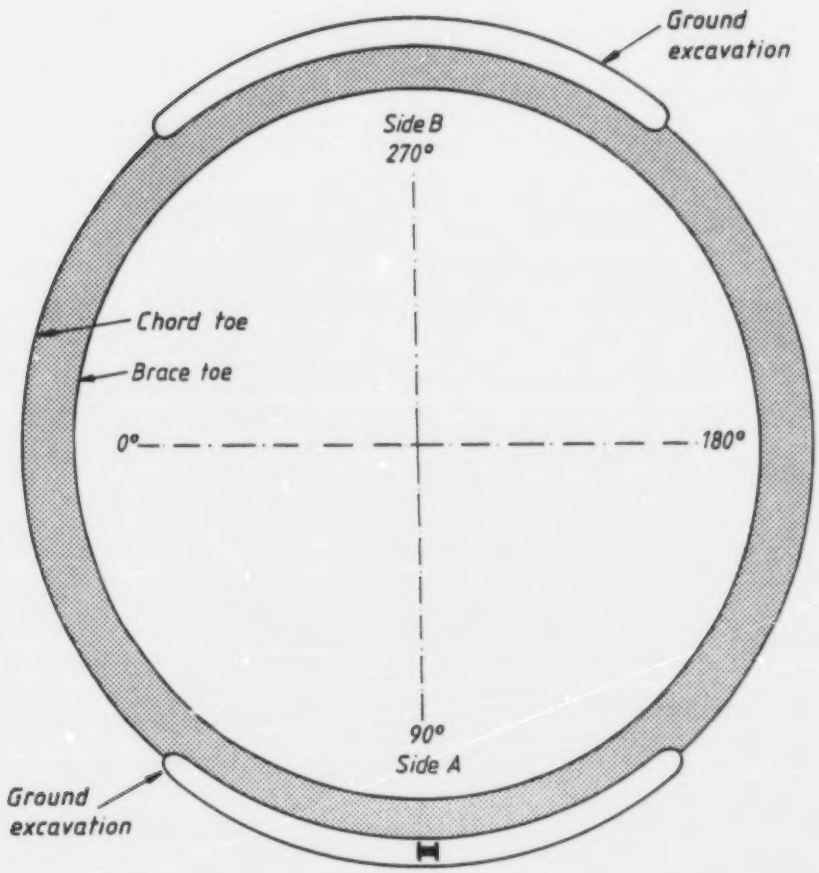

10mm

First detected cracking

Extent of final crack

APPENDIX A: Extent of cracking in tubular joints

Specimen No. 25
Burr ground
(6mm deep)

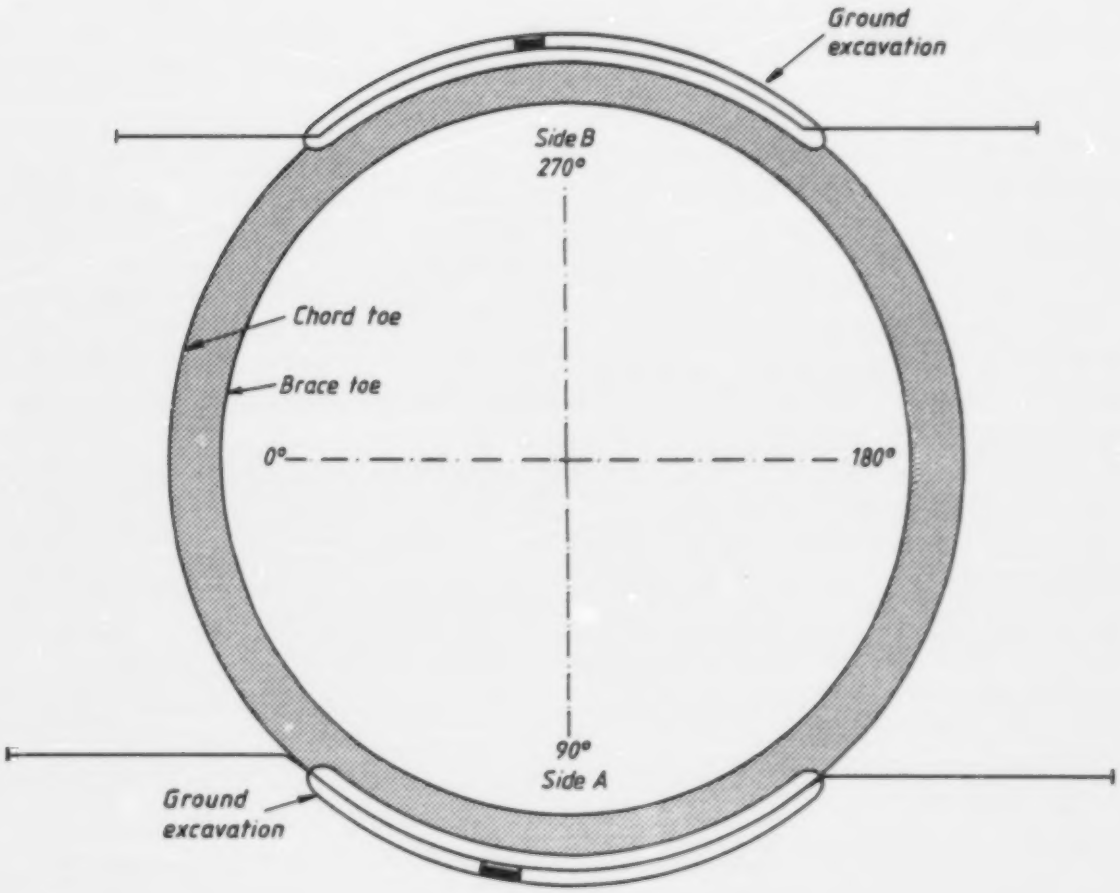

10mm

First detected cracking

Extent of final crack

APPENDIX B — Strain distributions in tubular joint specimens during precracking and after repair

The following graphs show the measured radial strain distributions in the chord wall plotted in terms of the strain range versus distance from the weld toe. The region assumed to be linear in the UKOSRP and ECSC guidelines (Ref.7 and 8 of main text) is shown on the diagrams. The strain gauges were arranged to give six measurement positions within this region. In some instances the strain values did not show a clear linear portion within these limits, see for example specimens 2 and 23. Nevertheless, to maintain consistency with the existing database of published results, the guidelines for hot spot strain determination were followed by fitting a straight line to the six points within the prescribed limits and extrapolating this to the weld toe. The lines were initially drawn by eye and the values so obtained are shown on each plot. For cases where the strains were particularly scattered subsequent checks by linear regression analysis were within 50 microstrain of the extrapolated values obtained by eye. Clearly many interpretations of the strain distributions are possible and, in the light of the results shown here, the validity of the guidelines may be questionable. However, for the purposes of the present investigation, a consistent interpretation has been adopted which allows comparisons between the results for the various repair methods and with published data.

The strain distributions measured during precracking are given for all specimens, and those measured after repair for repair welded specimens. Results of strain measurements in specimens repaired by grinding alone are presented in Appendix D.

APPENDIX B: Strain distributions in tubular joint specimens

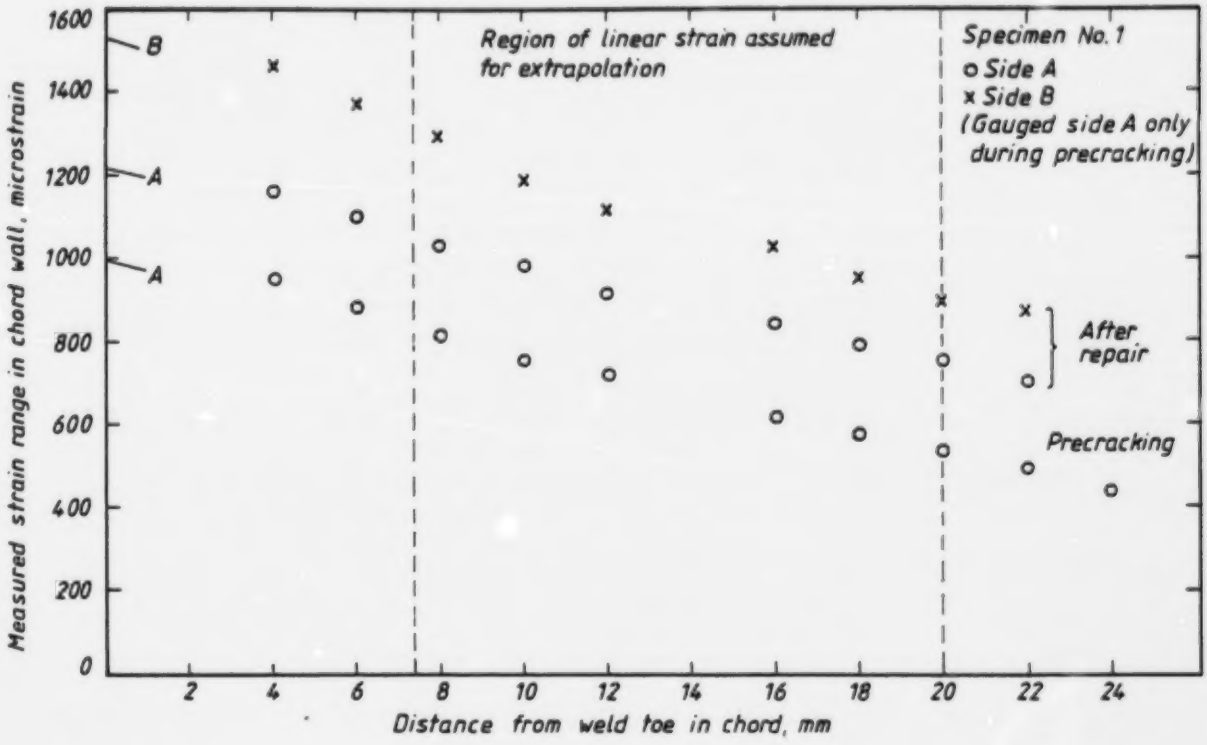

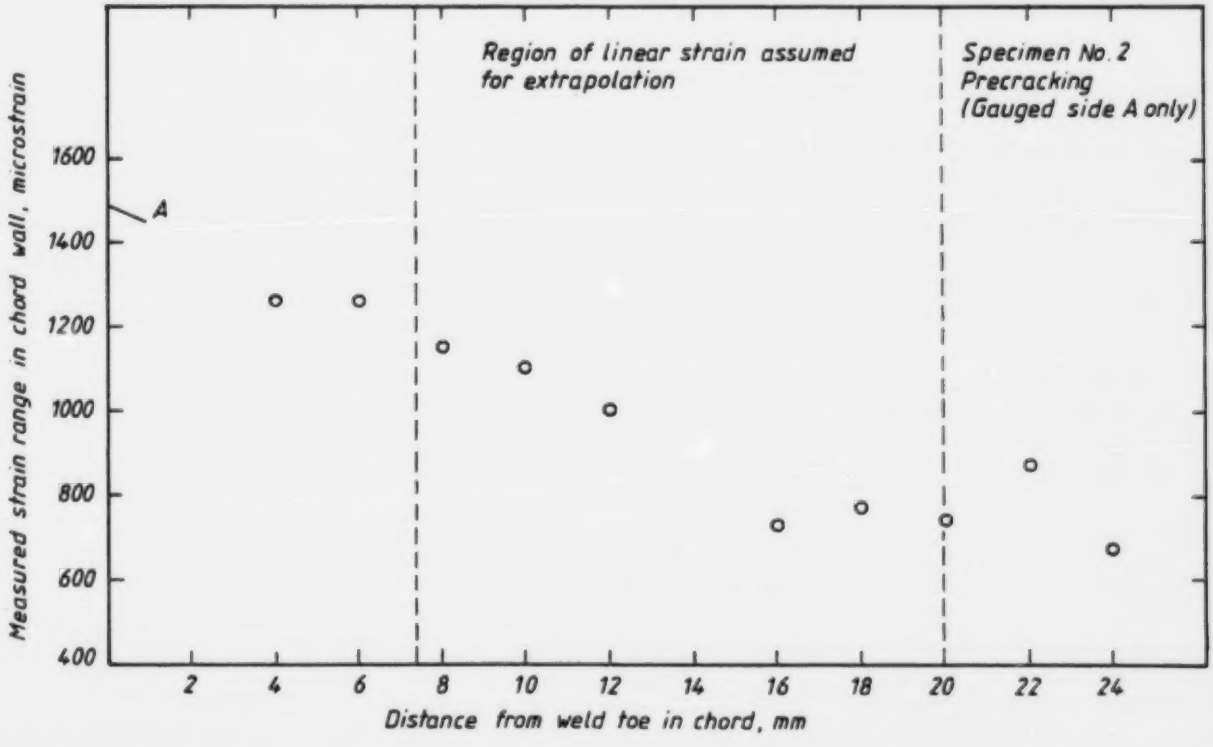

APPENDIX B: Strain distributions in tubular joint specimens

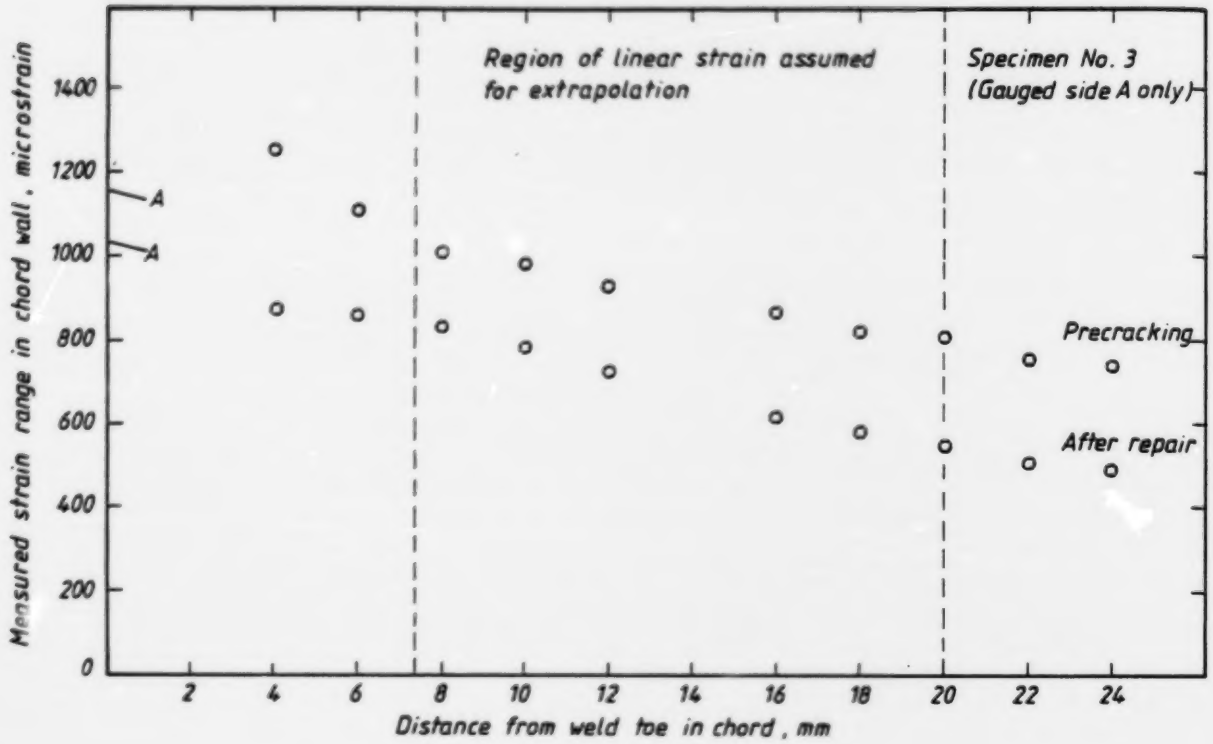

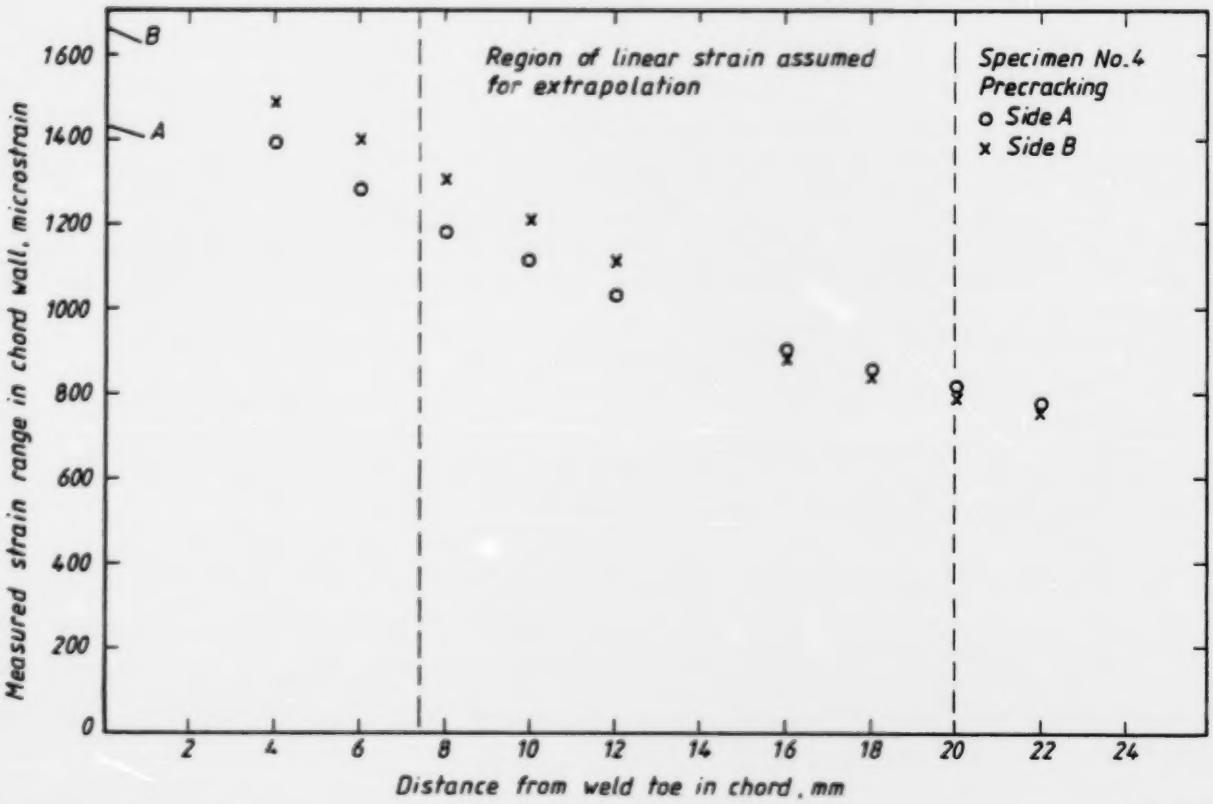

APPENDIX B: Strain distributions in tubular joint specimens

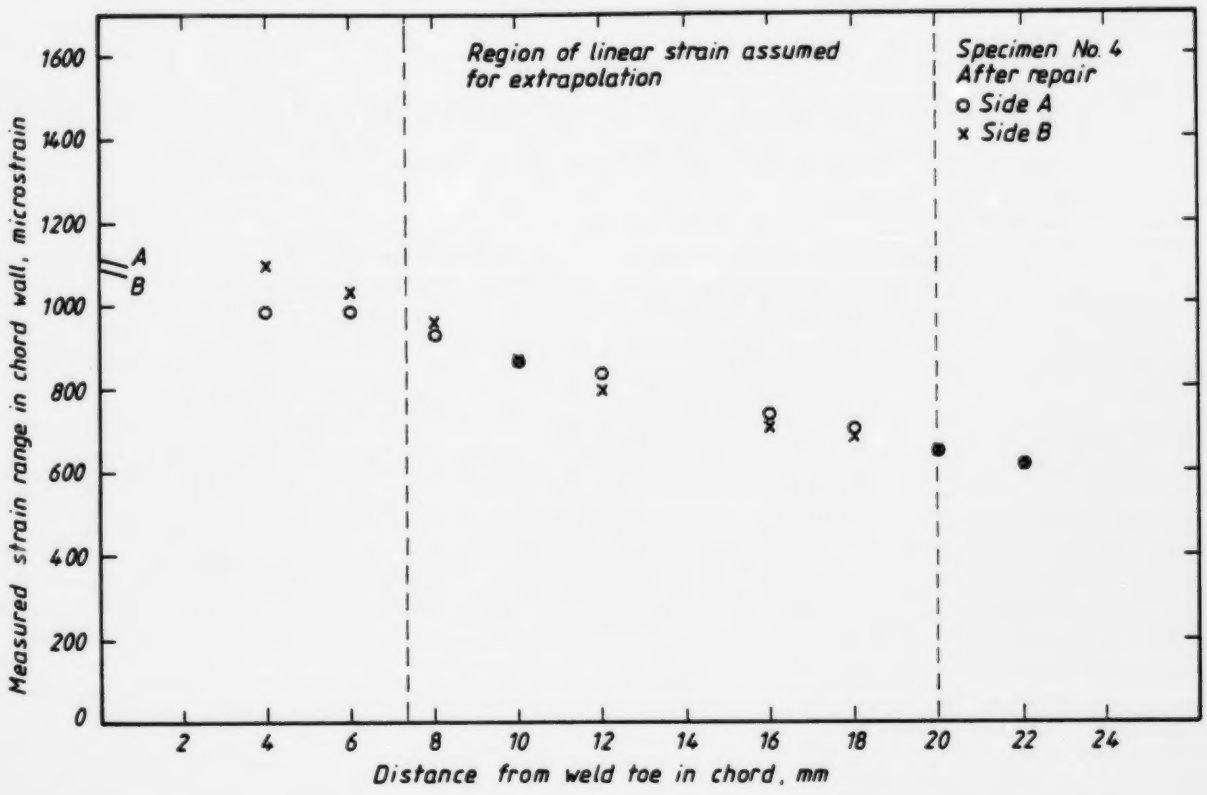

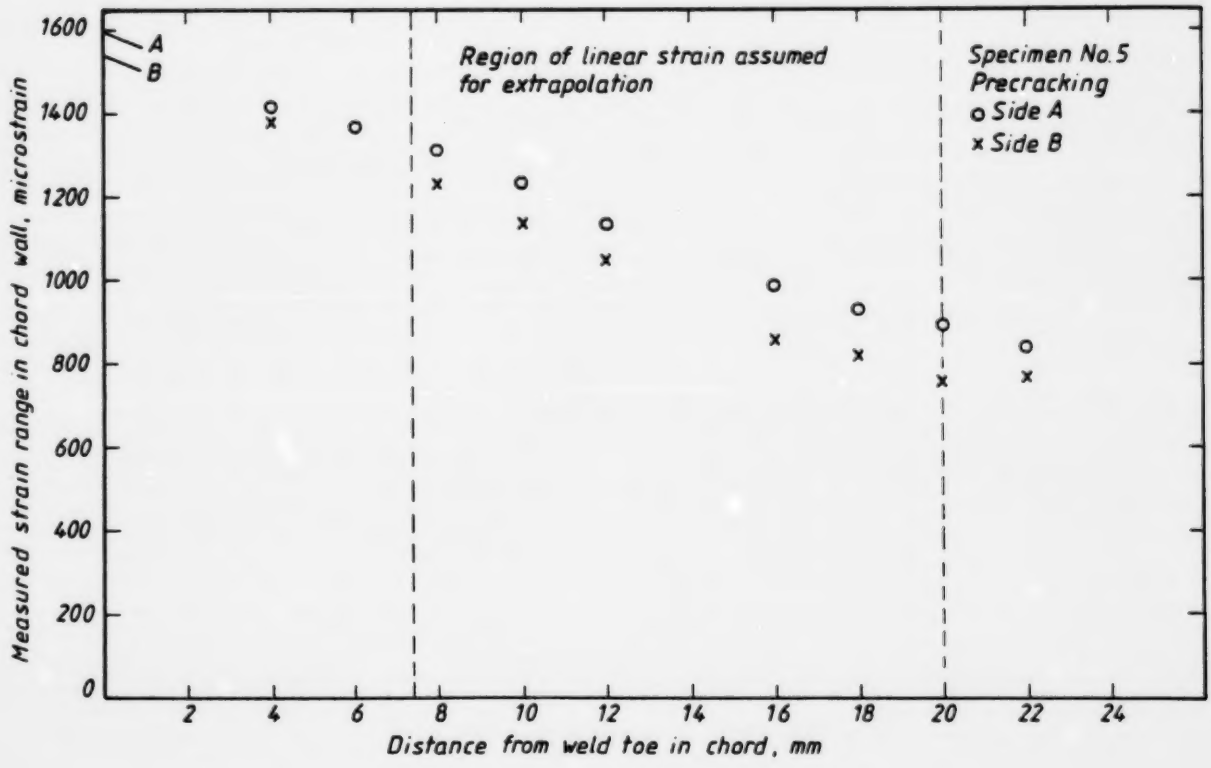

APPENDIX B: Strain distributions in tubular joint specimens

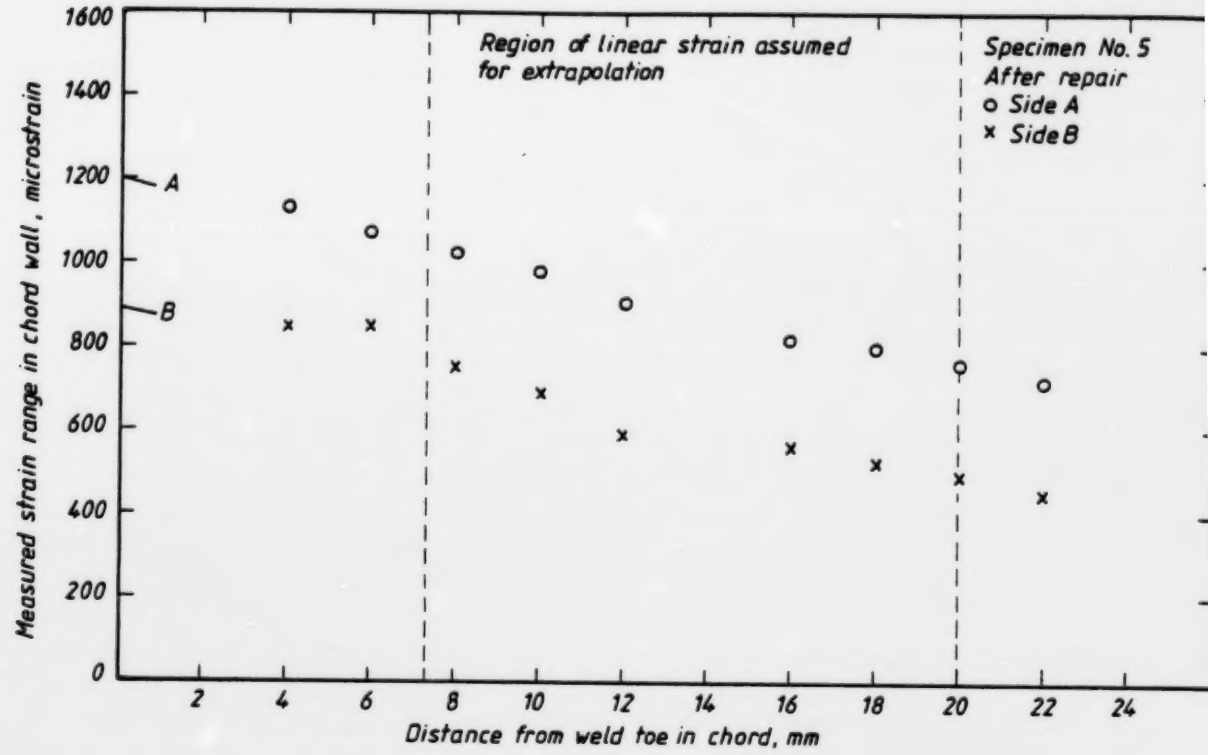

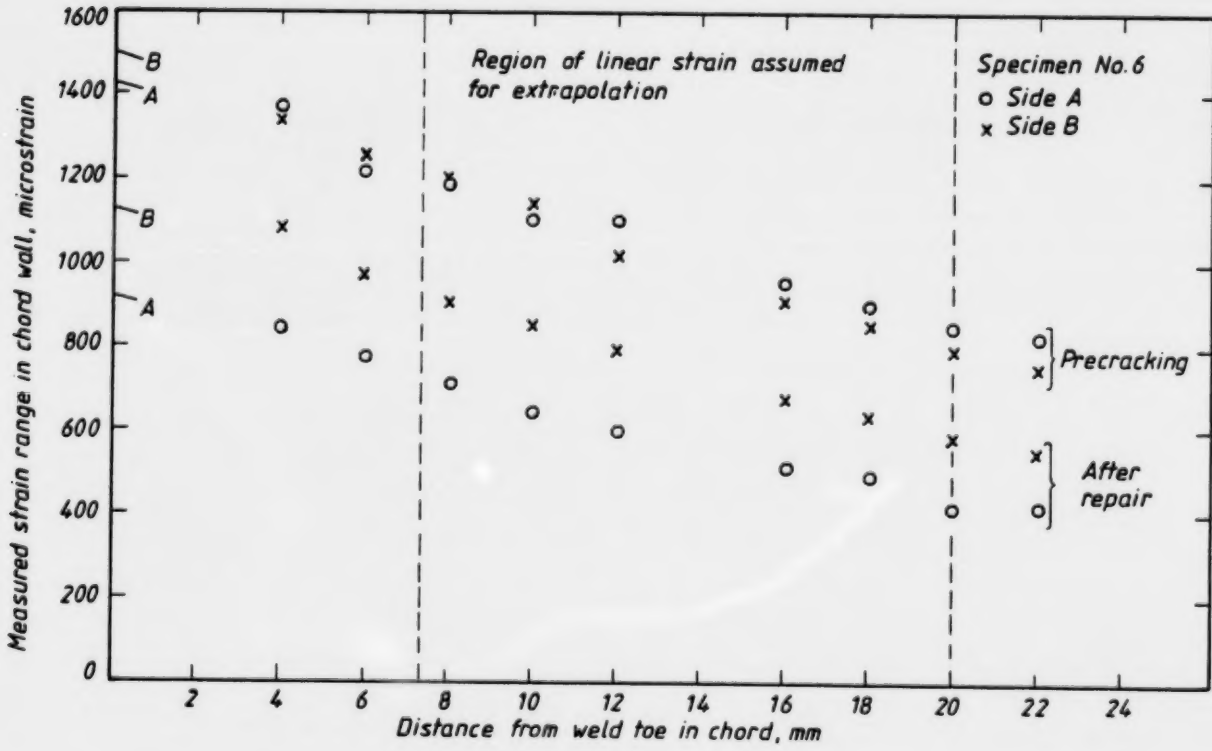
Region of linear strain assumed for extrapolation
Specimen No. 6
o Side A
x Side B
Precracking
After repair
Measured strain range in chord wall, microstrain
Distance from weld toe in chord, mm

APPENDIX B: Strain distributions in tubular joint specimens

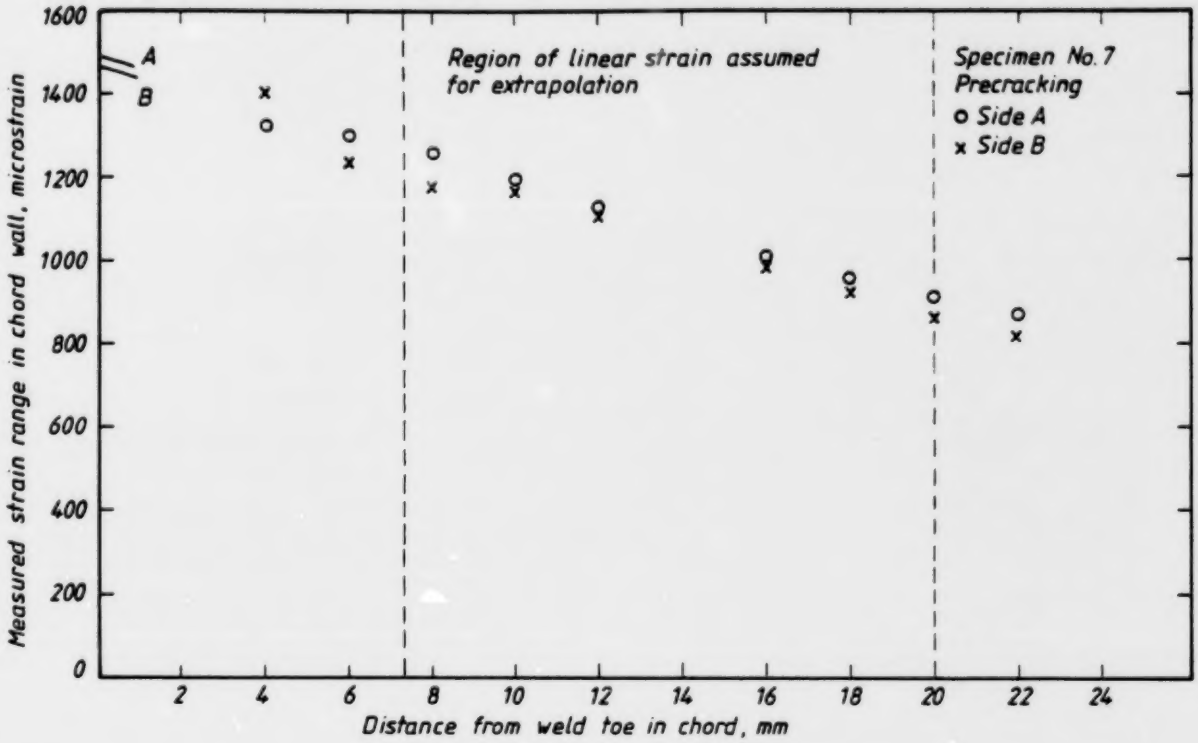

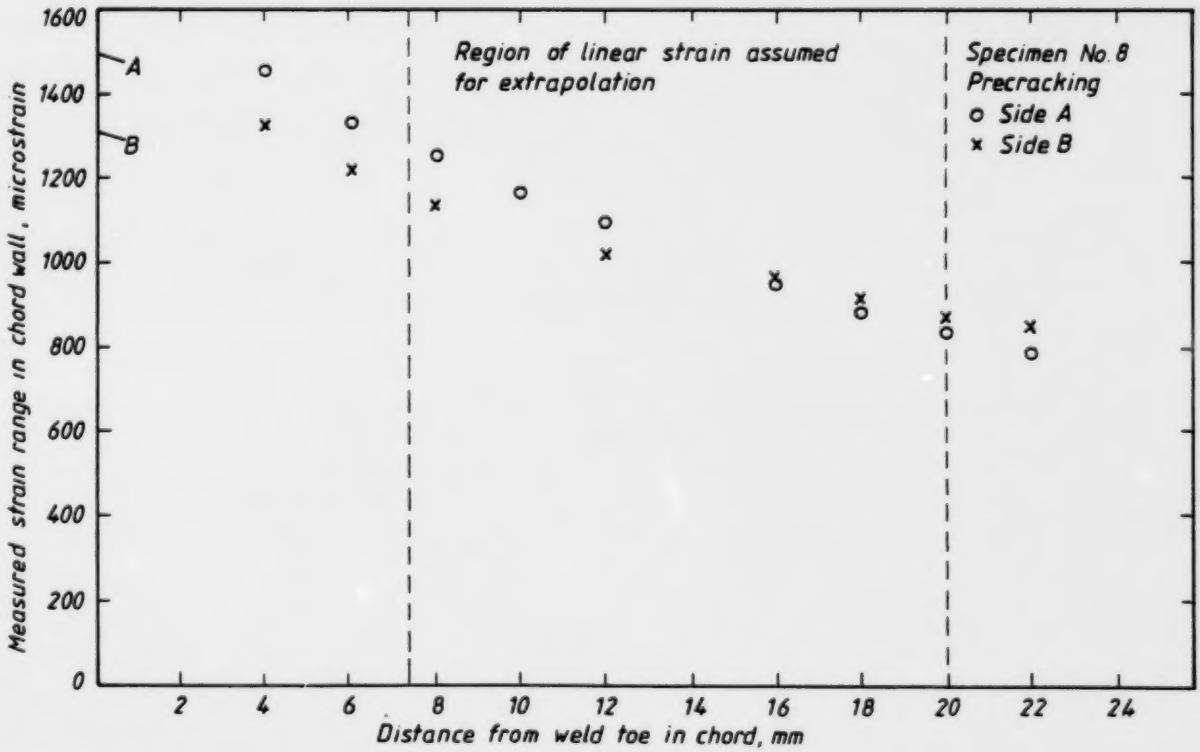

APPENDIX B: Strain distributions in tubular joint specimens

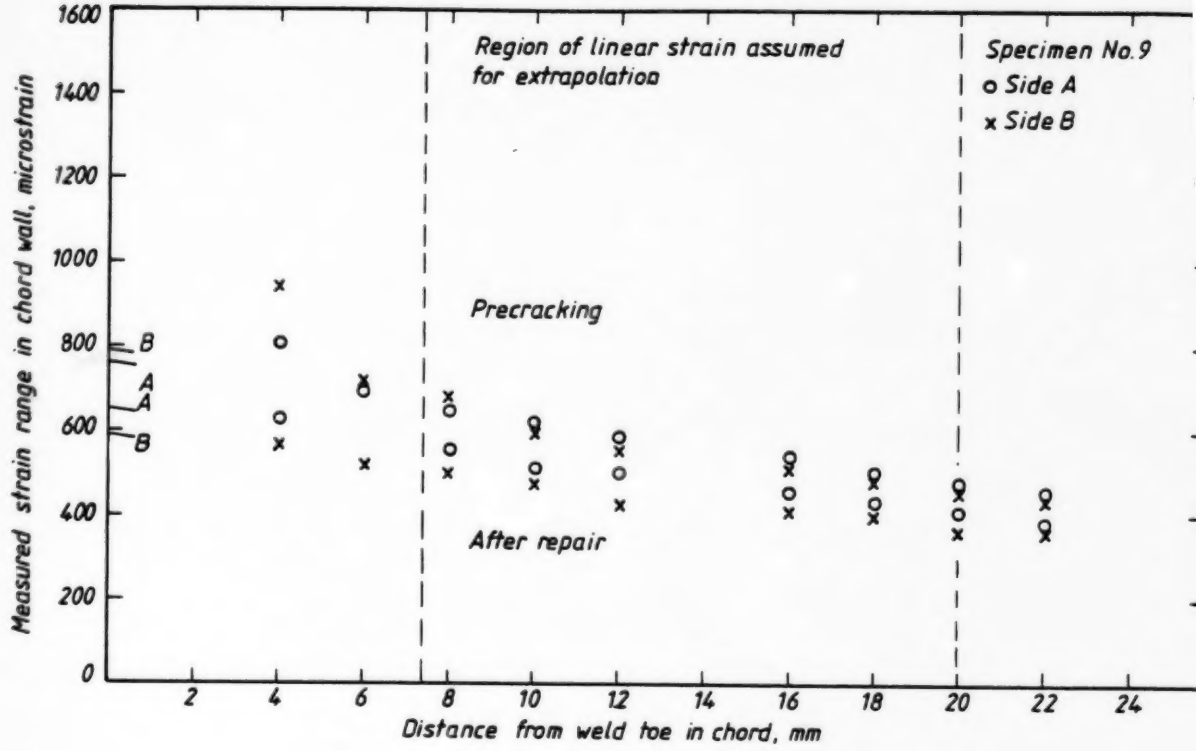

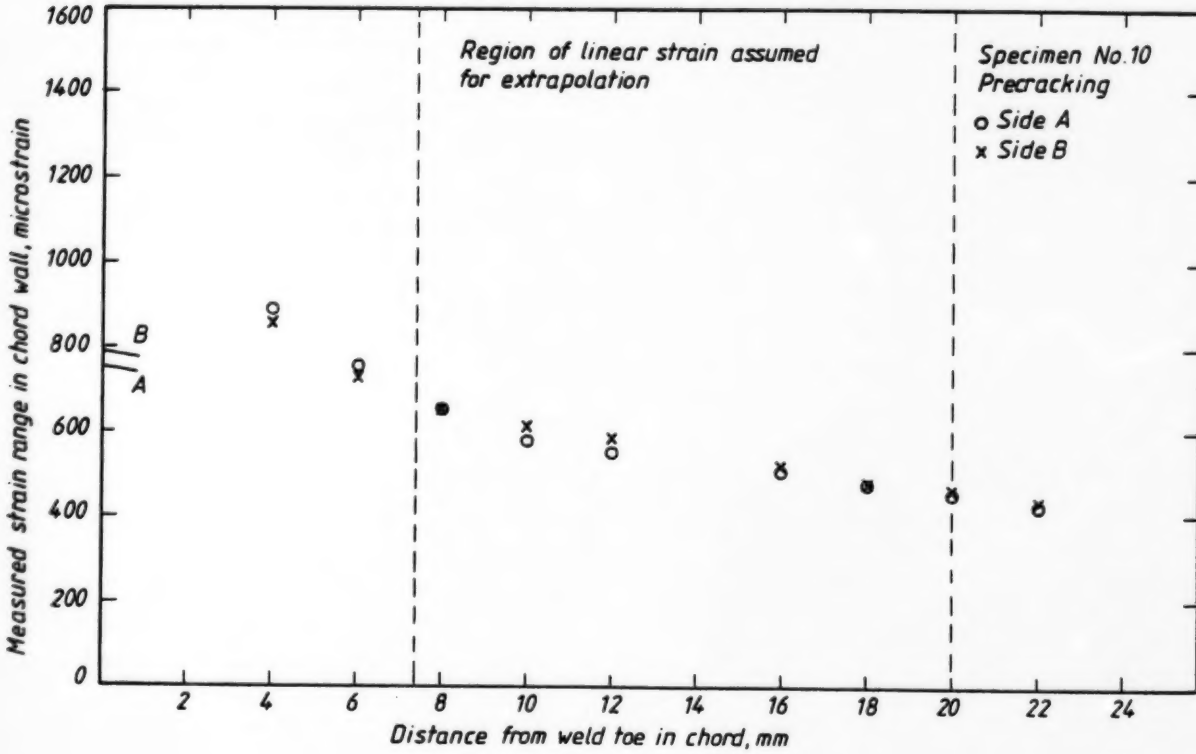

APPENDIX B: Strain distributions in tubular joint specimens

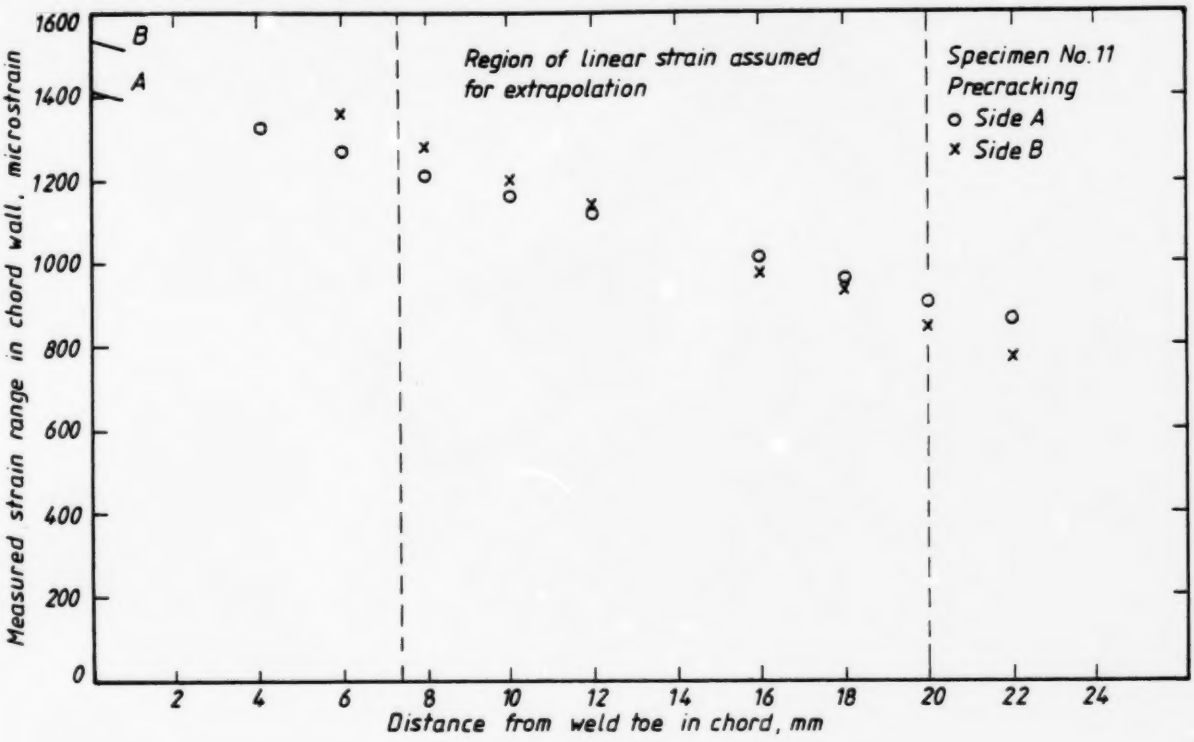

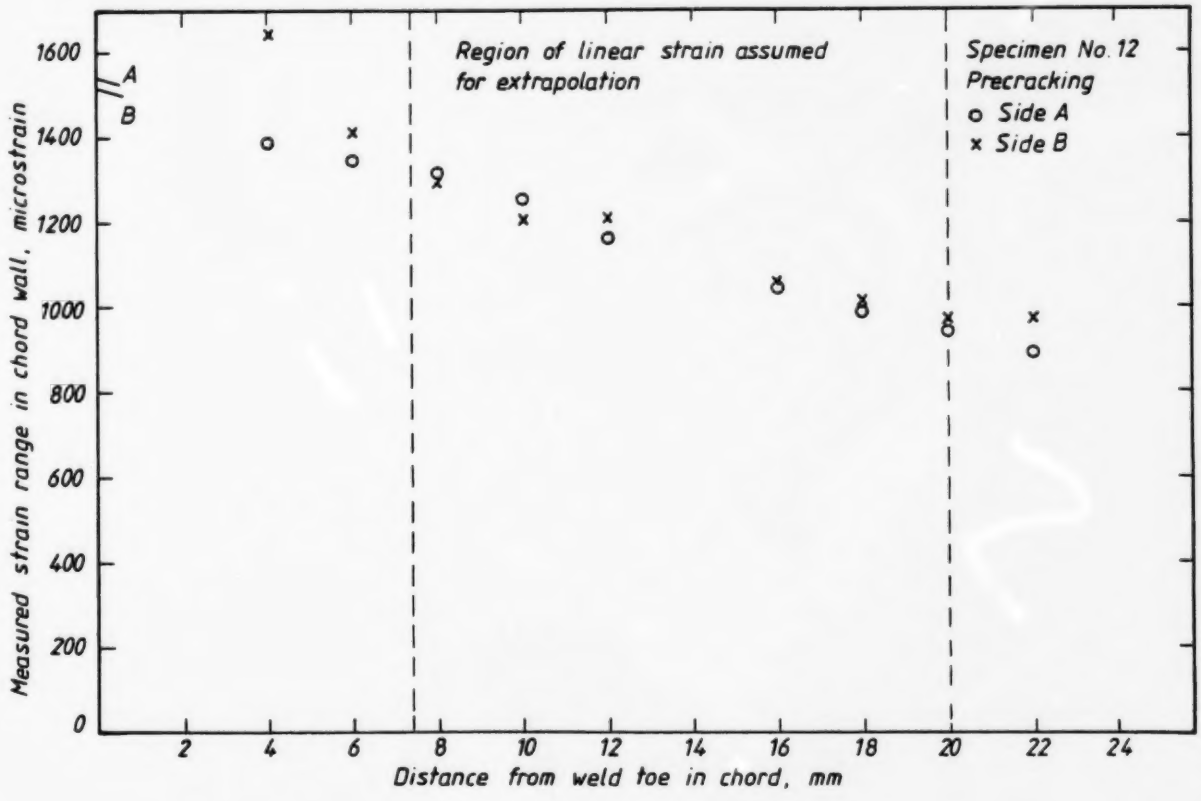

APPENDIX B: Strain distributions in tubular joint specimens

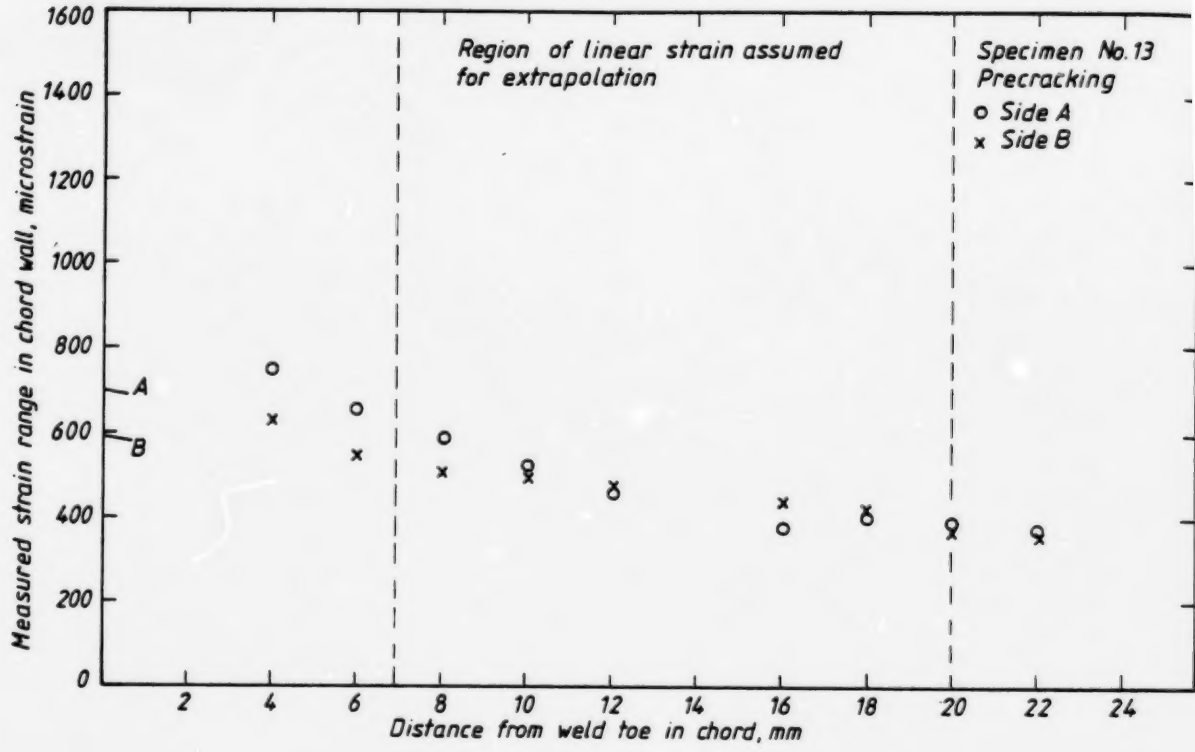

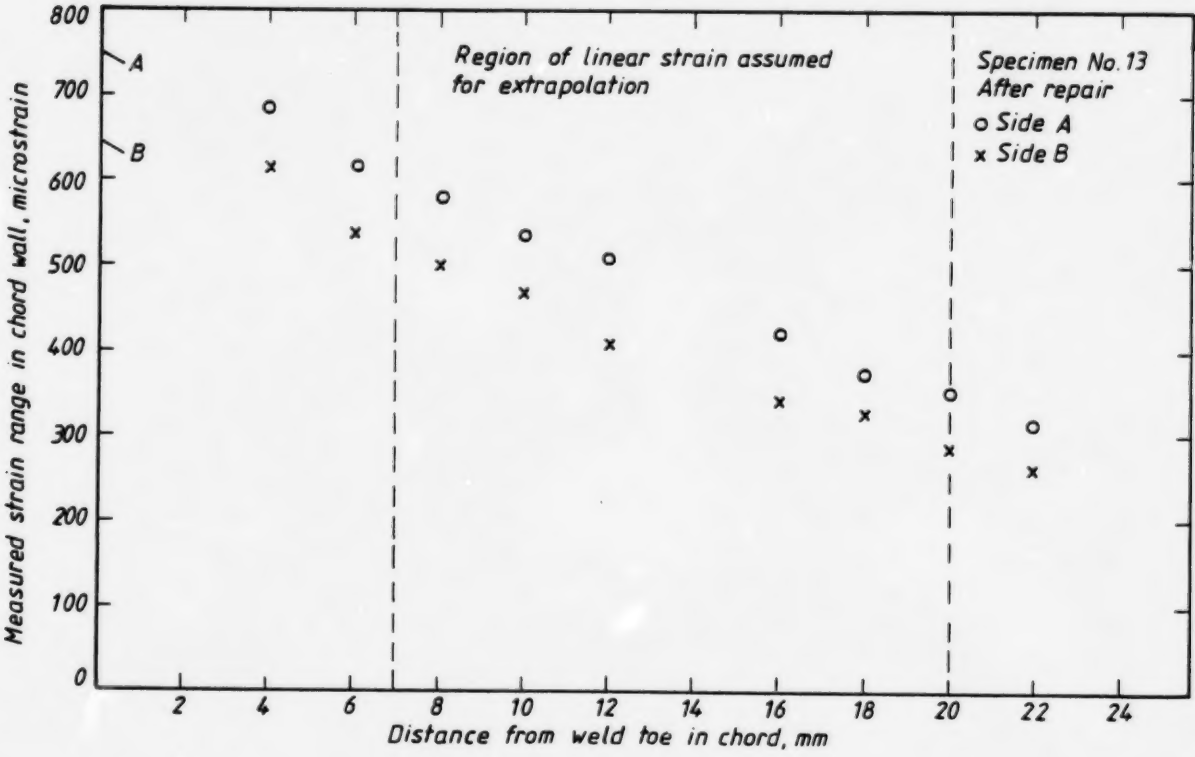

APPENDIX B: Strain distributions in tubular joint specimens

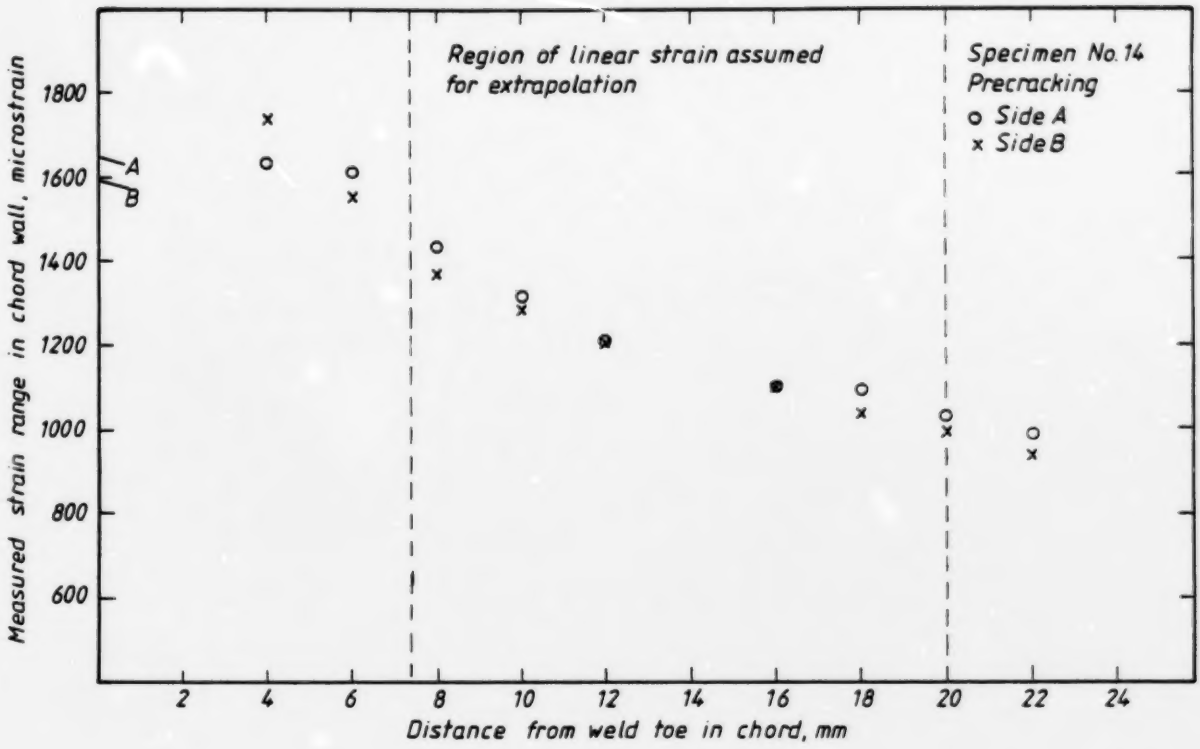

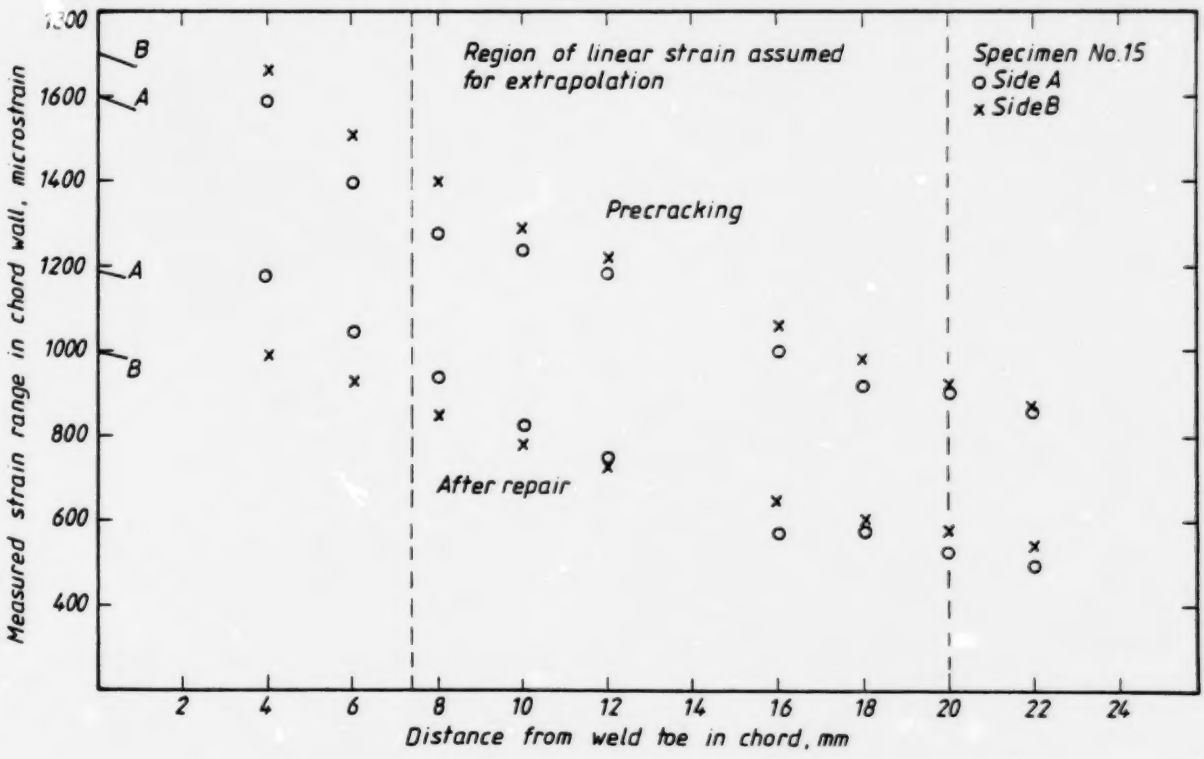

APPENDIX B: Strain distributions in tubular joint specimens

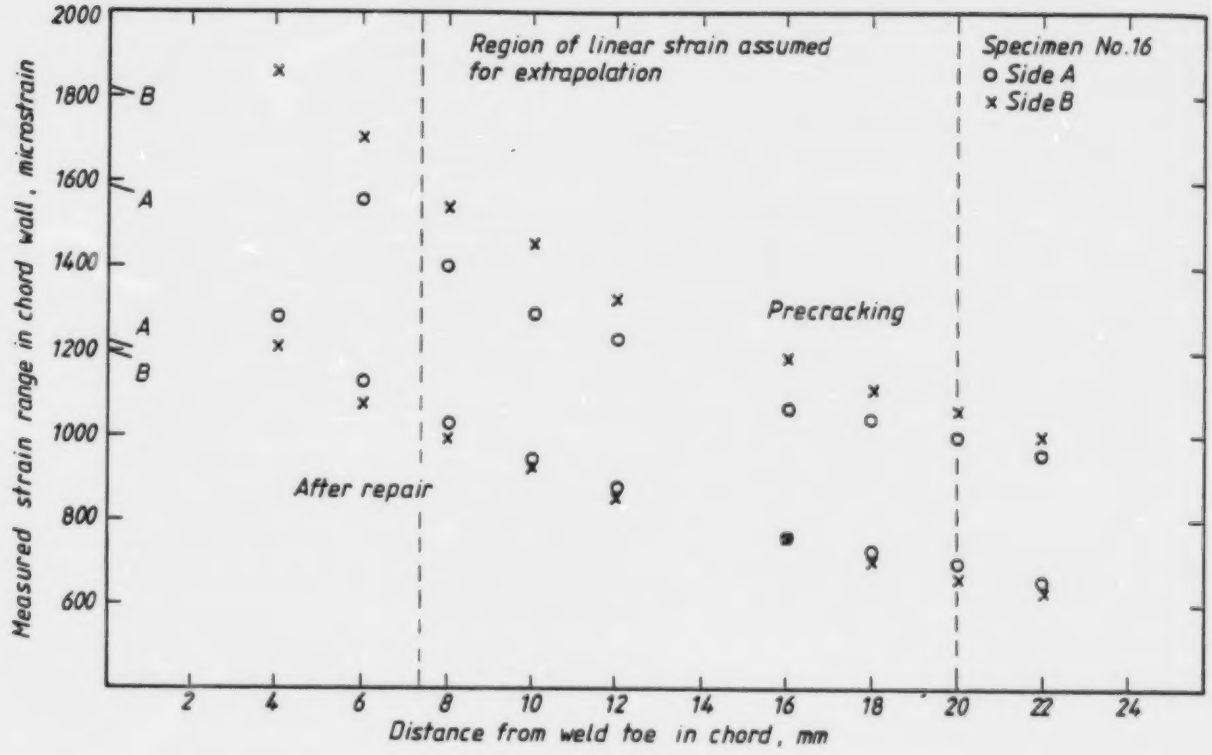
Region of linear strain assumed for extrapolation
Specimen No.16
o Side A
x Side B
Precracking
After repair
Measured strain range in chord wall, microstrain
Distance from weld toe in chord, mm

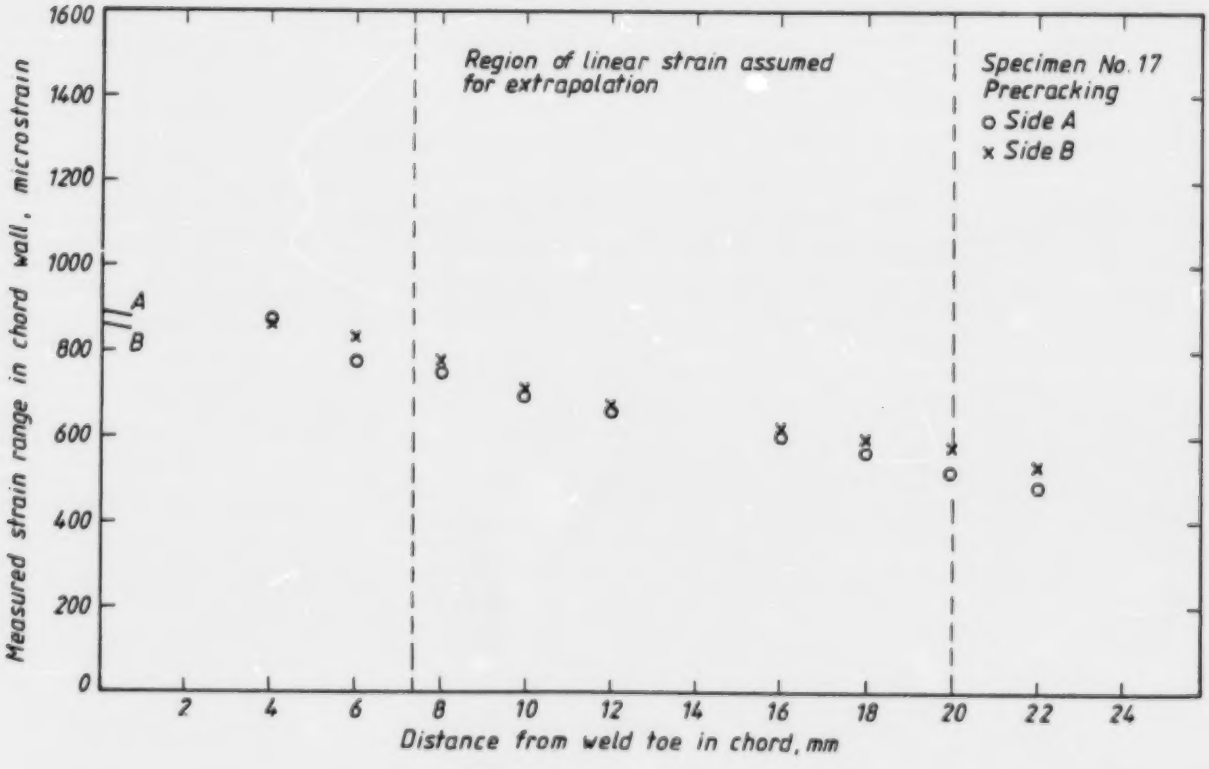
Region of linear strain assumed for extrapolation
Specimen No. 17
Precracking
o Side A
x Side B
Measured strain range in chord wall, microstrain
Distance from weld toe in chord, mm

APPENDIX B: Strain distributions in tubular joint specimens

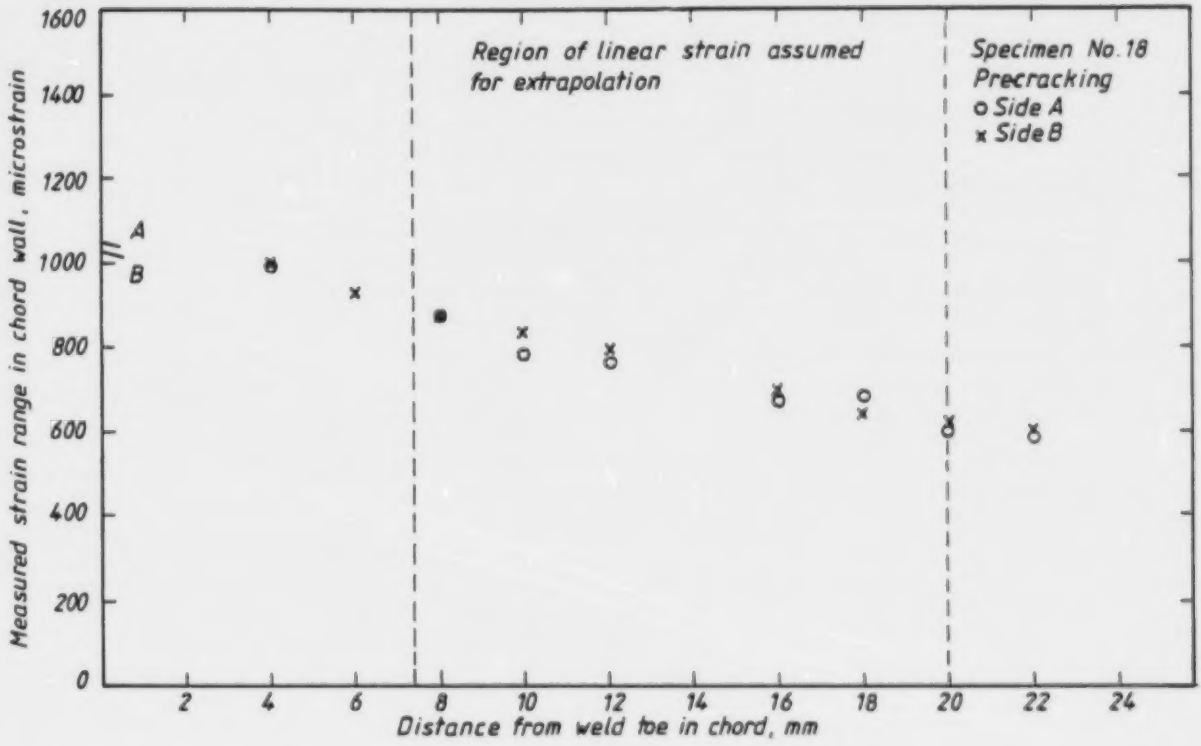

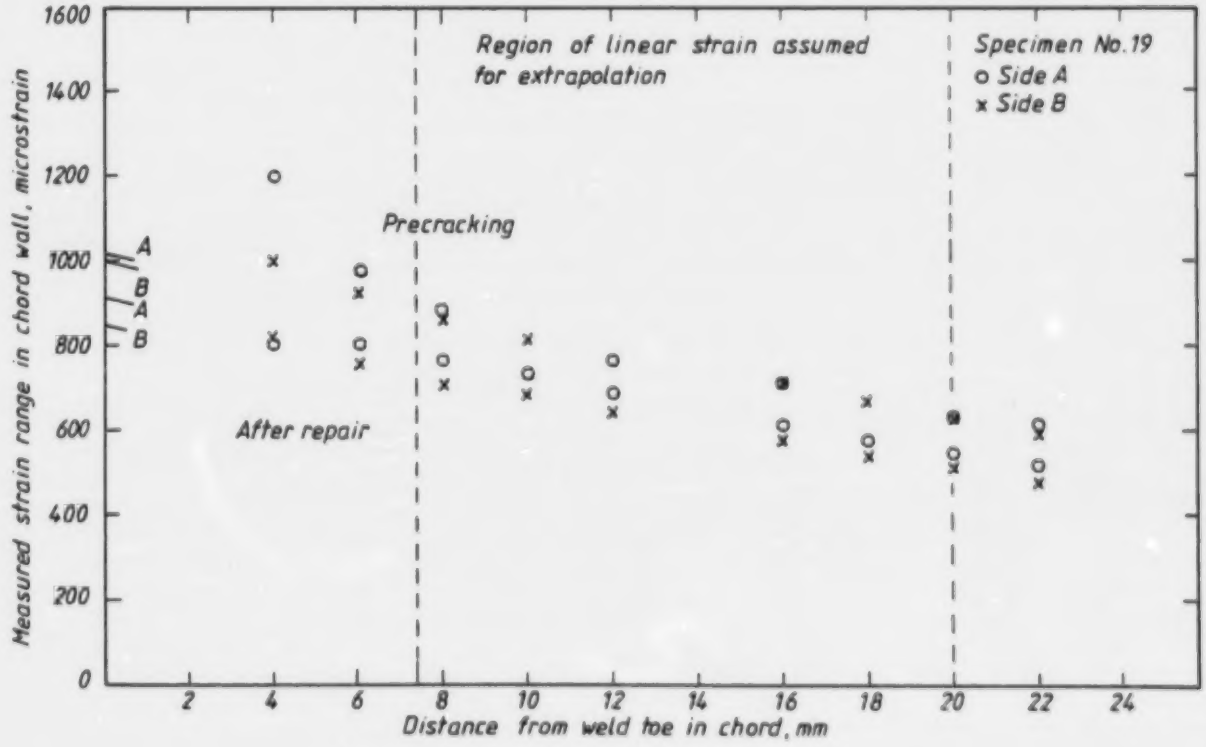

APPENDIX B: Strain distributions in tubular joint specimens

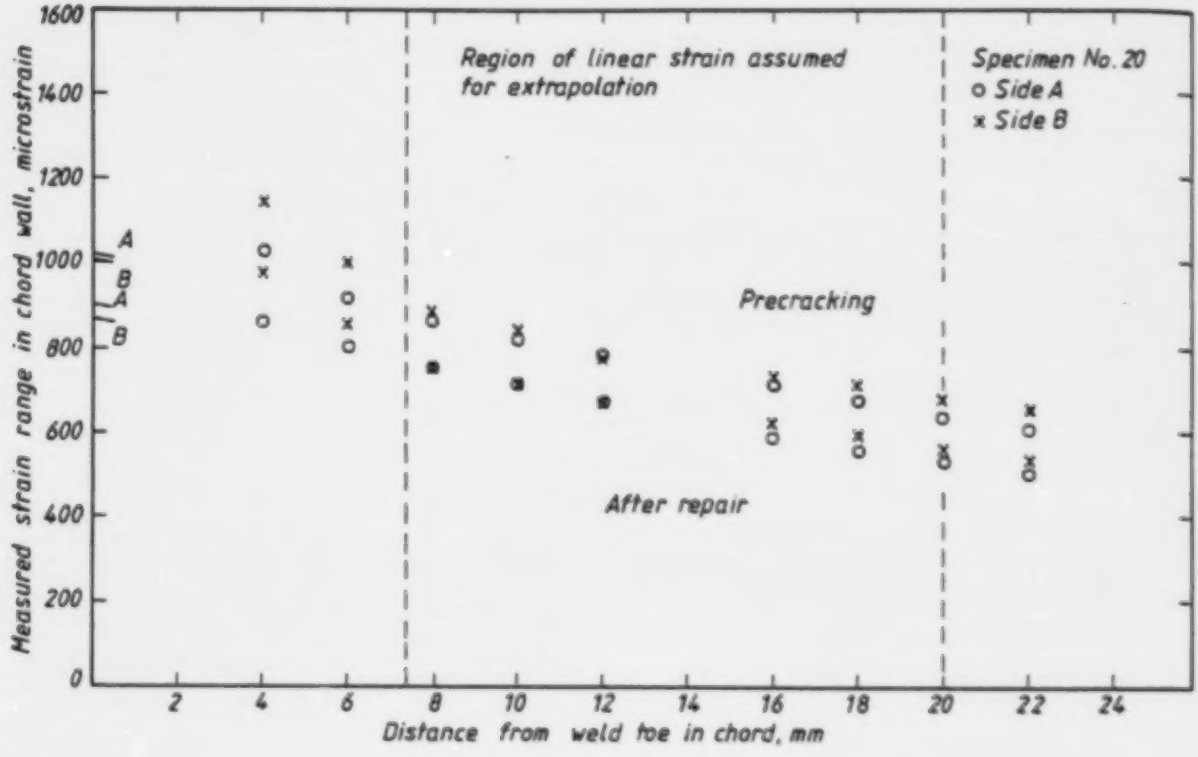

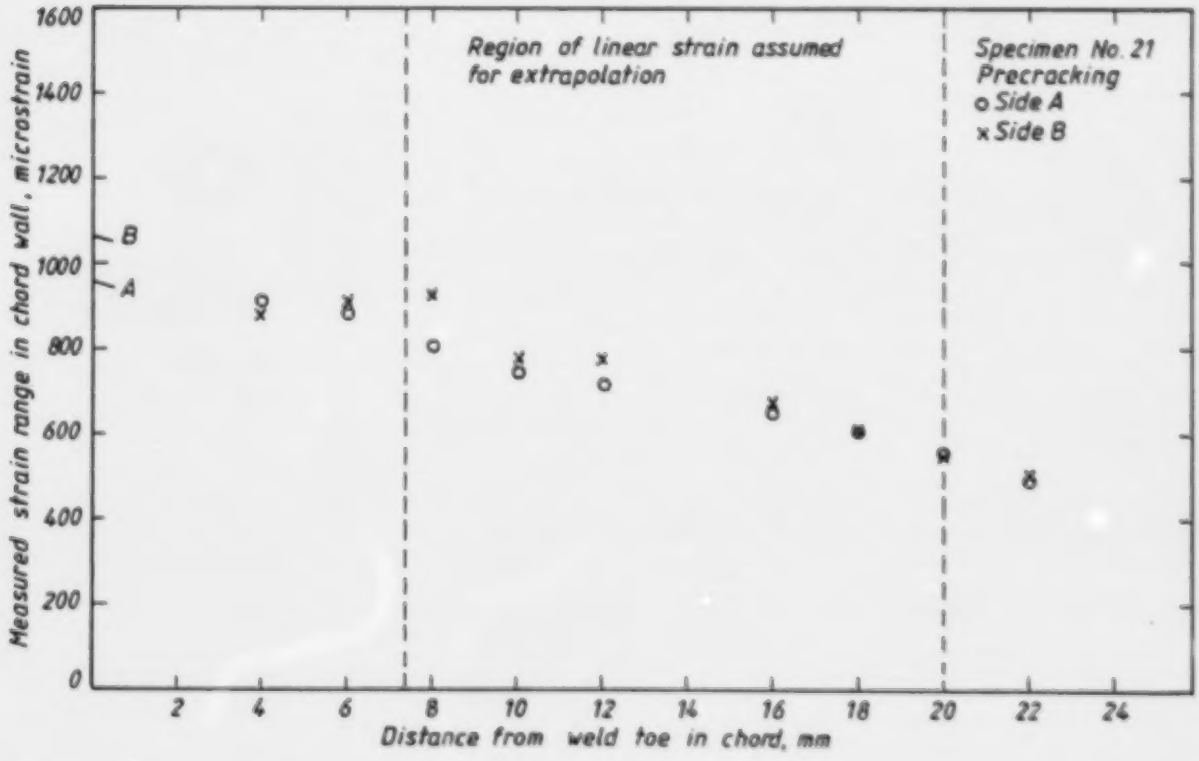

APPENDIX B: Strain distributions in tubular joint specimens

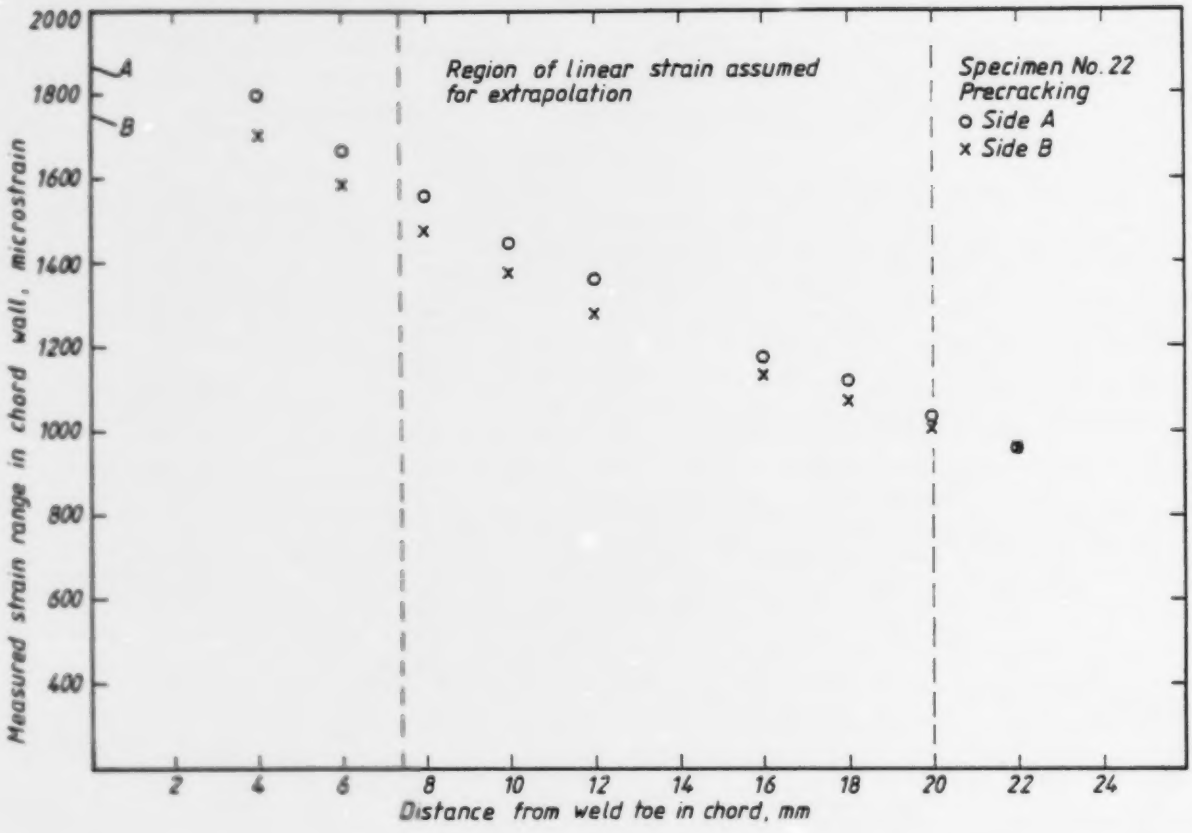

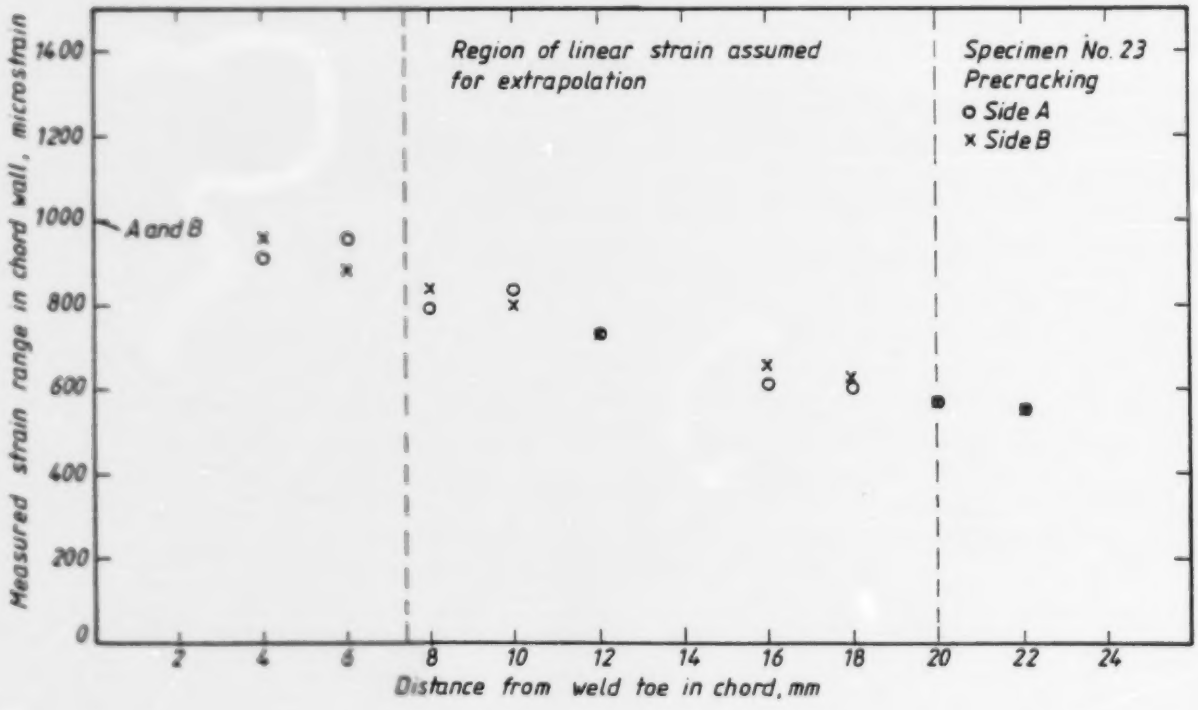
Region of linear strain assumed for extrapolation
Specimen No. 23
Precracking
o Side A
x Side B
A and B
Measured strain range in chord wall, microstrain
Distance from weld toe in chord, mm

APPENDIX B: Strain distributions in tubular joint specimens

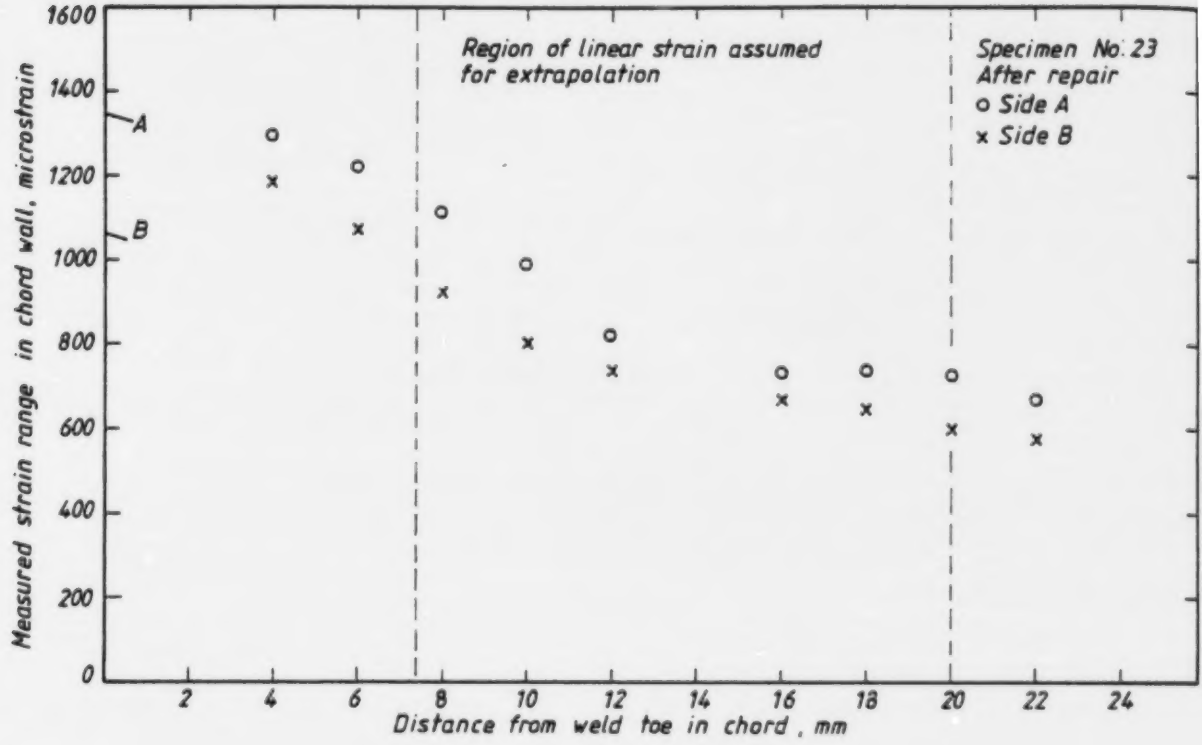

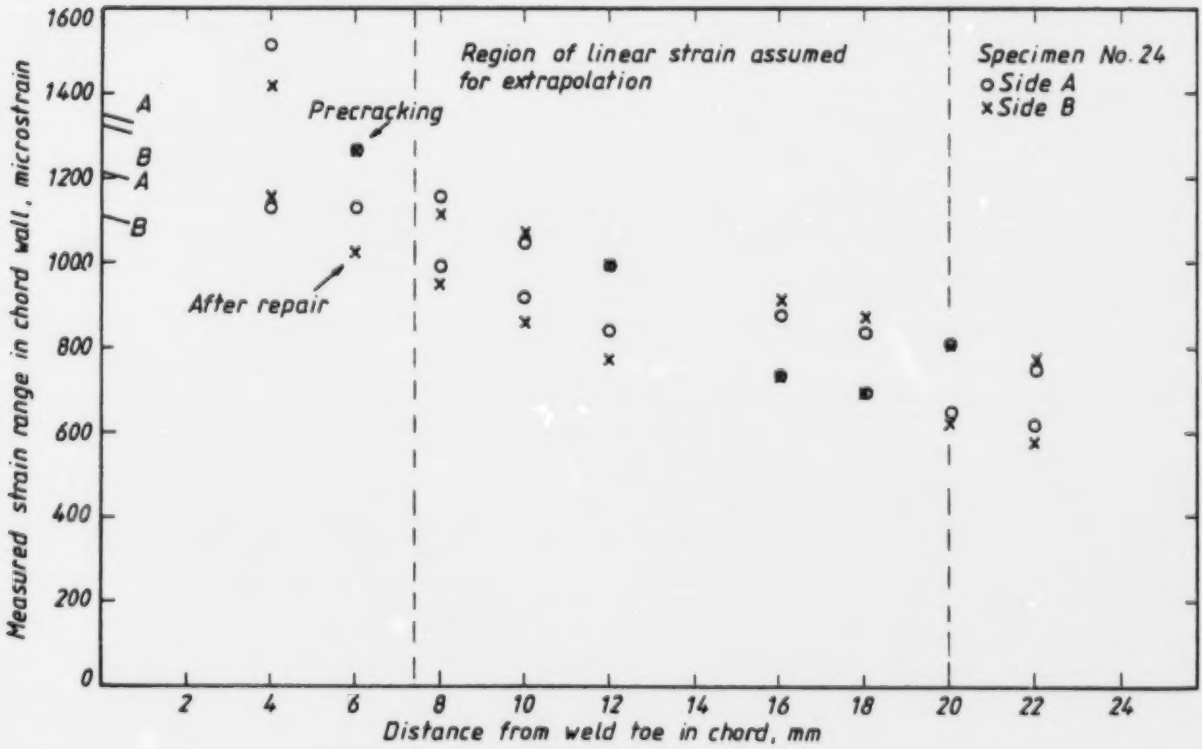

APPENDIX B: Strain distributions in tubular joint specimens

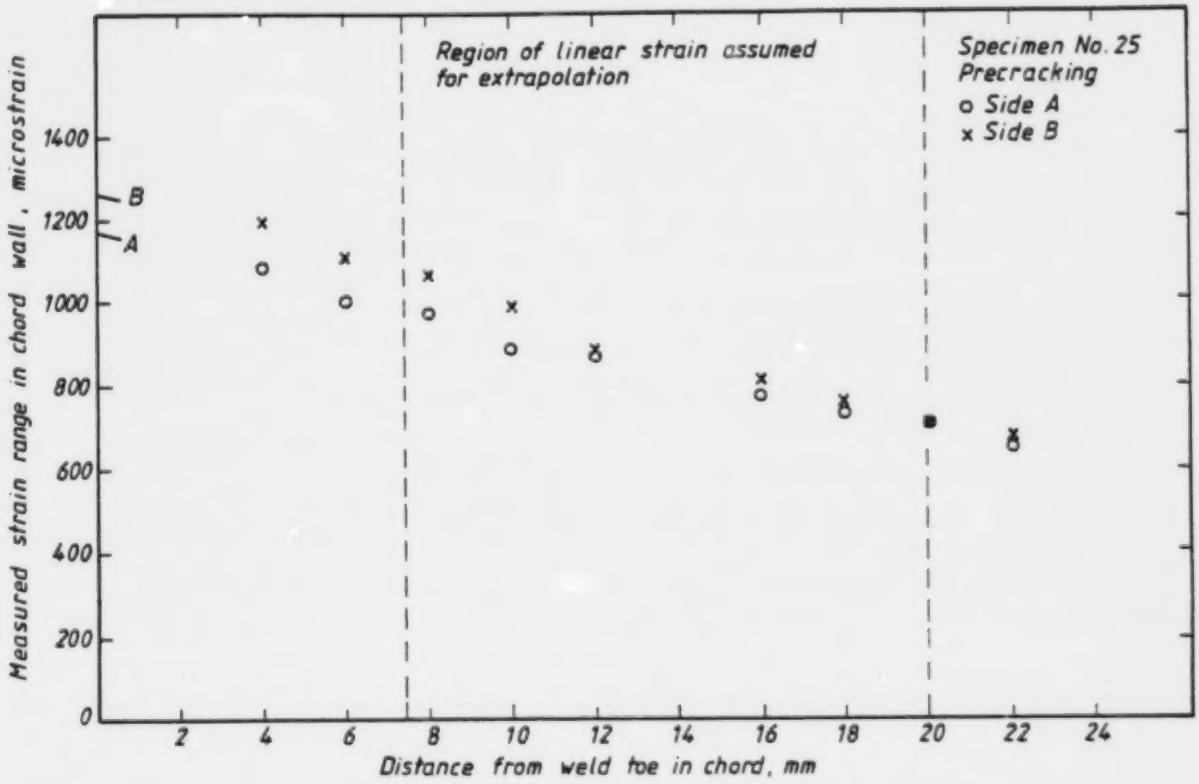

APPENDIX C — Macrosections from tubular joint specimens

The following Figures show etched macrosections taken from the tubular specimens. The sections were cut close to the brace centreline on each side of the joint, *i.e.* at the stress hot spots in the saddle areas. The cracks were opened to allow the fracture surfaces to be inspected. In some instances the two halves of the fracture did not fit back together perfectly with the result that the section shown does not reflect the true joint profile. The sections are grouped according to repair method and are presented in the order in which the test results are listed in Table 7 of the main text.

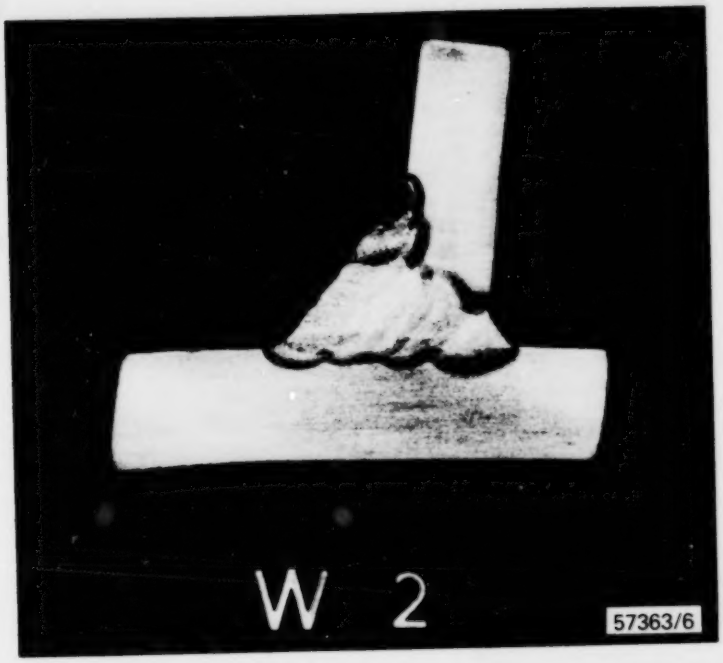

C1 *Etched macrosections from tubular joint specimen No.2 tested to failure without repair (note: section taken from crown position).*

C2 *Etched macrosection from tubular joint specimen No.1 (side A). Precracked through-thickness and repair welded.*

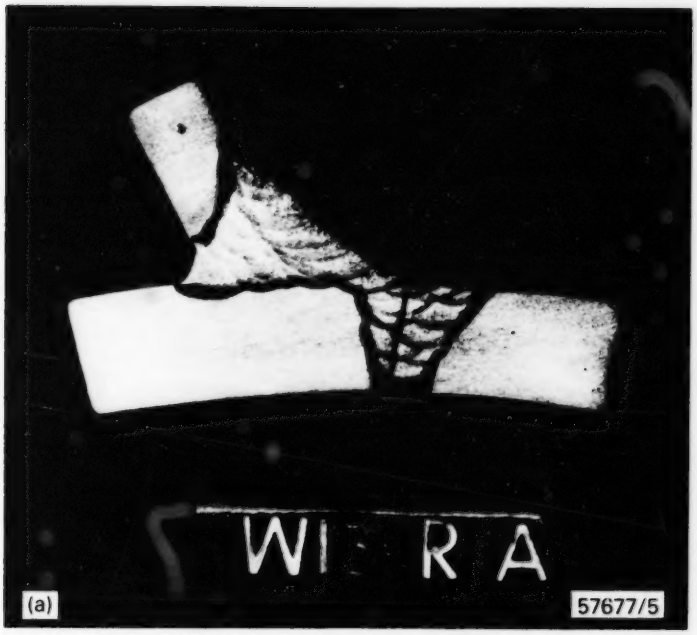

C3 *Etched macrosections from tubular joint specimen No.13. Precracked through-thickness and repair welded:* a) *Side A;* b) *Side B.*

C4 *Etched macrosections from tubular joint specimen No.19. Precracked through-thickness and repair welded:* a) *Side A;* b) *Side B.*

C5 *Etched macrosection from tubular joint specimen No.4 side A. Precracked through-thickness and repair welded.*

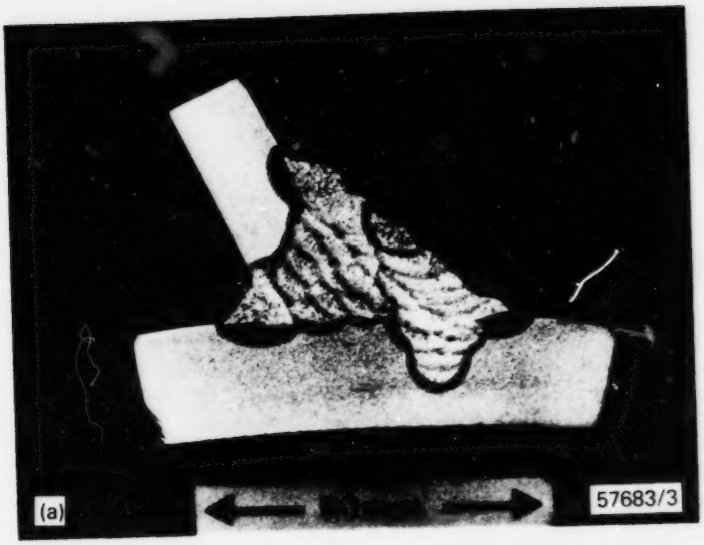

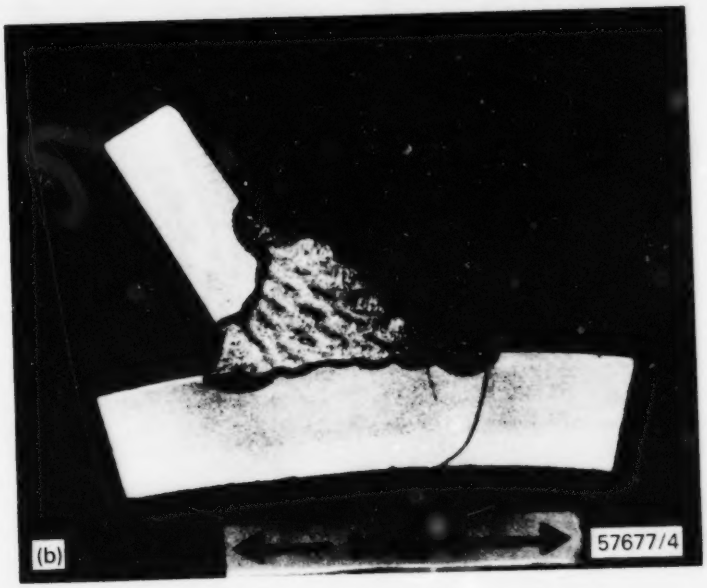

C6 *Etched macrosections from tubular joint specimen No.9. Precracked 50% of wall and repair welded:* a) *Side A;* b) *Side B.*

C7 *Etched macrosections from tubular joint specimen No.20. Precracked 50% of wall and repair welded:* a) *Side A;* b) *Side B.*

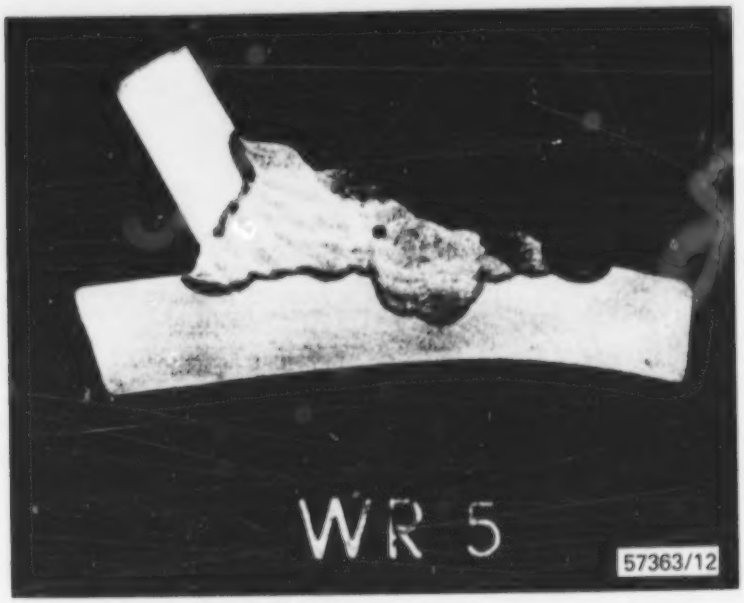

C8 *Etched macrosection from tubular joint specimen No.5 side B. Precracked 50% of wall and repair welded.*

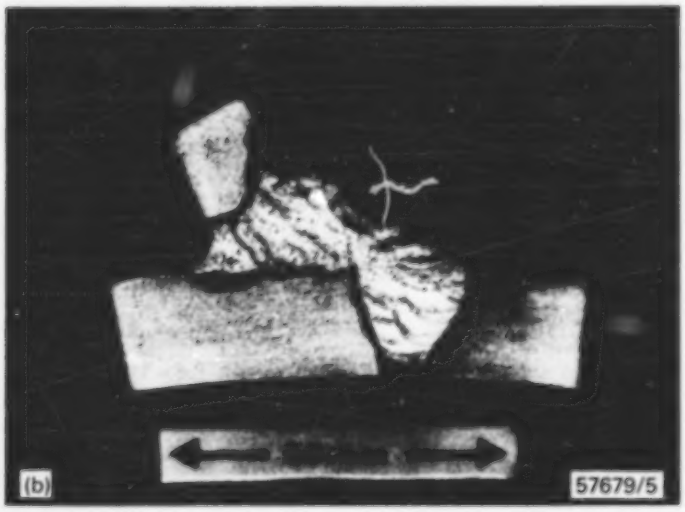

C9 *Etched macrosections from tubular joint specimen No.15. Precracked through-thickness, repair welded and burr ground:* a) *Side A;* b) *Side B.*

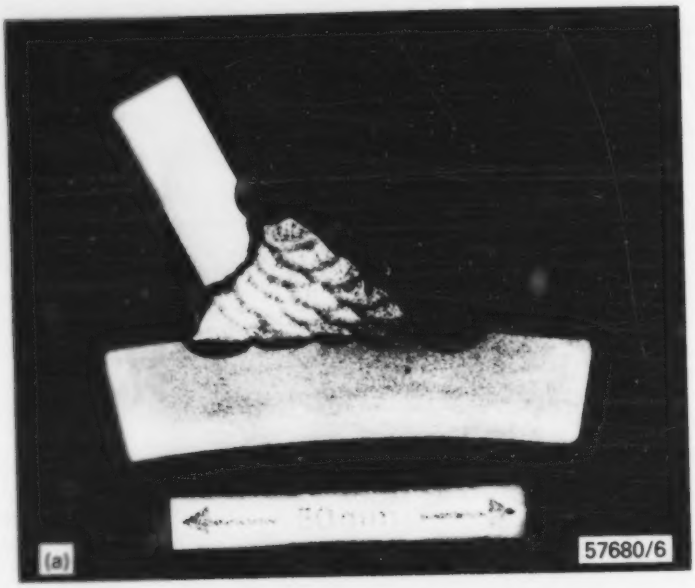

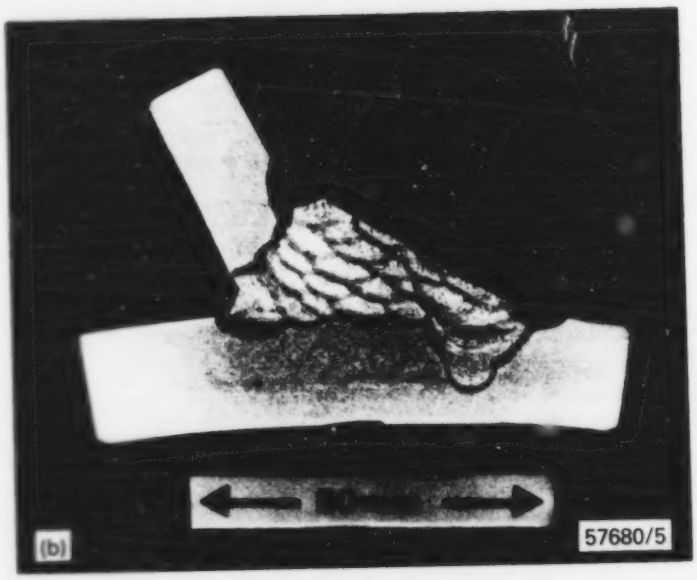

C10 *Etched macrosections from tubular joint specimen No.23. Precracked 50% of wall, repair welded and burr ground:* a) *Side A;* b) *Side B.*

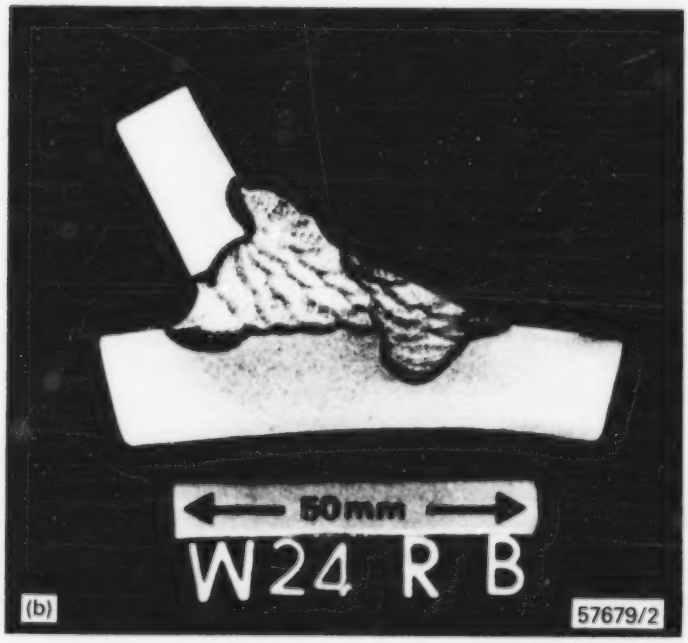

C11 *Etched macrosections from tubular joint specimen No.24. Precracked 50% of wall, repair welded and burr ground:* a) *Side A;* b) *Side B.*

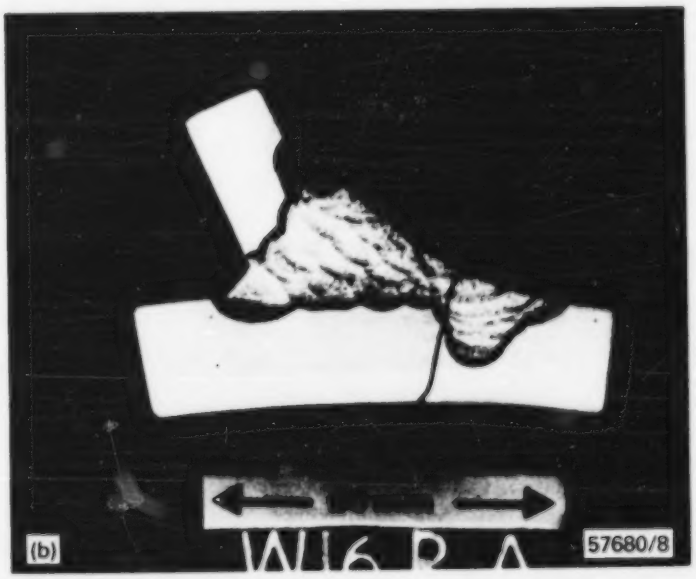

C12 *Etched macrosections from tubular joint specimen No.16. Precracked 50% of wall, repair welded and burr ground:* a) *Side A;* b) *Side B.*

C13 *Etched macrosections from tubular joint specimen No. 7. Through-thickness crack treated by hole drilling and cold expansion process:* a) *Side A;* b) *Side B.*

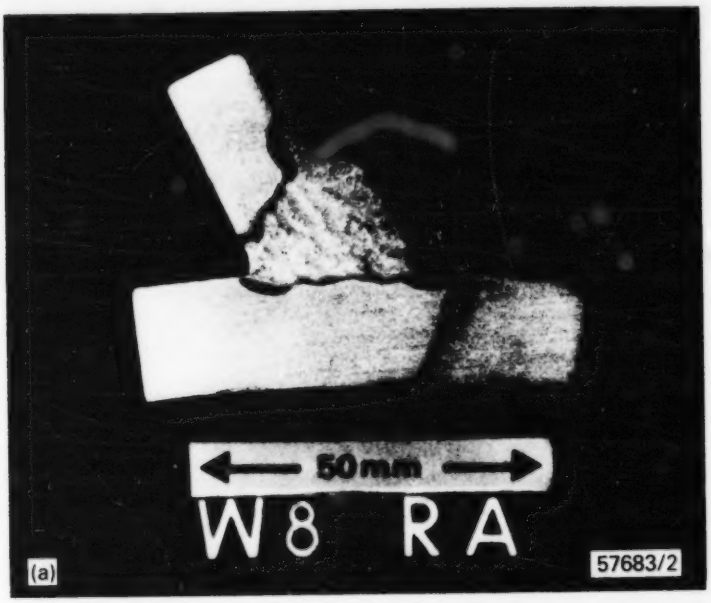

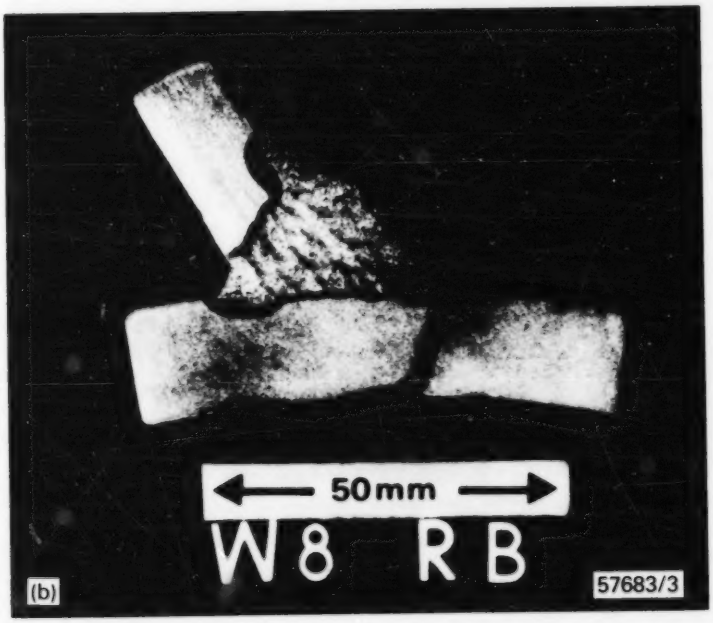

C14 *Etched macrosections from tubular joint specimen No.8. Crack 50% of wall treated by hole drilling and cold expansion process:*
a) *Side A;* b) *Side B.*

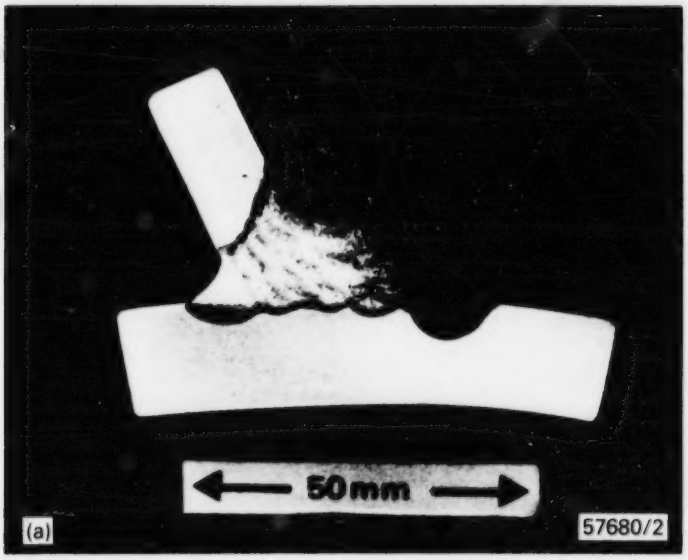

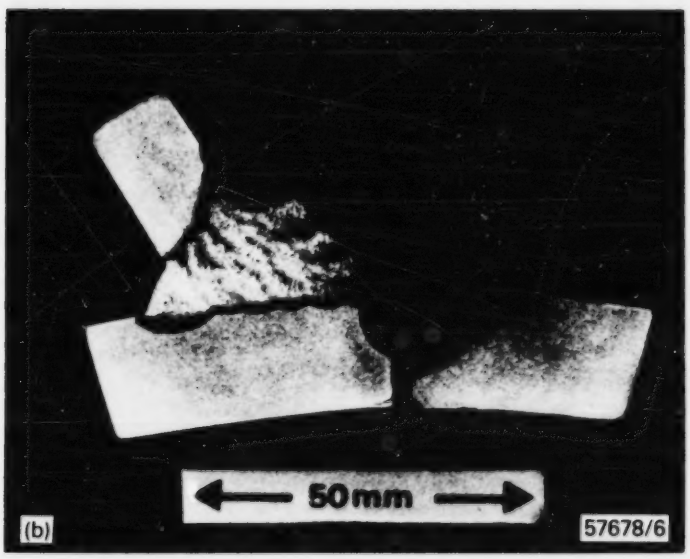

C15 *Etched macrosections from tubular joint specimen No.17. Crack 50% of wall repaired by grinding alone:* a) *Side A;* b) *Side B.*

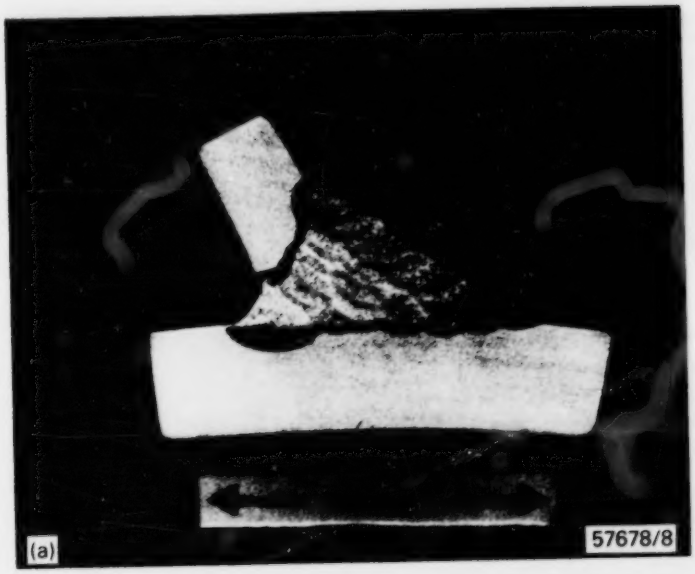

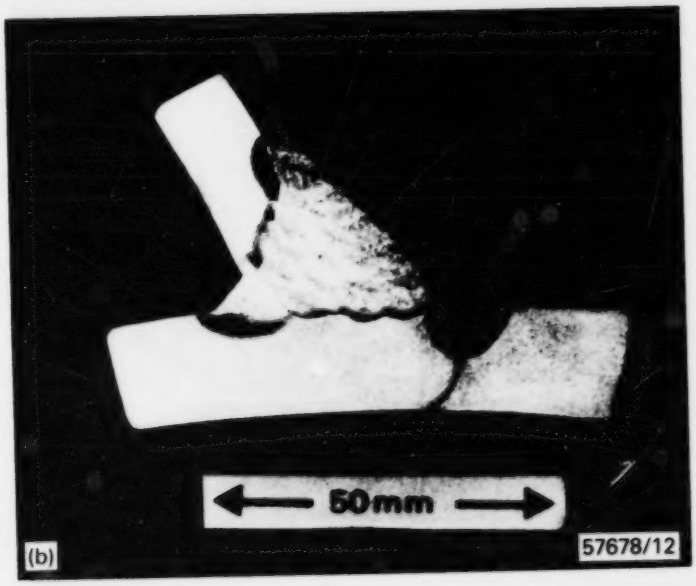

C16 *Etched macrosections from tubular joint specimen No.21. Crack 50% of wall repaired by grinding alone:* a) *Side A;* b) *Side B.*

C17 *Etched macrosections from tubular joint specimen No.11. Crack 50% of wall repaired by grinding alone:* a) *Side A;* b) *Side B.*

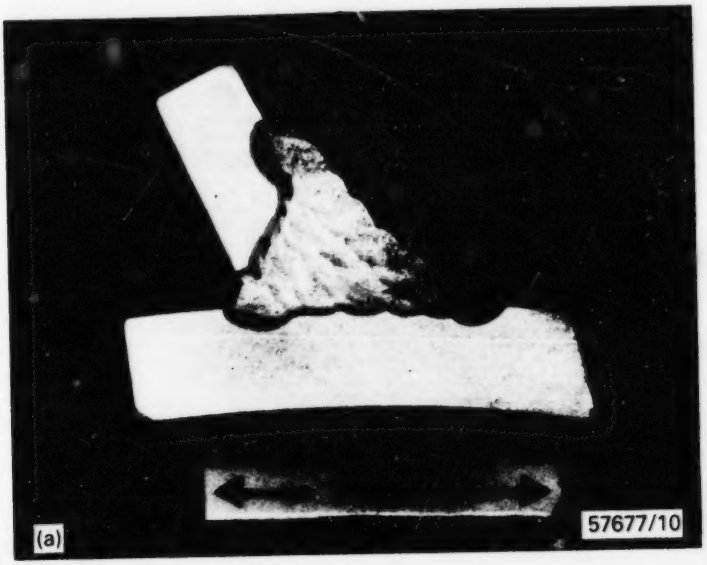

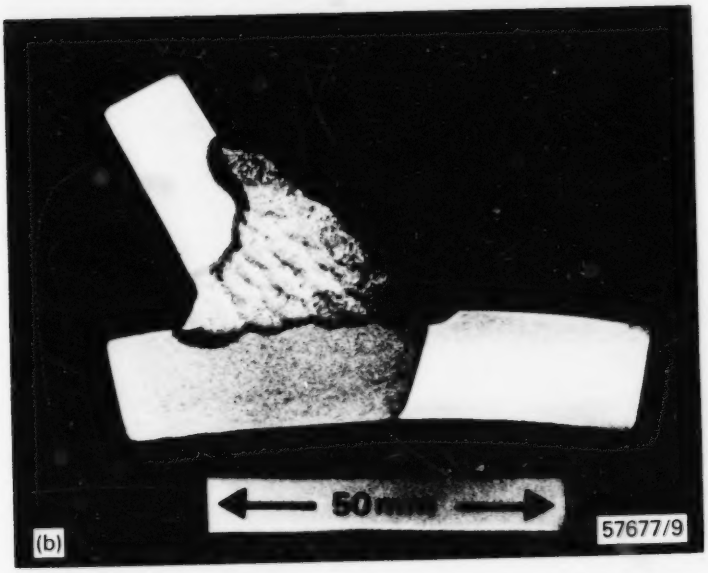

C18 *Etched macrosections from tubular joint specimen No.10. Crack 25% of wall repaired by grinding alone:* a) *Side A;* b) *Side B.*

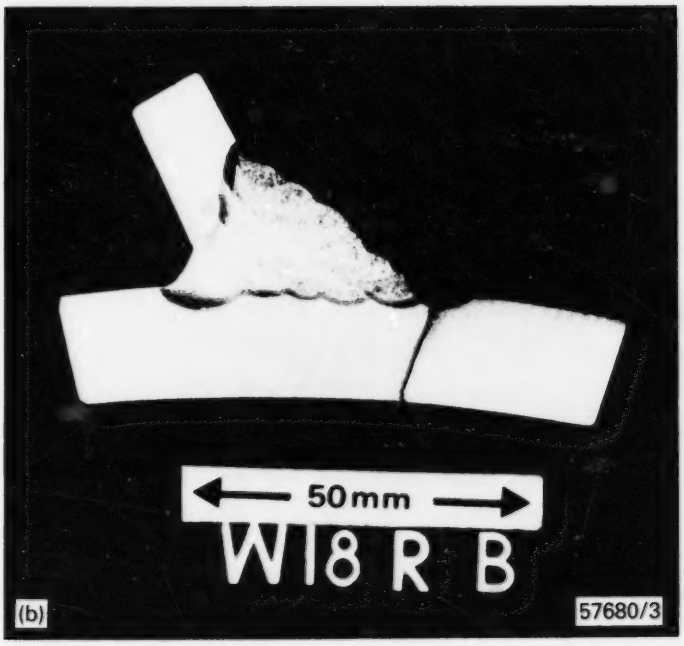

C19 *Etched macrosections from tubular joint specimen No.18. Crack 25% of wall repaired by grinding alone:* a) *Side A;* b) *Side B.*

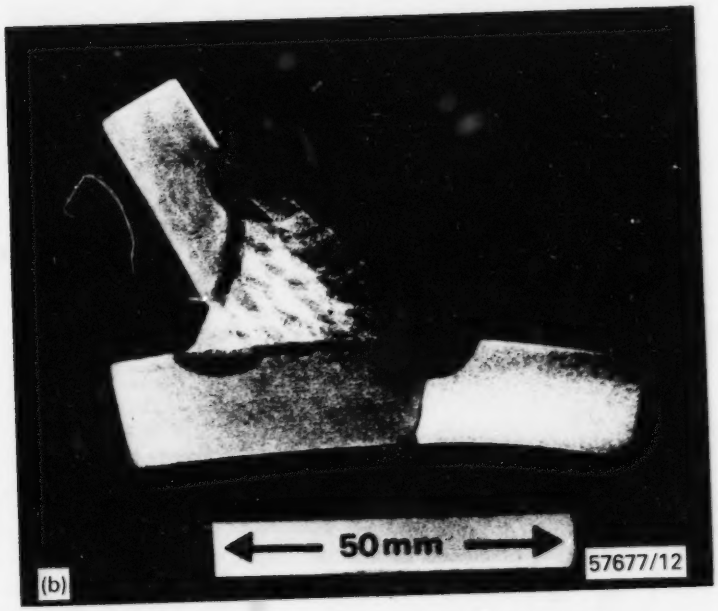

C20 *Etched macrosections from tubular joint specimen No.12. Crack 25% of wall repaired by grinding alone:* a) *Side A;* b) *Side B.*

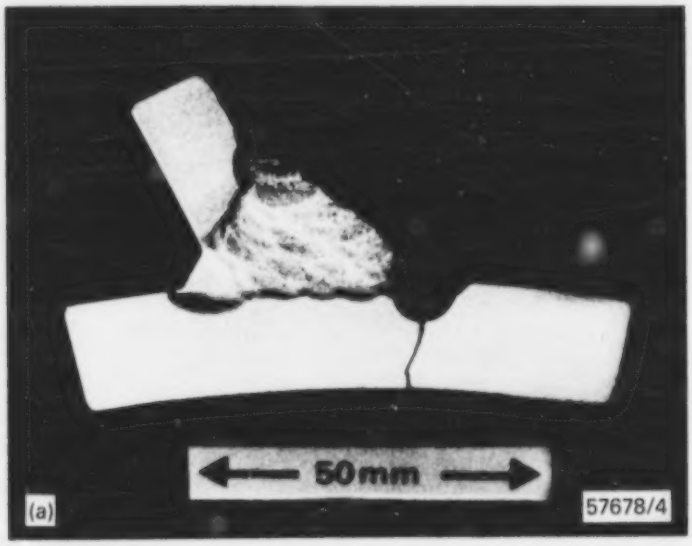

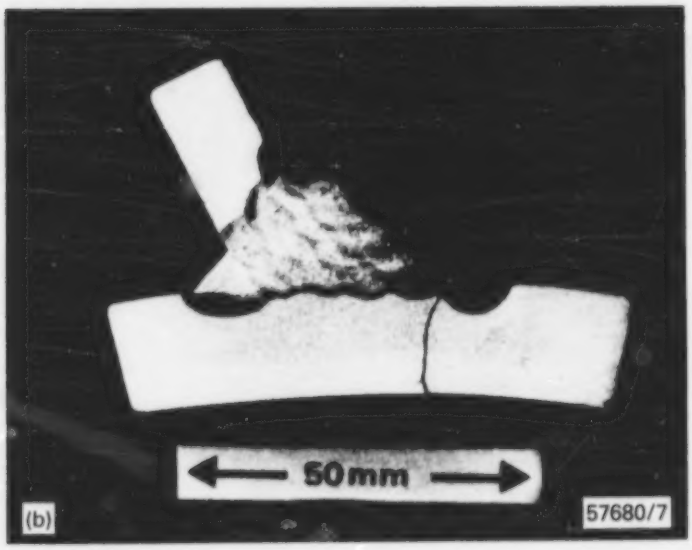

C21 *Etched macrosections from tubular joint specimen No. 14. Crack 25% of wall repaired by grinding alone:* a) *Side A;* b) *Side B.*

C22 *Etched macrosections from tubular joint specimen No.22. Repaired by grinding alone. Several excavation depths investigated:* a) *Side A;* b) *Side B.*

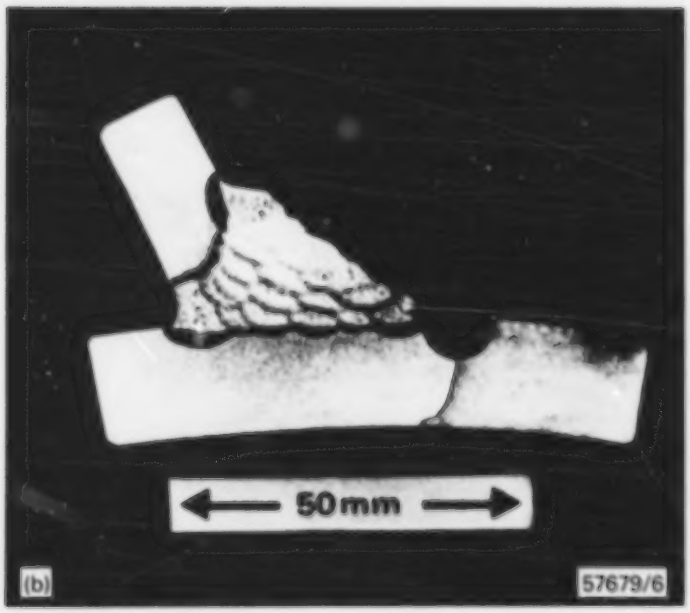

C23 *Etched macrosections from tubular joint specimen No.25. Repaired by grinding alone. Several excavation depths investigated.* a) *Side A;* b) *Side B.*

APPENDIX D — Burr ground excavations in tubular joints. Strain measurements and excavation profiles

Four specimens were instrumented with strain gauges according to the gauge plan shown in Fig.9 of the main text. Strains measured by the single element gauges in the bottom of the excavation are shown in Fig.D1-4. Figures D2 and 3 also show strains given by the row of gauges attached to the chord wall approximately 8mm from the edge of the excavation. The values measured here, and by the strip gauges on the chord, were very low by comparison with those in the excavation. These gauges were omitted in later tests.

The five remaining specimens with ground excavations were investigated using the SPATE system (described in Section 2.1.7 of the main text) to isolate the position of maximum stress. A rosette gauge of 1mm gauge length was then attached at this point to allow principal stresses to be estimated. The values obtained are given in Table 8 of the main text. Figure D5 shows a typical two dimensional 'stress map' obtained by SPATE analysis of the excavation in specimen No.14, side A. The position of maximum stress is indicated by the arrow. The parameter measured by the SPATE system is the sum of the principal stress ranges. Hence, in components where the ratio of the principal stresses varies significantly, the position of maximum principal stress range does not necessarily correspond with the maximum SPATE output. However, strain measurements from the rosette gauges indicate that within the excavation the ratio of the principal stresses is virtually constant with an average value of 0.3. Thus the SPATE output was a good indication of the position of maximum principal stress in this case.

Whilst the SPATE results were used here principally to select the positions for gauges, and were not intended to give absolute measurements, the output can be calibrated approximately using the measured principal stress values. It should be emphasised that this is not an accurate calibration because the stress gradient in the excavation is rather steep and ideally strain measurements should be made in an area of uniform stress. Figure D6 shows the variation of the principal stress sum on a line crossing the excavation at right angles in the vicinity of the position of maximum stress. Figure D7 shows the stress variation along the bottom of the excavation.

Figure D8 shows the variation in principal stress range estimated from rosette gauges in the excavations in specimen No.25. Three excavation depths were investigated as described in Section 3.1.5 of the main text.

Finally, Fig.D9-18 show depth profiles for all the excavations investigated.

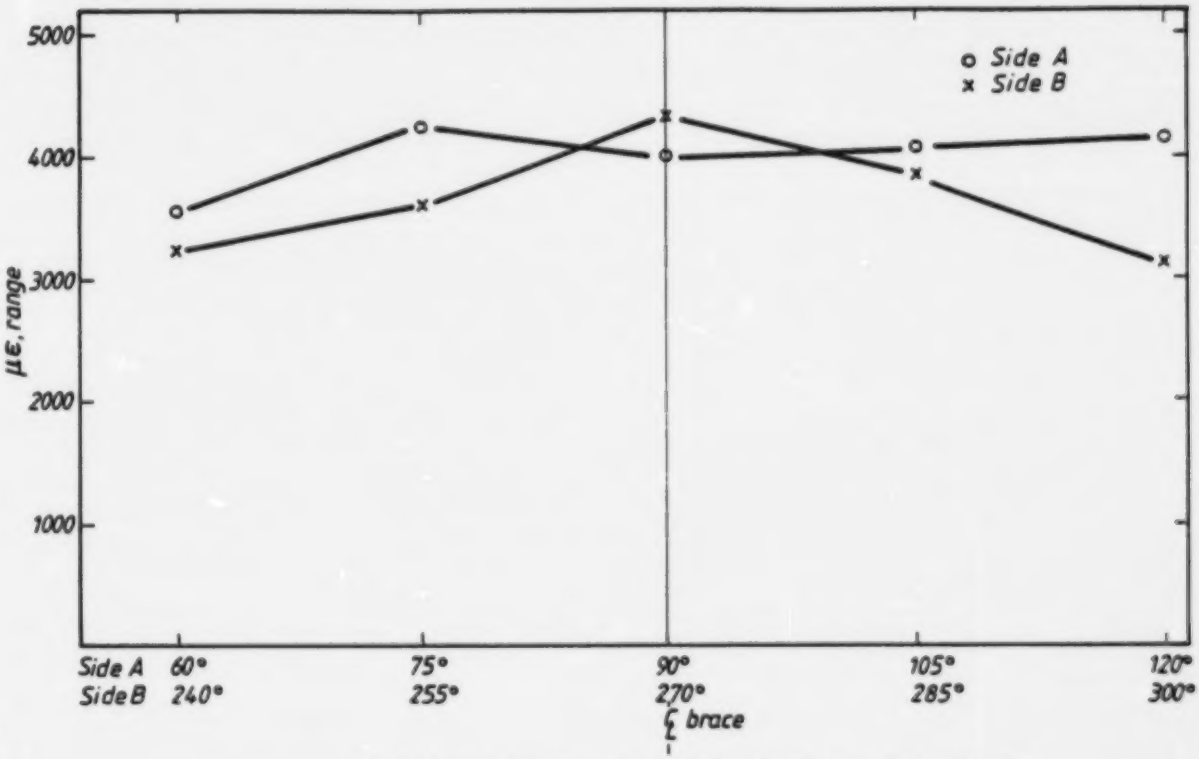

D1 *Strain variation along the ground excavation in specimen No.11.*

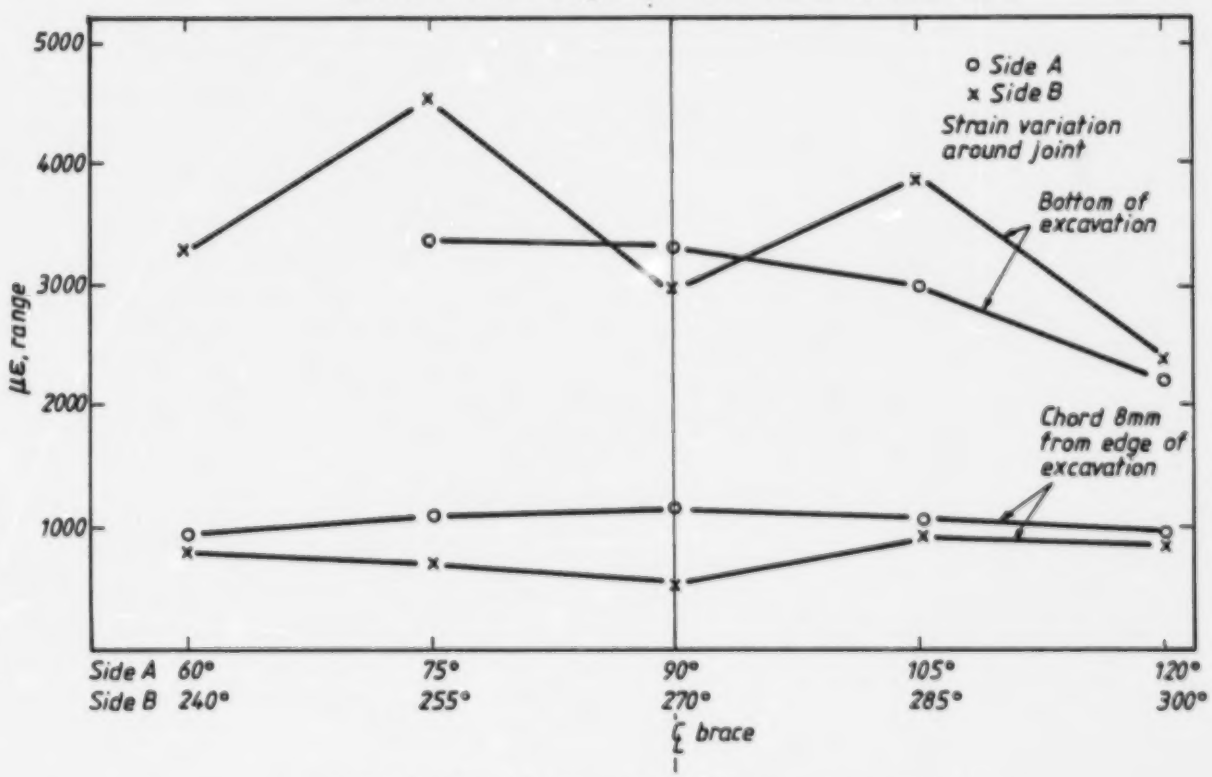

D2 *Strain variation along the ground excavation in specimen No.12.*

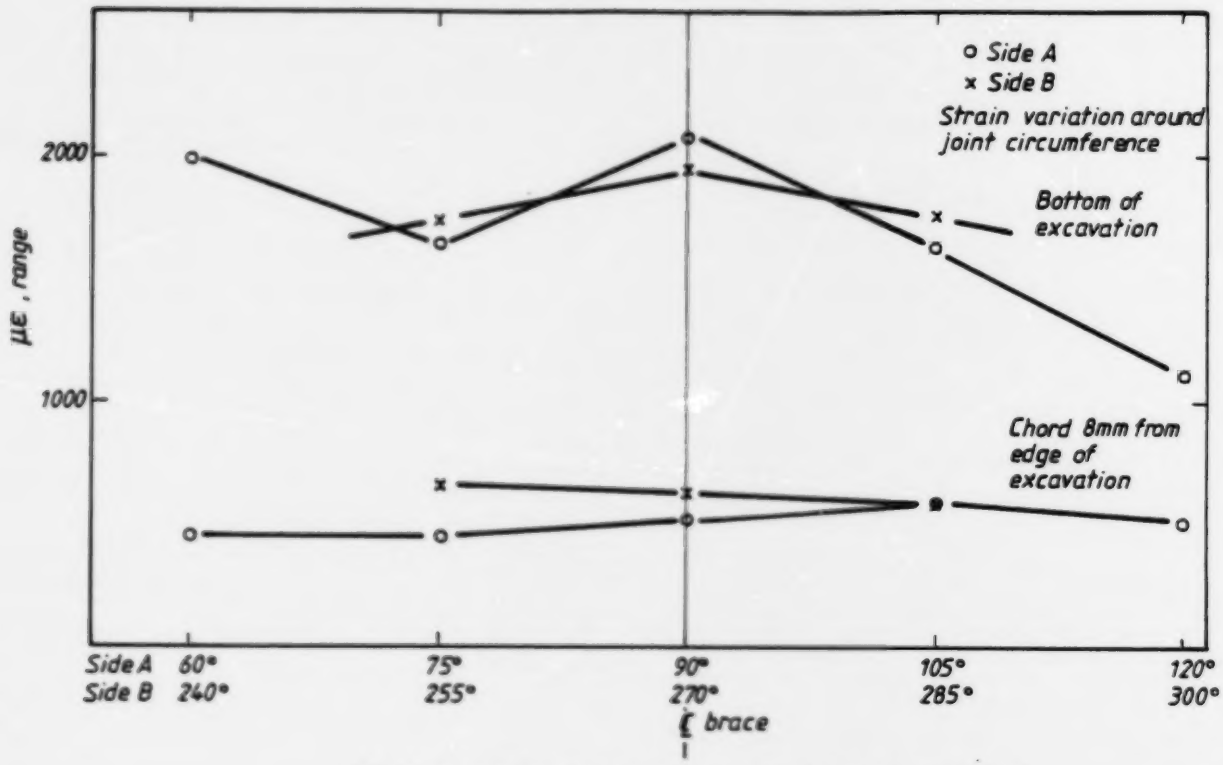

D3 *Strain variation along the ground excavation in specimen No.18.*

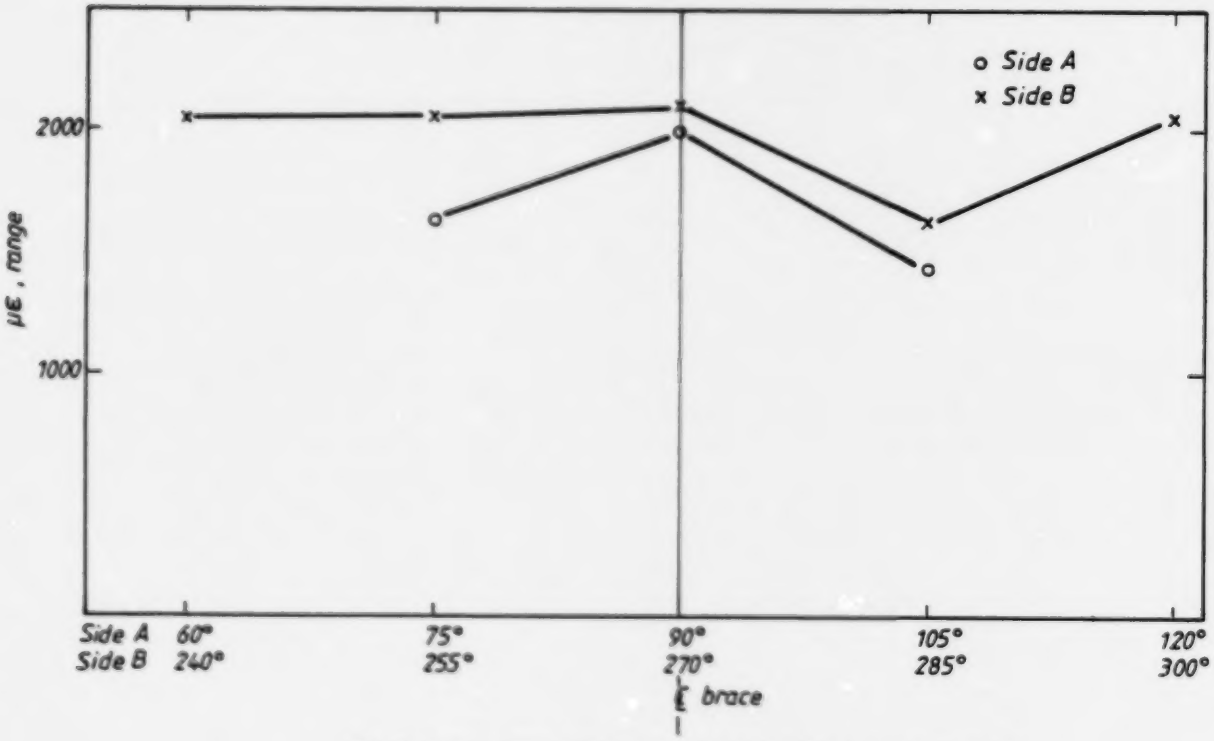

D4 *Strain variation along the ground excavation in specimen No.21.*

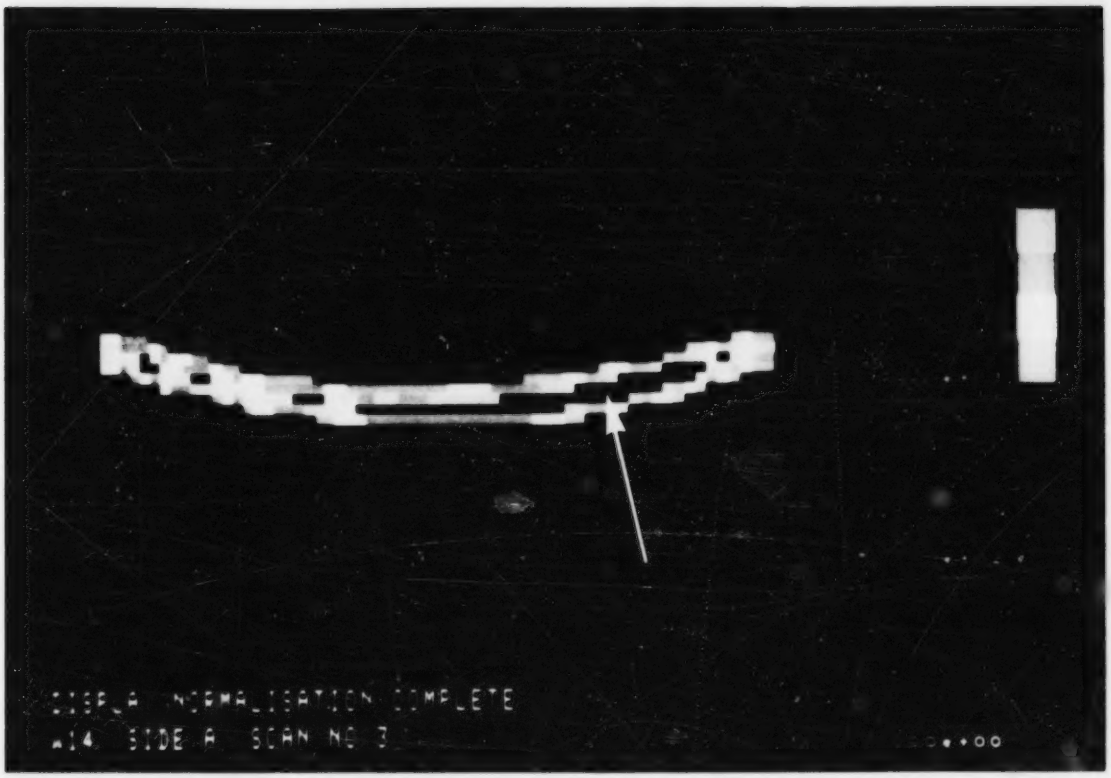

D5 *SPATE scan of the ground excavation in specimen 14, side A. The arrow indicates the position of maximum stress. Markers (+) indicate the edges of the excavation on the brace centreline.*

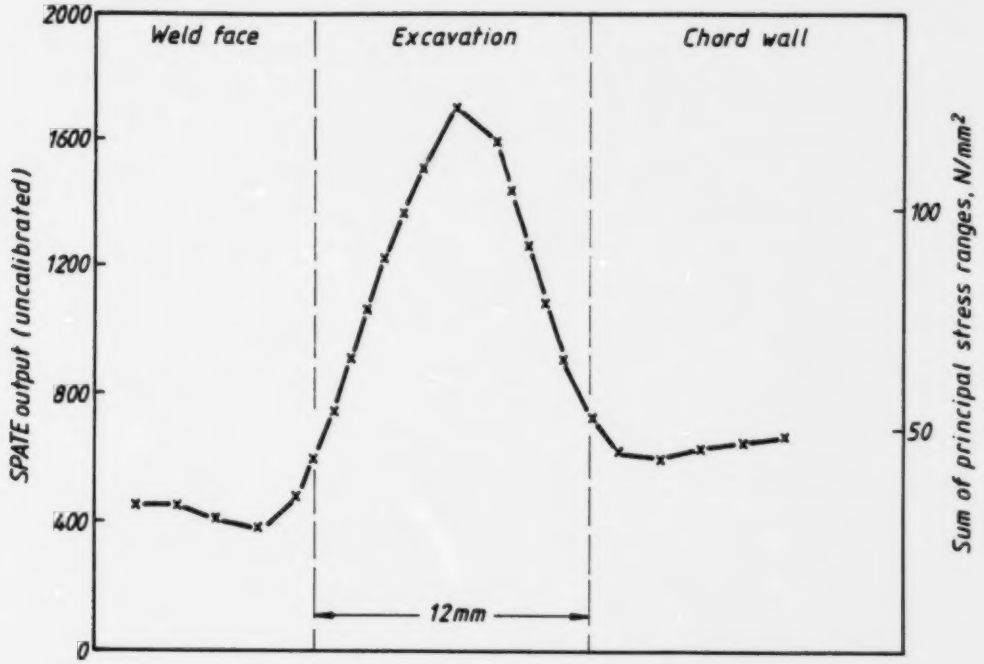

D6 *Stress variation indicated by SPATE measurements across the ground excavation at the position of maximum stress in specimen No.14 side A.*

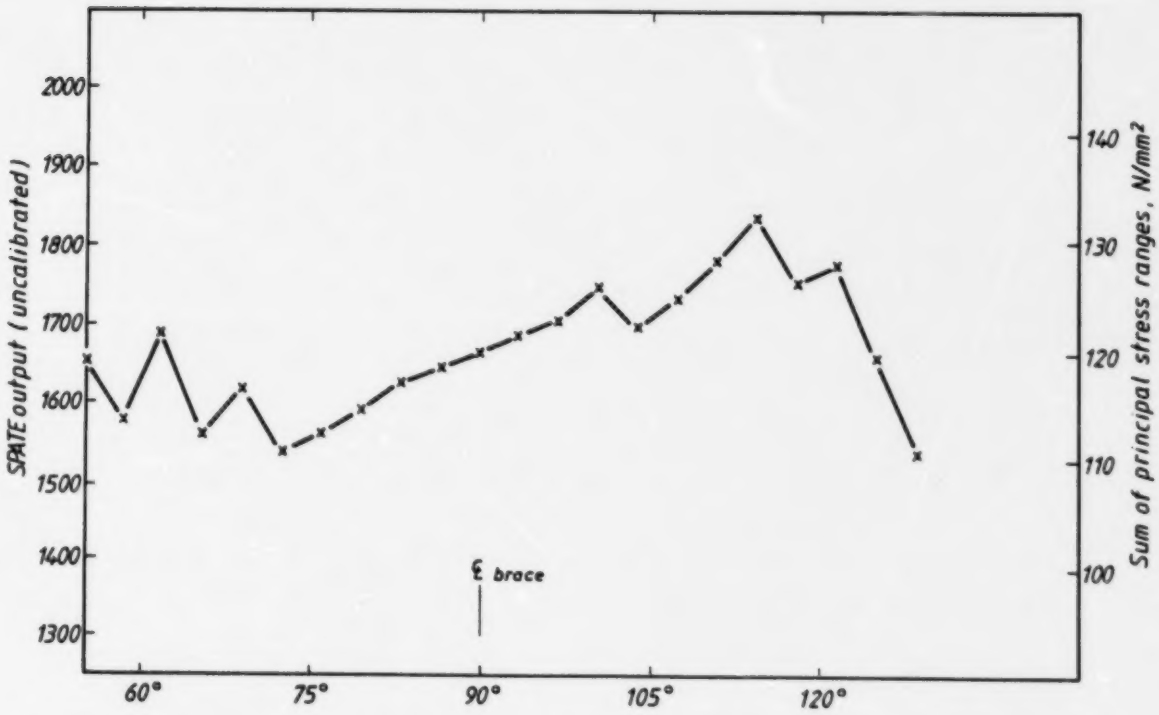

D7 *Stress variation indicated by SPATE measurements along the bottom of the excavation specimen No.14 side A.*

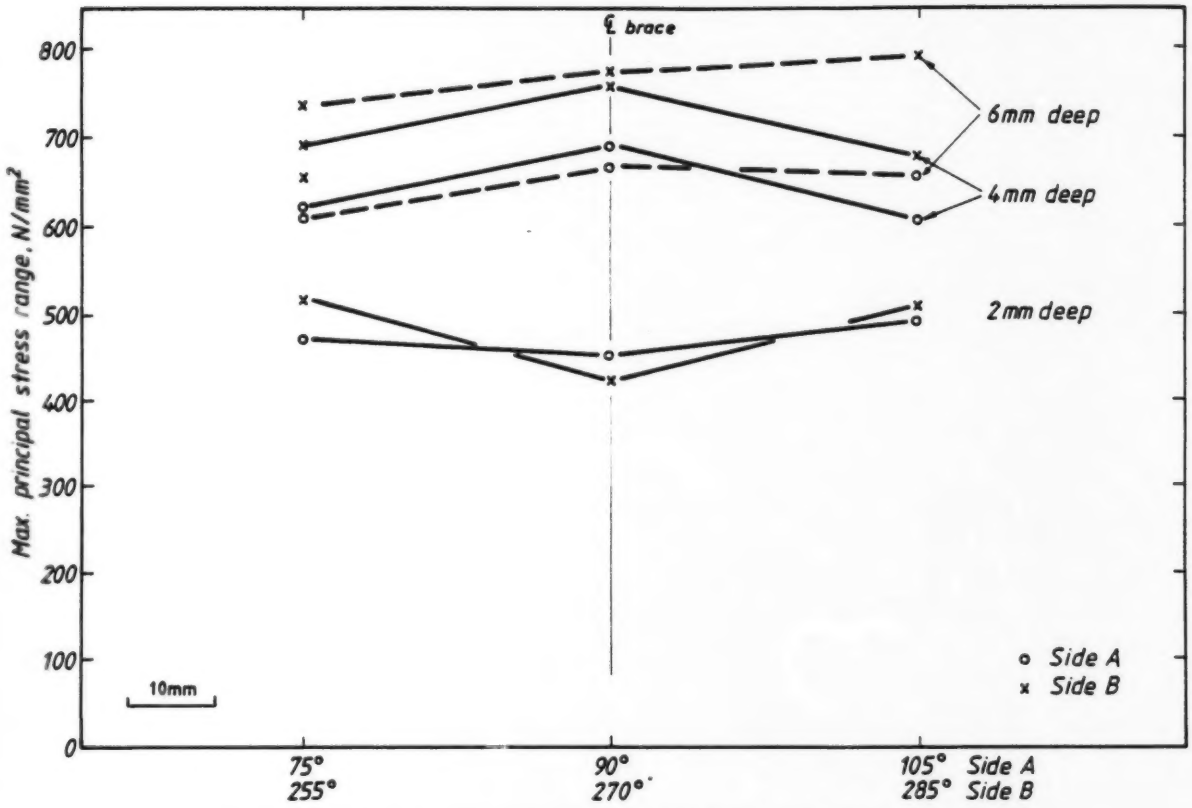

D8 *Variation of principal stress range distribution with excavation depth. Specimen No.25.*

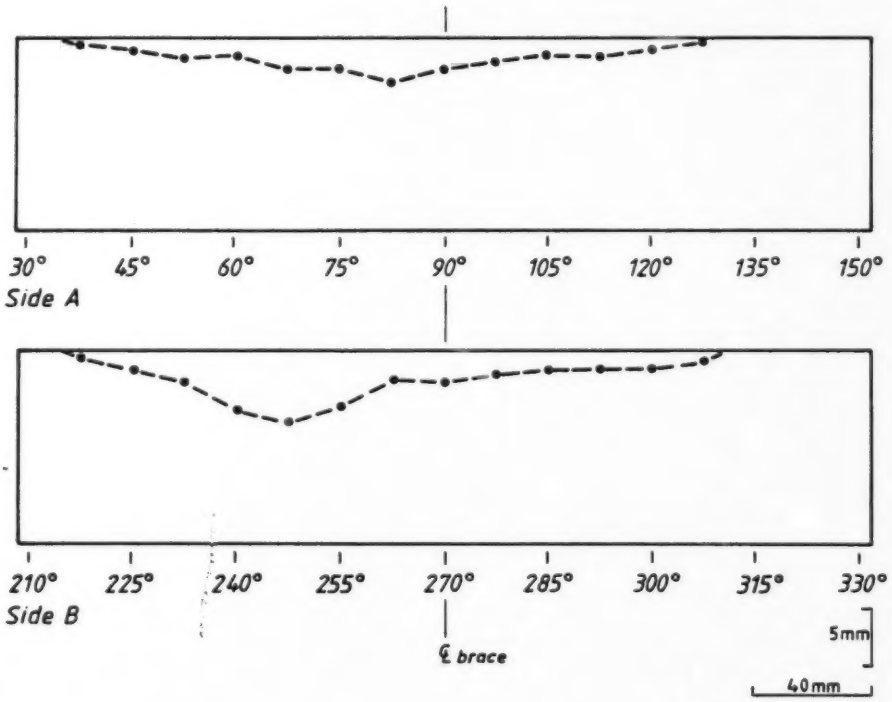

D9 *Profile of ground excavation, specimen No.10.*

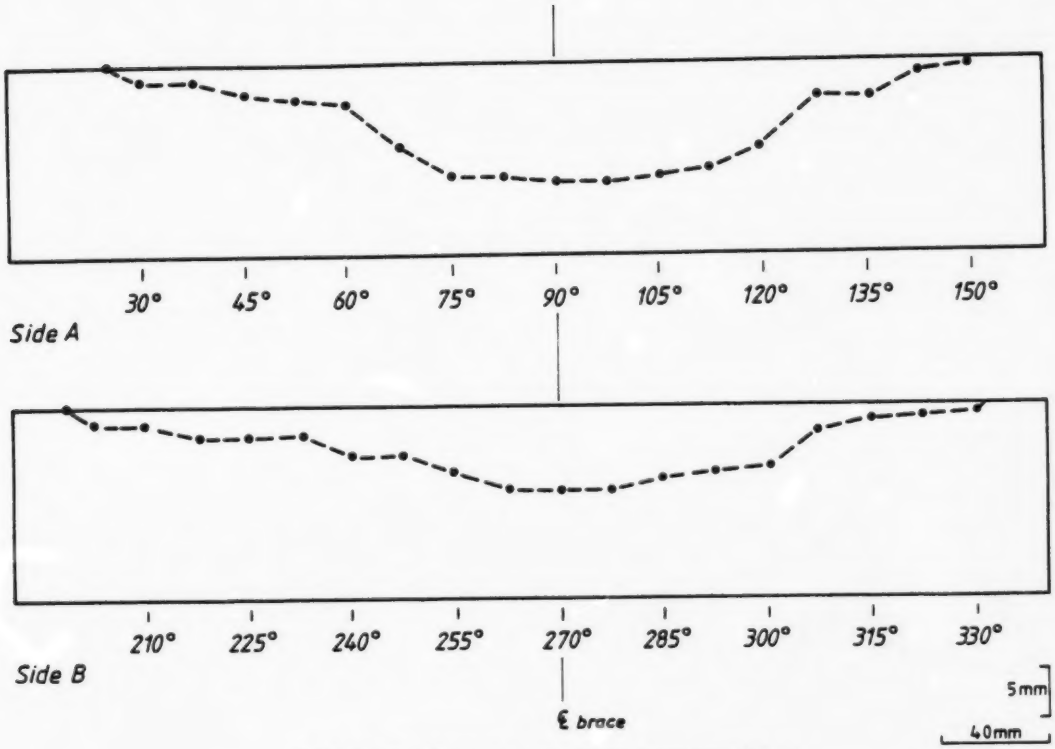

D10 *Profile of ground excavation, specimen No.11.*

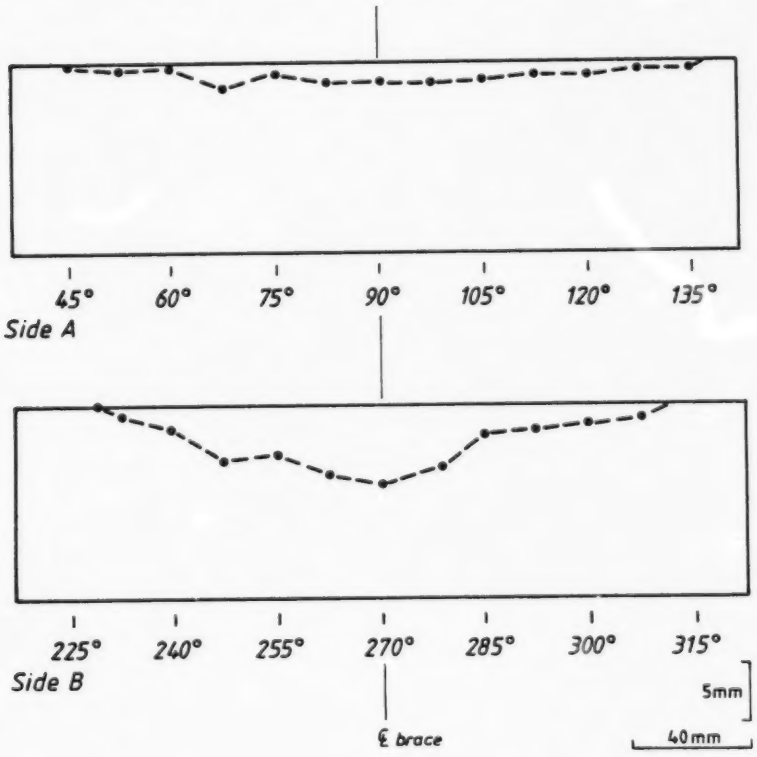

D11 *Profile of ground excavation, specimen No.12.*

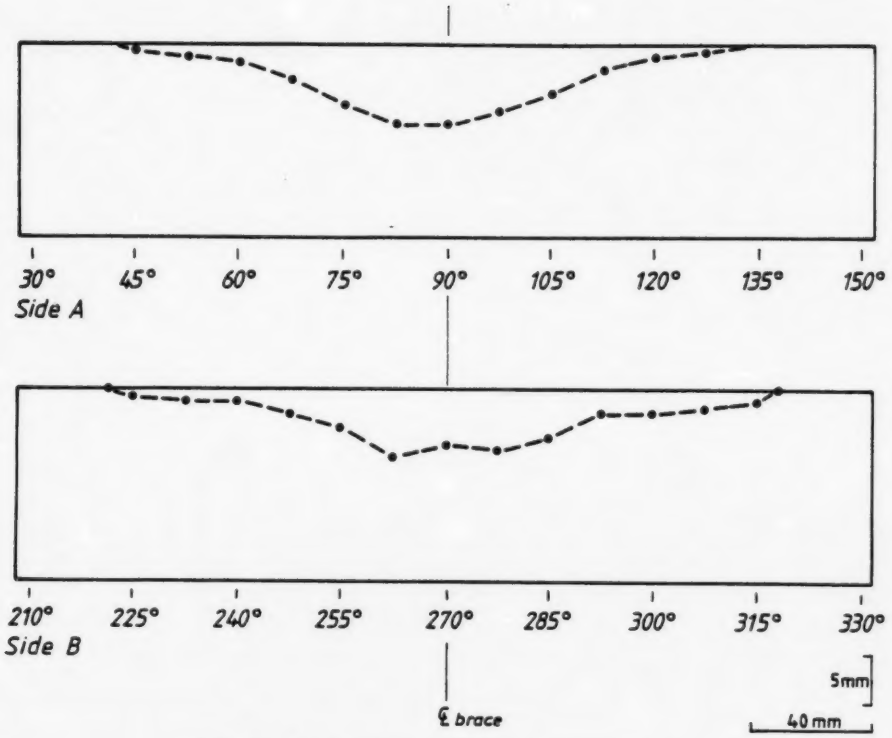

D12 *Profile of ground excavation, specimen No.14.*

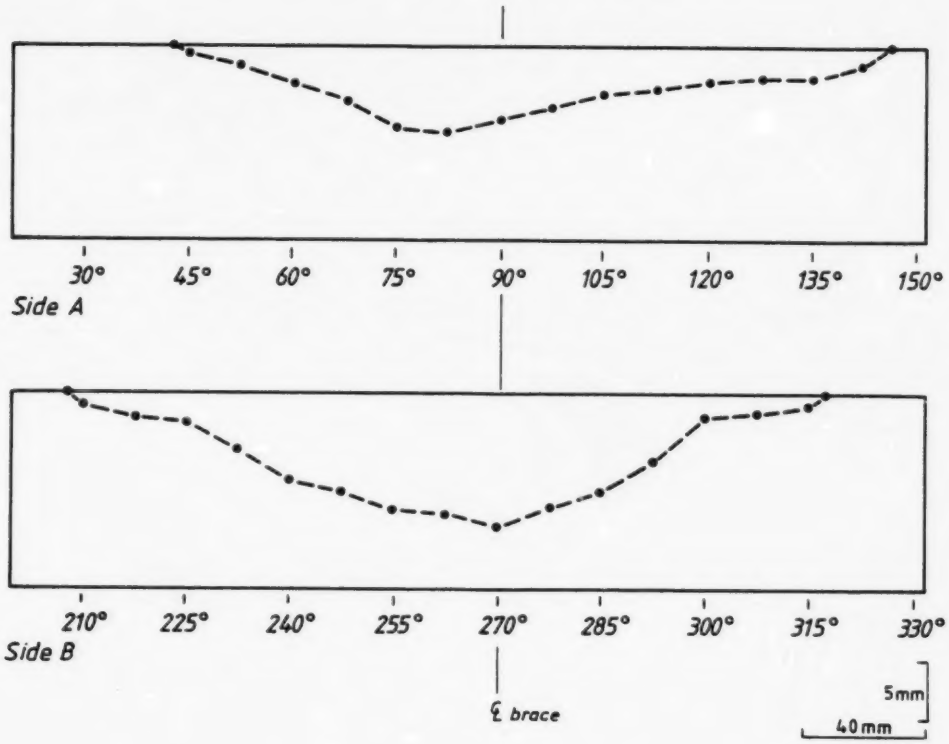

D13 *Profile of ground excavation, specimen No.17.*

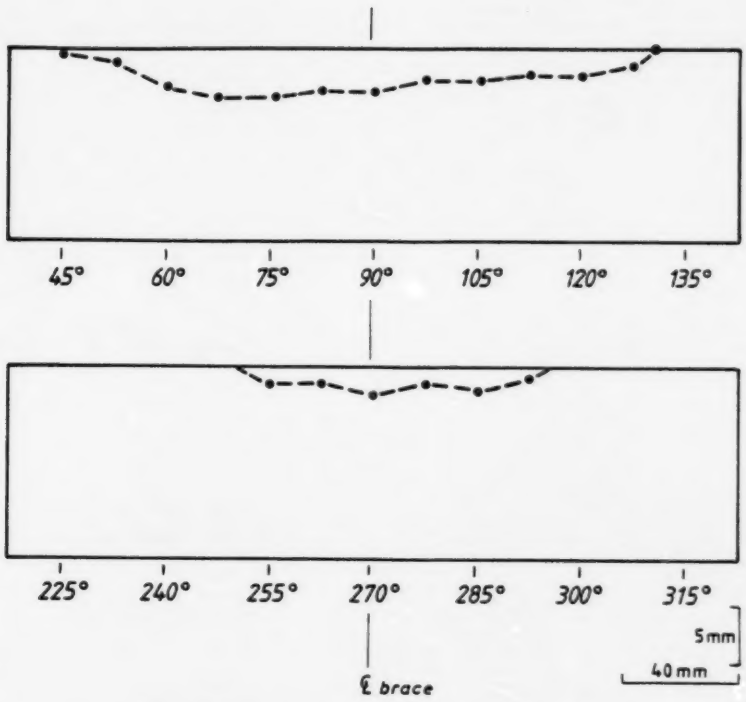

D14 *Profile of ground excavation, specimen No.18.*

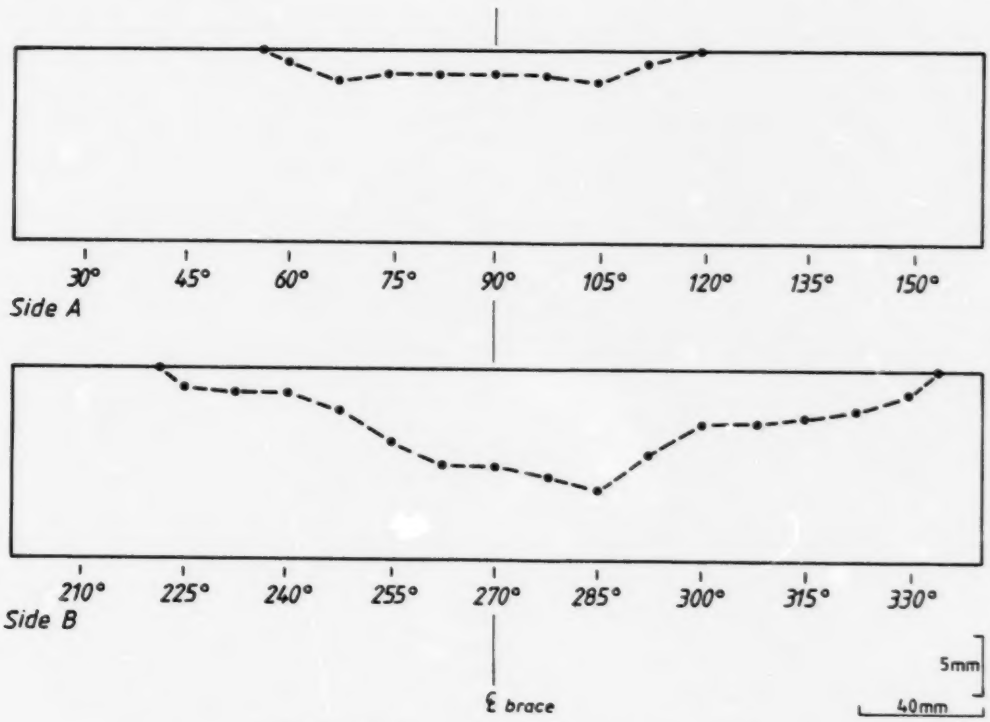

D15 *Profile of ground excavation, specimen No.21.*

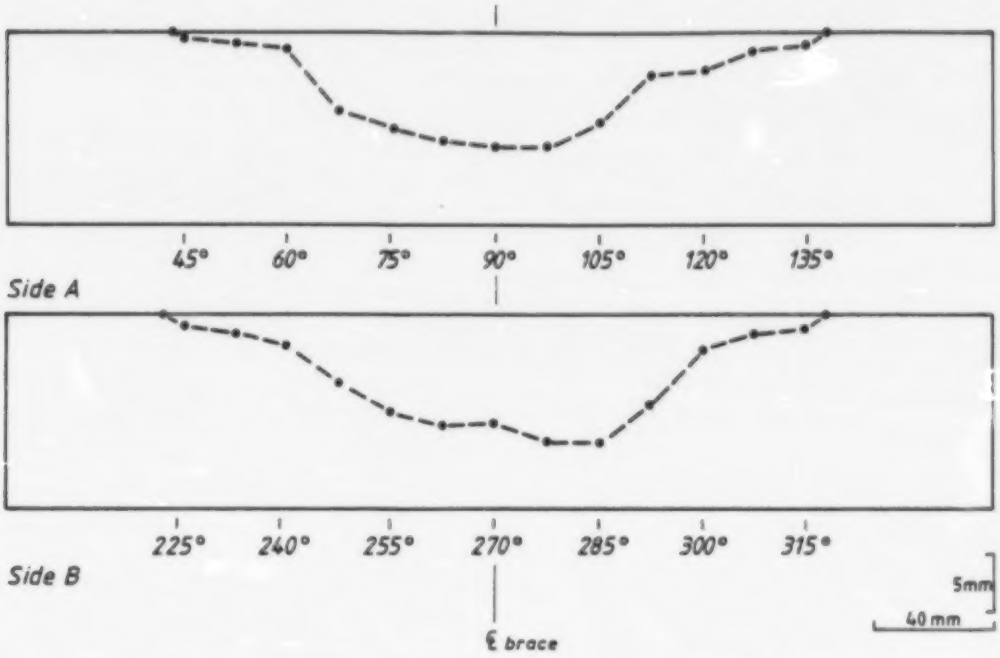

D16 *Profile of ground excavation, specimen No.22.*

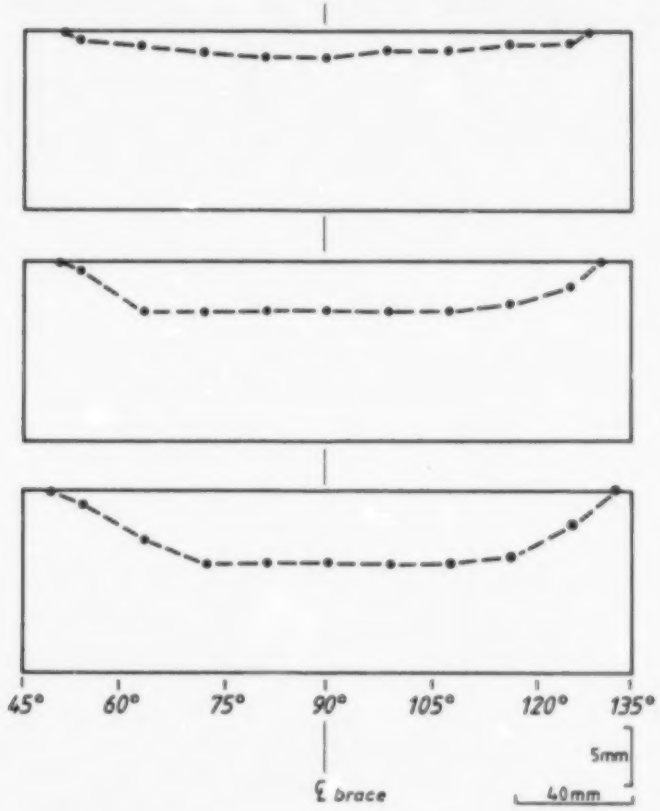

D17 *Profile of ground excavation, specimen No.25, side A.*

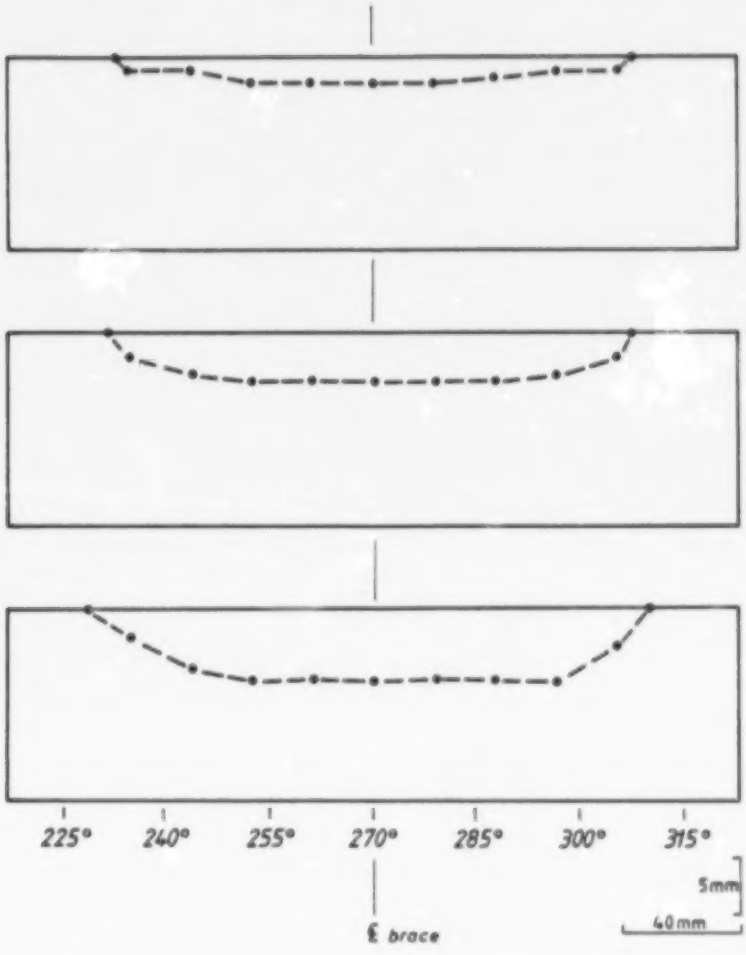

D18 *Profile of ground excavation, specimen No.25, side B.*

The Welding Institute

WORLD CENTRE
FOR WELDING
TECHNOLOGY

The Welding Institute, Abington Hall,
Abington, Cambridge CB1 6AL, UK
Telephone: 0223 891162; Telex: 81183
WELDEX G; Telefax: 0223 892588
A company limited by guarantee.
Registered No 405555 England.